Investigation of Human Gait Control Using Simulation and Sliding Mode Techniques

Thesis submitted for the degree of

Doctor of Philosophy

at the University of Leicester

by

Steven Lister

Department of Engineering

University of Leicester

September 2004

ProQuest LLC
789 East Eisenhower Parkway
P.O. Box 1346
Ann Arbor, MI 48106-1346

Investigation of Human Gait Control Using Simulation and Sliding Mode Techniques

by

Steven Lister

Declaration of Originality:

A thesis submitted in fulfillment of the requirements for the degree of Doctor of Philosophy in the Department of Engineering, University of Leicester, UK. All work presented in this thesis is original unless otherwise acknowledged in the text or by references. No part of it has been submitted for any other degree, either to the University of Leicester or to any other University.

Steven Lister
September 2004

They say the world is a stage, but obviously the play is unrehearsed and everybody is ad-libbing his lines. Maybe that's why it's hard to tell if we're in a tragedy or a farce.

-Calvin and Hobbes, Bill Waterstone (1993)

Acknowledgements

My thanks go first to my supervisors; to Barrie Jones for bringing me back to Earth when I was carried away by some of my wilder ideas, to Sarah Spurgeon without whom I would not have begun to understand sliding-modes, to Will Peasgood for his enthusiasm and support, and finally to Jon Scott whose medical perspective became an essential reference point.

Special thanks to Richard Thomas, John Twiddle, Anita Boardman and all the others who kept me sane throughout the highs and lows of the last three years. Their faith in me when even my supervisors were giving up kept me going.

My gratitude also goes out to the Leicester General Hospital for the use of their gait analysis equipment, and in particular to Mike Barnes of the Sports and Medicine department for giving us access as well as help and advice with the apparatus.

Contents

List of Figures

Abstract

This thesis deals with the novel application of non-linear sliding-mode control techniques to the fields of gait analysis and locomotion control. The aim of the study was to create a platform for the development of sliding-mode controlled FES (functional electrical stimulation) systems for subjects suffering neural gait disorders.

A model of the human locomotive system featuring 10 pin-jointed segments and 50 functioning muscles was created. A sliding-mode controller was applied to force the simulation to follow kinematic trajectories collected from subjects using gait analysis techniques and optimisation algorithms were developed to predict possible muscle activity patterns during the sampled gait sequences.

With accurate parameters, motion tracking by the system took place with an error of less than 0.25 degrees and joint moments were generated within 1 standard deviation of the expected reference curves. Significant features of the measured EMG (electromyogram) readings typically matched similar features in the simulated muscle activations.

Antagonism occurred in the simulated signals in the same periods as in the reference EMG readings, i.e. where the joint angles are most sensitive to moments acting on them. This is due to the switching nature of the sliding-mode controller. Sliding-mode techniques also provide insensitivity to model-plant mismatches reducing the need for accurate parameters, of which hundreds would be required and the majority of which would be difficult to obtain.

As a forward-dynamics neuro-musculo-skeletal model with an integral sliding-mode controller and optimised muscle activity estimator, the model can function both as a powerful tool for gait analysis and non-invasive EMG estimation and as a platform for the development of FES controllers for subjects with neuro-muscular gait anomalies, thus fulfilling the stated aim of the study.

Nomenclature

A reasonable level of biomechanics knowledge is assumed, but for the sake of clarity, some of the terms not explained in the text are defined here in the context appropriate to their use.

Actuator: a mechanism that generates an action.

Anteversion: the forward tipping or tilting of an organ as a whole without bending.

Biomechanics: the mechanics of a living body, and the study of it.

Cadaver: a dead body, especially for study.

Circumduction: swinging of the leg in a wide arc during gait to ensure ground clearance.

Closed-loop: a system controlled with feedback.

Coefficient: a number that is multiplied by a variable.

Diplegic: paralysis of corresponding parts on both sides of the body.

Dynamics: the study of the energy and motion of objects.

EMG (ElectroMyoGraphy): the study of, or measurement of the electrical activity of muscles as they contract.

Feedback: the return of some or all of the outputs of a system to the input.

Femoral nerve palsy: paralysis of the femoral nerve.

FES (Functional Electrical Stimulation): the stimulus of muscle activity using externally applied electrical signals.

Foot-drop: a condition where the foot of the subject hangs from the ankle during the swing phase due to inadequate dorsiflexor action or spastic plantarflexors.

Forward-dynamics: a method of modelling a system from cause to effect.

Gait: way of walking.

Ground reaction: the reactive forces and moments presented by the ground that prevent a person from sinking through the surface with each footstep.

Hill-type actuator: a model of human muscle behaviour [21, 120, 119].

Idiopathic: relating to a disease having no known cause.

Inertia: the tendency of a body to resist acceleration.

Interpolation: a method of finding missing points within a dataset by analysis of the relationships between the surrounding points.

Inverse dynamics: a method of modelling a system where the outputs are used to find the inputs.

Kinematics: the study of the motion of a system without consideration of the forces acting on it.

Kinetics: the study of the forces causing motion of and within a system.

Magnitude: size with no consideration of direction.

Moment: the measure of the tendency of a force to produce rotation about an axis. See section 2.4.3.

Moment of inertia: the tendency of a body to resist rotational acceleration.

Normalisation: a transformation applied uniformly to a data set so that the set shares certain properties. E.g. representing muscle force as a proportion of the maximum voluntary contraction for that muscle. The same muscle model can be used for every muscle.

Open-loop: a system without feedback, i.e. uncontrolled.

Optimisation: mathematical techniques used to make a system as efficient as possible in terms of the optimisation criteria.

Orthopaedics: the branch of medicine dealing with the skeletal system and associated muscle, joints and ligaments.

Parameter: one of a set of measurable factors that define a system.

Pathology: the nature, causes and effects of a disease or the study of it.

Pennation: the angle of muscle fibres to the path of the muscle.

Physiological cost index (PCI): A measure of the effort of walking based on the increase in heart rate from resting over the distance walked.

Plant: a real system being studied or modelled.

Trajectory: the path of a body or point moving through a space. The space may be a mathematical description of physical properties such as joint angles over time.

Trendelenburg sign: a symptom of weak hip abductor muscles where the pelvis sags over the swing phase leg during gait.

Chapter 1

Introduction

1.1 Research Motivation

Gait disorders have a significant impact on the quality of life of many people. Understanding of the motions and forces involved in human gait, and the associated muscle activations, could help in the diagnosis of underlying deficits and in developing appropriate therapies [92, 115, 116].

FES (functional electrical stimulation) is a technique increasingly employed for the rehabilitation of those with neurologically impaired limb function [40, 27, 90, 89]. In particular, work with paraplegics to restore some limited function to their paralysed legs has shown success in several areas from basic functions such as cycling [37, 45] and rowing [19], which require little or no feedback, to the more complex tasks such as standing [6, 36, 88, 87, 100] and walker supported walking [6, 36, 64, 100]. It has been demonstrated that it is possible to measure and identify in real time the distinctive EMG activity in upper trunk muscles that are produced when the subject wishes to take a right or left step, and to then stimulate the lower limb muscles in the appropriate sequence [40]. In this way practised subjects can typically take walks of 50 to 150 steps between rests. Obviously this has enormous benefits for the subject in terms not only of mobility, but also with cardiovascular circulation, and as a psychological boost for someone expecting to spend the rest of his/her life in a wheelchair [27].

Paraplegics are not the only people who can benefit from FES techniques; there are many other conditions that also affect lower limb function. Human gait is the outcome of interactions between the brain, spinal cord, peripheral nervous system, muscles, bones and joints [112]. A disorder of any part of this system will produce a change in gait pattern and as such, gait pathologies can

vary from a stubbed toe to complete paralysis. Amongst those relevant to this study are cerebral palsy, Parkinsonism, stroke, head injury, spinal cord injury, and multiple sclerosis [112]. Each of these can result in a failure, or reduction in quality, of the transmission of an activation signal to a muscle. In cases where only a small number of muscles are seriously affected the subject can still walk, albeit with an unusual gait pattern. Such methods of locomotion are clearly less than optimal; the speed is drastically reduced, stability and balance can be compromised, and there can be psychological factors such as lack of confidence and embarrassment that affect the subject.

It is these people that this study aims to benefit, and in particular those who have only recently been affected, as it is difficult to alter gait patterns that compensate for the problems, once they have become ingrained.

Using FES to stimulate inadequately functioning muscles in the appropriate sequence and by the required degree could allow a subject to produce a more normal gait pattern. This would improve stability and freedom of movement for the subject, which would have an enormous effect on his/her quality of life.

Stimulation techniques are applicable only where the muscles, bones and joints are still healthy and functional. Conditions affecting these organs will not be helped by artificial stimulation and may even by exacerbated. FES can only provide a substitute for the normal neural signals to the muscles.

Finding the appropriate sequence and the required level of activation for the inadequately functioning muscles requires a control system that can analyse the gait pattern in real time and generate stimuli to force the limbs to the required trajectories. This study aims to provide a method for development of controllers that can be applied to specific individuals with specific gait pathologies.

A typical example of the sort of problem that can be corrected is foot drop [10, 105, 107, 106]. Inadequate dorsiflexor control means that during the swing phase of gait the foot tends to hang from the ankle which causes the subject to employ one of a number of characteristic compensations to ensure that the toes clear the ground. As the average clearance in normal gait is only 1.29cm, almost any degree of foot drop is significant [47]. By employing FES stimulation to the dorsiflexor muscles during the swing phase, toe clearance can be produced, the compensations eliminated, and a more normal gait pattern resumed. In stroke patients, Taylor et. al. [106] produced a 27%

increase in walking speed through the use of FES over a four and a half month period, and in a similar study Burridge et. al. [10] produced increases in walking speed of 20.5% compared to 5.2% in the control group.

In addition to the increase in velocity, subjects using FES techniques to correct foot-drop cited a marked reduction in the effort of walking [107], a belief backed up by an improvement in the physiological cost index (PCI) of over 30% [10, 107].

Multiple sclerosis sufferers also showed an increase in walking speed and reduction in PCI to FES foot-drop correction, although generally not as large an improvement as the stroke victims over the same time period [105, 106].

Additional gait problems can also be corrected by adding more stimulation channels, as in the case of Burridge and Wood [11] who added calf or hamstring stimulus as appropriate to a group of subjects, producing significant benefits over foot-drop correction alone.

Glanz et. al. [39] showed that FES is a useful tool in the rehabilitation of stroke patients, especially in terms of promoting muscle strength, while Thrasher and Popovic [108] concluded that FES-assisted walking can be an effective short-term technique with long-term results in the treatment of incomplete spinal cord injuries.

Alternatively, FES can be used in conjunction with botulinum toxin A to treat spasticity [35, 53], the combination of the two treatments inhibiting and reducing the tone of a spastic muscle and increasing the tone and range of movement of it's antagonist.

As well as providing increased mobility with reduced effort [10, 105, 107, 106], FES can help to reduce abnormal joint stiffness [77] and prevent further damage to the musculoskeletal system from acute compensations for inactive muscles [66].

1.2 Neuro Musculo Skeletal Modelling and its Applications

Essential to this study is a 2-dimensional model of the human locomotor system comprising 10 rigid segments (upper body, pelvis, thighs, shanks, feet and toes) and a total of 50 musculotendon actuators.

Using the model, both normal and pathological gait patterns as well as any other movements of the lower limbs within the sagittal plane (Chapter

2) can be simulated. Through EMG and joint angle analysis, an individual subject's condition can be modelled and then compared with that of normal movement patterns. The compensations are then identified and removed from the simulation leaving only the pathological problems. From there it is a matter of selecting which muscles would be best stimulated to correct the motion and to then develop controllers to stimulate them in the correct sequence. Both of these can be performed on the model.

This information can then be used to develop an FES system customised for the specific subject, containing the controller or a part of it to ensure that the required movements are performed correctly.

The attraction of sliding-mode control is based on its order reduction properties and its insensitivity to certain types of uncertainty [29]. The sliding-mode system comprises a sliding surface that describes the required dynamic behaviour of the system, and a control law that drives the system onto the surface.

Using sliding-mode techniques, precise tracking of model to subject is possible even with such complex non-linear systems as the human body.

Various human locomotor system models have been developed in previous years [122, 123]. The majority are relatively simple, designed for a specific purpose with limited flexibility to other uses. Many employ only a few musculotendon units or simply operating using estimated joint torques [42, 65, 67, 68, 25]. Most are 2-dimensional and incorporate only a small number of segments and muscle groups [7, 31, 32, 44, 70, 83, 85, 89, 90, 95, 96]. The most complex examples are usually for gait analysis rather than control, operating on inverse dynamics principles alone [21].

Where control models do exist they are typically based around the knee [31, 32, 50, 49, 51, 52, 71, 96, 97] or ankle joints if not individual muscles [80, 111]. Larger models tend to be concerned only with paraplegia or robotics [19, 30, 90, 95].

Control models tend only to be concerned with producing the gross movements necessary for locomotion. This study focuses on finessing the motion of those who suffer some disability, but are still capable of producing the gross movements.

Parameters for both bones and musculotendon units were obtained from a surgical model [21, 22, 119] and used for this project to develop a large and versatile neuromusculoskeletal control model which would be used not

for severe paralysis, but for subjects with a only a few poorly functioning muscles. Ideally muscles which do not function correctly and are to be stimulated can be substituted in the model by an FES muscle simulation such as those demonstrated in the following citations [31, 32, 90, 95, 96, 111], possibly including the skin impedance model by Dorgan and Reilly [26]. This is however, beyond the scope of this project for which it is only required to represent only healthy muscles thus the use of the muscle model by Zajac et. al. [119].

1.3 Objectives

The main objective of this study is to produce a neuromusculoskeletal model and controller for the development of systems providing FES control of pathological human gait. This can be split into sub-objectives:

- The construction of a forward-dynamics neuromusculoskeletal model capable of simulating human gait.
- The development of a controller to force the model to follow observed gait trajectory data from real subjects.
- To use the controller output signals to estimate the muscle activation signals that are required to produce the gait pattern being followed.
- To provide an environment for the development of FES controllers.

Ultimately the model is designed to be used to develop smaller controllers for FES gait correction. The simplest method of applying these in practice would be through the use of commercial programmable stimulator systems such as the "Compex Motion" [58] providing control channels in multiples of four, controlled by external sensors. Alternatively a prototype system could be built specifically for the model in the manner of Ilic et. al. [46]. In this case strategies for activation level control [9] would need to be considered as well as techniques to compensate for fatigue effects [78] as the model aims to produce fine control.

Transcutaneous FES techniques are only useful for the superficial muscles, suggesting that only gait conditions affecting these can be treated, however surgical implants for FES make the stimulation of deep muscles a practical possibility. Memberg et. al. showed that an implanted electrode can maintain a stable position within the muscle and function correctly in vitro

[76]. Arabi and Sawan designed a four channel, programmable neuromuscular stimulator for implanting into subjects [3]. In conjunction with the implantable joint angle sensor of Johnson et. al. [54] and the sensory nerve signal interpretation of Strange and Hoffer [104], a completely implanted system can be envisaged.

However the stimulus is applied, the model and controller described here aim to provide a platform for the development and testing of FES gait control systems.

The research motivation has developed as an extension of work to help paraplegics regain motion and to correct foot-drop. The area of interest here, involving an intermediate level of neural gait disability, is one that is largely ignored by the FES community. The study also aims to provide a primer in appropriate biology, engineering and medical practices relating to this area of work in order to help researchers following up this project.

Chapter 2 provides an introduction into the research background necessary when reading the chapters that follow. It covers the basics of the sciences of anatomy, physiology and biomechanics as they apply to human locomotive gait.

Gait analysis is explained in Chapter 3 including the stages of the gait cycle and the techniques and equipment used. Methods are objectively examined as to their effectiveness in clinical diagnosis and as sources of data for simulation.

Chapters 4 and 5 deal with the collection and processing of gait data respectively, as performed for this study, including kinematics (joint angles and body trajectories), kinetics (forces and moments) and EMG signals (muscle activation levels). Data collected and processed in this way is used both to validate the model and as controller reference signals in Chapters 8 and 9.

The construction of the forward dynamics neuromusculoskeletal model is described in Chapter 6. Emphasis is given to the relationship between the mathematical equations and the biological and biomechanical processes they describe. Necessary approximations and assumptions are also introduced.

Chapter 7 details the development of the controller and the changes in the model its application permits. It also deals with the generation of approximate neuromuscular activation signals based in the joint moment outputs from the controller.

Chapters 8 and 9 describe the results of tracking experimentally obtained gait patterns with the model and controller. Chapter 8 refers to normal gait

patterns and Chapter 9 to pathological patterns. These simulation results include kinematic, kinetic and EMG analyses. The validation of the model is detailed here.

The conclusions in Chapter 10 cover the value of the model as a tool for gait analysis and therapy and introduce further work that could be undertaken to improve it.

Equations and parametric data are found in the appendices.

Chapter 2

The Neuro-Musculo-Skeletal System

2.1 Introduction

Before studying any system or process, it is necessary to have an understanding of the basic principles, components and disciplines involved. The human locomotive apparatus, relying on the complex interactions of a set of bones, joints, muscles, ligaments and nerves is no exception. Before moving onto the processes and pathologies of gait, therefore, this chapter will introduce the disciplines of anatomy, physiology and biomechanics as they relate to human locomotion. This section does not aim to teach these subjects in detail, merely to provide enough information to understand the chapters that follow.

Notable absences to the components of the human locomotive apparatus listed above are the brain, spinal cord and vascular system. While the brain and spinal cord are essential parts, the complex nature of their control system, relying on visual, tactile and balance sensory signals, is far beyond the scope of this project. Instead a simple motion tracking system will substitute for these organs (Chapter 7). The vascular system, while also essential, has only an indirect influence on gait and will therefore not be discussed.

2.2 Anatomy

The main functions of anatomy in this context are to provide a frame of reference for describing the positions of body parts and the movements of those body parts relative to each other. Unfortunately, there is no absolute

consensus on the anatomical terms used and as such they can vary from text to text. The terms used here are taken from Whittle [112] where "as far as possible the most common name has been used." Anatomical diagrams 2.3 to 2.9 were created using data from the Visible Human Project [82] with software made available by the Visible Human Server [16].

2.2.1 Anatomical terms

Figure 2.1 shows a body in the *anatomical position*, where a person is standing with their arms by their sides and their palms and face forward. The following terms are all made in reference to a body in this position. Alternative names are shown in brackets.

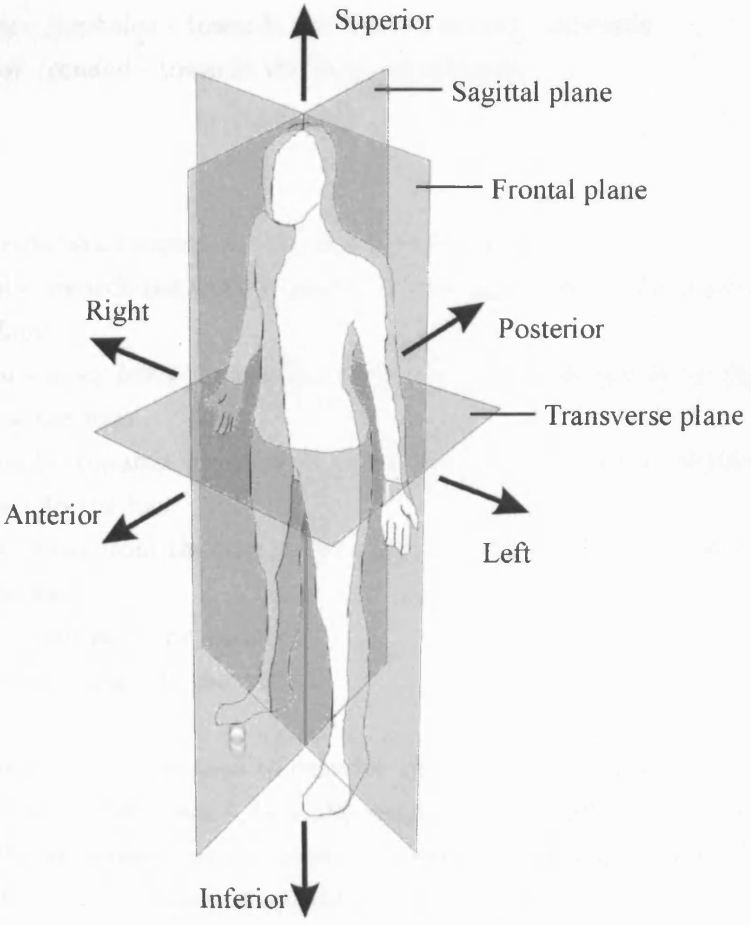

Figure 2.1: A body in the anatomical position with reference planes and directions.

Three reference planes divide the body (see figure 2.1) and are used in describing the motion of the limbs:

- *Sagittal* - divides the body or part of it into left and right portions. The median plane is the sagittal plane running through the body's midline dividing the body into halves.
- *Frontal (coronal)* - Divides the body or a body part into front and back portions.
- *Transverse (horizontal)(axial)* - Divides into upper and lower portions.

There are six fundamental direction terms used (Figure 2.1):

- *Anterior (ventral)* - forwards
- *Posterior (dorsal)* - backwards
- *Superior (cephalad* - towards the head*)(cranial)* - upwards
- *Inferior (caudad* - towards the tail*)* - downwards
- *Right*
- *Left*

A further six terms describe relative directions:

- *Medial* - towards the median plane, i.e. the big toe is on the medial side of the foot
- *Lateral* - away from the median plane, i.e. the little toe is on the lateral side of the foot
- *Proximal* - towards the rest of the body, i.e. the hip is proximal with respect to the foot
- *Distal* - away from the rest of the body, i.e. the foot is distal with respect to the hip
- *Deep* - away from the surface
- *Superficial* - towards the surface

Six basic terms are used to describe the rotation of joints (Figure 2.2):

- *Flexion* and *Extension* - typically occur in the sagittal plane and their directions depend on the joint in question. As a guideline, flexion is bending and extension straightening of the joint.
- *Abduction* - describes a frontal plane rotation moving distal parts away from the median plane.

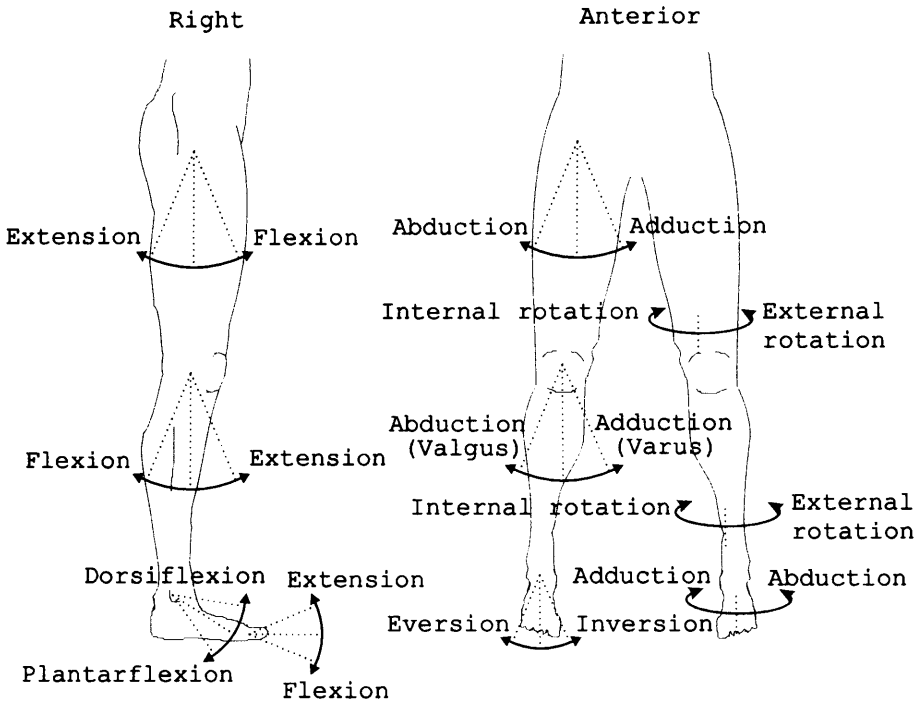

Figure 2.2: Joint movements

- *Adduction* - describes a frontal plane rotation moving distal parts towards the median plane.
- *Internal (medial) rotation* - transverse plane rotation of the anterior surface towards the median plane.
- *External (lateral) rotation* - transverse plane rotation of the anterior surface away from the median plane.

The terms varus and valgus are often used to describe, respectively, the adduction and abduction of the knee joints.

Rotation about the ankle joint causes the most problems for standardising leg movement terms. Rotations are described both in terms of the movements through the three reference planes described above, and about the natural axes of rotation within the ankle. In different texts, the meanings of the terms may be changed or interchanged.

Below is one of the more common systems for describing foot rotation:

- *Dorsiflexion (flexion)* - rotates the anterior foot upwards in the sagittal plane. Also used to describe the rotation about the talocrural joint of the ankle, which does not occur entirely in the sagittal plane.

- *Plantarflexion (extension)* - rotates the anterior foot downwards in the sagittal plane. Also used to describe the rotation about the talocrural joint of the ankle, which does not occur entirely in the sagittal plane.
- *Inversion (varus)(adduction)* - rotates the feet in the frontal plane bringing the soles of the feet together. Often interchanged with supination.
- *Eversion (valgus)(abduction)* - rotates the feet in the frontal plane moving the soles of the feet apart. Often interchanged with pronation.
- *Abduction (valgus)* - is a transverse plane rotation of the foot, moving the toes away from the median plane.
- *Adduction (varus)* - is a transverse plane rotation of the foot moving the toes towards the median plane.
- *Supination* - rotates the foot about the subtalar joint of the ankle. This combines mostly inversion with some planterflexion and adduction.
- *Pronation* - rotates the foot about the subtalar joint of the ankle. This combines mostly eversion with some dorsiflexion and abduction.

Rotation of the toes is simpler:

- *Extension* - is rotation of the toes upwards.
- *Flexion* - is rotation of the toes downwards.

For the purposes of this project it will be assumed that the toe joints do not articulate in any other direction.

2.2.2 The Skeleton

The skeleton provides a linked framework of rigid components with fixed muscle attachment sites to facilitate body movement.

Bone is the body's hardest substance after the enamel and dentin in the teeth. A highly vascular and metabolically active tissue, it has a large capacity for self-repair and adaptation to variation in mechanical demand [13]. It is a complex composite structure with mechanical properties uniquely evolved for the function it performs, but for the purposes of this project, it is assumed to be a perfect rigid structure with no flexibility and no capacity to break. During a normal (or even pathological) gait cycle there is not enough force to produce significant deformation of any of the bones. Over long periods, some gait patterns can cause damage ([81] pp. 45-47), but this is beyond the scope of this study.

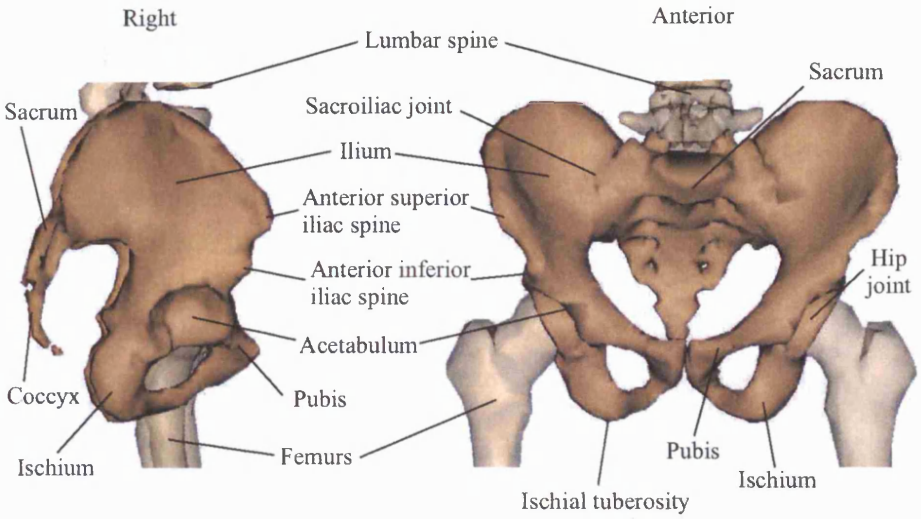

Figure 2.3: The bones and features of the pelvis

Most of the body's bones are used during locomotion; however, the movements of the arms and upper body are principally for balance. For practicality, only the legs and pelvis will be considered.

The *pelvis* is formed from a number of bones, in some cases fused together and in others tightly held by ligaments.

It can be considered as the following main parts:

- The *sacrum* is formed from five fused vertebrae and the superior surface attaches to the inferior of the lumbar spine.
- The *coccyx* is the vestigial tail.
- The two *innominate bones*, formed from a fusion of the *ilium*, *ischium* and *pubis* bones on either side, wrap around from the sides of the sacrum to meet at the anterior. These bones also form the *acetabulae*, which are the sockets of the ball-and-socket hip joints.

The result is a girdle of bone providing protection for the organs inside, as well as solid muscle attachment sites that provide large moment arms for more efficient movement. Little enough movement is possible between the bones of the pelvis that for gait analysis, it can be assumed to be a single rigid structure.

Distal to the pelvis are the *femurs* (Figure 2.4). These are the longest bones in the body. The head of the femur is a ball that articulates in the acetabulum of the pelvis. The neck of the femur runs inferior and lateral,

meeting the main shaft of the bone at a junction with two bony protuberances; the *greater* and *lesser trochanters*. These are muscle attachment sites that protrude to give greater moment arms. At the distal end of the shaft the bone widens into the *lateral* and *medial condyles*, which have rounded curves to articulate smoothly with the tibia distally and a groove between to articulate with the patella to the anterior.

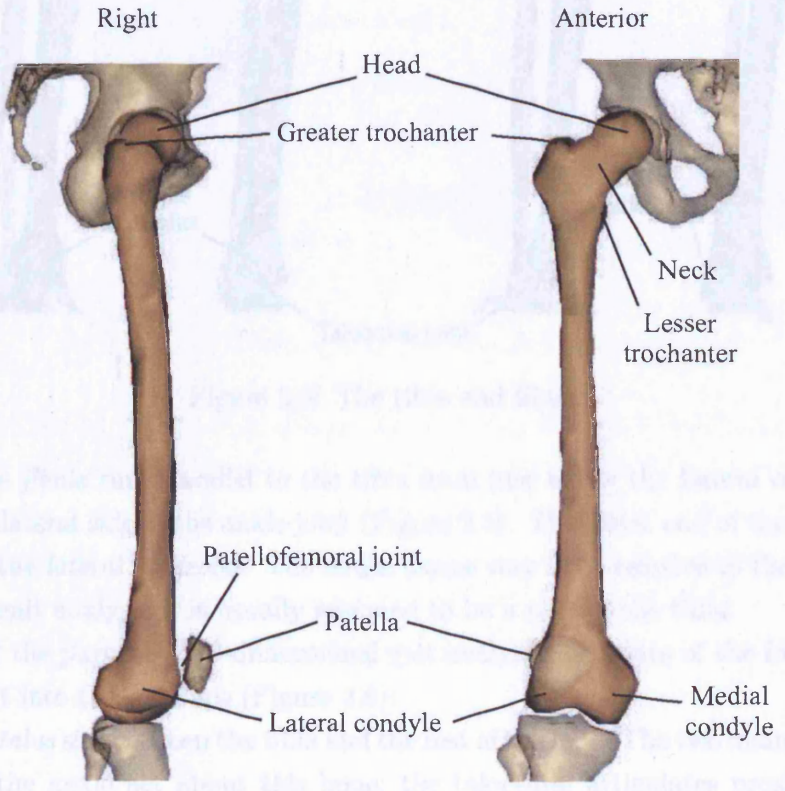

Figure 2.4: The femur and patella.

The *patella* or *knee cap* (Figure 2.4) is a *sesamoid* bone, which means it is contained within a tendon. It acts to increase the moment arm across the anterior of the knee allowing greater extension torques to be generated.

Proximally, the lateral and medial condyles of the *tibia* form an almost flat surface that articulates with the femur (Figure 2.5). A bony prominence on the anterior called the *tibial tuberosity* forms the attachment site of the *patellar tendon*. Distally the tibia attaches to the talus bone in the *talocrural* joint of the ankle. The medial prominence of the ankle is part of the tibia and is referred to as the *medial malleolus*.

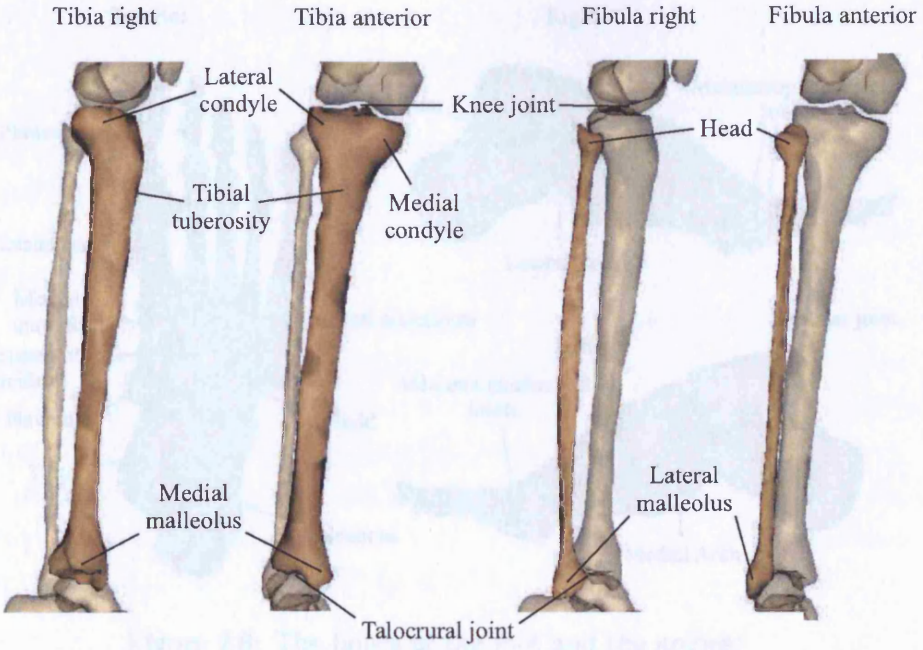

Figure 2.5: The tibia and fibula.

The *fibula* runs parallel to the tibia from just below the lateral condyle to the lateral side of the ankle joint (Figure 2.5). The distal end of the fibula forms the *lateral malleolus*. The fibula moves very little relative to the tibia, so for gait analysis it is usually assumed to be a part of the tibia.

For the purposes of 3-dimensional gait analysis the bones of the foot can be split into three groups (Figure 2.6):

- The *talus* sits between the tibia and the rest of the foot. The two main joints of the ankle act about this bone; the talocrural articulates proximally with the tibia and fibula, and the subtalar distally with the calcaneus. The talus also articulates to the anterior with the navicular, but little movement is made at this joint so it can be ignored.
- The *calcaneus* is the heel bone, but for the purposes here it is combined with the other bones of the foot: the *navicular*, the *cuboid*, the *lateral*, *intermediate* and *medial cuneiforms* and the five *metatarsals*. These will be referred to collectively as the *main foot*.
- The *phalanges* are the toe bones and these are grouped together, with the assumption that they move collectively with a simple flexion-extension motion only.

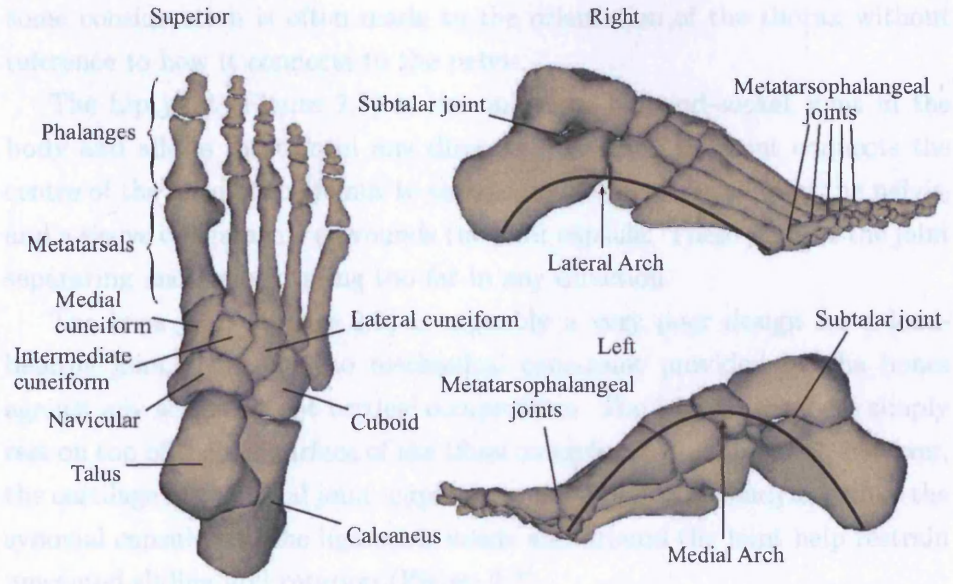

Figure 2.6: The bones of the foot and the arches.

This is a simplified view of the foot and does not allow for flexibility of the arches or of other movements within the body of the foot, however, for the purposes of gross gait analysis it is more than adequate, many similar systems ignore the subtalar joint and/or neglect the toes altogether [25, 38, 42, 59, 60, 74, 89, 90]. For 2-dimensional analysis the subtalar joint is ignored and the talus bone is grouped with the calcaneous and others in the main foot.

2.2.3 Joints and Ligaments

Simply put, a joint is the point where two or more bones meet. There are several types of joint, but for studies restricted to gross movements, only synovial joints are of interest. In these joints, the bone surfaces involved are covered in a layer of cartilage and the joint is contained within a synovial capsule, which secretes synovial fluid as a lubricant.

Ligaments are used to stabilise joints and limit unwanted motion. They are formed of fibrous tissue of limited elasticity.

The lumbar spine and its connection to the pelvis form a series of joints supported by assorted ligaments and muscles allowing flexibility about any axis, but this is too complex a system for basic gait analysis unless the spine is the specific area of study. The area is usually ignored, although

some consideration is often made to the orientation of the thorax without reference to how it connects to the pelvis.

The hip joint (Figure 2.3) is the only true ball-and-socket joint in the body and allows rotation in any direction. A small ligament connects the centre of the head of the femur to the centre of the acetabulum of the pelvis, and a sleeve of ligaments surrounds the joint capsule. These prevent the joint separating and from rotating too far in any direction.

The knee joint (Figure 2.5) is arguably a very poor design for a load-bearing joint. There is no mechanical constraint provided by the bones against any action except vertical compression. The femoral condyles simply rest on top of the flat surface of the tibial condyles. Inside the joint, however, the cartilage of the tibial joint 'cups' the rounded femoral condyles, while the synovial capsule and the ligaments inside and around the joint help restrain unwanted sliding and rotation (Figure 2.7).

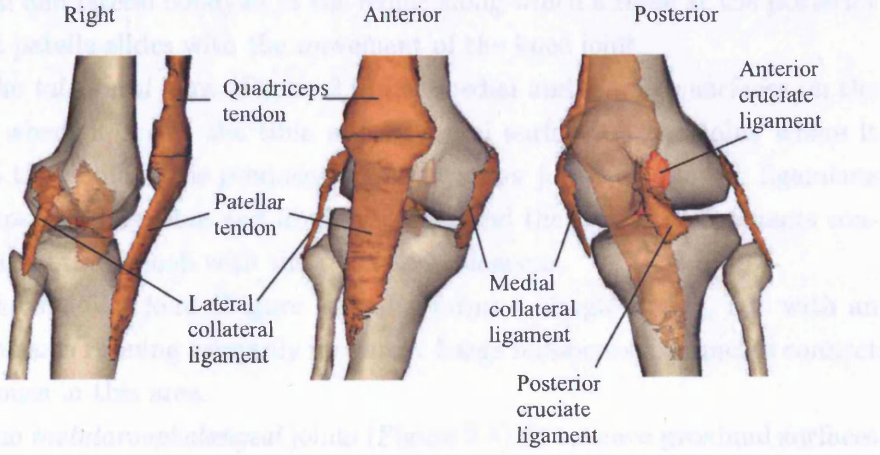

Figure 2.7: The knee ligaments

Five ligaments restrain the motion:

- The *medial collateral ligament (MCL)* across the medial side of the joint restricts abduction
- The *lateral collateral ligament (LCL)* across the lateral side of the joint restricts adduction
- The *posterior joint capsule* across the restricts of the joint prevents hyper-extension (excessive extension)
- The *anterior cruciate ligament (ACL)* is inside the joint, between the condyles and crosses from the anterior of the tibia to the posterior of

the femur. It prevents the tibia from sliding forward relative to the femur and restricts hyperextension.

- The *posterior cruciate ligament (PCL)* is also inside the joint between the condyles and crosses from the posterior of the tibia to the anterior of the femur. It prevents the tibia from sliding backwards relative to the femur and restricts hyperflexion.

The cruciate ligaments form a four-bar linkage forcing the joint to roll and slide simultaneously. This moves the contact point and the axis of rotation as the joint rotates.

At full extension the knee joint rotates externally a few degrees to 'lock' the joint, but healthy knees undergo very little adduction and abduction movement.

The *patellofemoral* joint (Figure 2.4) is essentially a groove between the medial and lateral condyles of the femur along which a ridge at the posterior of the patella slides with the movement of the knee joint.

The *talocrural* joint (Figure 2.5) has medial and anterior surfaces on the talus where it meets the tibia and a lateral surface on the talus where it meets the fibula. This produces a simple rocker joint. The major ligaments are those holding tibia and fibula together and the collateral ligaments connecting both malleoli with the talus and calcaneus.

The *subtalar* joint (Figure 2.6) also forms a simple rocker, but with an oblique axis running primarily forwards. Large numbers of ligaments connect the bones in this area.

The *metatarsophalangeal* joints (Figure 2.6) fit concave proximal surfaces into convex distal ones. As well as significant flexion/extension, some abduction/adduction is possible, but this can be neglected when treating them as a single joint for gait analysis.

There are many other joints in the foot, not least those forming the arches, which use the elasticity of the ligaments to act as two parallel curved springs (Figure 2.6), but in the interests of practicality these will be neglected in this study.

2.2.4 Muscles and Tendons

Muscles provide motive force for the body and are responsible for both voluntary and involuntary movements.

Tendons are pieces of strong, relatively inflexible (although their elasticity is important in muscle force transfer to the limbs), fibrous tissue very similar to ligaments, but instead of connecting bones to each other, they connect muscles to bones.

Together muscles and tendons form *musculotendon units*, but they are often referred to as muscles. Musculotendon units may cross one joint *(uniarticular muscles)*, two joints *(biarticular muscles)*, or many joints *(polyarticular muscles)*.

It is often the case that a muscle has a broad attachment site with a very short tendon at one end and narrows to a much longer and slimmer tendon at the other. Attachment sites are often referred to as the origin and insertion of the muscle, but these are poorly defined terms. For the purposes here the origin is defined as the proximal end of the musculotendon unit and the insertion, the distal end. It is not uncommon for a muscle to have a single attachment at one end and two or more at the other. The multiple attachments are referred to as *heads* and are often treated as separate muscles.

The following is a list of the muscles having a significant contribution to gait and their actions (not all of the muscles of the legs are included). Muscle action is influenced by joint position, particularly in the case of bi-articular muscles, as such the actions listed below are those that are significant during gait.

Crossing the lumbar joints (Figure 2.8):

- *Erector spinae* - a group of muscles including iliocostalis, longissimus and spinalis. Running from the sacrum and iliac crests to the spinous processes of vertebrae all the way up to the 7th cervical vertebra, they act to extend the trunk and provide lateral flexion and rotation.
- *External oblique* - from ribs 9-12, the external oblique muscle runs inferior and anterior, inserting onto the anterior iliac crest. It provides trunk flexion, lateral flexion and rotation to the opposite side.
- *Internal oblique* - from ribs 8-10, the internal oblique runs inferior and posterior, inserting onto the iliac crest and lumbar fascia. It provides trunk flexion, lateral flexion and rotation to the same side.

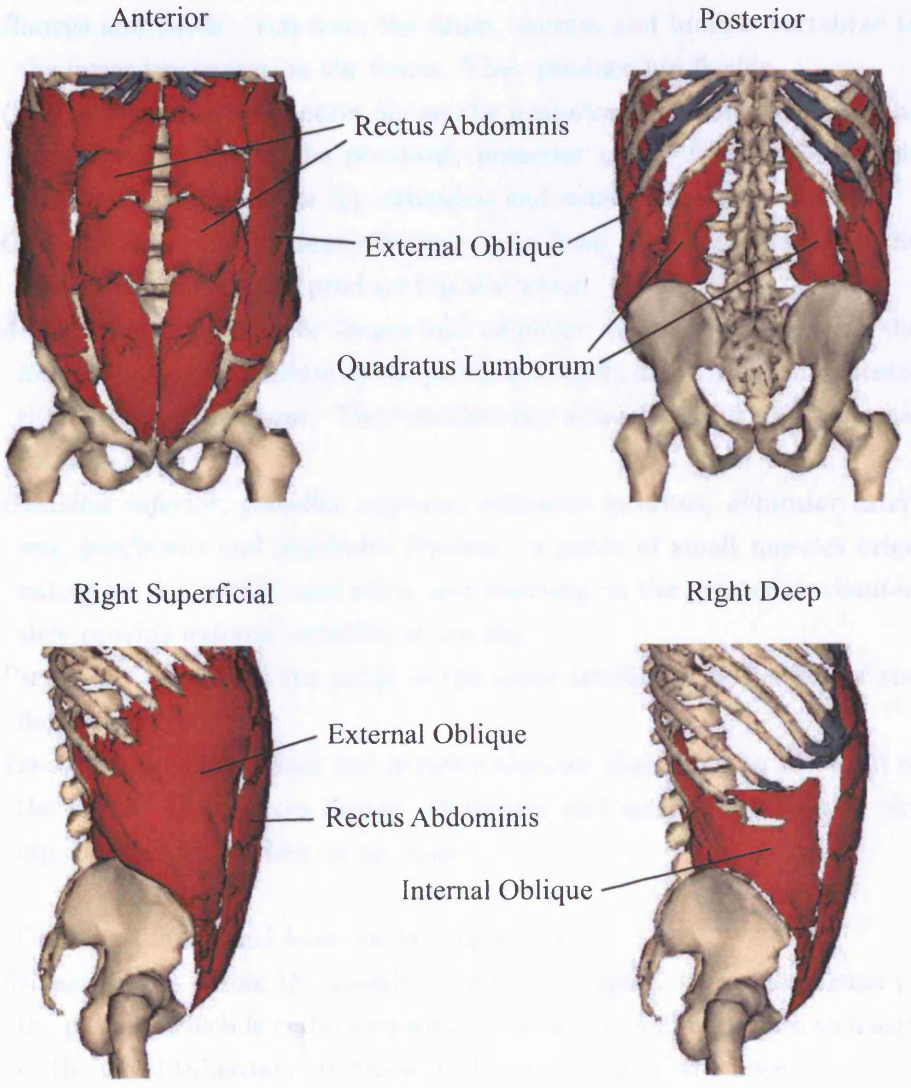

Figure 2.8: Muscles acting on the lumbar spine

- *Rectus abdominis* - run down the front of the torso from the lower ribs to the pubis. The two rectus abdominis muscles and the bands of ligament crossing them form the 'six-pack'. They produce trunk flexion.

Crossing the hip (Figure 2.9 except illiacus and psoas):

- *Illiacus* and *psoas* - run from the ilium, sacrum and lumbar vertebrae to the lesser trochanter on the femur. They produce hip flexion.
- *Gluteus maximus* - originates across the posterior pelvis and insert at the gluteal tuberosity at the proximal, posterior of the femur shaft. This muscle is responsible for hip extension and external rotation.
- *Gluteus medius* and *gluteus minimus* - run from the lateral pelvis to the greater trochanter and produce hip abduction.
- *Adductor brevis, adductor longus* and *adductor magnus* - originate at the inferior pubis and ischium of the pelvis and insert along the medial posterior length of the femur. They produce hip adduction and some internal rotation.
- *Gemellus inferior, gemellus superior, obturator internus, obturator externus, piriformis* and *quadratus femoris* - a series of small muscles originating on the ischium and pubis and inserting on the greater trochanter, they provide external rotation at the hip.
- *Pectineus* - runs from the pubis to the lesser trochanter and adducts and flexes the hip.
- *Tensor fascia latae* - from the anterior superior iliac spine to the head of the fibula. It produces flexion, abduction and internal rotation at the hip, but has little effect on the knee.

Crossing the hip and knee joints (Figure 2.9):

- *Rectus femoris* - from the anterior inferior iliac spine, this muscle runs to the patella, which is embedded within the tendon and continues to insert at the tibial tuberosity. It flexes the hip and extends the knee.
- *Biceps femoris long head, semimembranosus* and *semitendinosus* - run from the ischium of the pelvis to the medial tibia and both of its condyles. Along with biceps femoris short head, these muscles form the hamstring group and are responsible for hip extension and knee flexion.
- *Gracilis* - running from the pubis to the medial tibia, this muscle performs hip adduction and internal rotation and knee flexion.

- *Sartorius* - running from the anterior superior iliac spine to the medial tibia, this muscle performs hip flexion and external rotation and knee flexion.

Crossing the knee (Figure 2.9):

- *Biceps femoris short head* - the fourth hamstring originates at the shaft of the femur and inserts at the lateral condyle of the tibia. It is only involved in knee flexion.
- *Vastus lateralis, vastus intermedius* and *vastus medialis* - the vasti are knee extensors running from the superior anterior femoral shaft to the patella and on to the tibial tuberosity. The vasti and rectus femoris are the quadriceps femoris.
- *Popliteus* - this muscle has little effect on gait but it is important nonetheless. When the knee extends fully it goes through a small external rotation that locks the joint. Popliteus provides an internal rotation to unlock the joint and allow it to flex again.

Crossing the knee and ankle joints (Figure 2.9):

- *Gastrocnemius lateral head* and *gastrocnemius medial head* - the gastrocnemius has a head originating at each of the femoral condyles. Its tendon merges with the soleus' tendon to from the Achilles tendon, which inserts into the posterior of the calcaneus. The gastrocnemius plantarflexes the ankle and flexes the knee.

Crossing the ankle joints (Figure 2.9):

- *Soleus* - this muscle originates at the posterior of the tibia and fibula and inserts at the posterior of the calcaneus with the gastrocnemius which also plantarflexes the ankle. The soleus, plantaris (not included in this list) and gastrocnemius are also known collectively as the triceps surae.
- *Tibialis anterior* - from the upper lateral tibia to the first cuneiform bone in the foot, this muscle is the main dorsiflexor of the ankle. It also inverts the foot and supports the medial arch.
- *Tibialis posterior* - from the upper posterior tibia and the fibula to the inferior navicular, tibialis posterior inverts and plantarflexes the foot.
- *Peroneus brevis* and *peroneus longus* - running from the lateral tibia and fibula to the lateral foot, these muscles evert and weakly plantarflex the foot.

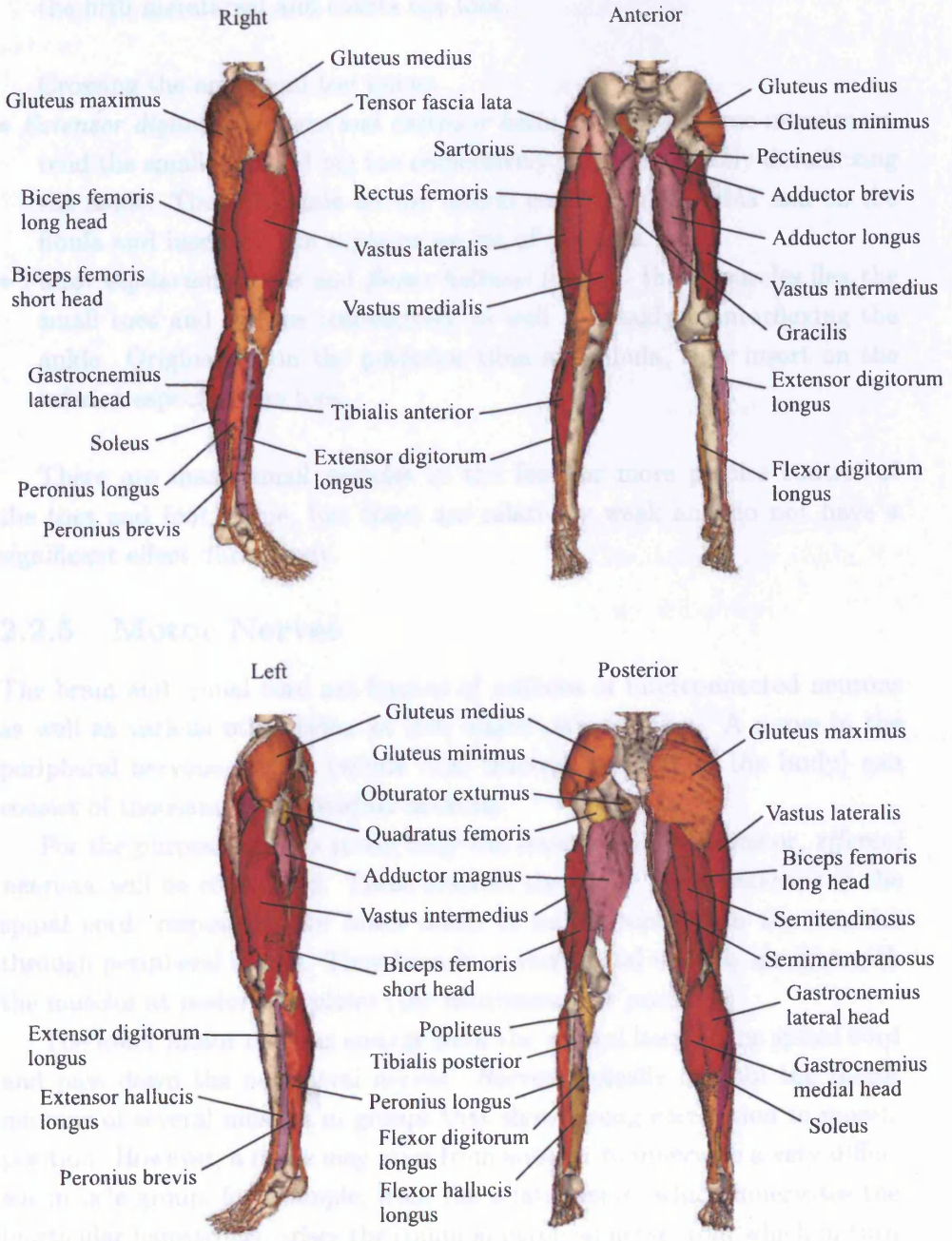

Figure 2.9: Muscles in the legs

- *Peroneus tertius* - this muscle is often distinguished from the other peroneal muscles as its action is different. It runs from the lower anterior fibula to the fifth metatarsal and everts the foot.

Crossing the ankle and toe joints:

- *Extensor digitorum longus* and *extensor hallucis longus* - these muscles extend the small toes and big toe respectively as well as weakly dorsiflexing the ankle. They originate on the lateral condyle of the tibia and on the fibula and insert on the superior aspect of the toes.
- *Flexor digitorum longus* and *flexor hallucis longus* - these muscles flex the small toes and big toe respectively as well as weakly plantarflexing the ankle. Originating on the posterior tibia and fibula, they insert on the inferior aspect of the toes.

There are many small muscles in the feet for more precise control of the toes and foot shape, but these are relatively weak and do not have a significant effect during gait.

2.2.5 Motor Nerves

The brain and spinal cord are formed of millions of interconnected neurons as well as various other types of cell, which service them. A nerve in the peripheral nervous system (which runs through the rest of the body) can consist of thousands of individual neurons.

For the purposes of this study, only the *lower motor neurons* or, *efferent neurons*, will be considered. These connect the *upper motor neurons* in the spinal cord, responsible for lower levels of motor control, to the muscles through peripheral nerves. They branch at their distal ends to *synapse* with the muscles at *motor end plates* (the neuromuscular junction).

The lower motor neurons emerge from the ventral horn of the spinal cord and pass down the peripheral nerves. Nerves typically contain the motor neurons of several muscles in groups that show strong correlation to muscle position. However, a nerve may arise from another to innervate a very different muscle group, for example; from the sciatic nerve, which innervates the biarticular hamstrings, arises the common peroneal nerve from which in turn arises the superficial peroneal nerve, which innervates the peroneus longus and brevis muscles. The following table illustrates the pattern of peripheral nerves relevant to the locomotive process using information from Whittle [112].

Nerve	Vertebral origin	Muscles innervated
Anterior lumbar nerves	Lumbar 2 - 3	Psoas major
Iliohypogastric	Thoracic 12 - lumbar 1	Abdominal wall
Ilioinguinal	Thoracic 12 - lumbar 1	Abdominal wall
Femoral	Lumbar 2 - 3	Iliacus, pectineus, sartorius, rectus femoris, vastus lateralis, vastus intermedius, vastus medialis
Obturator	Lumbar 2 - 4	Obturator externus, pectineus, adductor longus, adductor brevis, adductor magnus, gracilis
Superior gluteal	Lumbar 4 - sacral 1	Gluteus minimus, gluteus medius, tensor fascia lata
Inferior gluteal	Lumbar 5 - sacral 2	Gluteus maximus
Nerve to piriformis	Sacral 1 - 2	Piriformis
Nerve to obturator internus	Lumbar 5 - sacral 2	Obturator internus, superior gemellus
Sciatic	Lumbar 4 - sacral 3	Biceps femoris, semimembranosus, semitendinosus, adductor magnus
Tibial	Lumbar 4 - sacral 3	Gastrocnemius, plantaris, soleus, popliteus, tibialis posterior, flexor digitorum longus, flexor hallucis longus
Superficial peroneal	Lumbar 4 - sacral 2	Peroneus longus, peroneus brevis
Deep peroneal	Lumbar 4 - sacral 2	Tibialis anterior, extensor hallucis longus, extensor digitorum longus, peroneus tertius

Table 2.1: Motor nerve innervation pattern.

2.3 Physiology

While anatomy is concerned with the locations of organs, physiology describes their composition and operation. Knowledge of this is essential for accurate modelling and simulation as well as for understanding the problems that can occur to affect the gait cycle.

2.3.1 Nerves

Nerve cells, or *neurons*, appear to vary greatly in structure, but they all share the same basic components (Figure 2.10) [14]:

- *Cell body (soma)* - this contains the nucleus and other parts of the cell not directly involved in signal transmission. It also synthesises various chemical mediators for transmission between neurons and gives rise to the dendrites and axon. It is the integrative component of the neuron.
- *Dendrites* - these are the receivers of the cell, picking up signals from adjacent neurons. The tree-like branches may receive signals from a large number of other cells around them.
- *Axon* - usually not as branched as dendrites the axon may still form branches to several thousand other cells. They take the form of cables providing fast signal transfer along distances from 0.1 mm to 3 m from the cell body to the presynaptic terminals. To increase transfer speed and reduce signal losses and interference, long axons are wrapped in a fatty *myelin sheath.* The sheath is interrupted at intervals called *nodes of Ranvier*, which regenerate the signals. Transient electrical signals pass along the axon with an amplitude of around 100 mV and duration of about 1 ms at between 1 and 100 ms^{-1} [55].
- *Presynaptic terminals* - these release *neurotransmitter* chemicals into the *synapse*, which is the space between the presynaptic terminals and the dendrites of another neuron. This stimulates the *post-synaptic cell.* These are the output components of the neuron.

In a typical resting neuron, a negative electrical potential of around -65 mV is maintained on the inside of the cell wall (*membrane*) relative to the outside (the *resting membrane potential*) (Figure 2.11) [55]. All cells have a membrane potential, but nerve and muscle cells can alter theirs by changing the permeability of the cell membranes to sodium (Na^+) and potassium (K^+)

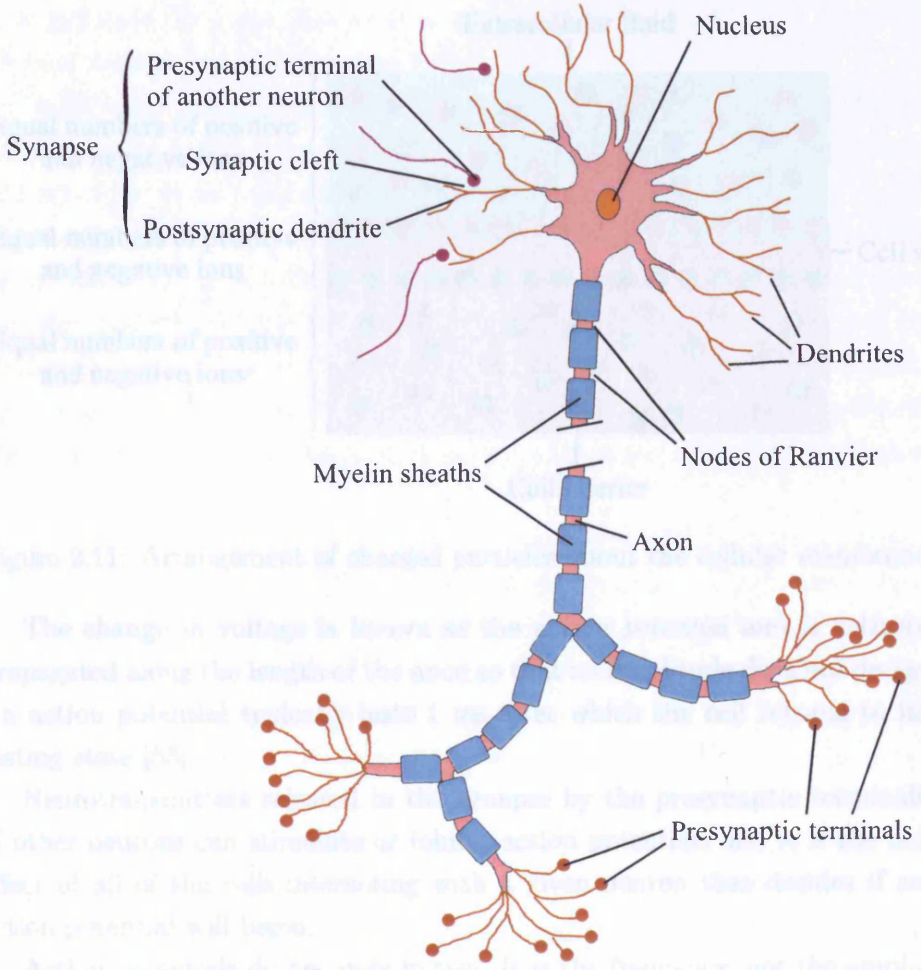

Figure 2.10: Structure of a neuron

ions. Depolarising a neural cell's membrane potential by 10 or 15 mV makes the cell wall permeable to Na^+, the influx of which increases the membrane potential to +40 mV. This increase makes the membrane permeable to K^+ ions which rapidly leave the cell, restoring the resting potential [112]. A membrane protein then pumps the exchanged Na^+ out of the cell and K^+ back into it [55].

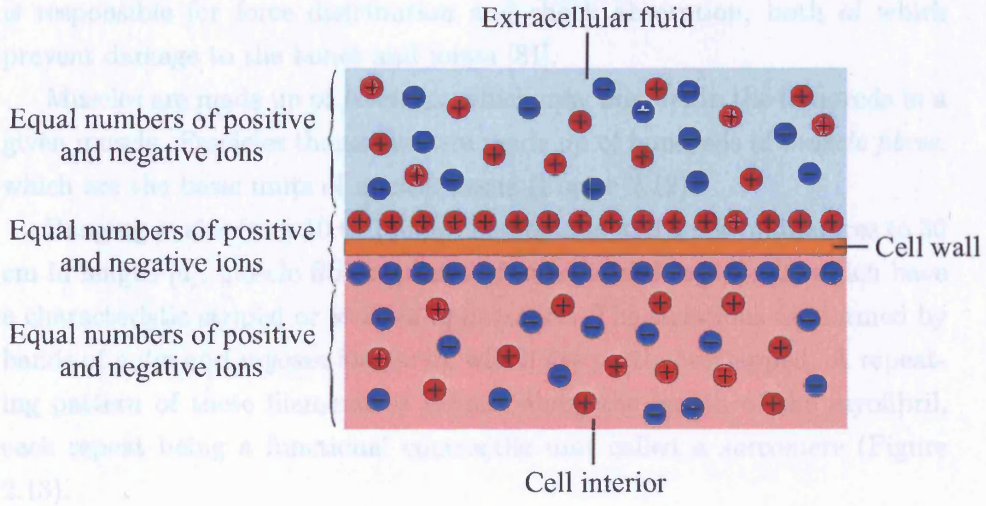

Figure 2.11: Arrangement of charged particles about the cellular membrane

The change in voltage is known as the *action potential* and is actively propagated along the length of the axon so that its amplitude does not decay. An action potential typically lasts 1 ms after which the cell returns to its resting state [55].

Neurotransmitters released in the synapse by the presynaptic terminals of other neurons can stimulate or inhibit action potentials and it is the net effect of all of the cells interacting with a given neuron that decides if an action potential will begin.

Action potentials do not vary in size. It is the frequency, not the amplitude, which transmits the information.

2.3.2 Muscles

There are three types of muscle within the body: *cardiac*, which makes up the heart; *smooth* (*nonstriated*)(*involuntary*), which lines hollow organs and performs plastic contractions and relaxations; and *skeletal muscle* (*striated*)(*voluntary*), which is responsible for body movement. This section is

only concerned with skeletal muscle, as the other types have no direct influence on gait.

The more than 430 skeletal muscles of the human body typically contribute 40-45% of total body weight making it the most abundant tissue in the body [81].

As well as producing movement and maintaining posture, skeletal muscle is responsible for force distribution and shock absorption, both of which prevent damage to the bones and joints [81].

Muscles are made up of *fascicles*, which may number in the hundreds in a given muscle. Fascicles themselves are made up of hundreds of *muscle fibres*, which are the basic units of muscle tissue (Figure 2.12).

Ranging in size from 10 to 100 μm in diameter and a few millimetres to 30 cm in length [4], muscle fibres consist of hundreds of *myofibrils*, which have a characteristic striped or *striated* appearance. The striations are formed by bands of *actin* and *myosin* filaments, which are partly overlapped. A repeating pattern of these filaments is formed along the length of the myofibril, each repeat being a functional contractile unit called a *sarcomere* (Figure 2.13).

The striation pattern seen in figure 2.12 and figure 2.13 can be explained as follows: the A band covers the length of the myosin filaments; the I band covers the region not intruded on by myosin filaments across two sarcomeres; the paler H zone is the region where the myosin is not overlapped by the actin; the Z lines are the origins of the actin filaments and form dividers between the sarcomeres. Filaments of elastic *titin* hold the myosin filaments in place.

Changing the overlap between the actin and myosin bands produces change in muscle length. Muscle fibre can contract to about 57% of its resting length [4]. Contractions are produced by the *cross-bridges*, or *myosin heads*, which emerge from the myosin filaments and attach to the actin. These cross-bridges go through a cycle of pulling, releasing from the actin and reattaching to it further on. Cross-bridges go through several cycles to produce significant contractions in a manner similar both to rowing and pulling hand over hand on a rope, although without any coordination between individual cross-bridges [81].

An action potential through a motor neuron causes *acetylcholine* to be released at the motor end plate. This causes a wave of depolarisation to pass

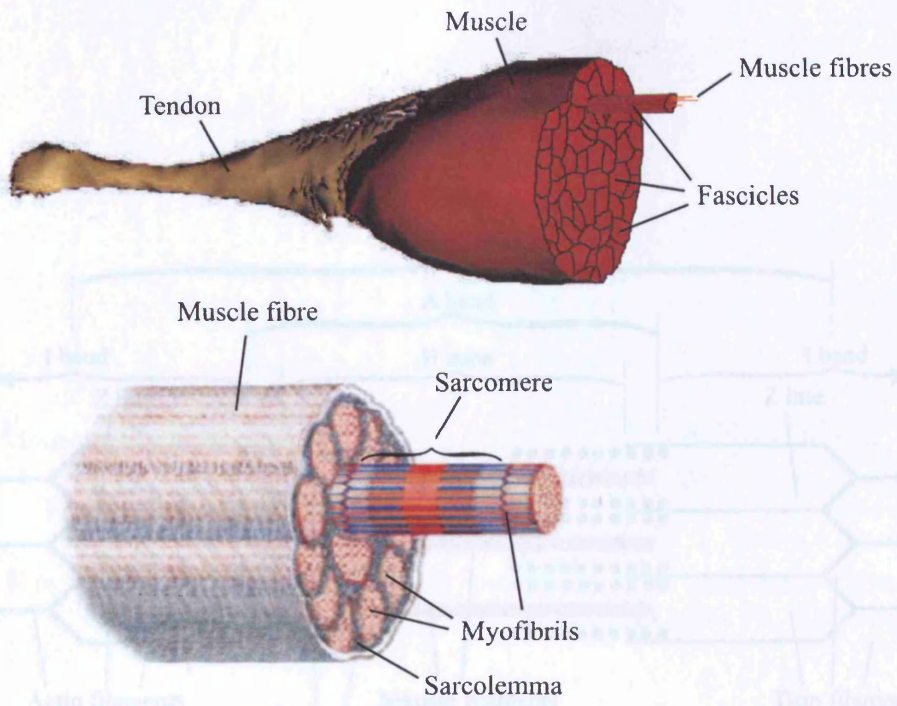

Figure 2.12: Cross-sections through muscle and muscle fibre

along the muscle fibre membrane (*sarcolemma*), which in turn causes a release of calcium ions (Ca^{2+}) from the *sarcoplasmic reticulum*, a network of sacks and tubules surrounding the myofibrils. The Ca^{2+} ions allow the actin (A) in a myofibril to bind to the myosin (M) adenosine triphosphate (ATP) forming cross-bridges. A reaction to split the ATP takes place, releasing energy in the form of movement, pulling the actin and myosin filaments towards each other [81, 112]:

$$A + M \cdot ATP \rightarrow A \cdot M \cdot ATP \rightarrow A \cdot M + ADP + P_1$$

New ATP then bonds to the myosin releasing the actin and breaking the cross-bridge:

$$A \cdot M + ATP \rightarrow A + M \cdot ATP$$

This process continues in a cycle as long as calcium ions are present in concentration. A calcium pump removes the ions back into the sarcoplasmic reticulum, so to maintain the Ca^{2+} levels, constant neuromuscular stimulation is necessary [81, 112].

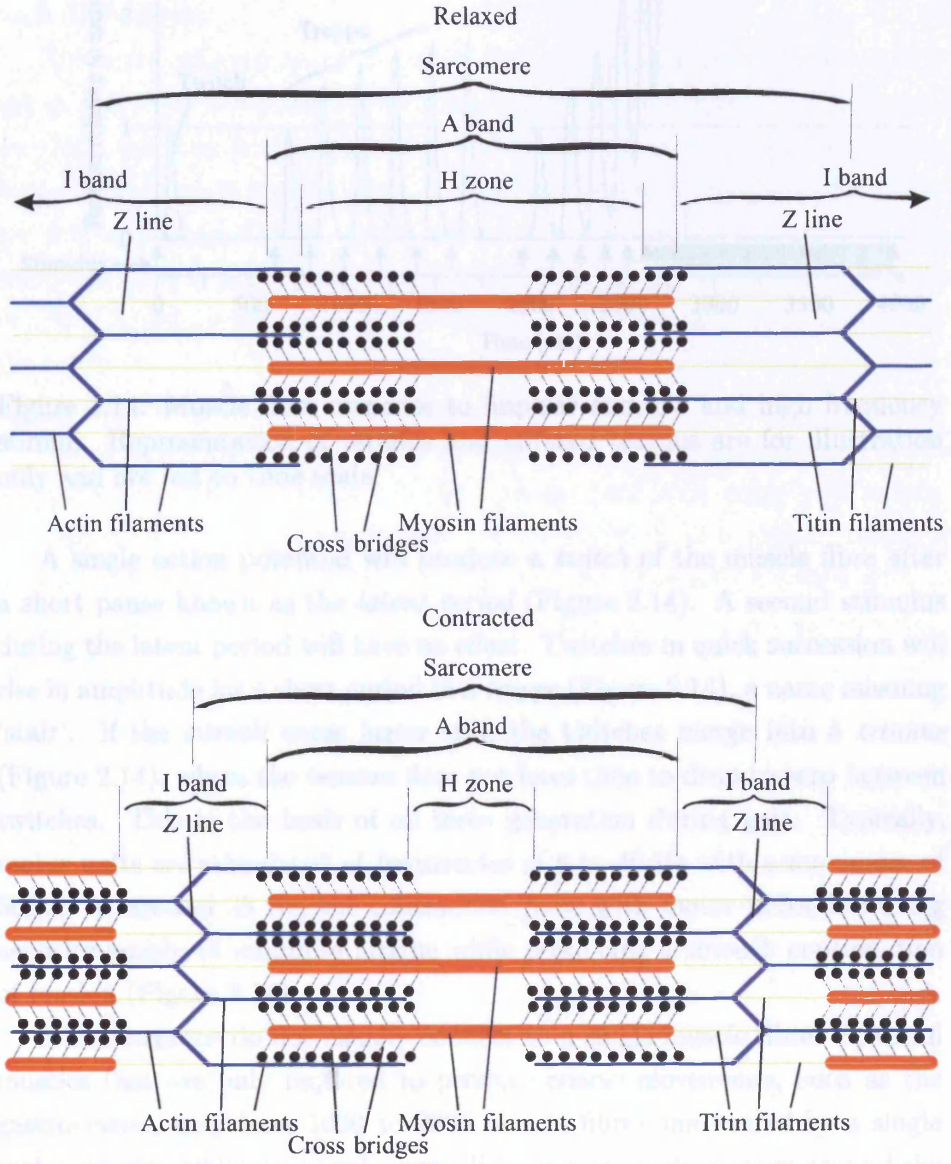

Figure 2.13: Sarcomere components when relaxed and contracted

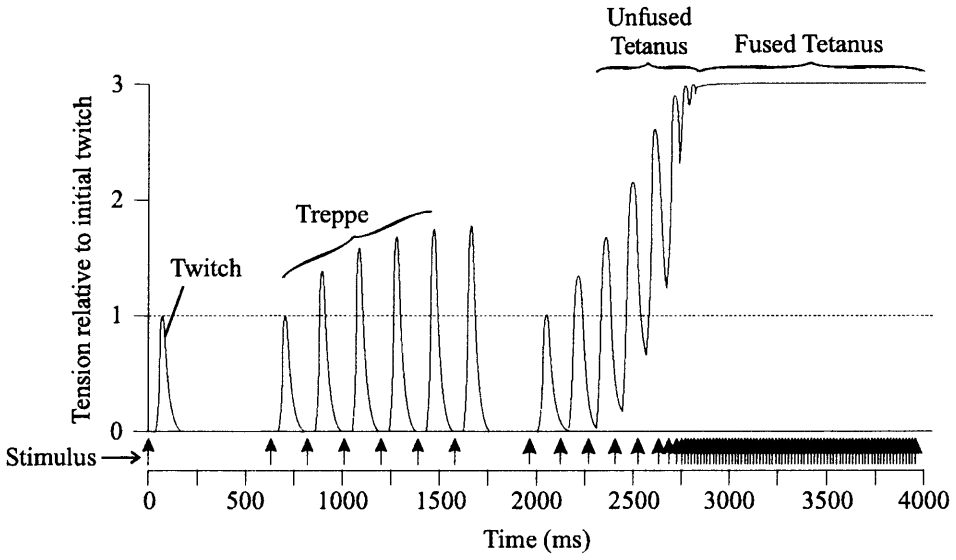

Figure 2.14: Muscle fibre response to impulse and low and high frequency stimuli. Representation of tetanus and unfused tetanus are for illustration only and are not to time scale.

A single action potential will produce a *twitch* of the muscle fibre after a short pause known as the *latent period* (Figure 2.14). A second stimulus during the latent period will have no effect. Twitches in quick succession will rise in amplitude for a short period in a *treppe* (Figure 2.14), a name meaning 'stair'. If the stimuli come faster still, the twitches merge into a *tetanus* (Figure 2.14), where the tension does not have time to drop to zero between twitches. This is the basis of all force generation during gait. Typically, motor units are stimulated at frequencies of 8 to 40 Hz with a maximum of 50Hz. At around 25 Hz, the contraction *fuses* with motor units activating asynchronously to minimise fatigue while producing a smooth continuation of tension (Figure 2.14).

Motor neurons do not usually connect to a single muscle fibre. Powerful muscles that are only required to produce coarse movements, such as the gastrocnemii, may have 1000 to 2000 muscle fibres *innervated* by a single motor neuron, while very finely controlled muscles, such as those around the eyes, may connect only 10 or less muscle fibres to each neuron [81].

A motor neuron and the muscle fibres it innervates are known as a *motor unit*, and a stimulus from the neuron or *motor unit action potential (MUAP)* activates all of the muscle fibres within the motor unit simultaneously. Muscle fibres in a motor unit are distributed throughout the muscle to contract

large portions of the muscle. Greater force can be produced by increasing the stimulation frequency (up to maximal tetanus) or by stimulating more motor units (*recruitment*). During a muscle contraction, the motor units activated change over time to distribute the work between them. This allows each time to rest.

There are different types of muscle fibre (although those in a motor unit are all the same type) the main ones being type I and type II [112]. Type I are dark coloured, slow acting fibres. They are resistant to fatigue and can be active for long periods without tiring. For this reason they are invaluable for postural muscles such as the soleus, which maintains the angle of the talocrural joint of the ankle during still standing. The soleus is mainly formed of type I fibres, whereas the gastrocnemius, which lies directly posterior to the soleus is about 75% made up of faster, paler type II fibres making it more useful for powerful bursts of activity such as running and jumping.

Fibres in a muscle often lie at an angle to the line of the muscle. This is called the *pennation angle*. While a larger pennation angle will reduce the length of the fibres, the muscle can be made up of a greater number of shorter fibres. Pennated fibre muscles are therefore slower acting with a smaller range of movement but can generate larger forces then non-pennated muscles.

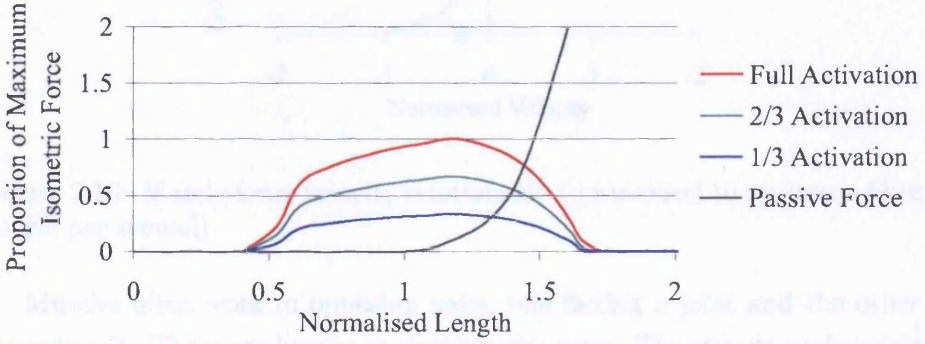

Figure 2.15: Muscle active and passive force-length relationships (length normalised to optimum fibre length)

The contractile element of muscle generates force as a function of stimulation and fibre length. A stretched fibre has very little overlap between the actin and myosin filaments. This means that few cross-bridges (and therefore

little tension) can be generated. A contracted fibre has little room to contract further and can therefore generate little extra tension. This produces an approximate bell curve relating length and force (see figure 2.15).

The contractile element of a muscle is it's sarcomeres, while the the sarcolemma and the connective tissue about the muscle fibres provide an elastic element preventing overstretch and returning the muscle to its resting length after contraction. It generates passive force as a function of fibre length (Figure 2.15) and is independent of muscle stimulation.

The sarcomeres are also subject to a force-velocity relationship (Figure 2.16). If the external force is greater than the internal muscle contraction force then stretching of muscle fibres occurs (*eccentric contraction*) as in figure 2.16. If the external force is smaller the muscle shortens (*concentric contraction*). If the forces balance, the muscle does not change length (*isometric contraction*).

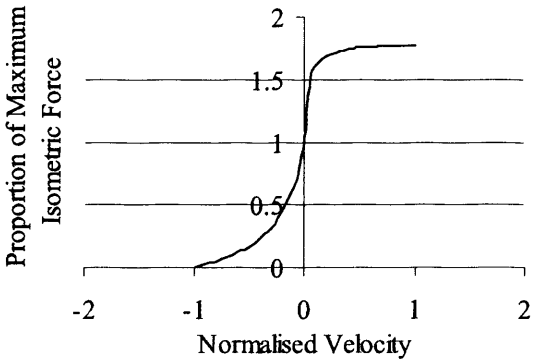

Figure 2.16: Muscle force-velocity relationship (normalised to optimum fibre length per second)

Muscles often work in opposing pairs, one flexing a joint and the other extending it. These are known as *antagonistic pairs*. The muscle performing a given action is the *agonist*, and the muscle opposing it is the *antagonist*. The antagonist is usually *reciprocally inhibited* from activity during agonist contraction [112].

2.3.3 Bones, Joints and Ligaments

For the purposes of this study bones, joints and ligaments are assumed to be much simpler structures than is actually the case. A detailed examination of

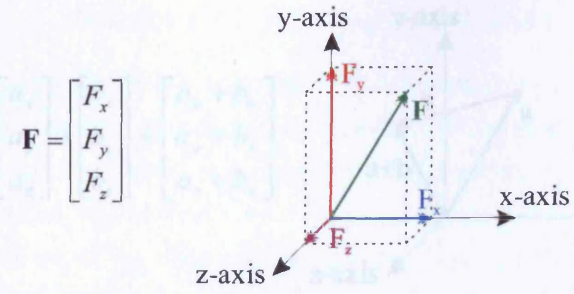

Figure 2.17: A force vector in a 3-dimensional space

their actual physiology and mechanical properties would only be misleading in this context.

It is assumed that the bones are rigid structures with no capacity for deformation or fracture; joints are assumed to rotate with fixed internal friction; and ligaments are simple springs.

2.4 Biomechanics

Biomechanics as a discipline involves the application of mechanical engineering and mathematical principles to describe a biological system. Human locomotive gait is a mechanical operation performed by a biological system, making biomechanical analysis appropriate.

2.4.1 Terminology

There are a number of terms essential to understanding this section:

- *Scalar* - a quantity having a magnitude (size) but not a direction, e.g. mass has magnitude but no direction.
- *Vector* - a quantity having both magnitude and direction, e.g. forces can act in any direction. Vectors are represented by bold typeface on a symbol, e.g. **F** represents a force vector (Figure 2.17). Column vectors are used with the components of the x-, y- and z-axes respectively in the rows (z-axis is only required for 3-dimensional vectors).
- *Vector sum* - Summing vectors is a matter of summing the values in each row (Figure 2.18).

$$\mathbf{a}+\mathbf{b}=\begin{bmatrix}a_x\\a_y\\a_z\end{bmatrix}+\begin{bmatrix}b_x\\b_y\\b_z\end{bmatrix}=\begin{bmatrix}a_x+b_x\\a_y+b_y\\a_z+b_z\end{bmatrix}$$

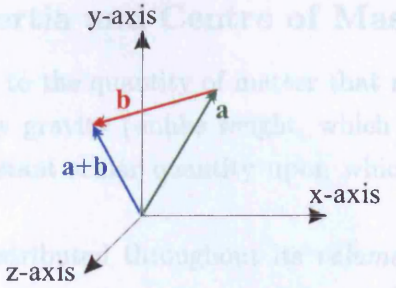

Figure 2.18: Summation of vectors

$$\mathbf{a}\times\mathbf{b}=\begin{bmatrix}a_x\\a_y\\a_z\end{bmatrix}\times\begin{bmatrix}b_x\\b_y\\b_z\end{bmatrix}=\begin{bmatrix}a_yb_z+a_zb_y\\a_zb_x+a_xb_z\\a_xb_y+a_yb_x\end{bmatrix}$$

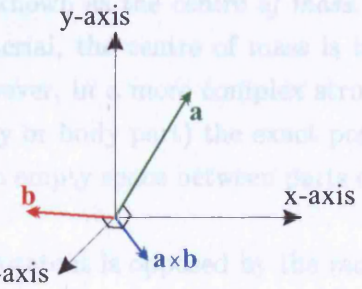

Figure 2.19: Vector multiplication

- *Scalar product (dot product)* - a scalar product of two vectors is found by multiplying the values in each row and summing the resulting products:

$$\mathbf{a}\cdot\mathbf{b}=\begin{bmatrix}a_x\\a_y\\a_z\end{bmatrix}\cdot\begin{bmatrix}b_x\\b_y\\b_z\end{bmatrix}=a_xb_x+a_yb_y+a_zb_z$$

- *Vector product (cross product)* - a vector product of two vectors is found as in figure 2.19.

  It should be noted that:

$$\mathbf{a}\times\mathbf{b}=-\mathbf{b}\times\mathbf{a}$$

and

$$\mathbf{a}\times(\mathbf{b}\times\mathbf{c})\neq(\mathbf{a}\times\mathbf{b})\times\mathbf{c}$$

- *Constant* - a quantity that does not change during the period in which it is considered.
- *Variable* - a quantity that can change during the period of use.

2.4.2 Mass, Moment of Inertia and Centre of Mass

Every object has *mass*, which equates to the quantity of matter that makes it up. Mass is therefore unaffected by gravity (unlike weight, which is often confused with it). Mass is a constant scalar quantity upon which the equations of motion of the body act.

While the mass of an object is distributed throughout its *volume* (the space it occupies), it can be assumed to act through a single point during translational (non-rotational) motion. This point is the mean position of all of the mass within the object and is known as the *centre of mass*. In a cube or sphere of a uniform density material, the centre of mass is in the exact geometric centre of the object, however, in a more complex structure of variable density (such as a human body or body part) the exact position must be measured and could even lie in an empty space between parts of the object.

When a moment causes an object to rotate it is opposed by the *moment of inertia* in the same way that the mass of an object resists acceleration by a force (section 2.4.3). If the mass were only considered as a point source (having no volume) at the centre of mass, any moment would instantly accelerate the object to infinite rotational velocity.

A moment acts to accelerate all of the particles making up an object relative to their distance from the centre of rotation. When rotating about the centre of mass the total linear acceleration adds up to zero, as particles on different sides of the object are accelerating in opposite directions. The moment of inertia is defined as the sum of the masses of all of the particles within an object individually multiplied by the square of its scalar distance from the axis of rotation.

$$I = \sum m_i r_i^2$$

Figure 2.20 shows the difference in moment of inertia moment arm for a ring and a disc of equal depth, mass and uniform density. More force is required to accelerate the rotation of the ring as the mass is distributed further from the centre of mass.

Moments of inertia can differ about differing axes, so for 3-dimensional calculations a matrix is usually used. This takes the form of a diagonal matrix of moments of inertia for rotations about the x-, y- and z-axes of the object unless rotating about another set of axes.

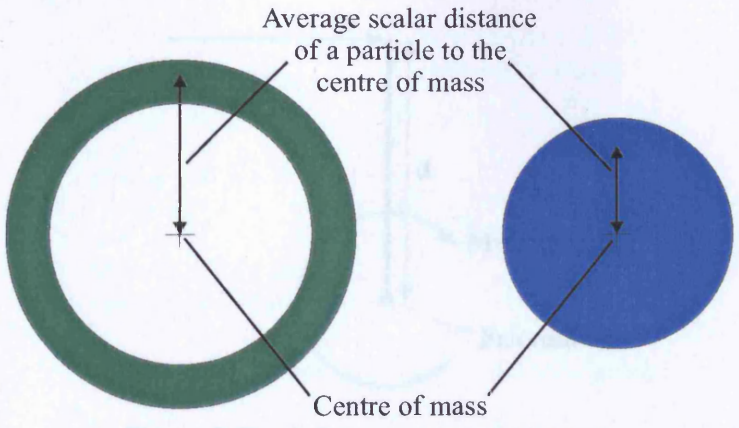

Figure 2.20: The distribution of equal mass in a ring and a disc

Using the moment of inertia, equations of rotation about the centre of mass can be produced. To rotate about any other point inside or outside of the body involves combining a translation as well as a rotation about the centre of mass.

2.4.3 Force and Moment

A force is a mechanical disturbance acting on an object. All forces and objects are subject to Newton's three laws of motion:

- A body remains at rest or moves at constant velocity in a straight line unless an external force acts upon it.
- A body will accelerate in the direction of a force acting upon it. To produce a given acceleration (a), the force (F) must equal the mass (m) of the body multiplied by that acceleration:

$$F = ma$$

- For every action there is an equal and opposite reaction.

Forces are measured in *Newtons* (N), which are defined as the force required to accelerate a 1 kg mass at 1 ms^{-2}.

Forces are vector quantities, which can act in any direction. Combinations of forces can oppose each other or combine by simple mathematical summation and are balanced by accelerations according to Newton's second law.

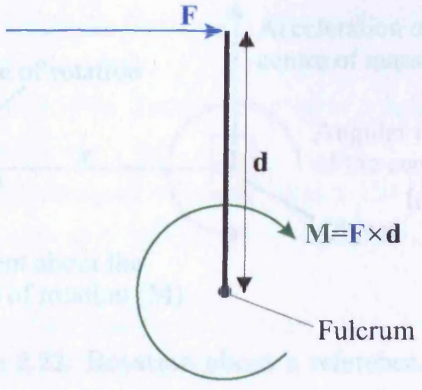

Figure 2.21: A force generated moment

Moments, also known as torques, are forces acting to produce rotation. They act about pivot points or fulcrums and are defined as the product of the force and the distance to the fulcrum (vector product when in three dimensions):

$$M = F \times d$$

For a 2-dimensional system, only the z-axis rotation is applicable. The distance (d) from the point of application of the force to the fulcrum is known as the moment arm or lever arm (figure 2.21).

Moments about the same fulcrum can combine or oppose each other in the same way as forces, and any remaining force is balanced by rotational acceleration with reference to the moment of inertia.

It is often convenient to measure all of the forces acting on a particular object relative to a particular point. This may be the centre of mass or a joint centre or any other point inside or outside the object (see figure 2.22). The forces (F) are summed to find the acceleration of the centre of mass (a) relative to the reference point. The sum of the vector product of each force and its distance to the reference point equates to the moment acting about the reference point. This is balanced by the angular acceleration ($\dot{\omega}$) multiplied by the moment of inertia (I) plus the mass (m) multiplied by the acceleration vector of the centre of mass (a) multiplied by the distance from the centre of mass to the reference point (r).

$$\sum F = ma$$

$$M = \sum (F \times d) = I\dot{\omega} + ma \times r$$

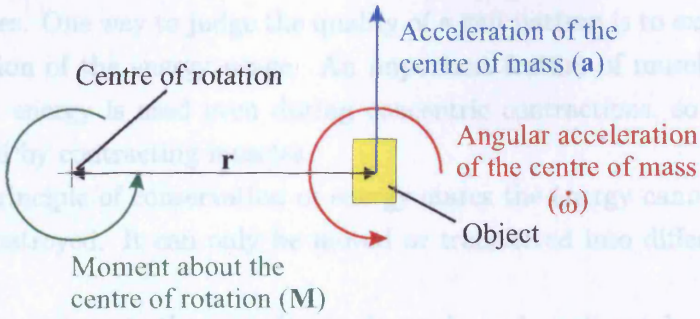

Figure 2.22: Rotation about a reference point

2.4.4 Kinetics and Kinematics

Kinetics and *kinematics* are two terms used frequently within the field of gait analysis. Kinetics refers to the forces, moments, masses and moments of inertia of the objects involved, while kinematics is the study of the positions and orientations of those objects.

Force plates are generally used to provide kinetic data for gait analysis. They take readings of the forces and moments applied by the foot to the ground, which from Newton's third law is opposed by the reaction of the ground to the foot (the *ground reaction*) (see Chapters 3 and 4).

Kinematic analysis often involves the use of cameras to record the positions of anatomical features on the limbs (see Chapters 3 and 4).

Combining kinetic and kinematic data allows calculation of internal joint forces and moments as well as work, energy and power. This makes a quantitative analysis of gait activity possible.

2.4.5 Energy, Work and Power

There are two types of energy of particular significance here, kinetic and potential. *Potential energy* is the energy an object has by virtue of its position and the forces acting on it. It is stored energy. *Kinetic energy (KE)* is the energy an object has by virtue of its velocity (v) and takes the form:

$$KE = \frac{1}{2}mv^2$$

The square is a scalar product.

Transfers between kinetic and potential energy occur in cycles during gait in a process that attempts to minimise the metabolic energy required from

the muscles. One way to judge the quality of a gait pattern is to examine the optimisation of the energy usage. An important feature of muscles is that metabolic energy is used even during concentric contractions, so energy is not gained by contracting muscles.

The principle of conservation of energy states the energy cannot be created or destroyed. It can only be moved or transferred into different types of energy.

Energy represents the capacity to do work, and work can be measured as the change in kinetic energy of an object. More often, it is defined as the force acting scalar-multiplied by the distance moved. Work provides a measure of the activity of a system over the time of observation, which can be a useful measure of optimisation.

Mechanical joint power is an increasingly common method of analysis during study of gait. Power (P) is the rate of doing work and as such can be used to observe when and where activity occurs. This aids identification of gait anomalies and their causes. The calculation is a scalar product of the moment (M) and the angular velocity (ω):

$$P = M \cdot \omega$$

2.5 Summary

This chapter serves as an introduction to the disciplines of anatomy, physiology and biomechanics, which is sufficient to provide a basis and reference for understanding the chapters that follow.

Anatomical terms are described in this chapter, which will be used as a consistent frame of reference throughout this text. As the meanings of these terms can and do vary from text to text, it is advisable to take note of the definitions used before reading any document further.

The physiological basis of human gait was described in terms relevant to the description of both gait analysis (Chapter 3) and modelling (Chapter 6).

The biomechanics section explains the principles necessary for simulation of the human locomotor apparatus as a mechanical entity. The same principles were used during the development of the model.

Chapter 3

Gait Analysis

3.1 Introduction

Gait analysis is a scientific discipline involving the study and evaluation of locomotive patterns in humans and animals. It is commonly used in the diagnosis of disorders of the locomotor apparatus and to assess and guide the performance of treatment of those disorders.

Measures of performance of gait will typically include an analysis of the motions of the limbs (kinematics - section 3.3.2), forces and moments acting at joints and between the feet and the ground (kinetics - section 3.3.3) and muscle activity (EMG - section 3.3.4).

This chapter aims to introduce gait analysis. It will explain the different phases of gait and the mechanical activity of the limbs and muscles during these stages. Typical gait analysis techniques and apparatus will then be described in detail with particular attention to those used in the collection of data for this project.

Computer simulation as a method of gait analysis will also be introduced as a precursor to later chapters.

3.2 Principles and Parameters

Walking can be considered as a repeating sequence of events known as the gait cycle. This cycle is defined as the period between two successive occurrences of the same event [112], although it is usually the case that the instant one of the feet contacts the ground *(initial contact)* is chosen.

There are 4 basic criteria for a successful gait pattern:

- Production of leg swing - the ability to move each leg to an advanced position.
- Stance capability - the strength in each leg to support the body while the other leg swings.
- Maintenance of balance - static or dynamic balance is required at all times.
- Generation of momentum - the body must be able to begin, maintain and end a forward motion.

A subject with a pathology that prevents any one of these will be unable to walk, however, a pathology that only restricts the performance of any or all of the criteria would still permit a limited form of gait. It is convenient to subdivide the gait cycle for more detailed analysis. The most basic division is into swing and stance phases of a given leg.

The stance phase covers the period in which the relevant foot is on the ground and typically occupies 60% of the gait cycle of that leg. It begins with the instant the heel contacts the floor and ends when the toe lifts off. During this phase the leg supports and propels forward the mass of the body.

The remainder of the cycle is taken up by the swing phase where the foot is moved forward and positioned to take the weight of the body once more. During a walking gait the swing phase is entirely contained within the stance phase of the opposite leg.

For a more detailed subdivision of the gait cycle, more events must be defined:

- Initial contact (heel strike)
- Opposite toe-off
- Heel rise
- Opposite initial contact (opposite heel strike)
- Toe-off
- Feet adjacent
- Tibia vertical (there are two tibia vertical events. The relevant one occurs between feet adjacent and the next initial contact)

As with the stance and swing phases, these events relate to the cycle followed by one leg. An identical set of events divides the cycle of the opposite leg.

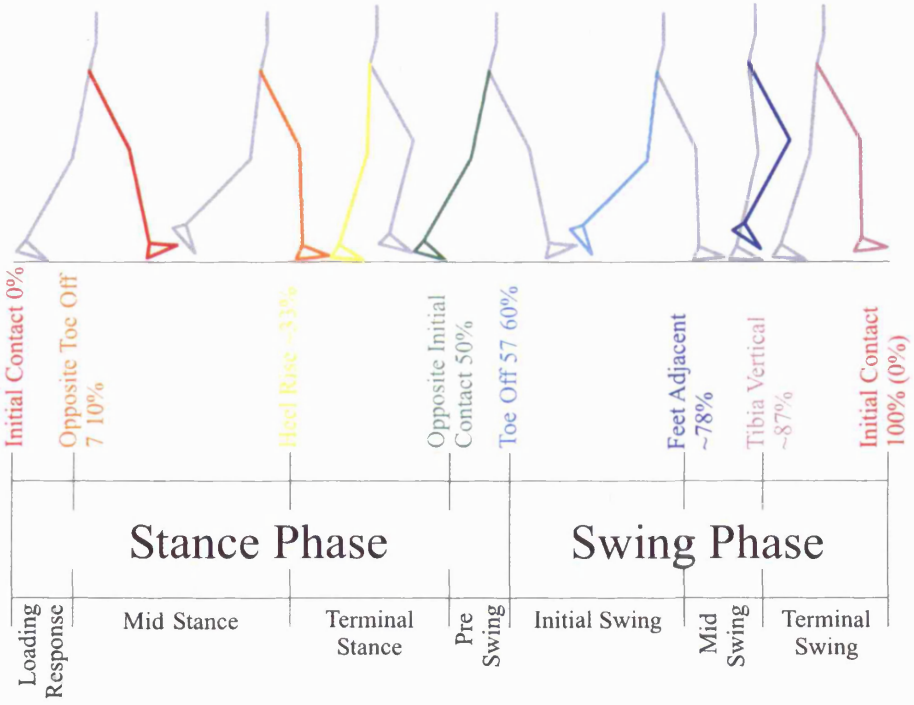

Figure 3.1: Phases and events of the gait cycle.

Using these events the stance and swing phases can be divided into the sub-phases below (and in figure 3.1).

Stance phase:

- Loading response
- Mid-stance
- Terminal stance
- Pre-swing

Swing phase:

- Initial swing
- Mid-swing
- Terminal swing

Examination of velocities and distances is an important part of gait analysis. A number of terms must be defined to facilitate this:

- Step - a step is defined as the movement from the initial contact of one foot to the initial contact of the other. Consecutive steps may not necessarily be symmetrical.

- Step length - (Figure 3.2) the distance along the direction of motion between initial contact points during a step.
- Stride - a stride is the movement from the initial contact of one foot to the next initial contact of the same foot.
- Stride length -(Figure 3.2) the distance between consecutive initial contact points of one foot.
- Walking base - (Figure 3.2) the lateral distance between the midpoints of the backs of the heels.
- Toe out - (Figure 3.2) the angle of the foot to the direction of motion
- Cadence - the number of steps taken in a given time period (usually a minute). This is a very common measurement, but care should be taken as it does not use SI units.
- Cycle time - the time taken to complete a full gait cycle. Cycle time is equivalent to dividing 120 by the cadence.
- The speed of the subject can then be defined as stride length divided by the cycle time.

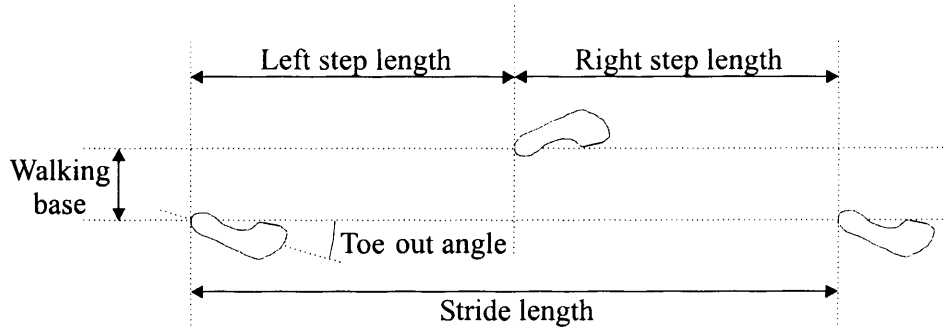

Figure 3.2: Definitions of foot placement terms.

3.3 Methods of Gait Analysis

Systematic study of human gait dates from the Renaissance with the works of Leonardo da Vinci, Galileo and Newton. Gait analysis methods have since evolved from the basic qualitative observational techniques into a multidisciplinary science, quantitatively measuring motion, force and muscle activity. This section explains the systems and techniques typically used in gait analysis.

3.3.1 Observation

Before the advent of the camera, gait analysis relied entirely on the experience and skill of the observer. With no method of making permanent recordings, all analysis had to occur as the movements took place and high-speed events could easily be missed or misinterpreted. There was also no way to examine muscle activity or force and moments acting at the joints. Nonetheless, visual examination by a skilled observer was and still is a very powerful tool for gait analysis.

The human brain is still the most complex computer system available and it is one that has evolved to recognise human gait patterns very effectively. A person can distinguish and identify others using no more information than the way that they walk. This gives a head start when observing gait.

Gait analysis purely by observation is inevitably a subjective process. Misinterpretation and misdiagnosis is not uncommon so quantitative methods of analysis, introduced to support pure observation, have risen to dominate the field.

3.3.2 Kinematics

Kinematics is the study of motion without consideration of mass and force. In the context used here it is a quantitative form of observational gait analysis. Generally, kinematic analysis involves examination of gait velocity, stride length and joint angles over time as one or more gait cycles are completed.

Early kinematic studies involved taking multiple photographic images on a single plate of subjects walking, using a technique known as stroboscopic flash exposure [72]. In the 1870s Marey took multiple exposures of a subject wearing black with brightly lit stripes on their limbs [112]. Later studies, at the end of the 19^{th} century, generated 3-dimensional trajectories, velocities and accelerations. Combining this data with the known masses of the body segments allowed estimates to be made of the forces acting throughout the gait cycle.

Modern video capture systems have come a long way from the early days of kinematics. Commonly used systems use several cameras that reflect ultraviolet light (Figure 3.4) from markers (Figure 3.3) attached to anatomical landmarks on the subject's body. Within seconds, 3-dimensional motion

Figure 3.3: Marker for motion capture.

tracking analyses can be generated with joint angle calculations and measurements of speed, stride length, cycle time and any other desirable readings.

Systems are also available which can analyse ordinary video footage to identify and measure gait motion. These have the advantage of practicality outside the gait laboratory but can be much less accurate.

Camera systems are limited to line of sight readings, which may be obscured by body parts or other objects. With reflective marker based systems, accurate placement is essential or joint centres will be miscalculated and the resulting calculations of angles, forces and moments will be inaccurate not just at the joint in question, but at those around it as well.

Nevertheless video motion capture is the method of choice in kinematic data capture. It is fast, accurate and reliable in the hands of experienced operators and is a non-intrusive method of data collection, which does not interfere with the subject's natural gait pattern.

Another valuable kinematic tool is the goniometer. This device measures angular displacement at joints. For static joint angle readings goniometers can be very effective despite the high probability of error in manually aligning the device over the joint axis, which may change position with angle [109]. However, the usefulness of goniometers is limited by their impracticality for dynamic readings.

The electrogoniometer solves this problem by providing a constant reading for sampling. Common types of electrogoniometer include potentiometer devices, which use rotary variable resistors, and flexible strain gauges, where the variation in the electrical properties of a strip of metal is measured as it bends. Proper calibration of these devices is required, but once this is complete the readings will provide accurate angle measurements even if the

centre of rotation of the goniometer does not coincide with the centre of rotation of the joint [109]. Using three electrogoniometers simultaneously on a joint can generate three-dimensional joint angle readings.

With the increasing use of motion capture video systems the use of goniometers is declining [112], however, they still have applications in cases where cost is a greater factor than versatility. Likewise, electrogoniometers are portable and inconspicuous making them appropriate for neuromuscular control applications in the environment outside the lab.

3.3.3 Kinetics

Kinetics is the study of the forces and moments acting on an object as both cause and effect of its motion. Direct measurement of the forces acting in the joints would involve the surgical implantation of force transducers. This is obviously infeasible, so an indirect method is required.

Measuring the force of the foot on the ground is possible using a force plate, which measures the forces and moments the ground applies in reaction to the pressure of the foot. By Newton's third law, this *ground reaction* is the equal and opposite of the force and moment applied by the foot.

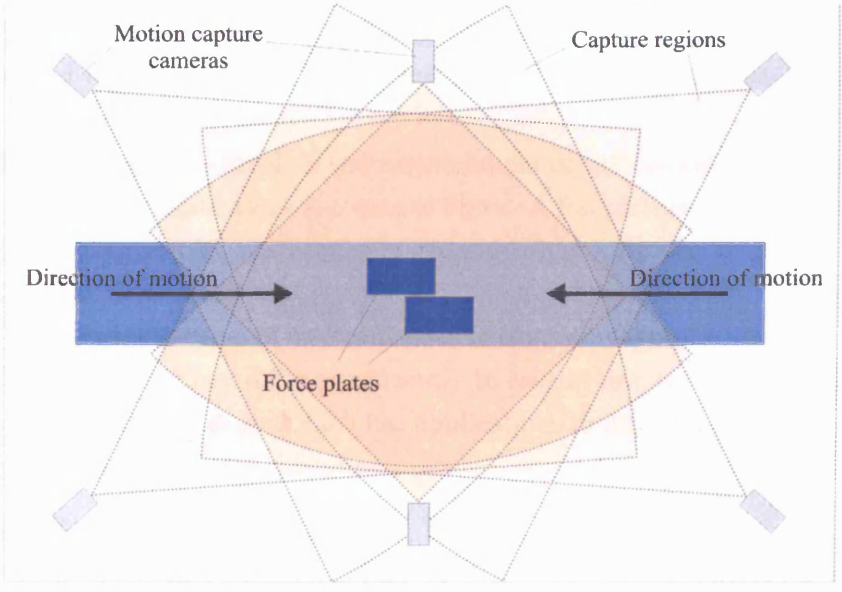

Figure 3.4: Typical camera and force plate set up for kinematic and kinetic data capture.

Combining the ground reaction with kinematic data and physical parameters of the body segments, such as mass and moment of inertia, allows the calculation of internal joint forces and moments.

Force plates typically use strain gauges or piezoelectric transducers to measure the ground reaction in six degrees-of-freedom (forces in the x-, y- and z-axes and moments about the x-, y- and z-axes). The plates are buried in the floor or have platforms built around them so that their upper face is at the same level as the walking surface. Ideally the plate should be indistinguishable from the rest of the floor so that the subject will not alter their gait pattern by aiming towards it.

Two force plates are required to collect kinetic data for both legs (Figure 3.4), and for longer gait sequences a series of force plates would be beneficial.

For a correct reading the footprint of one foot should be entirely within the area of the plate surface, and the footprints of the other foot entirely out of it. If more than one foot is on the plate at the same time the reading will be the sum of the ground reactions of both. It may take several passes before the subject steps on the plate(s) correctly.

3.3.4 Electromyography

In order to fully understand gait it is necessary to know when each muscle is active and by what degree. This is where electromyography (EMG) comes in.

Electromyography involves the measurement of the muscle action potentials as they propagate along the muscle fibres. A full picture of the muscular role in gait is given by synchronising these readings with the kinematic and kinetic measurements.

There are three types of electrode used in electromyography; surface, needle and fine wire. They differ significantly in ease of use, comfort and precision of EMG pickup, as such each has applications in different circumstances [4].

Surface Electrodes

Surface electrodes (Figure 3.5) consist of silver-silver chloride disks that detect the current on the skin through skin-electrode contact. They are widely available, require minimal training for use and give little discomfort to the subject [4].

These electrodes read the MUAPs from multiple motor units, performing spacial averaging within the detection region. This makes surface electrodes the common choice in volume measurement of EMG signals [4].

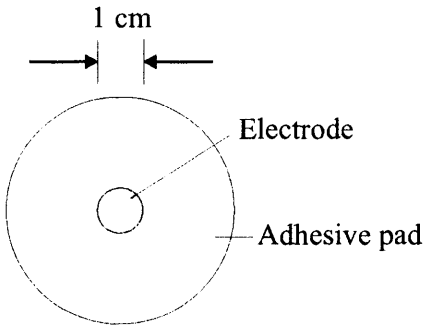

Figure 3.5: Surface electrode for gross surface electromyography.

Surface electrodes are limited by a range of only 2-2.5 cm depth from the point of application [4, 112]. This means that they are only practical when taking readings from the most superficial muscles.

Crosstalk is also a problem with surface electrodes. Adjacent muscle activity may be registered when the examined muscle is quiescent resulting in misleading results. It has been shown to be advantageous to place the electrode in the midline of the muscle belly to detect the signal with the largest amplitude and frequency spectrum and to reduce the likelihood of crosstalk.

Needle Electrodes

Needle electrodes are inserted through the skin directly into the muscle. The most common type is the concentric electrode. In a monopolar configuration a single insulated wire runs through the cannula of the needle to its tip (Figure 3.6). The end of the wire is bared to provide a detection surface. Bipolar needles have two wires running through the cannula to give two detection surfaces.

Needle electrodes are capable of conveniently detecting individual MUAPs and can be easily repositioned to examine other locations within the muscle or to improve signal quality [4]. They are useful for investigating the characteristics of MUAPs and the control properties of motor units [4], but do not give an overview of muscle activity.

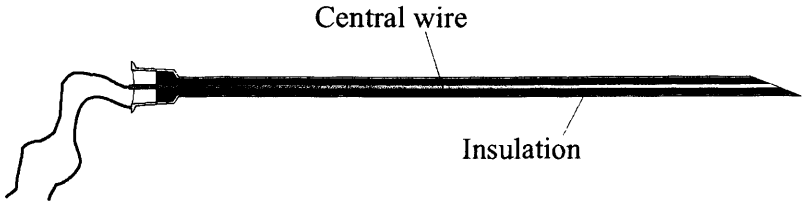

Figure 3.6: Monopolar needle electrode for detailed and deep electromyography.

The chief disadvantage to the use of needle electrodes is the discomfort they can produce. This is an invasive technique, which may involve the insertion of multiple needles that remain in place during motion. As such they can often be uncomfortable or even painful.

Fine Wire Electrodes

Fine wire electrodes are also inserted into the muscles using needles (Figure 3.7), but the needles are withdrawn after insertion leaving the wires, of as little as 25 μm diameter, to protrude through the skin [4].

An alloy of 90% platinum-10% iridium is recommended by Basmajian and De Luca [4] to offer the appropriate chemical inertness, mechanical strength and stiffness. Teflon or nylon insulation is also recommended.

The wires are hooked at the ends (Figure 3.7) so that the needle withdraws without them and are than taped to the skin surface to reduce the risk of accidental removal. The electrodes can be pulled out painlessly as the wires are flexible enough that the hooks straighten with almost no resistance [4].

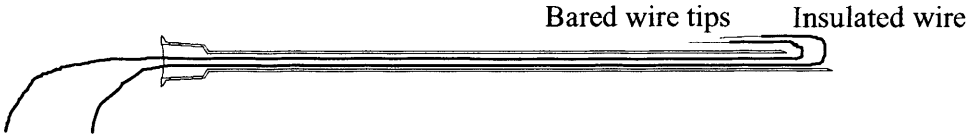

Figure 3.7: Fine wire electrode and insertion needle for relatively painless, detailed and deep muscle electromyography.

These electrodes may migrate slightly, so the muscle should be contracted and relaxed a few times before taking readings [4].

Fine wire electrodes are useful for studies of deep muscle activity, in particular where comfort is a priority. Their chief disadvantage is the time and effort used in setting them up for recording. The needle must be removed

over the ends of the wires after insertion into the muscle, so the wires cannot be pre-attached to the equipment. Analysis can include large numbers of electrodes, so a long period of preparation must be allowed for.

EMG Signal Processing

EMG readings are composites of the signals from multiple motor units as well as noise signals. This produces a frequency spectrum with peak signal strengths typically between 5-200 Hz and a lesser component at 1 kHz [72].

Muscle electrical signals are very small and signal strength diminishes with distance to the electrode. Differential amplifiers are typically used to produce readable signals and to limit noise. Noise is removed from bipolar electrodes by subtracting the two signals using differential amplification [72]. Each is measured relative to the ground electrode. The result should filter out unwanted signals.

Band-pass filtering can eliminate some noise and 'artefact' caused by movement of cables etc. Filters are usually set to a range of around 5 Hz to 500 Hz to eliminate low and high frequency interference but retain the action potentials.

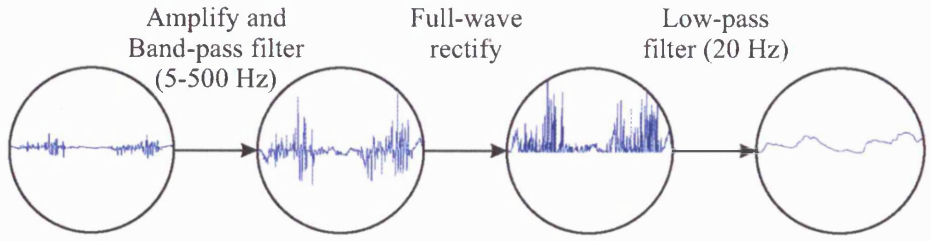

Figure 3.8: Surface EMG signal processing.

Digitisation of the signal is very common to allow offline post-processing by computer. Typical processes include further amplification, full-wave rectification and low pass filtering to produce a relatively smooth muscle activation curve (Figure 3.8) that resembles the muscle tension curve.

Muscle activation signals are calculated relative to the maximum voluntary contraction of the muscle under examination. This must therefore be ascertained as a part of the data collection routine before any post-processing can occur.

3.3.5 Simulation

The increasing quality and precision of biometric and sampled motion data has allowed a perfusion of computer simulation into the field of gait analysis. These models permit rapid analysis, diagnosis and assessment of gait, making possible estimates of muscle activations and joint forces, which in some cases cannot be measured directly even using invasive procedures.

Simulations cannot generate the precise values of moment or activation actually used within the body, as no simulation is perfect and redundancy within the body systems means that there is often no unique solution to the calculations. The readings offer a possible solution, similar to the actual values, without the need for invasive techniques.

Models are constructed using biometric parameters to individualise a normalised system [44, 101, 119, 121]. Dynamics equations define the motion of the body and separate normalised musculotendon models are used with musculotendon parameters to dictate the actions of the muscles [21]. More advanced models will also include joint behaviour definitions and ligament equations. Experimental kinematic, kinetic and EMG readings serve as inputs to the model and reference signals for comparison with the outputs when checking validity.

Different methods of neuromusculoskeletal modelling have arisen to serve different purposes. The most significant techniques will be discussed in the following sections.

Forward Dynamics

The forward dynamics approach to system modelling involves the simulation of a system from cause to effect through all of the processes in between. In the case of the neuromusculoskeletal system, the inputs are the muscle activation signals, sampled from measured EMGs. These activations then drive musculotendon models, which generate muscle forces and moments about the joints. Combined with moments and force from the ground reaction, gravity and ligaments, these serve as inputs to a motion dynamics model formed from a set of deterministic ordinary differential equations, which generates a unique solution in the form of body segment trajectories.

A forward dynamics neuromusculoskeletal model will take a form similar to the following:

$$M(\theta) \cdot \ddot{\theta} = n(\theta, \dot{\theta}) + g(\theta) + m_{mt}(\theta, \dot{\theta}) + GR \tag{1}$$

Where:

- θ ,$\dot{\theta}$ and $\ddot{\theta}$ are the vector joint (or segment) angles, angular velocities and angular accelerations respectively.
- $M(\theta)$ is a matrix of the part of the motion dynamics that have an acceleration component and $n(\theta, \dot{\theta})$ is a vector of the coriolis and centrifugal moments, which represent the remainder of the motion dynamics.
- $g(\theta)$ is a vector of the moments due to gravity.
- $m_{mt}(\theta, \dot{\theta})$ is a vector of the moments due to muscle activity.
- GR is the ground reaction.

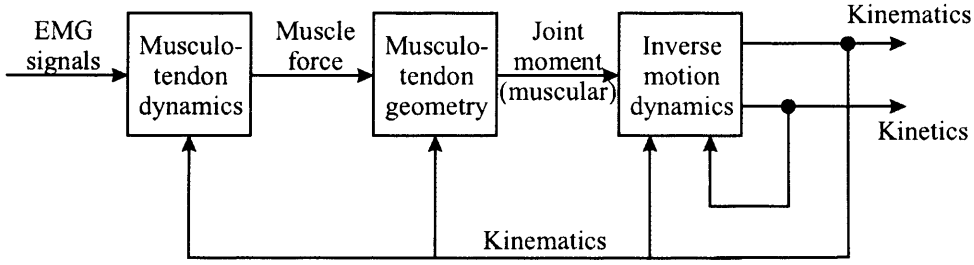

Figure 3.9: Forward dynamics neuromusculoskeletal model flow chart.

The forward dynamics approach is an intuitive, deductive process, which describes a system from cause to effect making it very appealing to simulation designers. A forward dynamics musculoskeletal model will use muscle activations to calculate muscle forces, which in turn are used to find joint moments and ultimately system kinematics (figure 3.9). But the human locomotive apparatus is a fundamentally unstable system and the measurements used as parameters and inputs are prone to error and inaccuracy. In many cases they may be merely convenient approximations. Under these conditions, the cumulative error over a period of a fraction of a gait cycle will drive any forward dynamics system beyond its error bands making such a system unsuitable for gait modelling.

Inverse Dynamics

As the name suggests, the inverse dynamics method involves approaching the modelling of a system from the opposite direction to the forward dynamics method. The experimental data, kinematic and kinetic in the case of gait analysis, is used to find the internal joint moments and muscle activation

levels. This is referred to as an inductive process and it yields a result that may be only one of many possible outcomes. The joint muscular moments can be found by rearranging the forward dynamics motion equation (3.1) to give:

$$m_{mt} = M(\theta) \cdot \ddot{\theta} - n(\theta, \dot{\theta}) - g(\theta) - GR$$

There are many more muscles than joints, groups of which produce approximately the same effect. As such there is not a single mathematically determinate solution to inverse dynamics muscle activity models. Inverse dynamics models are limited by their need for accurate mathematical modelling and parameters, both of which are difficult to obtain for biological systems. Common simulation problems associated with inverse dynamics models occur because of the models' mismatch as well as measurement and derivative estimation errors [121].

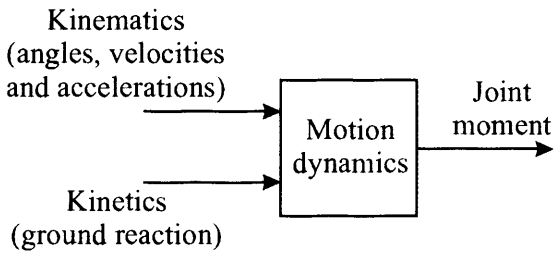

Figure 3.10: Inverse dynamics body segment model flow chart.

The inverse dynamics approach is also subject to inflexibility in its models. The behaviour of a system is described for a particular set of inputs. In the case of a musculoskeletal model, the inputs are the joint angle trajectories and the parameters are the masses, moments of inertia and lengths of the body segments (figure 3.10). Due to the closed loop nature of the musculoskeletal system any variation to these will have incremental effects throughout the rest of the cycle. An inverse dynamics model cannot account for these incremental variations and therefore any experimental variation of inputs or parameters may yield only meaningless results.

Optimisation

Optimisation is a technique for dealing with systems with more unknowns than system equations [86]. The method relies on decreasing the number of unknowns or increasing the number of system equations until they match.

An optimisation algorithm is applied based on a set of assumptions or optimisation criteria within the system constraints 3.11. Rather than being a modelling approach in its own right, optimisation serves as a component of another approach.

When calculating muscle activation levels using an inverse dynamics approach, it quickly becomes clear that there is a far greater number of muscles than there are joints. Optimisation can be used to address this problem in two ways. Firstly, many muscles cross the same joints and perform approximately the same actions. It is a common technique to group such muscles to reduce the number of unknowns. Secondly, human gait has evolved to be as close to optimal as possible [2], and therefore a set of criteria based on minimising the total work done can be applied as extra system equations [20].

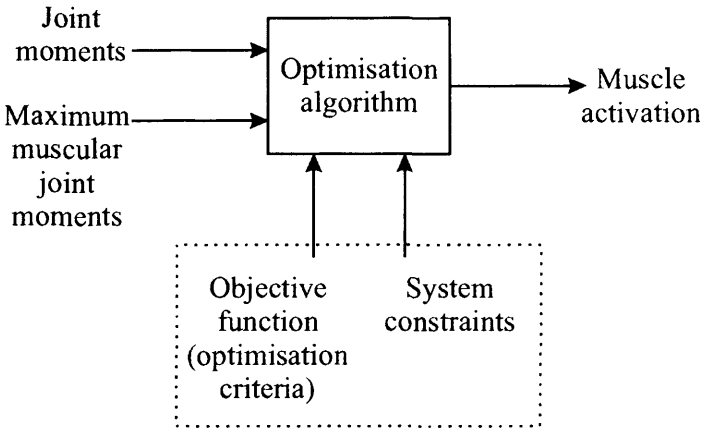

Figure 3.11: Muscle activation optimisation model flow chart.

Optimisation of human gait modelling typically produces predicted muscle activity that correlates poorly or inconsistently with measured EMG activity [2, 20, 72]. Metabolic energy consumption 50% higher than measured and extreme sensitivity to kinematics and kinetics can be expected. This may be due to inaccuracies in the non-trivial assumptions made to form the optimisation criteria, especially as the physiological basis for muscle control is so poorly understood, or to oversimplification in the lumped-parameter musculotendon models commonly used in human biomechanical modelling [2].

Neural Network

Artificial neural networks also offer a method of neuromusculoskeletal modelling [1, 91]. The functional relationship between input and output is not of interest in this approach. Instead neural networks attempt to find a set of rules, based on example data, to describe the relationship between input and output signals.

The main disadvantage of using this approach for gait modelling is that no insight is offered into the biomechanical processes at work.

Control

Unmodelled dynamics, parameter variation, simplifications, disturbances and non-linear interactions are inherent problems when modelling actual gait samples. Open-loop models can make no allowance for these discrepancies, producing inaccurate results. The solution is to build a controller into the system to close the loop and allow feedback to compensate for any plant/model inconsistencies.

Various types of control system have been applied to gait models in an attempt to force the simulation to follow a set of required trajectories. Most of these require a degree of robustness that is difficult to realise in a practical situation especially given the non-linear nature of the human locomotive apparatus. These problems have led to research interest in a novel control methodology known as sliding-mode control.

Sliding-mode is a type of variable structure control system (VSCS). These VSCSs emerged from Russia in the mid 1970s following pioneering work by Emel'yanov and Barbashin in the early 1960s [29]. As the name suggests, variable structure control systems vary their control law during operation according to a set of predefined rules. Sliding-mode controllers use a two-state control law, which switches back and forth between two powerful, opposing feedback signals as the system crosses a 'switching surface' at high frequency (see Chapter 7 for greater detail). Under these conditions, the closed-loop model behaves as a reduced-order system, insensitive to plant/model mismatches and certain types of disturbance [29].

Figure 3.12 shows a flow chart of the complete system. The forward dynamics section represents the body of a subject during gait. The sliding-mode and inverse dynamics blocks close the system loop, the controller generating the required accelerations to match the system trajectories and the inverse

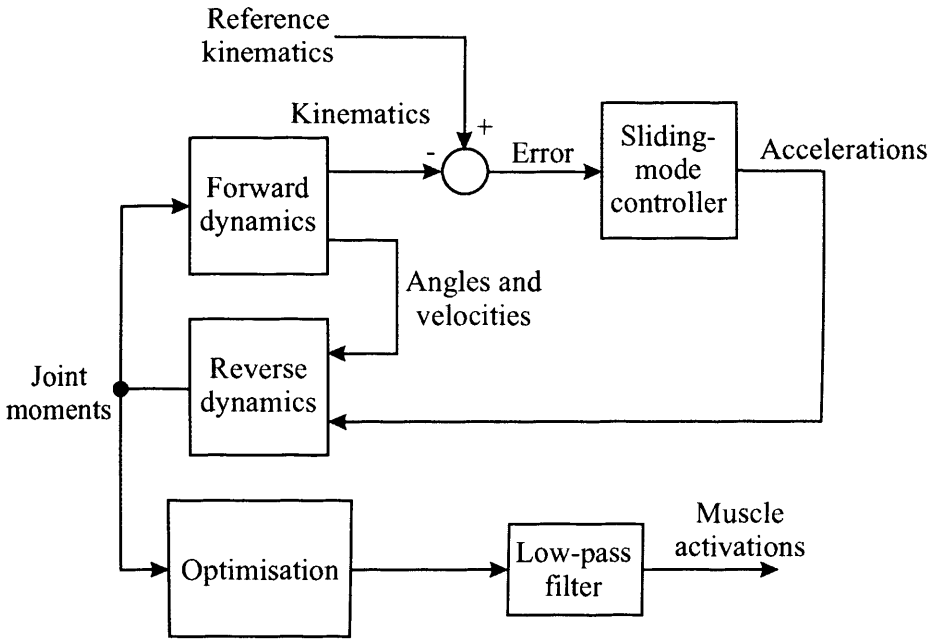

Figure 3.12: Flow chart of a neuromusculoskeletal model utilising sliding-mode control in conjunction with forward and inverse dynamics and optimisation techniques.

dynamics converting them into the joint moments necessary to drive the subject along those trajectories. The moments are distributed amongst the muscles according to the rules of the optimisation algorithms and then divided by the maximum moment those muscles can generate in order to find the magnitude of muscle activity necessary to generate those moments. The end result is low pass filtered with a cut-off frequency of 20Hz to remove the switching noise from the sliding-mode controller.

The muscles activities are calculated outside the closed loop as there are delays inherent to the muscle system that cause the controller to crash.

As a non-linear technique with robustness to parameter variations and disturbances, sliding-mode control is particularly suited to the inaccuracies of measurement and poorly understood processes of the field of neuromusculoskeletal modelling.

3.4 Summary

This chapter represents an overview of the basic principles and techniques of gait analysis. The particular methods used depend on the available equip-

ment, and those used in this study will be described in detail in the next chapter.

The fundamental characteristics and phases of the gait cycle were introduced to provide a frame of reference for the analysis of results in later chapters, as well as the four criteria required for successful gait, which is the focus of this study.

Observational gait analysis was introduced as the first stage in examination of a subject, before the quantitative version, kinematics, was described. Kinematics involves the study of body position and joint angles using equipment such as multiple exposure cameras, goniometers, electrogoniometers and motion capture video systems, which were compared in terms of accuracy, applications and cost.

Kinetics is the study of the forces and moments relating to an objects motion. The use of force platforms for this purpose has been introduced. Combination of ground reaction force plate data with kinematic measurements allows the calculation of internal joint forces and moments.

Three types of electrode used in electromyography were described and compared in terms of clinical situations. Surface electrodes are preferred for gait analysis due to their ease of use, comfort, non-intrusive nature and their envelope detection and spacial averaging of a large volume of MUAP signals. Needle electrodes can be very uncomfortable or even painful so are less popular, while the use of fine wire electrodes is increasing in situations where measurement of signals from deep muscle or investigation of individual MUAPs is required.

Simulation techniques combine the kinematic, kinetic and EMG data to provide estimates of the internal forces, moments and muscle activity not possible without extreme invasive techniques. They can offer a tool to help explain results and offer insight into the biomechanical processes and interactions of the human locomotive apparatus [72].

The neural network approach removes much of the desired insight by effectively bypassing the functional relationship between input and output signals.

Forward and inverse dynamics approaches both have their disadvantages, which make them independently unsuitable, however by combining these techniques with sliding-mode and optimisation, the inherent problems associated with gait modelling; measurement inaccuracy and unmodelled dynamics, can be suppressed to offer more accurate results.

A combination of techniques is the best way to perform thorough gait analysis.

Chapter 4

Data Acquisition

4.1 Introduction

In order to validate and to provide input data for the neuromusculoskeletal model, experimental readings needed to be taken from human subjects. Data was obtained from two sources; the Department of Sports Medicine within the Leicester General Hospital, which permitted the use of its gait analysis equipment for this project and the Internet, where various groups have made available kinematic, kinetic and muscle activation data samples [63].

This chapter describes the methods used in sampling data using the gait analysis equipment at the Leicester General hospital and highlights the selection processes and criteria used in collecting data from the Internet.

4.2 Kinematics

4.2.1 System

Kinematic motion tracking data was obtained using a ProReflex Motion Capture/Analysis System (Qualysis AB, 411 12 Gothenburg, Sweden) comprising six infrared video cameras and the associated markers, reference structures, calibration wands and software.

The ProReflex MCU (Motion Capture Unit) is an infrared camera with an array of infrared LEDs around the lens (Figure 4.1). The infrared light projected from the unit is reflected from small spherical markers (Figures 3.3 & 4.1) attached to the subject and picked up by the camera to generate a 2-dimensional image of the marker positions (Figure 4.1).

Using a second MCU allows marker positions to be triangulated in the 3-dimensional space observed by both cameras. For gait analysis the markers

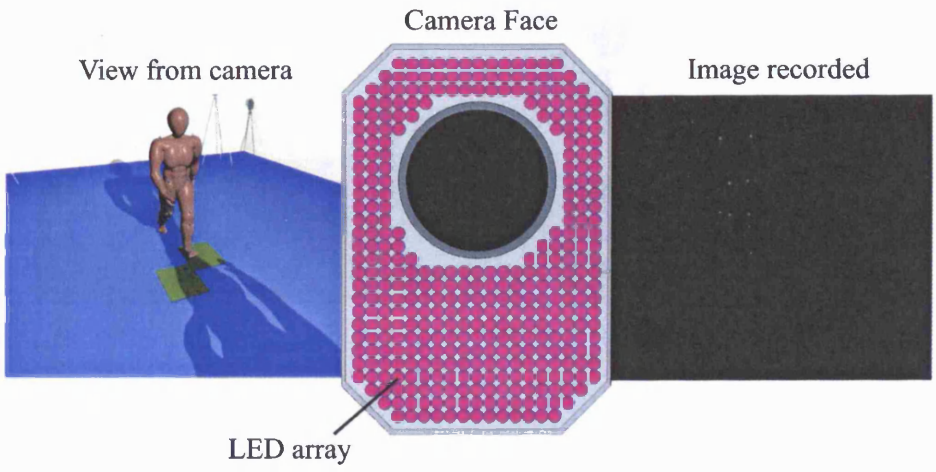

Figure 4.1: Camera face and 2-dimensional image.

are arranged on all sides of the body, so several cameras are required in order to keep track of all of the markers simultaneously. With body movement and in particular arm swing obscuring the view of markers at intervals, a minimum of six MCUs is recommended for bilateral gait analysis.

A 120 Hz motion capture system was used to provide a high enough sampling rate to observe all of the features of walking gait. ProReflex MCU systems of up to 1 kHz are available for kinematic analysis of more rapid actions such as sporting activity.

4.2.2 Camera Set-up

The MCUs are ideally arranged in a six-by-ten metre rectangular arrangement with three cameras equally spaced along each long side (Figure 4.2). The dimensions of the room used to collect the data did not permit this idealised setup, so four cameras were moved as far as possible into the corners of the room while the remaining two were lined up as far opposite each other as possible across the force plate, perpendicular to the walking direction.

The focus and aperture of the cameras was adjusted as in the ProReflex MCU user guide to obtain the best image possible throughout the capture region for the position of each camera.

In order to prevent the LEDs of the other cameras from being in the frame of view, each camera was raised on its tripod above the shoulder height of the tallest subject and tilted down until the other cameras no longer registered (Figures 4.1 & 4.2). It is necessary to ensure that the shoulder markers can

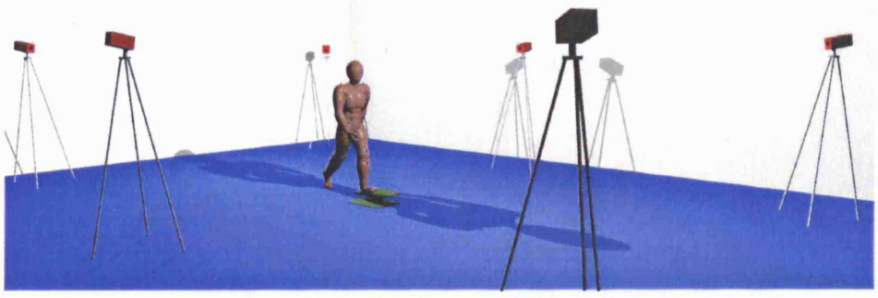

Figure 4.2: Camera arrangement.

still be observed throughout the capture region by examining the real-time camera output. If the markers cannot always be observed, the camera should be raised and tilted further.

False signals can be generated by smooth surfaces such as computer screens, plastic casings and even laminated paper. Anything generating a false signal was removed or covered before proceeding as the results could be distorted even if the false signal only registers on a single camera.

4.2.3 Calibration

Prior to motion capture, the system requires calibration. The position and orientation of each camera relative to the others must be known in order to accurately triangulate marker positions.

The calibration process took place at the beginning of every session and every time any of the cameras was moved or even nudged. If a camera is moved without re-calibrating, then data from it becomes invalid resulting in markers being missed and extra markers identified in inaccurate locations.

Calibration is performed using a reference structure and calibration wand. The reference structure is an L-shaped metal frame with markers at precisely measured points. It is laid on the ground with the longer bar pointing in the direction of walking motion (Figure 4.3).

The calibration wand comprises a T-shaped frame with a marker on each end of the precisely measured cross bar and a handle on the end of the shaft (Figure 4.3).

During calibration, the computer records the positions of the markers on the reference structure and wand over a period of seconds set by the user (usually 30). The wand is waved in motions roughly parallel to each axis in

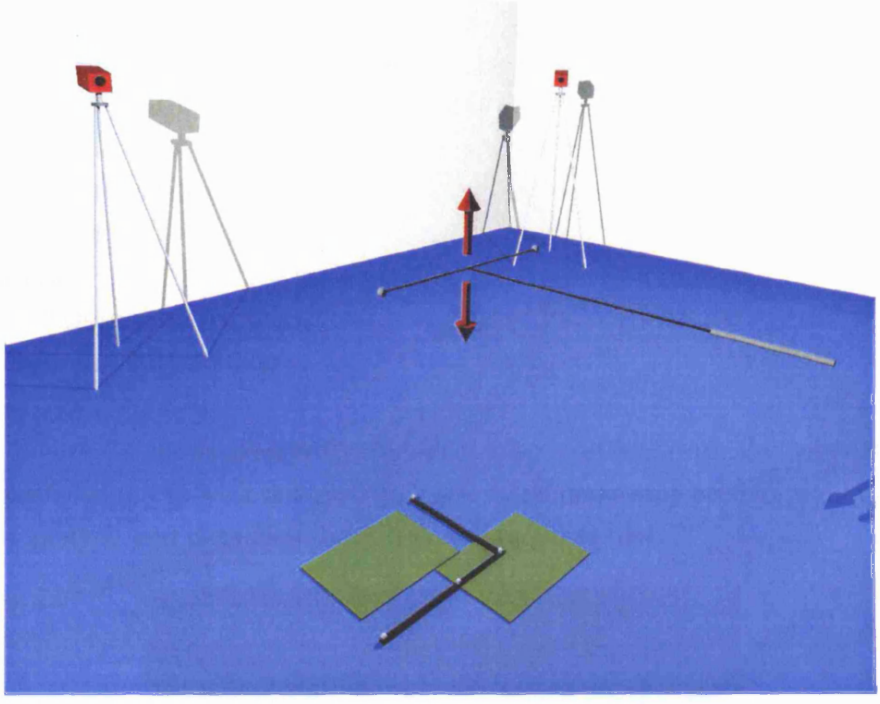

Figure 4.3: Calibration equipment.

turn throughout the capture region to calibrate the cameras for the entire area in all orientations.

The data is then processed to identify the six markers in each camera view. Identifying the markers and knowing the distances between them provides enough information to calculate the position of the cameras relative to the reference structure and therefore relative to each other. The movement of the wand provides information regarding the characteristics of the camera to signals from areas throughout the capture region. The data processing is automatically carried out by the software included.

4.2.4 Subject Preparation

Subjects first had their height and weight measured and their details recorded along with the filenames of their gait samples. Markers were then attached to the skin at anatomical landmarks with double-sided tape (Figure 4.4). The landmarks are points where the skin moves very little with the motion of the joints, they are:

- Right and left toe

- Right and left heel
- Right and left ankle
- Right and left tibial tuberosity
- Right and left knee joint
- Right and left patella
- Right and left ASIS
- Sacrum
- Twelfth thoracic vertebra
- Right and left shoulder

Figure 4.4 shows greater trochanter marker positions with the associated boxes faded out as with this system, these markers are only used for unilateral gait analysis and data from both legs was required here.

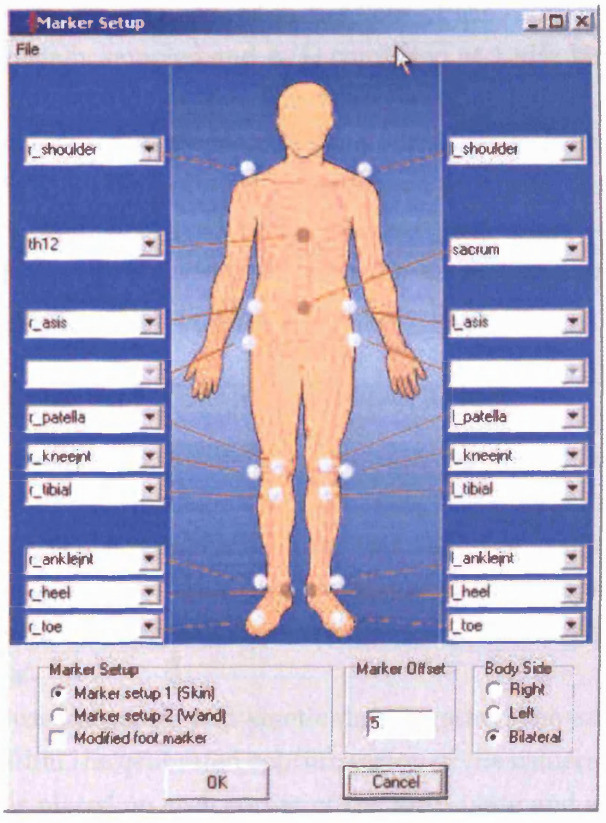

Figure 4.4: Marker positioning.

Instructions for identifying these landmarks are included in Appendix A.

With the markers in place and before any motion capture takes place, subjects are asked to walk up and down the capture route several times to relax them into a normal and comfortable gait.

Subjects often look down at their feet as they walk or aim to step on the force plates in order to be helpful. Both of these distort the gait patterns. To prevent this, a small piece of tape was attached to the wall at approximately the eye-level of the subject, who was then told to walk towards the piece of tape ignoring everything else in the room.

4.3 Kinetics

4.3.1 System

Kinetic measurements were taken using a single Bertec 4060-10 strain-gauge force plate (Bertec Inc.) embedded in the floor of the room. The data from the plate was initially sampled and A/D converted at 1 kHz but the software resampled the data to match the camera frequency of 120 Hz.

Forces are measured in three orthogonal axes (vertical, lateral and fore-aft) and moments are measured about the same axes providing six degrees-of-freedom. Six-component load transducers are used to perform this.

The force plate was synchronised with the kinematic camera system to ensure simultaneous data collection for useful calculation.

4.3.2 System and Subject Preparation

The force plate requires a few minutes to warm-up once first switched on. This period was usefully occupied by calibrating the cameras and preparing the subject for kinematic analysis. After this time the system was zeroed. Examination of the output signals occasionally revealed some signal drift and the need for further zeroing at a later interval when the force plate was used for long periods.

In order to use kinematic and kinetic data together, the force plate must be identified within the calibrated capture region of the cameras. To perform this, a marker is placed on each corner of the force plate and a short motion capture run is made. This data sample can be used to link the kinematic and kinetic data from subjects within the same system calibration.

It is often the case that a subject will not step on the force plate correctly. The footprint may lay partly off the plate, miss the plate altogether or part

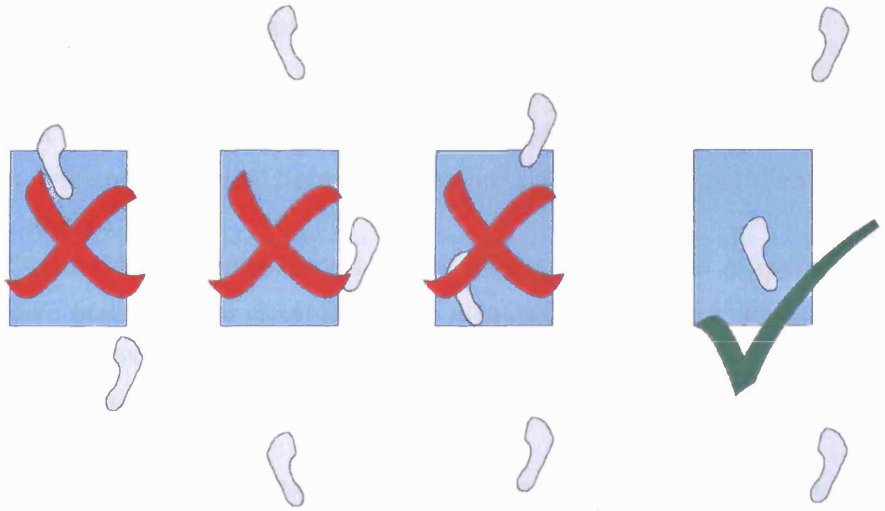

Figure 4.5: Force plate footprints.

of a second footprint could fall on the plate (Figure 4.5). The kinetic data obtained in these cases is useless; only a single, full footprint on the surface of the plate is acceptable (Figure 4.5). However, the subject should not be informed of this, as their gait pattern will be distorted if they aim for the plate. Instead, in each case the subject was asked to start from a slightly different place until an acceptable reading was produced.

4.4 EMG Acquisition

4.4.1 System

A BIOPAC EMG acquisition system (BIOPAC Inc.) was used to collect EMG data in synchrony with the kinematic and kinetic data.

Sets of silver-silver chloride surface electrodes were applied to the subjects each including a positive, negative and ground electrode. These signals fed into a BIOPAC TEL 100M portable transmitter, which accepts four channels of EMG data input. The unit converts the EMG signals into a modulated bit stream to transmit over a single, 10-metre, lightweight cable to the TEL 100D receiver. The receiver demodulates the data and transmits it to an MP100 console connected to a computer for recording and analysis.

In order to synchronise the EMG data collection with the kinematic and kinetic acquisition, the BIOPAC system permits the use of triggering. The TEL 100D monitors a cable from the kinematic acquisition system continuously and when the signal turns high EMG acquisition begins.

4.4.2 Subject Preparation

To lower the electrical impedance of the skin and provide a good electrical contact the site of electrode attachment was first shaved with a disposable razor, to remove hair and lightly abrade the skin surface [4], and then cleansed with alcohol.

Disposable, self-adhesive electrodes were applied to the prepared areas. Positive and negative electrodes were attached within a few millimetres of each other over the body of the muscle to be examined, while the ground electrode was attached to a site with no muscle tissue nearby eg. over the lateral femoral condyle.

To minimise movement artefact, the cables from the electrodes were taped to the subject's legs, allowing enough slack for the joints to move unimpeded.

The cables connect to the BIOPAC TEL 100M unit, which is attached at the subject's waist using a belt clip on the back of the casing.

The weight of the cable from the TEL 100M unit to the receiver module is insignificant in terms of its effect on the subject's gait. However, it is important to ensure that the cable will not snag on any objects or cross the path of the subject during acquisition as this will affect the locomotive pattern.

Only four simultaneous EMG recordings can be taken using the unit, typically a selection from the rectus femoris, vasti, hamstrings and triceps surae muscles and muscle groups of both legs as these are the most easily accessible of the muscles having a significant effect on gait. When validating the model a much wider spectrum of muscle activity readings is desirable, comparing only 4 out 22 muscle groups may be poorly representative of the system performance. In addition, before taking measurements during gait, each of the muscles being analysed must be maximally contracted by the subject to provide a maximum voluntary contraction (MVC) reference signal to measure the rest of the readings against, but the expertise and equipment required to take these readings properly was unavailable.

As a result, it was decided that normal muscle activity approximations from Perry [84] would be used for comparison with model outputs, supplemented with more gait analysis data sets from Internet sources [63, 110] that included a larger selection of EMG readings.

4.5 Motion Capture

With the equipment set up and the subject prepared, motion capture could begin. The subject was arranged at the starting position and the computer systems activated. When the system initiation finished and recording started, the subject was asked to begin walking back and forth across the capture region towards marks on the walls.

A capture period of twenty seconds was typically chosen as it would allow two or three full passes depending on how quickly the subject moved. Shorter time periods would permit only one pass and increase the time spent in preparation and initiation, while longer periods would waste more time in the event of an error such as a marker coming loose and would not allow adjustment of the subject's start position to increase the probability of him/her stepping on the force plate correctly.

Any pass of the subject where a marker comes loose is effectively useless for the purposes of this project, as the joint angles cannot be calculated properly without all of the markers. If an electrode comes loose, the rest of the data can still be used but a better option is to reattach the electrode and record another pass to obtain a full data set. Samples where the force plate was not stepped on correctly were also removed from the results.

Owing to difficulties described in section 4.5.2, data was only collected from four subjects and useful data could only be obtained from three of those. The subjects acceptable data was taken from were male, ranging in age from 23 to 25 with heights of 1.75 to 1.87m and weights of 75 to 78kg.

4.5.1 Initial Motion Analysis

The initial motion analysis is essentially a check that all of the equipment has functioned correctly. It was carried out as quickly as possible so as not to keep the subject waiting too long.

Qualysis provides software to generate a 3-dimensional image of the markers over time as they move through the capture region (Figure 4.6). The markers were manually identified and tracked from their first appearance within the region until they left it. Small gaps were considered acceptable up to 20 frames (at 120 Hz) including trimming, where the marker data for the first and last four frames of each marker is ignored. This is performed because the moment when a marker is picked up or lost by a camera is the

region that tends to have the greatest error. In most cases the removal of four frames is enough to account for this. All of the markers were required to be visible to the cameras for a minimum of two complete steps beginning and ending at a heel strike to facilitate normalisation. Kinematic data that fulfils this criterion was considered acceptable.

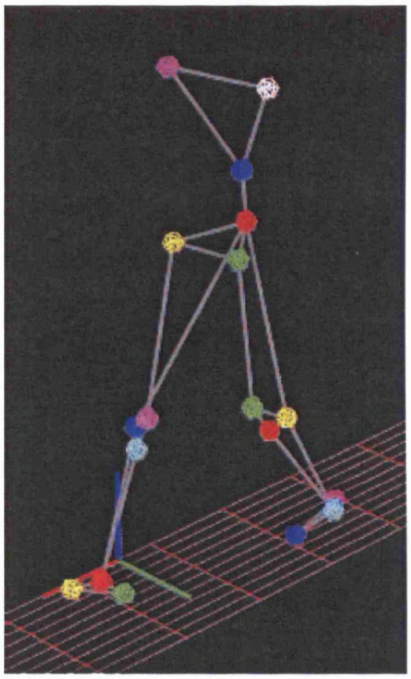

Figure 4.6: Kinematic analysis.

Visual analysis of the kinetic data was used to confirm that the subject had stepped on the force plate correctly. Normal gait forms a distinctive set of curves in the six-degrees of freedom of the ground reaction (Figure 4.7). A cursory examination was enough to confirm that these appeared to be correct and to pass the sample for the next stage of analysis and processing.

It was also necessary to confirm that the ground reaction measurement corresponded to one of the acceptable steps of the kinematic analysis.

A visual examination of the EMG samples was also sufficient to confirm that strong signals are being received on each of the channels and that the movement artefact and other noise signals are kept to a minimum. Of the signals shown in figure 4.8 the strong and medium EMG signals are acceptable, as filtering will remove the unwanted artefacts. It may be possible to

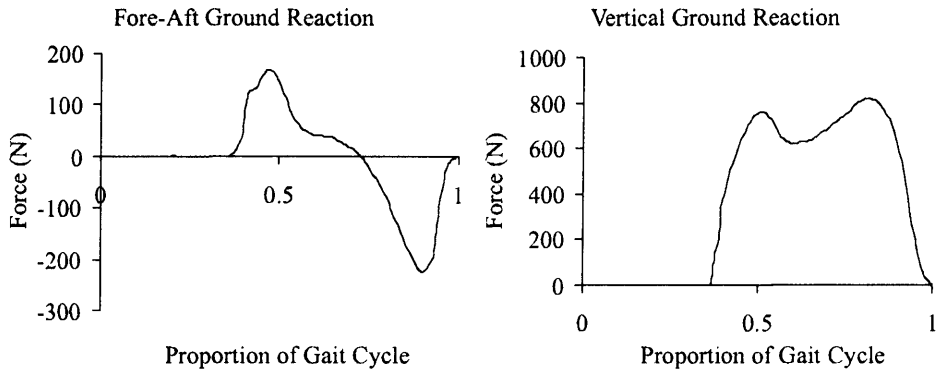

Figure 4.7: Typical ground reaction curves.

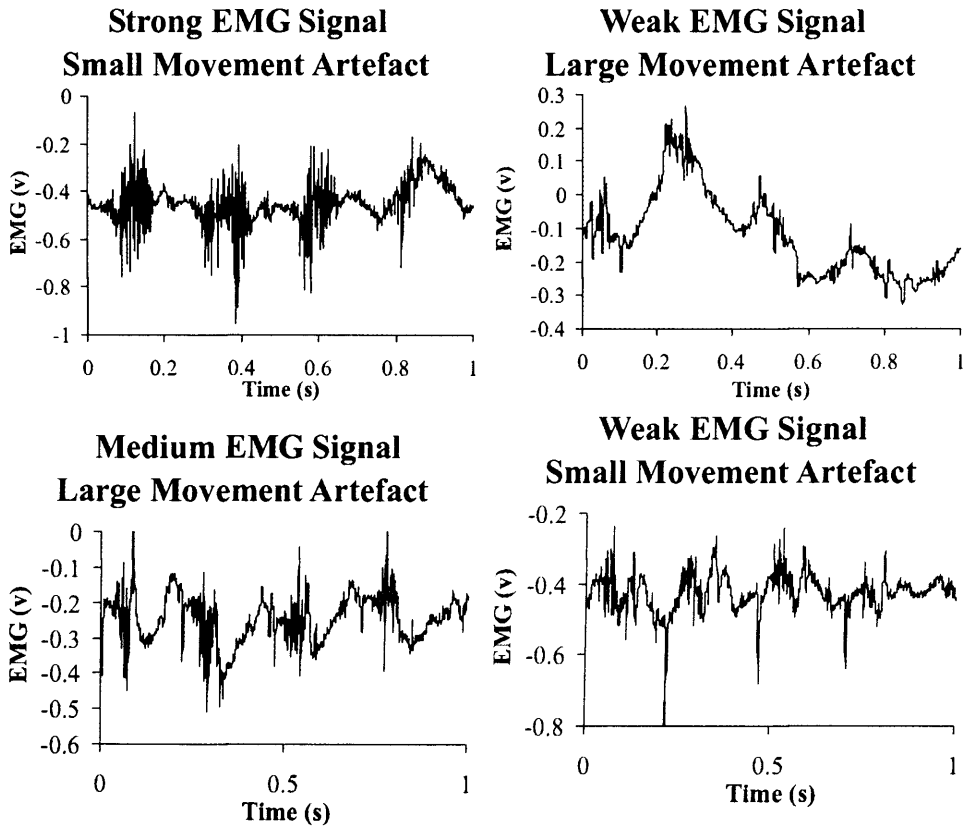

Figure 4.8: Example EMG samples.

obtain data from the other signals, but such data cannot be trusted. It may include noise from other muscles as well as from other sources.

If all of the data from a sample were seen to be acceptable then the files were saved under the subject's name with the date and time.

4.5.2 System Limitations

In the absence of a more formal arrangement, experimental protocol was set by the author, based around the instructions in the equipment user guides. The author also applied the markers, as the gait lab had no skilled technicians to perform this task.

The joint moments are calculated from the motion data and force plate readings by both the gait analysis software and the simulation. Inaccurate marker positioning due to inexperience becomes less important in this context, providing that the motion data falls within normal gait bounds. It is the relationship between the gait analysis software and simulation generated moments that are under examination here, both of which are calculated from the same motion data.

This is not the case with the EMG and calculated muscle activations as the EMG signals are measured and not calculated, however EMG measurements for these gait samples were not used due to the absence of trained personnel to take MVC readings and the limitations of a four-channel system.

With such a new system there were inevitably teething troubles, which delayed data acquisition and resulted in invalid data sets.

Initially, the chief problem was the size of the room used. With the cameras moved as far as possible into the corners it was just possible to take a data set for one full gait cycle including a step on the force plate. However, a great deal of time and effort was required to find the optimum camera positions to accomplish this.

Once data collection had begun, a problem arose in the processing of the force plate data. Using the sensitivity matrix and gain formula provided by the manufacturer, the resulting force and moment calculations were gibberish. Communications with the manufacturers and installers over a period of several months were fruitless and in the interim, alternative data was sought out on the internet. Ultimately, analysis of the sensitivity matrix and gain formula offered a solution.

The sensitivity matrix is a 6*6 matrix describing the interactions between the 6 transducers in the force plate to input in the system's 6 degrees of freedom. As such it is an approximately diagonal matrix:

$$\begin{bmatrix} 1218.4 & 12.2 & -9.4 & 9.3 & 1.9 & -5.7 \\ -13.6 & 1232 & 4.1 & -2.8 & 2.7 & -2 \\ -33.6 & -6.8 & 1917.9 & 3 & 2.9 & 17.3 \\ 0.3 & -76.4 & -1.6 & 703.8 & 0.6 & -0.1 \\ 73 & -1.7 & 1.4 & 4 & 495.9 & -0.2 \\ 0.9 & 0 & 0.4 & 4.5 & -3.2 & 285.5 \end{bmatrix}$$

The gain formula applies the voltage and channel gains to each element in the matrix as appropriate and was given as:

$$a_{ij} = 1/(s_{ij} \times 10^{-6} \times V_j \times G_j)$$

Each element 's_{ij}' of the matrix is adapted to compensate for gain 'G_j' and excitation voltage 'V_j' levels set by the user. This equation clearly cannot be correct as it inverts each element of the matrix causing the major diagonal to tend to zero.

Logically, the equation must take the form:

$$a_{ij} = \frac{xs_{ij}}{V_j G_j}$$

Where x is a value to be ascertained.

Over enough time, the average vertical ground reaction equals the weight of the subject 'mg', assuming no other external forces are in effect, therefore a value for x can be found using the first row of the sensitivity matrix:

$$\frac{mg}{x} = \sum_{n=1}^{6} \frac{s_{n,1}}{VG} \times v_n$$

Where v is the average voltage output from the force plate.

A value of 500 was found for x, to 2 significant figures (the technique is only as accurate as the scales used to weigh the subject).

Varying the gain and excitation voltages when taking samples confirmed that the equation was arranged correctly, but without specialist equipment, precise calibration of the system would be impossible, particularly in the other 5 degrees of freedom. Fortunately, the same equation and value of x applies to every degree of freedom.

Of more than 80 gait samples recorded, 30 were put forward from the initial analysis for more detailed examination before conversion to a format suitable for simulation. The detailed examination revealed that the majority of samples were incomplete in one detail or another. Many did not cover a complete gait cycle or when they did, the force plate readings did not occur entirely within that cycle making the readings invalid. Eventually, only six complete data sets emerged, so it was decided to supplement them with samples discovered on the internet, time shortage, equipment difficulties and lack of expert staff combining to make this the best alternative.

4.6 Internet Data Acquisition

Many other gait researchers have made data samples from their own work available over the Internet to provide a broader experimental reference base for future work [63, 110]. The nature of these data files is biased towards the purpose for which they were collected and as such most are of limited use to this project. Some of the data samples were collected in better-equipped gait laboratories with a sufficiently large room for high quality kinematic measurement, two force plates for bilateral analysis and EMG systems capable of analysing more than four channels of activity at once. These can offer exactly the required data for this project and while few are available, they provide a valuable supplement to the data obtained from the Leicester General hospital gait analysis equipment.

4.7 Summary

Collection of experimental data is necessary to provide reference signals to drive the model. Kinematic data provides the trajectories that the segments of the model are forced to follow and kinetic ground reaction data give the information necessary to calculate accurate internal moments.

EMG data is only necessary for validation of the model, to confirm that the muscle activations generated by the simulation bear close similarity to the actual activity in the muscles.

The facilities available in the Department of Sports Medicine of the Leicester General Hospital give the capacity to generate large quantities of relevant data in a very short period. These experimental measurements are, however,

inevitably incomplete owing to the limitations of the equipment. For this reason complete data sets were sought out over the Internet to augment the set of measured samples.

The processing of these data files into a format that is acceptable to the model is detailed in the next chapter.

Chapter 5

Data Processing

5.1 Introduction

Data generated by different gait analysis equipment and software may be stored in a number of formats. The most commonly supported data storage method is the C3D format, which is capable of storing synchronised 3-dimensional motion and analogue data samples [12, 118]. However, the use of C3D is by no means exclusive throughout the field of gait analysis, many other formats may be used at the analyst's discretion. Normal gait data for this project has been collected and processed from many different types of file, those used are listed in Table 5.1.

Filename	Source	Data Content
<files 1-6>.tsv	Gait lab	Marker displacement
<files 1-6>_A.tsv	Gait lab	Force plate output
<files 1-6>.qgt	Gait lab	Joint kinematics
Old.gcd	CGA database [63]	Kinematics and Kinetics
Young.gcd	CGA database [63]	Kinematics and Kinetics
dundee.gcd	CGA database [63]	Kinematics and Kinetics
man.apm	ISB software resources [110]	General parameters
man.emg	ISB software resources [110]	EMG readings
man.fpl	ISB software resources [110]	Force plate output
man.kin	ISB software resources [110]	Kinematics

Table 5.1: Normal gait data files used with the model.

Before input, the data samples must first be processed into a format acceptable to the model. With so much variation in file types it was decided that the data would be converted into a format created for the model, to take advantage of features of the programming language used. It would have been possible to convert all of the data into one of the formats listed above and develop code to read this file type, but with only small sample groups used in any given format, this would be less efficient.

This chapter details the methods used to process the data file types listed above in order to generate a suitable trajectory file for the model.

5.2 TSV, _A.TSV and QGT

These are the native file-types of the Qualisys Motion Capture/Analysis System described in Chapter 4 and data in files of these types was collected specifically for this project.

Much of the data in a given capture sample is inevitably unusable as the subject will walk into and out of the capture region observed by the cameras. Data output to the TSV file consists of the marker positions for a period of useful data, collected following the rules for Initial Motion Analysis as detailed in section 4.5.1. Small gaps in the observed marker positions are automatically interpolated and extra markers falsely detected by the cameras ignored.

Ground reactions are saved in a _A.TSV file simultaneous to the saving of the TSV file and covering the same frames.

QGT files contain a further processed form of the TSV and _A.TSV data including joint angles found by applying a predefined set of equations to the marker data.

A program was developed in the MATLAB environment, to reformat the data into a form appropriate to the model (Appendix B). For this program to function correctly it is essential that the markers be stored in the same order in every TSV file, as follows:

1. 12th thoracic vertebra
2. Sacrum
4. Right shoulder
5. Right ASIS
6. Right knee joint

7. Right patella
8. Right tibial tuberosity
9. Right ankle joint
10. Right heel
11. Right toe
12. Left shoulder
13. Left ASIS
14. Left knee joint
15. Left patella
16. Left tibial tuberosity
17. Left ankle joint
18. Left heel
19. Left toe

See Appendix A for detailed descriptions of marker positioning.

TSV, _A.TSV and QGT format files follow a delimited spreadsheet format allowing data to be read into the MATLAB workspace using the 'dlmread' command. The data can then be processed in the same way as any other matrix in the workspace.

The initial conditions of the model cannot easily be completely or accurately predicted and a settling time is therefore required before useful outputs are generated (7.4.1). For this reason the program was designed to format data for a single gait cycle and repeat it for output as two identical gait cycles. To accomplish this, the frames for the start and end of the cycle must first be manually identified.

The 'dlmread' command is used to read the 12th thoracic, right ankle and left ankle marker positions from a TSV file, the joint angles from a QGT file, the ground reactions forces from a _A.TSV file and the force plate corner coordinates from a separate TSV file:

```
% Input data
fplmarkers=dlmread(fpl,'\t',10,0)/1000;
groundreaction=dlmread(atsv,'\t',[12+start,0,12+stop,5]);
thoracicmarker=dlmread(tsv,'\t',[9+start,0,9+stop,2])/1000;
rightanklemarker=dlmread(tsv,'\t',[9+start,21,9+stop,23])/1000;
leftanklemarker=dlmread(tsv,'\t',[9+start,45,9+stop,47])/1000;
Trajectories=dlmread(qgt,'\t',[289+start,0,289+stop,23]);
```

Data from TSV files are divided by 1000 to convert it from millimetres to metres and the joint angles from the QGT files are converted from degrees to radians. The delimiter '\t' identifies tabs as the separator between values. The start and stop values locate the required data within the matrices. Data regarding the force plate coordinates comes from a separate, non-synchronised file collected at the beginning of the laboratory session. As such the start and stop values do not apply and all of the data is useful.

5.2.1 Ground Reactions

Data from the force plate must first be zero offset to ensure that when there is no pressure applied, the measured output is zero.

An acceptable ground reaction data file should contain the entire measured ground reaction, and therefore the first and last frames of data should be zero for all channels. These are therefore used as a reference; the offset applied being the negative of their average.

```
% Zero offset ground reactions
offset=(groundreaction(1,:)+groundreaction(noofframes,:))/2;
for i=1:6
    groundreaction(:,i)=groundreaction(:,i)-offset(i);
end
```

As the transducers in the force-plate are not precisely aligned to their axes, a sensitivity matrix is required to calculate the forces exactly and to convert the voltage outputs of the force plate transducers into Newton and Newton-metre readings of the actual forces and moments respectively. This matrix is supplied with the force plate by the manufacturer and is unique to it. The matrix elements were derived empirically, taking the form:

$$\begin{bmatrix} 1218.4 & 12.2 & -9.4 & 9.3 & 1.9 & -5.7 \\ -13.6 & 1232 & 4.1 & -2.8 & 2.7 & -2 \\ -33.6 & -6.8 & 1917.9 & 3 & 2.9 & 17.3 \\ 0.3 & -76.4 & -1.6 & 703.8 & 0.6 & -0.1 \\ 73 & -1.7 & 1.4 & 4 & 495.9 & -0.2 \\ 0.9 & 0 & 0.4 & 4.5 & -3.2 & 285.5 \end{bmatrix}$$

Each element 's_{ij}' of the matrix is adapted by an equation to compensate for gain 'G_j' and excitation voltage 'V_j' levels set by the user:

$$a_{ij} = \frac{500 s_{ij}}{V_j G_j}$$

For every sample taken, the excitation voltages for the six channels were set as follows, where 'F' and 'M' refer to forces and moments about the stated axis respectively:

F_z	F_x	F_y	M_z	M_x	M_y
20	20	10	20	20	20

The gains were set to:

F_z	F_x	F_y	M_z	M_x	M_y
500	500	500	500	200	200

The adjusted sensitivity matrix for these values is therefore:

$$\begin{bmatrix} 60.92 & 0.61 & -0.94 & 0.465 & 0.2375 & -0.7125 \\ -0.68 & 61.6 & 0.41 & -0.14 & 0.3375 & -0.25 \\ -1.68 & -0.34 & 191.79 & 0.15 & 0.3625 & 2.1625 \\ 0.015 & -3.82 & -0.16 & 35.19 & 0.075 & -0.0125 \\ 3.65 & -0.085 & 0.14 & 0.2 & 61.9875 & -0.025 \\ 0.045 & 0 & 0.04 & 0.225 & -0.4 & 35.6875 \end{bmatrix}$$

Each frame of ground reaction data was multiplied by this matrix in order to generate the force and moment readings required.

In order to calculate ground reaction moments acting on the ankle joints, the position of the joints relative to the centre of the force plate must be known. The force plate centre can be found by averaging the coordinate data for the four corners from the appropriate TSV file and subtracting the radius of the markers and the thickness of the material covering the force plate from the vertical value.

The talocrural joint position can be approximated as the ankle marker position offset by the vector $(0.0315i + 0.010j - 0.0235k)$. This vector was obtained by adapting equations from the Qualysis user manual and must be rotated to match the shank orientation.

In order to identify which foot steps on the force plate, the vertical ground reaction force is analysed to find the point where the reading first exceeds 100 N. The ankle marker position closest to the force plate centre at this frame is assumed to be attached to the foot stepping on the plate. The value of 100 N is high enough to avoid transient errors and low enough to function with data from the lightest individuals.

The cross product of the ground reaction forces with the vector distance from force plate centre to ankle joint added to the ground reaction moments gives the moment acting at the ankle joint.

As the equipment used to collect data in this format only included one force plate and therefore can only take readings from a single step, the ground reaction data must be duplicated for the other leg by offsetting the data by half a gait cycle with the assumption that ground reactions for each leg are symmetrical.

5.2.2 Angles, Angular Velocities and Angular Accelerations

The joint angle trajectories extracted from the QGT file, once converted into radians are used to calculate body segment angle trajectories:

```
Pelvis_Trajectory=Trajectories(:,2);
Body_Trajectory=-Trajectories(:,1)-Pelvis_Trajectory;
R_Thigh_Trajectory=Trajectories(:,3)+Pelvis_Trajectory;
R_Shank_Trajectory=-Trajectories(:,4)+R_Thigh_Trajectory;
R_Foot_Trajectory=Trajectories(:,5)+R_Shank_Trajectory;
R_Toes_Trajectory=R_Foot_Trajectory;
L_Thigh_Trajectory=Trajectories(:,7)+Pelvis_Trajectory;
L_Shank_Trajectory=-Trajectories(:,8)+L_Thigh_Trajectory;
L_Foot_Trajectory=Trajectories(:,9)+L_Shank_Trajectory;
L_Toes_Trajectory=L_Foot_Trajectory;
```

These files include no data for the toe angles, so they are assumed to match the foot angles. As the influence of the ground reactions is calculated relative to the ankle joint, limiting toe joint motion will have little effect.

The pelvis angle is included in the QGT file, so for a 2-dimensional model the other segment angles can be found by adding and subtracting the appropriate joint angles as above. It should be noted that in the case of the knee joint angles the z-axis is inverted so that flexion is positive.

The start and end of the angle trajectories are interpolated to produce a smooth transition when the cycle is repeated, as described in 7.4.2.

```
% Interpolate beginning and end
yi=interp1([1:4 9:12]',[Trajectories(noofframes-5:noofframes-2,:) ...
            Trajectories(3:6,:)],1:12,'spline');
Trajectories(noofframes-1:noofframes,:)=yi(5:6,:);
Trajectories(1:2,:)=yi(7:8,:);
```

Differentiating the trajectories generates the angular velocities and accelerations ('AngularVelocities' and 'AngularAccelerations') needed by the controller. Disregarding any physical limits, noise from the differentiation

can be eclipsed by raising the switching function co-efficient of the sliding-mode controller (see Chapter 7), but for practical purposes a low-pass filter with transfer function:

$$\frac{1}{0.0004s^2 + 0.04s + 1}$$

accompanied each differentiation.

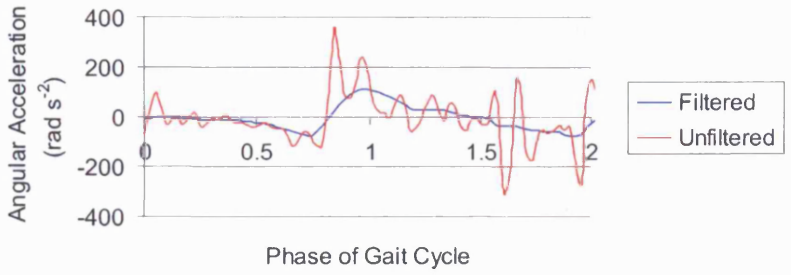

Figure 5.1: Filtered and unfiltered angular accelerations

Figure 5.1 shows the outcome of applying the 50Hz low-pass filter during differentiation. The most likely cause of the high frequency oscillation removed by the filter is wobbling of the skin markers.

5.2.3 Other Data Required

The initial conditions of the body segment positions are defined as the first frame of either the segment angles or orientation matrices depending on the number of dimensions of the model used.

The 12th thoracic marker is assumed to occupy approximately the same position as the centre of mass for the upper body. Its acceleration, found by differentiation, can therefore be used as an approximate for that of the upper body segment for reference by the controller. The initial velocity of the upper body centre of mass is found as the first frame of the differential of the marker position.

Mass and height are measured and recorded separately and stored in the data file for the model under the names 'TotalMass' and 'TotalHeight'.

A frequency of 120 Hz was used during motion capture, so the total time ('TotalTime') of the simulation is the number of frames examined divided by this frequency and multiplied by two (because the cycle is repeated). A

single time step (1/frequency) must then be subtracted from the total to take into account that the simulation begins at frame zero.

'StepSize' defines the model time step. According to the Nyquist rule, the simulation step frequency should be set to at least twice the maximum frequency of data input to model. EMG data is filtered at 500Hz (see section 3.3.4), and accordingly the model step frequency was set at four times this (to err on the side of generosity) giving a step size of 0.0005 seconds.

A final variable by the name of 'GaitPhase' gives the time values for every step of the simulation.

5.3 GCD

The GCD format is another common system for storing gait data. This format does not have a file type of its own as in the case of TSV and QGT; it is typically stored in files of type HTM.

The 'dlmread' command is used to copy the required data from the file with a space as the delimiter. However, files in GCD format often contain a variable length quantity of unnecessary data at the beginning, so the point at which the data falls into standard format must be identified manually as the number of the line on which '!Cadence 237' falls.

Data in GCD format is usually the average from both legs of a number of subjects and therefore provides only unilateral information. The data is used for the right leg and then offset by half a gait cycle for the left leg.

5.3.1 Ground Reactions

Ground reactions forces can be read in directly from lines 1738 to 1788 below the '!Cadence 237' line, but as there is no recording of marker or joint positions the moment cannot be calculated as it would be for TSV and _A.TSV files. Instead the moment calculated at the ankle is assumed to be entirely due to the ground reaction and is read from lines 958 to 1008 below '!Cadence 237'.

```
GroundReactions=dlmread(gcdhtm,' ',[cadence+1738,0,cadence+1788,2]);
TotalMass=sum(GroundReactions(:,3))*2/(9.81*51);
Momentz=dlmread(gcdhtm,' ',[cadence+958,0,cadence+1008,1])*TotalMass;
```

The mass of the subject is not included in the file, so it is found by averaging the vertical ground reaction for both feet over the 51 frames and dividing by gravitational acceleration (9.81 ms^{-2}).

The moments are normalised by division by the subject's mass, so they must be multiplied by the mass to find the result in Nm.

Offsetting for the left leg is carried out in the same way as for TSV files above as is repetition of the gait cycle to negate initial condition errors.

```
%Ground reactions
Force(:,1)=GroundReactions(:,1);
Force(:,2)=GroundReactions(:,3);
Force(:,5)=Momentz(:,1);
%Offset for other foot
Force(:,3)=[GroundReactions(27:51,1);GroundReactions(1:26,1)];
Force(:,4)=[GroundReactions(27:51,3);GroundReactions(1:26,3)];
Force(:,6)=[Momentz(27:51,1);Momentz(1:26,1)];
```

The order of: right leg forces, left leg forces, right leg moment, left leg moment is for convenience when organising the data in the model.

5.3.2 Angles, Angular Velocities and Angular Accelerations

Pelvis, hip knee and ankle data are read using the dlmread command and converted into radians.

```
Pelvis_Trajectory=-dlmread(gcdhtm,' ',[cadence+22,0,cadence+72,0])*pi/180;
Hip=dlmread(gcdhtm,' ',[cadence+178,0,cadence+228,0])*pi/180;
Knee=dlmread(gcdhtm,' ',[cadence+334,0,cadence+384,0])*pi/180;
Ankle=dlmread(gcdhtm,' ',[cadence+490,0,cadence+540,0])*pi/180;
```

The same processing is used to convert these joint angles into segment angles as for QGT data above except that with no data for the lumbar joint it is assumed that the body follows the same trajectory as the pelvis.

```
% Angles
Body_Trajectory=Pelvis_Trajectory;
R_Thigh_Trajectory=Hip+Pelvis_Trajectory;
R_Shank_Trajectory=-Knee+R_Thigh_Trajectory;
R_Foot_Trajectory=Ankle+R_Shank_Trajectory;
R_Toes_Trajectory=R_Foot_Trajectory;
L_Thigh_Trajectory=[Hip(27:51,1);Hip(1:26,1)]+Pelvis_Trajectory;
L_Shank_Trajectory=-[Knee(27:51,1);Knee(1:26,1)]+L_Thigh_Trajectory;
L_Foot_Trajectory=[Ankle(27:51,1);Ankle(1:26,1)]+L_Shank_Trajectory;
L_Toes_Trajectory=L_Foot_Trajectory;
```

Interpolation and differentiation are also carried out in the same way using identical commands.

5.3.3 Other Required Data

GCD format files carry less data than TSV and QGT files so some assumptions must be made. An average height of 1.70 m is assumed in the absence of any other information regarding height, gender or age.

Initial conditions of the body segment positions are defined as the first frame of the segment angles. No data is available for the motion of the 12th thoracic marker so a constant zero acceleration is assumed. However the initial forward velocity can be found in the file using:

```
TotalTime=dlmread(gcdhtm,' ',[cadence+2,0,cadence+2,0])*2;
InitialVelocity=[dlmread(gcdhtm,' ',[cadence+20,0,cadence+20,0])/1000,0];
```

The gait cycle is normalised to 51 frames so the total time ('TotalTime') is double the stride time.

'StepSize' and 'GaitPhase' are defined in the same way as for TSV files.

5.4 APM, EMG, FPL and KIN

APM, EMG, FPL and KIN files contain body parameters EMG readings, force plate outputs and kinematic marker position data respectively. Unfortunately, the format of the data precludes the use of MATLAB code to read in the data. Every useful numerical value is preceded by text, which prevents MATLAB commands such as 'dlmread' from functioning.

A word processor's find-replace command was used to extract all of the text and other non-essential characters from each file. This leaves a matrix in each file, which can be read using 'dlmread'.

A sample of the marker position format used in a KIN file before the unnecessary text is removed is shown below:

TIME 0.02 SECONDS

Number	Name	X (m)	Y (m)	Z (m)
1	R.Metatarsal Head V	0.238	0.192	0.025
2	R.Heel	0.072	0.216	0.033
3	R.Lateral Malleolus	0.125	0.189	0.062
4	R.Tibial Tubercle	0.152	0.232	0.415
5	R.Femoral Epicondyle	0.071	0.176	0.453
6	R.Greater Trochanter	-0.052	0.122	0.838
7	R.ASIS	-0.022	0.185	0.945
8	L.Metatarsal Head V	-0.407	0.356	0.042
9	L.Heel	-0.508	0.227	0.087
10	L.Lateral Malleolus	-0.483	0.327	0.117
11	L.Tibial Tubercle	-0.228	0.348	0.374
12	L.Femoral Epicondyle	-0.264	0.386	0.451
13	L.Greater Trochanter	-0.165	0.451	0.829
14	L.ASIS	-0.075	0.425	0.935
15	Sacrum	-0.225	0.242	0.936

5.4.1 Ground Reactions

The ground reaction data in the FPL file is sorted into alternate six channel vectors from the two force plates. The first step is therefore to rearrange these so that each column relates to only one channel:

```
groundreaction=[groundreaction(1:2:152,:),groundreaction(2:2:152,:)];
```

Examination must be made to identify which foot steps on which plate. Identification of the ankle marker closest to the first plate when the ground reaction signals from it rise over 100N is used to perform this.

Horizontal forces are multiplied by the sign of the difference between the sacrum marker end and start positions to account for the direction of motion.

Column four and five of the output matrix for each force plate contain the horizontal centre of pressure coordinates (vertical is always zero). The cross product of the ground reaction force readings in the first three columns with the distance from these coordinates to the talocrural joint of the ankle

TIME 0.02 SECONDS

Number	Name	X (m)	Y (m)	Z (m)
1	R.Metatarsal Head V	0.238	0.192	0.025
2	R.Heel	0.072	0.216	0.033
3	R.Lateral Malleolus	0.125	0.189	0.062
4	R.Tibial Tubercle	0.152	0.232	0.415
5	R.Femoral Epicondyle	0.071	0.176	0.453
6	R.Greater Trochanter	-0.052	0.122	0.838
7	R.ASIS	-0.022	0.185	0.945
8	L.Metatarsal Head V	-0.407	0.356	0.042
9	L.Heel	-0.508	0.227	0.087
10	L.Lateral Malleolus	-0.483	0.327	0.117
11	L.Tibial Tubercle	-0.228	0.348	0.374
12	L.Femoral Epicondyle	-0.264	0.386	0.451
13	L.Greater Trochanter	-0.165	0.451	0.829
14	L.ASIS	-0.075	0.425	0.935
15	Sacrum	-0.225	0.242	0.936

5.4.1 Ground Reactions

The ground reaction data in the FPL file is sorted into alternate six channel vectors from the two force plates. The first step is therefore to rearrange these so that each column relates to only one channel:

```
groundreaction=[groundreaction(1:2:152,:),groundreaction(2:2:152,:)];
```

Examination must be made to identify which foot steps on which plate. Identification of the ankle marker closest to the first plate when the ground reaction signals from it rise over 100N is used to perform this.

Horizontal forces are multiplied by the sign of the difference between the sacrum marker end and start positions to account for the direction of motion.

Column four and five of the output matrix for each force plate contain the horizontal centre of pressure coordinates (vertical is always zero). The cross product of the ground reaction force readings in the first three columns with the distance from these coordinates to the talocrural joint of the ankle

(found as for TSV files using as above) gives the joint moment due to ground reaction forces.

The frames covering one gait cycle need to be identified and isolated. To perform this the points where each vertical ground reaction first exceed 100N and first fall below 100N are identified.

```
% Find point where first ground reaction first exceeds 100N
j=0; a=0;
while j<1 ; a=a+1; j=groundreaction(a,3)>100; end

% Find point where first ground reaction falls below 100N
b=a;
while j==1 ; b=b+1; j=groundreaction(b,3)>100; end

% Find point where second ground reaction first exceeds 100N
j=0; c=0;
while j<1 ; c=c+1; j=groundreaction(c,9)>100; end

% Find point where second ground reaction is to be less 100N
d=c;
while j==1 ; d=d+1; j=groundreaction(d,9)>100; end
```

The start frame is identified as the first ground reaction to rise above 100N. The halfway point between the ground reaction rising over 100N and falling below it again is calculated as the sum of the two frame numbers divided by two. The number of the stop frame is calculated as twice the distance between the two halfway points plus the number of the start frame.

```
if c>a
    start=a;                % 'start' and 'stop' mark the beginning
    stop=a+(c+d)-(a+b);     % and end of the gait cycle that contains
else                        % ground reaction data for both feet.
    start=c;
    stop=c+(a+b)-(c+d);
end
```

However, ground reactions are only included for two steps. There are short periods at the beginning and end of the cycle where dual support phase ground reactions from one leg is not measured. To solve this the ground reaction forces and moments occurring outside the period from the start to stop frames are wrapped around, those before the start frame being offset to end at the stop frame and those after the stop frame beginning at the start frame.

```
if c>a
    GroundReactions(1:stop-start+1,[1:2,5])=Force([start:stop...
        -start+1,1:start-1],[1:2,5]);
    GroundReactions(1:stop-start+1,[3:4,6])=Force([stop+1:stop...
        +start,start+start:stop],[3:4,6]);
else
    GroundReactions([1:2,5],:)=Force([1:2,5],[stop+1:stop...
        +start,start+start:stop]);
    GroundReactions([3:4,6],:)=Force([3:4,6],[start:stop...
        -start+1,1:start-1]);
end
```

5.4.2 Angles, Angular Velocities and Angular Accelerations

Body segment angles are found using the marker positions. There are no thoracic or shoulder markers, so the upper body is assumed to follow the same angles as the pelvis.

Sacrum, right ASIS and left ASIS markers form a plane through the pelvis. The angle of this plane is therefore the angle of the pelvis.

Greater trochanter and femoral epicondyle markers give the thigh angle and the femoral epicondyle and ankle malleolus markers give the shank angle. It is assumed that when placed on a body in the anatomical position these markers form a vertical line.

Heel and metatarsal head markers should be placed on the body at the same vertical height from the floor and therefore can be used to find the foot angle.

Marker data is extracted from the KIN file in a matrix of three columns containing x-, y- and z-axis data. Every frame contains fifteen rows of data each relating to one marker, so to find all of the data for one marker every fifteenth row of data is needed

```
righttoemarker=kinematics([1:15:noofframes*15],:);
rightheelmarker=kinematics([2:15:noofframes*15],:);
rightanklemarker=kinematics([3:15:noofframes*15],:);
rightkneemarker=kinematics([5:15:noofframes*15],:);
righttrochmarker=kinematics([6:15:noofframes*15],:);
rightasismarker=kinematics([7:15:noofframes*15],:);
lefttoemarker=kinematics([8:15:noofframes*15],:);
leftheelmarker=kinematics([9:15:noofframes*15],:);
leftanklemarker=kinematics([10:15:noofframes*15],:);
leftkneemarker=kinematics([12:15:noofframes*15],:);
lefttrochmarker=kinematics([13:15:noofframes*15],:);
leftasismarker=kinematics([14:15:noofframes*15],:);
sacrummarker=kinematics([15:15:noofframes*15],:);
```

The inverse tangent function can then be used to find the appropriate angles:

```
Pelvis_Trajectory=-atan(((rightasismarker(:,3)+leftasismarker(:,3))/2...
    -sacrummarker(:,3))./((rightasismarker(:,1)+leftasismarker(:,1))/2...
    -sacrummarker(:,1)));
```

The data is trimmed to the start and stop frames and differentiated to find the angular velocities and accelerations.

5.4.3 Other Required Data

In the absence of a thoracic marker, the sacrum marker data is substituted to find the body acceleration and initial velocity.

The mass is read from the APM file and 'TotalTime', 'StepSize' and 'GaitPhase' are calculated as normal.

Dividing the default model height of 1.75m (the height of the default simulated individual represented by the model, not the average subject height used in section 5.3.3) by the sum of the distances from hip to knee and knee to ankle (0.85m) and multiplying by the same distances from the APM file (averaged for the two legs) generates 'TotalHeight' based on the assumption that subject and model are proportionally similar.

```
TotalHeight=(1.75/0.85)*sum(parameters([3,4,7,8]))/2;
```

Data in the EMG file is read as a single vector, so must be reordered by muscle. Eight muscles are involved so every eighth element must be extracted for each one. The names of each muscle are included in a separate matrix for clarity.

```
% Reorder EMG signals into a more organised form
Muscles=['Erector Spinae    ';'Gluteus Maximus   ';'Gluteus Medius    ';...
         'Hamstrings        ';'Rectus Femoris    ';'Adductor Longus   '; ...
         'Tibialis Anterior';'Triceps Surae     '];

for i=0:8:(noofframes-1)*8
    EMG(i/8+1,:)=muscleactivity(i+1:i+8,1)';
end
```

5.5 C3D, DAT and XLS

C3D files can be converted into TSV, _A.TSV and QGT files using the Qualisys software. Those files can then be processed by the code described above.

The DAT files processed contained filtered EMG data from the acquisition in the Leicester General Hospital. Data extracted from them could then be

reordered by muscle and interpolated as necessary for comparison with model outputs. Data files are prepared separately from TSV, _A.TSV and QGT files as many of the samples do not include EMG readings.

XLS files obtained from the web contain data from other file types converted into a form which any user can easily access and read without specialist software. This data was either converted into appropriate file types for processing or processed manually.

5.6 Summary

File types are created with different purposes in mind, so it is inevitable that they will contain different data to one another. No single file type or group of file types described here contains all of the information ideally required by the model, so assumptions and approximations are used in every case. For the most part these will have little impact as their effect is indirect and limited. However, a set of minimum conditions is required for simulation:

- Pelvis, thigh, shank and foot angle trajectories.
- Ground reaction forces and some means of calculating the moment arm at the ankle

From these, every other value can be calculated, approximated or assumed with only minor effect to the driving moments of the controller.

EMG readings are not necessary to run a simulation but are required for comparison with the muscle activation outputs of the model.

Chapter 6

The Neuro-Musculo-Skeletal Model

6.1 Introduction

A forward dynamics approach was used to model the neuromusculoskeletal system incorporating ten segments moving in the sagittal plane about pin joints, all of which have internal friction values independent of velocity. Only those muscles having a significant effect on the flexion/extension of any of the joints were used in the model.

The model was constructed chiefly within the *Simulink* environment of the *MATLAB* computing and programming application. MATLAB is a high-level programming tool for describing and solving static and dynamic systems. Simulink is a graphical user interface (GUI) for the MATLAB programming language, which allows the construction of simulation models in the form of block diagrams.

Use was made of both the simplicity and convenience of the Simulink user interface, as well as the power of the raw MATLAB language to produce the model.

6.2 2 Dimensions or 3 Dimensions

A 3-dimensional model would be preferable as normal human gait involves a lateral sway as the centre of mass shifts towards the weight bearing leg as well as a lateral roll of the foot against the ground. Figure 6.1 shows a typical example of the frontal plane motion of the centre of mass for a normal subject over one gait cycle. The range of motion seems small (less than 5

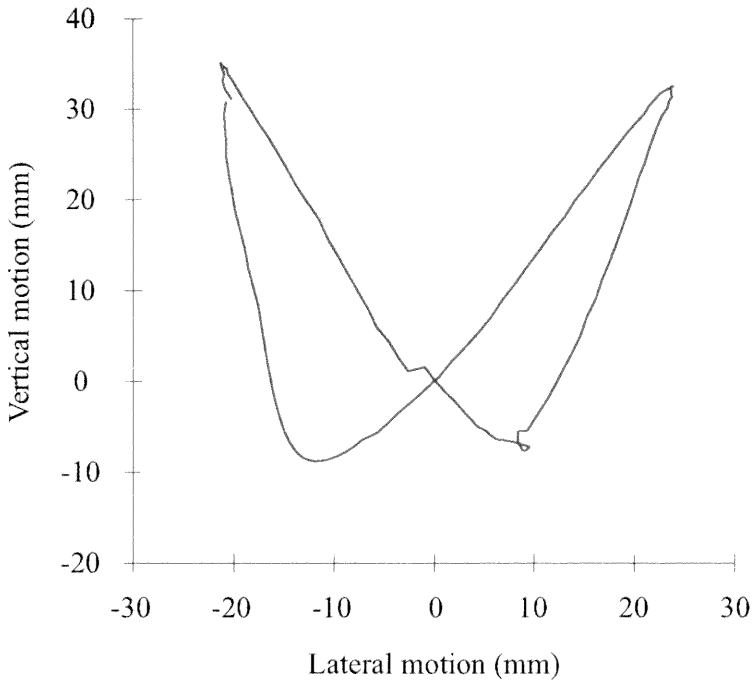

Figure 6.1: Frontal plane motion of the twelfth thoracic vertebra of a normal subject during gait at a cadence of 103 steps min^{-1} with a stride length of 1.4 m.

cm compared to the forward motion, which in this case was 1.4 m) but it is significant to the balance of the subject.

Figure 6.1 is a view from behind the subject with the direction of gait being into the paper. Values are given relative to the zero point of the motion tracking system. The data represented is part of a sample that was collected as described in chapter 5.

Many pathological gait patterns involve a more pronounced lateral motion that is likely to be asymmetric. Intuitively, pathological gait cannot be symmetrical unless the pattern of abnormality in nerve and muscle is at least approximately symmetrical.

To maintain balance during gait, the torso shifts laterally over the weight bearing (stance phase) leg. The longer the stance phase, the closer the centre of mass must move towards a position above the centre of pressure with the ground. If an asymmetry causes a difference in the length of the stance phase for each leg then a non-symmetrical lateral motion will result.

The lateral roll of the foot against the ground can also be important in pathological gait as it can play a part in trips, falls, twisted ankles etc. The

peroneus muscles in particular act almost entirely in the frontal plane and are the chief evertors of the foot. Failure of these muscles increases the risk of those injuries.

The forces on the knee, ankle and toe joints in the axes other than their axis of rotation could also be examined using a 3-dimensional model. This would be useful for confirming that the stimulated gait patterns will not cause discomfort to a real subject.

Ultimately it was decided that the model would be limited to 2-dimensions as a 2-dimensional model would be simpler to design and build and faster both to build and to run.

Constraining the knee, ankle and toe joints to their appropriate axes of rotation in a 3-dimensional model is difficult to achieve without dramatically slowing the running speed of the model. Applying extra equations to absolutely constrain the motion to one axis of rotation increases the size of the operating matrix, which slows the model. Absolute constraints in this form can also cause the matrix to become singular if they interfere with the ground reactions. Alternatively, applying forces opposing motion in unwanted axes tends to reduce the integration step size to unacceptably small values.

Vertical and horizontal ground reactions are needed that allow the segments to roll, that provide friction to restrain sliding and that prevent movement into the ground but allow the feet to lift off it. These must be applied to all of the foot and toe segments and must not interfere either with each other or with the joint constraints under any conditions. If this happens, a positive feedback loop can be generated with exponentially increasing forces needed to maintain the constraints, driving the operating matrix towards singularity.

Many models do not include a foot segment or fix one or both feet to the ground for all or part of the simulation period [25, 67]. This avoids the transition from swing to stance, which is essential for a practical simulation [38] .

Walking motion is primarily restricted to the sagittal plane particularly in the case of individual limbs. The lateral movement of the foot relative to the hip during normal gait is very small. In the example shown in figure 6.2 the range of lateral motion for the toe marker is 72 mm. The maximum vertical distance between the ASIS (front of hip) and toe joint markers for the sample period was 0.992 m (Figure 6.3). Assuming the knee does not

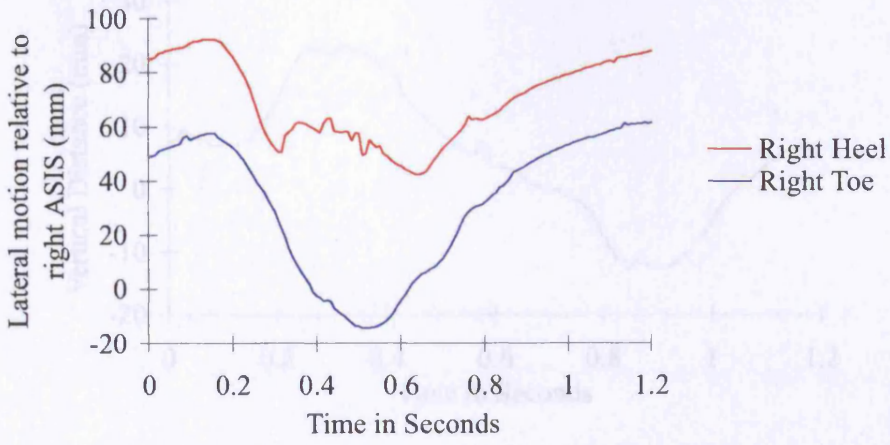

Figure 6.2: Motion of the right heel and toe markers relative to the right ASIS marker in the y-axis over 1 gait cycle for a normal subject walking at a cadence of 103 steps min^{-1} with a stride length of 1.4 m.

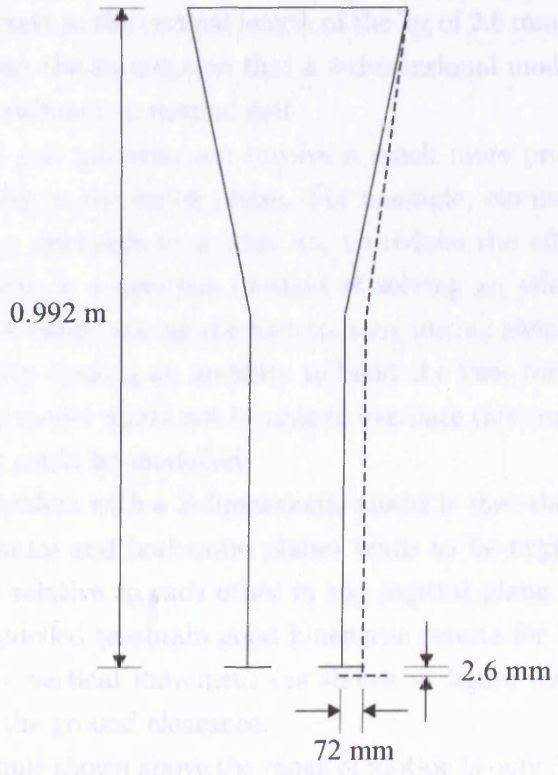

Figure 6.3: Effective leg extension produced by lateral motion of the foot relative to the hip. This diagram is not a representation of the body's frontal plane motion during gait.

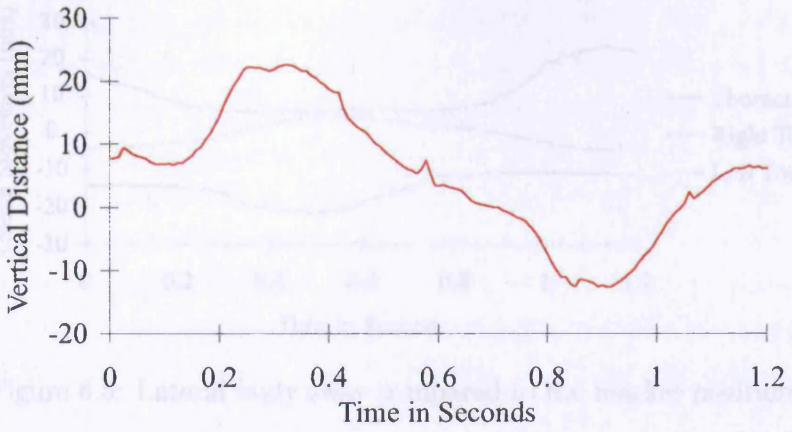

Figure 6.4: Vertical difference between right and left ASIS during gait at a cadence of 103 steps min^{-1} with a stride length of 1.4 m. The offset is due to an offset in the marker positioning.

bend in the frontal plane, the lateral movement of the foot produces an effective contraction in the vertical length of the leg of 2.6 mm. This negligible contraction allows the assumption that a 2-dimensional model can provide a reasonable approximate to normal gait.

Pathological gait patterns can involve a much more pronounced lateral motion, especially in the swing phase. For example, circumduction (where the leg is swung outwards in a wide arc to reduce the effective length in the sagittal plane) is a common method of solving an effective leg length discrepancy (foot drop causing the foot to hang during swing phase or weak hamstring activity causing an inability to bend the knee for example) [112]. A 2-dimensional model would not be able to simulate this correctly but other gait pathologies could be modelled.

The main problem with a 2-dimensional model is that the rotation of the pelvis in the frontal and horizontal planes tends to be neglected [38]. The hip joints move relative to each other in the sagittal plane during gait and this must be modelled to obtain good kinematic results for both legs. Most important is the vertical movement (as shown in figure 6.4) as this has a direct effect on the ground clearance.

For the example shown above the range of motion is only 3 cm, but during the swing phase, the minimum ground clearance is approximately 1.29 cm [85]. Without taking this into account, the margin for error in the ground clearance will be significantly distorted over most of the gait cycle.

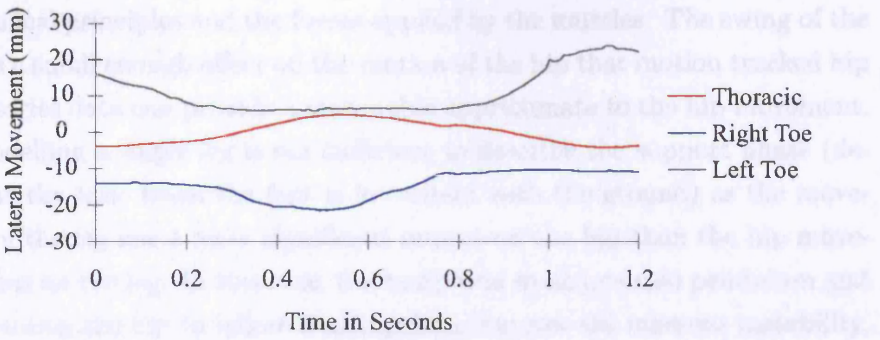

Figure 6.5: Lateral body sway compared to toe marker position.

Evolution has optimised human gait to minimise as far as possible the energy use when walking. Minimum metabolic energy used per unit distance travelled can therefore be used as a measure of walking performance [2]. Lateral sway during gait is therefore also close to optimal. The walking base (the side to side distance between the footprints, usually measured at the midpoints of the heels) for normal gait is usually in the range 50-100 mm ([112] p. 131). Compare this to a total range of upper body lateral sway of about 46 mm [84]. All this suggests a simple and predictable oscillation where the centre of mass approaches a stable point above the centre of pressure before being allowed to swing back towards the other leg (Figure 6.5). In figure 6.5 the thoracic marker appears to be offset to the left. This can be caused by inaccurate marker placement, a minor gait deviation or a slight physical asymmetry, the precise reason can easily be found by closer examination of the subject and/or gait pattern.

6.3 Skeletal Model

Central to the biomechanical model is the skeleton and its dynamics. The dynamic equations used simulate the motion of the limbs based on the forces and moments applied by the muscles and the ground.

6.3.1 Dynamic Model Segments Required

Modelling of a single leg is an extremely useful way of simulating the swing phase of gait. The swing phase is defined as the period when the foot of the leg being studied is not in contact with the ground. The motion of the hip is provided from motion tracking data and the leg swings based on its

mechanical principles and the forces applied by the muscles. The swing of the leg has a small enough effect on the motion of the hip that motion tracked hip trajectories data can provide a reasonable approximate to the hip movement.

Modelling a single leg is not sufficient to describe the support phase (defined as the time when the foot is in contact with the ground) as the movement of the leg has a more significant impact on the hip than the hip movement has on the leg. In this case, the body acts as an inverted pendulum and constraining the hip to follow tracking data removes the inherent instability, which it is the aim to control. For this reason, it is necessary to produce a model of both legs with a pelvis segment between them.

Many investigators model the pelvis and torso as a single segment [25, 59, 60, 67, 89, 90], however in doing so the interactions between thigh and pelvis will be distorted by the need to keep the torso upright at the expense of the pelvis angle [38]. Muscle behaviour around the hip will be changed, as it is dependent on the muscle length and therefore the joint angle [85, 119]. The ligament that restrains hyperextension of the leg is also dependent on the joint angle between pelvis and thigh [85] and would therefore influence the gait pattern if the pelvis cannot tilt. This may be acceptable in a model concerned only with ankle and foot behaviour, but this model is concerned with the entire leg and therefore requires a separate upper body segment.

The model comprises torso and pelvis segments as well as two legs, each with thigh, shank, foot and toe segments as shown in figure 6.6. The toe segment is modelled independently of the foot to generate more accurate toe-off results.

6.3.2 Motion Dynamics

The motion dynamics form the heart of the model, describing how the body moves based on the moments and forces produced by the musculotendon units, the ligaments, the ground reactions and gravity.

The motion dynamics of the model were developed from LaGrange's equations. The generalised model described by the equations below was developed and can be used to model the behaviour of any similar segmented, ball-jointed or pin-jointed system. It can be applied in 2 or 3 dimensions and calculates the acceleration of the first segment centre of mass and the angular accelerations of all of the segments based on the generalised forces acting.

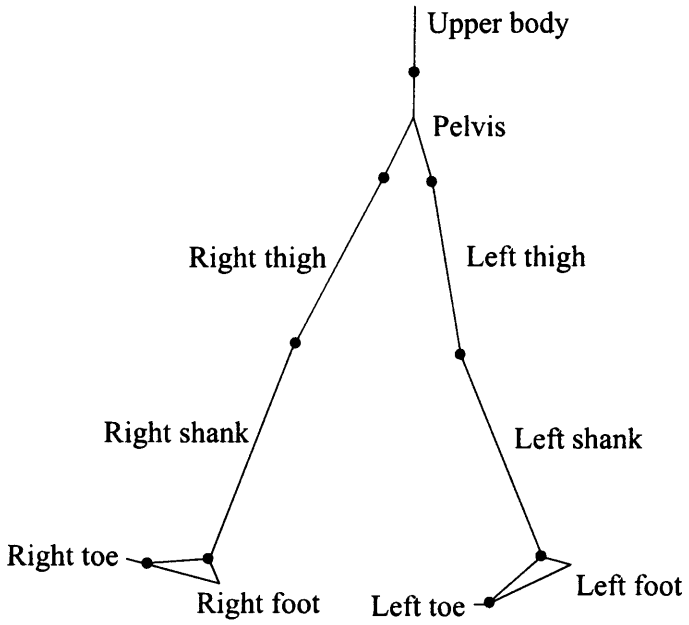

Figure 6.6: Stick figure of the body segments.

$$\sum_{i=1}^{n} m_{c,i} a_{c,i} = \sum_{i=1}^{n} F_{c,i} \tag{6.1}$$

$$\begin{aligned} I_{c,j}\dot{\omega}_{c,j} - \sum_{i=j}^{n}(r_{c,j} \times (m_{c,i}a_{c,i} - F_{c,i})) + \sum_{k=c}^{b_j}\sum_{i=j+1}^{n}(d_{c,j} \times (m_{k,i}a_{k,i} - F_{k,i})) \\ = \sum_{k=1}^{b_j}\sum_{i=j+1}^{n}((r_{k,j} - d_{k,j}) \times F_{k,i}) + \sum_{i=j}^{n}(\omega_{c,j} \times (r_{c,j} \times m_{c,i}v_{c,i})) \\ - \sum_{k=c}^{b_j}\sum_{i=j+1}^{n}(\omega_{c,j} \times (d_{k,j} \times m_{k,i}v_{k,i})) + d_{Fj} \times F_{c,j} \end{aligned} \tag{6.2}$$

$$p_{c,i+1} = p_{c,i} + d_{c,i} - r_{c,i+1} \tag{6.3}$$

$$v_{c,i+1} = \dot{p}_{c,i+1} = v_{c,i} + \omega \times d_{c,i} - \omega \times r_{c,i+1} \tag{6.4}$$

$$a_{c,i+1} = \dot{v}_{c,i+1} = a_{c,i} + \dot{\omega} \times d_{c,i} + \omega \times (\omega \times d_{c,i}) - \dot{\omega} \times r_{c,i+1} - \omega \times (\omega \times r_{c,i+1}) \tag{6.5}$$

- n is the number of segments along the branch in question.
- j is the current segment.
- c is the current limb.
- m is the segment mass.
- I is the segment moment of inertia.

- p is the centre of gravity of the current segment.
- v is the velocity of the centre of gravity of the current segment.
- a is the acceleration of the centre of gravity of the current segment.
- ω is the angular velocity of the current segment.
- r is the position of the proximal joint relative to the centre of mass.
- d is the position of the distal joint of the branch in question relative to the centre of mass.
- dF is the point about which the forces and moments act relative to the centre of mass.
- F and M are the forces and moments respectively acting on the segment.
- b_j is the number of distal joints on the segment (=1 except for the pelvis).

The motion dynamics based on these equations follow the form:

$$f = Ma$$

- f is a vector of the forces and moments applied as well as any effects due to angular velocities and positions.
- M is a 12*12 mass and moment of inertia matrix.
- a is a vector of the x-axis and y-axis accelerations of the first segment and the angular accelerations of all of the segments.

Rearranging this equation allows the accelerations to be calculated from the forces and moments acting on the body.

$$a = M^{-1}f$$

The velocities and positions of the segments can then be found by integration.

The system is not based around the joint angles, as errors would be cumulative from one segment to the next. Instead, segment angles, angular velocities and angular accelerations are calculated relative to the zero axes.

Testing the model

Any large model requires a considerable debugging procedure.

Initial tests of the motion dynamics involved developing 2 and then 3 segment models using the same equations described in section 6.3.2. In this way, the fundamental validity of the equations could be tested before expanding the system to a full sized model.

Having confirmed the system's principles with these tests on two and three segment models a full 10-segment model was created and similar tests applied in order to validate and debug the system. A selection of test results are presented in Tables 6.1 to 6.3 (N.B. where the zero time results offer no useful additions to the data they are not included in the tables).

Null test: no input forces or moments, zero initial velocities. No motion is expected during the null test regardless of how long the simulation lasts.

Gravity test 1 (G1): constant vertical acceleration of -9.81ms-2, zero initial conditions.

Gravity test 2 (G2): constant vertical acceleration of -9.81ms-2, zero initial velocities, various segment alignments tested. Initial segment angles of [0.1 -0.5 -0.8 0.2 0.6 -0.8 -0.3 -0.1 -0.5 -0.2] radians are demonstrated in Table 6.1.

Gravity test 3 (G3): different strengths and directions of gravity examined. Test G3 demonstrates changing the gravity of G2 to [-12 5] ms^{-2}

Gravity test 4 (G4): a selection of initial angular and lateral velocities introduced. Segment angular velocities of [0 0.5 -0.8 1.2 3 -1.5 0.6 0.2 0.4 -0.8] rad s^{-1} and upper body segment lateral velocity of [1.2 -0.5] ms^{-1} are introduced to change test G3 to G4. No expected angular velocity data is included in test G4 in Table 6.1 as such a prediction would require the construction of a second model to map the complex interactions of the segments relative to each other.

In each gravity test, the constant acceleration equations:

$$v = u + at$$

and

$$x = ut + \frac{1}{2}at^2$$

were used to confirm that the average position and velocity of the simulated segments was as expected at the halfway point and end of each simulation.

Where zero initial velocities were set, the segment alignment was expected to remain the same, otherwise the parallel axis theorem:

$$I_t = \sum I_{segment} + m_{segment} r^2_{segment}$$

Test	Time (s)		x_t (m)	v_t (ms^{-1})	ω_t ($^cs^{-1}$)	$I_t\omega_t$ (Nms)	$\sum \frac{1}{2}mv^2$ (J)
Null	0.5	Expected	[0 0]	[0 0]	0	0	0
		Simulated	[0 0]	[0 0]	0	0	0
	1	Expected	[0 0]	[0 0]	0	0	0
		Simulated	[0 0]	[0 0]	0	0	0
G1	0.5	Expected	[0 -1.226]	[0 -4.905]	0	0	926.5
		Simulated	[0 -1.226]	[0 -4.905]	0	0	926.5
	1	Expected	[0 -4.905]	[0 -9.81]	0	0	3706
		Simulated	[0 -4.905]	[0 -9.81]	0	0	3706
G2	0.5	Expected	[0 -1.226]	[0 -4.905]	0	0	926.5
		Simulated	[0 -1.226]	[0 -4.905]	0	0	926.5
	1	Expected	[0 -4.905]	[0 -9.81]	0	0	3706
		Simulated	[0 -4.905]	[0 -9.81]	0	0	3706
G3	0.5	Expected	[-1.5 0.625]	[-6 2.5]	0	0	1627
		Simulated	[-1.5 0.625]	[-6 2.5]	0	0	1627
	1	Expected	[-6 2.5]	[-12 5]	0	0	6508
		Simulated	[-6 2.5]	[-12 5]	0	0	6508
G4	0	Expected	[0 0]	[1.257 -0.485]	-	-1.975	71
		Simulated	[0 0]	[1.257 -0.485]	-0.232	-1.975	71
	0.5	Expected	[-0.871 0.382]	[-4.743 2.015]	-	-1.975	1024
		Simulated	[-0.871 0.382]	[-4.743 2.015]	-0.263	-1.975	1024
	1	Expected	[-4.743 2.015]	[-10.74 4.515]	-	-1.975	5230
		Simulated	[-4.743 2.015]	[-10.74 4.515]	-0.292	-1.975	5230

Table 6.1: Motion dynamics test samples: Null, G1, G2, G3 and G4. Data included are the centre of mass position (x_t), centre of mass velocity (v_t), angular velocity (ω_t) and angular momentum ($I_t\omega_t$) for the system and the sum of the kinetic energy due to the lateral motion of each segment ($\sum \frac{1}{2}mv^2$).

can be used to find the total angular velocity (I_t) of the system from an angular momentum calculation:

$$I_t\omega_t = \sum I_{segment}\omega_{segment} + m_{segment}r_{segment}v_{segment}$$

where I is the moment of inertia, m is the mass, r is the distance from the centre of gravity of the segment to the centre of gravity of the model and v is the velocity of the segment perpendicular to the line of r.

In the absence of any external forces this system angular momentum ($I_t\omega_t$) will remain constant, but where an external force (F) is applied, the angular momentum will change according to the force and the position of the centre of mass relative to the point of application (d):

$$I\omega = \int (F \times d)dt$$

Angular and lateral velocity test 1 (A1): the simulated model was made to spin at various speeds about the centre of mass without joint movement by applying appropriate initial velocities and angular velocities to each of the segments. The centres of mass must be arranged in a straight line to avoid joint motion caused by centrifugal force. Test A1 in Table 6.2 shows the result of spinning the model at 1 rad s^{-1}. As expected, all values remain constant. A lateral kinetic energy greater than zero results despite the fact the centre of mass of the system does not move as the segments are moving relative to each other.

Angular and lateral velocity test 2 (A2): by changing the initial velocity of the above test the model would spin as before, but a lateral component would be added to the movement of the system causing the velocity and lateral kinetic energy increase of A2 over A1 seen in Table 6.2.

Angular and lateral velocity test 3 (A3): the simulated model was spun without the lateral component but under the influence of gravity generating an increasing velocity and lateral kinetic energy (Table 6.2).

Force test 1 (F1): the rotation and lateral motion and velocities of the model are examined when a force of 100 N is applied horizontally to the upper body segment. The results can be seen in Table 6.3.

Force test 2 (F2): forces of $[-100sin(t)0]$ and $[080sin(t)]$ were applied to the pelvis and right shank segments respectively and the resulting motion examined and displayed in Table 6.3.

Test	Time (s)		v_t (ms^{-1})	ω_t ($^cs^{-1}$)	$I_t\omega_t$ (Nms)	$\sum \frac{1}{2}mv^2$ (J)	$\sum \frac{1}{2}I\omega^2$ (J)	$\frac{1}{2}I_t\omega_t^2$ (J)
A1	0.5	Expected	[0 0]	1	9.461	4.414	0.3164	4.73
		Simulated	[0 0]	1	9.461	4.414	0.3164	4.73
	1	Expected	[0 0]	1	9.461	4.414	0.3164	4.73
		Simulated	[0 0]	1	9.461	4.414	0.3164	4.73
A2	0.5	Expected	[0 0.1]	1	9.461	4.799	0.3164	4.73
		Simulated	[0 0.1]	1	9.461	4.799	0.3164	4.73
	1	Expected	[0 0.1]	1	9.461	4.799	0.3164	4.73
		Simulated	[0 0.1]	1	9.461	4.799	0.3164	4.73
A3	0	Expected	[0 0]	1	9.461	4.414	0.3164	4.73
		Simulated	[0 0]	1	9.461	4.414	0.3164	4.73
	0.5	Expected	[0 -4.905]	1	9.461	930.9	0.3164	4.73
		Simulated	[0 -4.905]	1	9.461	930.9	0.3164	4.73
	1	Expected	[0 -9.81]	1	9.461	3710	0.3164	4.73
		Simulated	[0 -9.81]	1	9.461	3710	0.3164	4.73

Table 6.2: Motion dynamics test samples: A1, A2 and A3. Data included are the system velocity (v_t), angular velocity (ω_t) and angular momentum ($I_t\omega_t$), the segment lateral ($\sum \frac{1}{2}mv^2$) and rotational ($\sum \frac{1}{2}I\omega^2$) kinetic energies and the system rotational kinetic energy ($\sum \frac{1}{2}I_t\omega_t^2$).

Test	Time (s)		v_t (ms^{-1})	ω_t ($^cs^{-1}$)	$I_t\omega_t$ (Nms)	$\sum \frac{1}{2}I_t\omega_t^2$ (J)	$\frac{1}{2}I_t\omega_t^2$ (J)
F1	0.5	Expected	[0.649 0]	1.575	13.39	16.23	42.18
		Simulated	[0.649 0]	1.575	13.39	16.23	42.18
	1	Expected	[1.298 0]	2.289	18.66	64.92	18.66
		Simulated	[1.298 0]	2.289	18.66	64.92	18.66
F2	0.5	Expected	[-0.093 -0.1]	-0.016	-0.104	0.715	0.001
		Simulated	[-0.093 -0.1]	-0.016	-0.104	0.715	0.001
	1	Expected	[-0.239 -0.057]	-0.614	-2.949	2.319	0.906
		Simulated	[-0.239 -0.057]	-0.614	-2.949	2.319	0.906

Table 6.3: Motion dynamics test samples: F1 and F2. Data included are the system velocity (v_t), angular velocity (ω_t), angular momentum ($I_t\omega_t$) lateral kinetic energy ($\sum \frac{1}{2}m_tv_t^2$) and rotational kinetic energy ($\sum \frac{1}{2}I_t\omega_t^2$).

These tests are designed to examine the functioning of the mathematical components of the model and confirm the viability of the model to simulate a 10 segment pin-jointed system in the form of a human body.

6.3.3 Skeletal Parameters, Joints and Ligaments

A set of parameters defining the masses, moments of inertia and relative positions of joints and centres of mass is used for each of the segments. These can be adjusted as necessary to individualise the model. Data from a variety of sources using cadaver measurements of these features were averaged to provide the set of default parameters used in the model [21, 68, 85] (Appendix C).

The motion dynamics equations can simulate other systems that involve rigid segments connected by pin joints in 2 dimensions or ball and socket joints in three dimensions. Any number of limbs can be modelled and any number of segments. Further development of the equations could also allow for non-rigid segments and more complex joints.

A small amount of damping is applied to the joints to simulate internal friction effects. A figure of 0.5 Nms rad-1 taken from data in the literature [102] is applied to all of the joints as an approximation.

During normal motion, the limit to the angles the joints can cover is not reached except for the extensions of the hip and knee joints. In these cases, the minimum joint angle is a very important feature during gait. Most gait patterns rarely come close to the other joint limits, especially patterns caused by muscle activation failures, as a lot of force is needed to overcome the passive resistance to stretching of the muscles across the joints before the angle limits can be reached.

Regression equations taken from the literature [85] are used to model the behaviour of the hip and knee ligaments that limit hyperextension.

The equations are:

$$M_{Hip} = 54.1 \times e^{-0.111 \times (-\theta_{Hip} \times \frac{360}{2\pi} - 9.96)}$$

$$M_{Knee} = 30.2 \times e^{-0.207 \times (-\theta_{Knee} \times \frac{360}{2\pi} - 0.03)}$$

M represents the moments generated and θ is the joint angle.

They produce angle dependant moments that oppose hyperextension of the hip and knee. This provides a simple and effective way of constraining the joint angles.

6.4 Musculotendon model

There are two main aspects to muscle dynamics; the activation dynamics, which describe the excitation of muscle tissue in response to neural or FES stimulus, and the contraction dynamics, which describe the forces generated by a muscle under the level of excitation specified and the conditions given.

6.4.1 Activation Dynamics

The activation dynamics describe the chemical response of the muscles to an electrical signal. This begins with the release of Ca^{2+} ions into the muscle fibres causing the breakdown of ATP, which provides energy to activate the cross-bridges between the myosin and actin filaments and thus generate force (see Chapter 2). The effect is of a low pass filter between the neural excitation signal and the muscle fibre activation level, delaying the rise and fall of the signal. This behaviour was approximated by a first-order equation [85]:

$$\frac{da(t)}{dt} = 41.67(u(t) + 1)(u(t) - a(t))$$

The neural input signal is represented by $u(t)$ and the activation by $a(t)$.

Activation dynamics can vary from muscle to muscle particularly in the case of muscles formed largely of slow twitch fibres compared to those comprising mainly fast twitch fibres. However, attempting to accurately measure and model the activation dynamics of every muscle of each subject is impractical. The general approximation above is therefore used for all of the muscles.

6.4.2 Contraction Dynamics

The contraction dynamics are the heart of each muscle, describing the force produced based on the level of activation and the conditions under which the muscle is acting. A Hill-type musculotendon actuator model (Figure 6.7) simulates this as a contractile element with parallel and series elastic elements [24, 44, 120, 119]. No allowance is made for differences in fibre types by this model.

The Hill-type model is built around four relationships. A stress-strain curve describes the spring-like behaviour of the tendon (Figure 6.8). The relationship is linear with a gradient of 37.5 Nm^{-2} except in the toe region.

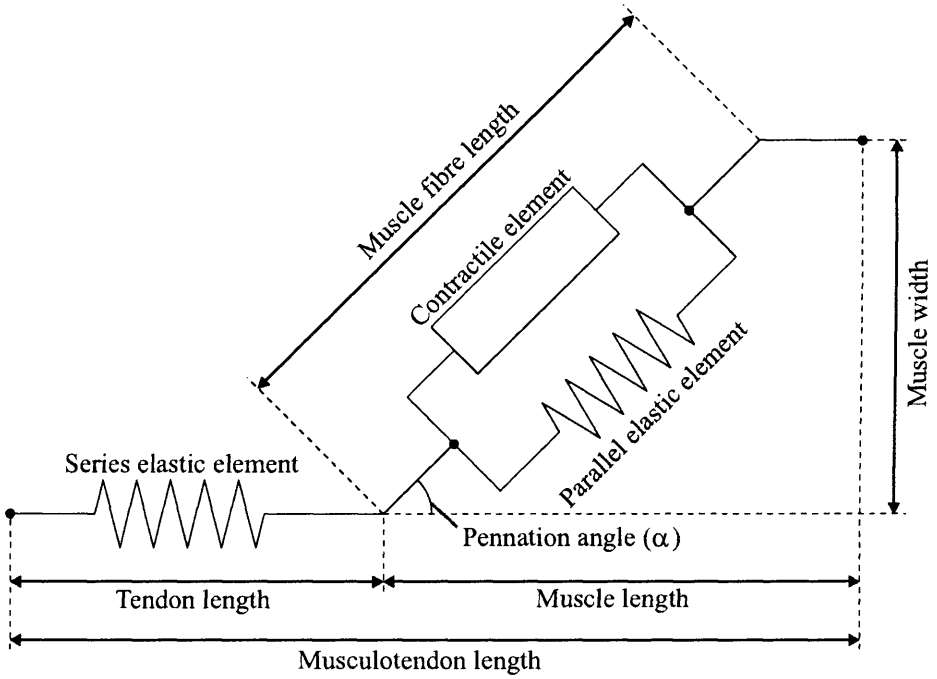

Figure 6.7: Hill-type musculotendon model.

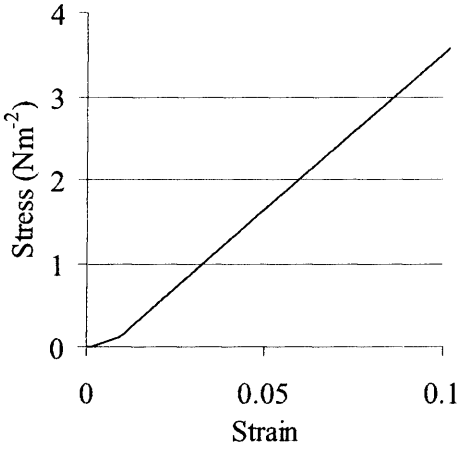

Figure 6.8: Tendon stress-strain relationship.

No provision is made for tendon failure under excessive force, as the model does not aim to simulate injuries. Differences in muscle fibre types are not taken into account (2.3.2). As gait does not involve long postural activations or fast powerful contractions, which could require more precise modelling, it is assumed that all of the muscles simulated respond to stimuli in the same way. Fatigue can also be neglected as few gait cycles are involved.

The pennation angle (α) is the angle of the muscle fibres to the line of the muscle.

The passive element models the resistance of the muscle to stretching beyond the optimal fibre lengths [24, 44, 120, 119]. It represents the elasticity of the connective tissue sheaths around the fibres. The force generated is a function of the muscle fibre length and is independent of muscle stimulation (Figure 2.15).

The remaining two relationships involve the contractile element of the muscle.

The force-length characteristic of muscle fascicles is related to the overlap of the actin and myosin filaments [112]. With too small an overlap, few cross-bridges can form and therefore little force can be generated. With too large an overlap there is not enough space for the muscle to contract further. In either case the amount of force that can be generated drops off (Figure 2.15). The contractile force is also a linear function of the activation.

A force-velocity relationship also occurs within the contractile element of the muscle. Greater forces can be generated when muscles are being stretched than when they are shortening (Figure 2.16) [41, 112, 120].

6.4.3 Parameters and Normalisation

The musculotendon model is normalised so that a set of four parameters can be used to scale it to simulate the behaviour of any muscle.

Contraction in muscle fibres occurs as a change in the overlap of many bands of actin and myosin filaments arranged in sarcomeres along the length of the fibre (Chapter 2) [41, 112]. The longer the fibre, the more bands of these filaments are present, so contraction occurs in the same way regardless of fibre length. This makes the *optimal fibre length* a useful starting point in the normalisation process and all lengths are calculated relative to it [24, 44, 119, 120].

The *tendon slack length* (the length of the tendon when no force is applied) must be known to find the strain acting on it (the strain is the extension divided by the original length), which relates to the energy stored in it.

Muscle fibres are often arranged at an angle to the line of action of the muscle [24, 44, 119, 120]. The maximum force generated by the muscle is therefore related to the cosine of this *pennation angle.*

The final parameter needed is the *maximum isometric force* that the muscle can generate, which is the maximum force that can be generated with no change in muscle length.

Parameters for 43 muscles were obtained from the ISB website [21]. These describe all of the significant muscles in the right leg for a generic, normal individual. For the left leg of the model, the muscles used in the right leg are reflected.

The parameters were found by averaging incision measurements from human cadaver samples from various sources [8, 21, 22, 24, 33, 113]. In the case of the maximum force potential, an indirect method is required, as live muscles are required to generate accurate results. However, muscle force potential is directly proportional to cross-sectional area, as it is related to the number of muscle fibres [8, 33, 113]. This measurement can therefore be used to estimate the maximum isometric force.

6.4.4 Testing

Testing of the muscle model components was also required.

A previously constructed version of the contraction dynamics Hill-type model was available for comparison with that of the model. This version was not used within the model as the construction of it was untidy and inefficient and did not include the force-velocity relationship, however as a test of the other components it was adequate.

Figure 6.9 shows the outputs from both models to a sine wave of amplitude 1 at 0.5 Hz entered for the musculotendon length and a sine wave of amplitude 1 with a frequency decreasing from 1 to 0.1 over the 10-second time frame for the activation. The force-velocity component of the model was disabled for this test.

The results are identical as would be expected. This does not prove conclusively that the models are correct, but the chance of producing identical errors without reference to the other model is small enough to be neglected.

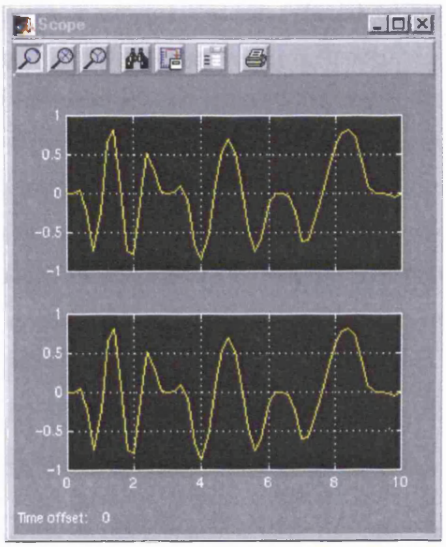

Figure 6.9: Comparison of normalised contraction dynamics block with the same for a previous model.

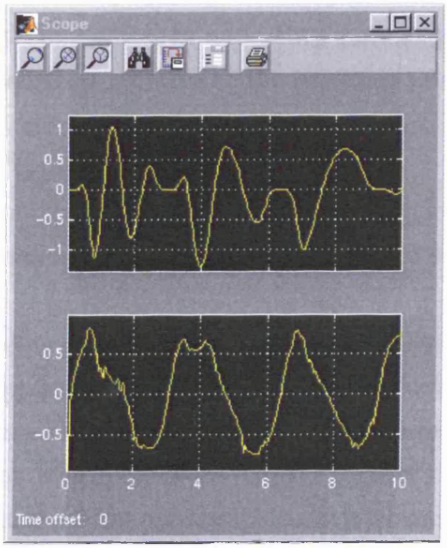

Figure 6.10: Normalised contraction dynamics including velocity behaviour and velocity.

In every case the results were very close, small differences were noted in the response times producing an error related to the slope of the curve. These are small enough to be ignored.

The force-velocity characteristic involves a single multiplier and as such minimal observation that high positive velocities (extension) producing increases in magnitude and large negative velocities (contraction) a decrease confirms that it has been applied correctly. Figure 6.10 shows that with such large and fast oscillation, the force-velocity relationship comes to dominate by opposing the activation component of the system and magnifying the force-length component.

6.5 Musculoskeletal Geometry

While the contraction dynamics dictate the amount of force a muscle can generate, it is the attachments and orientations of a muscle on and about the bones of the skeleton that define its action on the body. Muscle may cross more than one joint, wrap around bones and be restricted by ligaments. These factors must all be taken into account when modelling musculoskeletal anatomy.

The source used to find the musculotendon parameters [21] includes coordinate data for the attachment sites and other contact points of the muscles to the bones in 3-dimensions, relative to the proximal joint of the appropriate segment. From these, straightforward geometry is used to find the directions of force and moment arms as the muscles act.

The muscle parameters are 3-dimensional and calculations based on them must, therefore, be made in 3-dimension even when the rest of the model is 2-dimensional.

Each musculotendon unit follows a path from origin to insertion points via some or no wrapping points representing obstructions such as bones, ligaments or other muscles that divert the route. Points fixed to the same bone have a constant length between them, so this can be calculated in advance as a static length. The dynamic geometry occurs between adjacent points on different bones and must be calculated for the joint position in every frame of the simulation.

Each attachment and wrapping point is defined relative to a reference point and reference axes at the centre of rotation of the proximal joint of

the relevant bone. Before any other calculations can take place, the points on the bones are rotated and translated to match the reference frame of the ground.

The orientation of the body segments are represented as a 3×3 matrix formed by placing the direction vectors of the three axes of the segment relative to the ground axes in rows. To calculate the absolute position of a point on the bone (p_0), the position vector relative to the centre of rotation (p_1) is multiplied by the orientation matrix (N), and then the absolute position of the joint centre of rotation (r) is added:

$$p_0 = N \cdot p_1 + r$$

With two points (a and b) in the same reference frame the scalar distance (d_s) and vector distance (d_v) between them are found by as follows:

$$d_s = \sqrt{(a-b) \cdot (a-b)}$$

The forces from the muscles act on the bones at the contact points. Forces between points on the same bone cancel so can be ignored. Only the forces between bones need to be considered. The forces act at the contact points with a magnitude calculated using the contraction dynamics model above (section 6.4.2) and in the direction of the direction vector ($\hat{d}$) of the distance between the two points:

$$\hat{d} = \frac{d_{vector}}{d_{scalar}}$$

Muscle forces always pull the bones together so the negative of the force is applied to the distal bone.

To find the moment (Mj) applied by a force at a joint, the vector product of the force (F) and the distance from the contact point to the joint centre (r_j) is used:

$$M_j = F \times r_j$$

The same 3-dimensional geometry is used throughout the model.

6.5.1 Testing

Regression equations for the musculotendon lengths of 10 muscles [43], all of which cross the knee and some of which also cross the ankle and hip, were used to test the geometric method developed for this model. The equations are only valid in two-dimensions while the geometric lengths must be in three-dimensions, but as the model motion is constrained to two-dimensions this is not a problem. These two methods are based on different parameters and as such will not produce identical results, however the outcomes were similar enough to confirm the validity of the geometric method used.

Three sine waves at frequencies of 5, 5.5 and 6 rads s^{-1} generated joint angles at hip knee and ankle respectively. Amplitudes and offsets were set to match the range of motion allowed by the joints according to Delp [21].

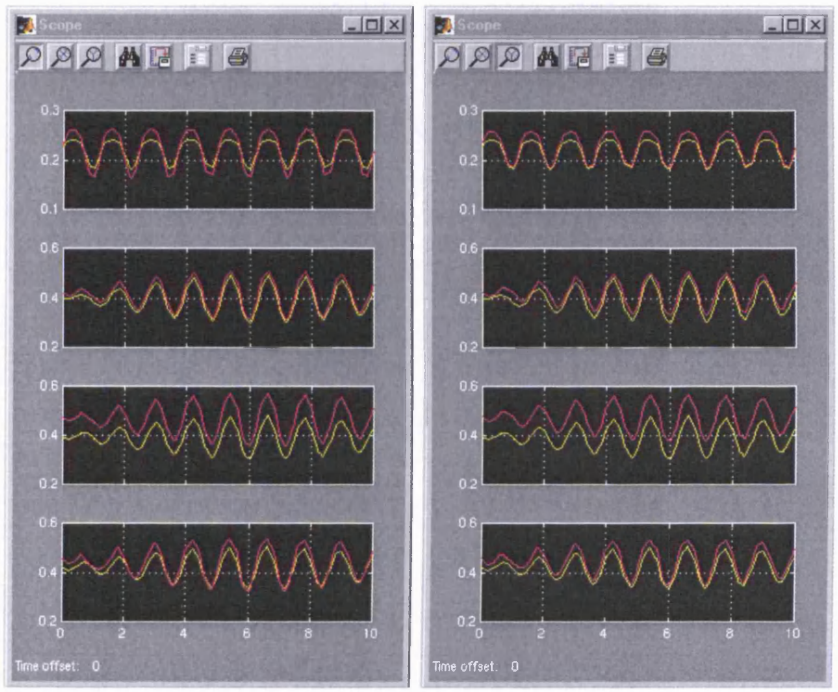

Figure 6.11: Hamstring lengths: biceps femoris short head, semimembranosus, semitendinosus and biceps femoris long head descending respectively. Simple knee joint on the left and variable-centre-of-rotation joint on the right. Regression equation outputs - yellow, geometrically calculated - magenta

The greatest error between geometric and regression equation muscle lengths occurs near to the extremes of angle (Figures 6.11 and 6.12). The

simplified model knee explains some of these differences as can be seen by comparison of the simple knee joint and variable-centre-of-rotation results. This more complex knee joint was not used in the model as it is far more difficult to integrate it into the motion dynamics of the simulation.

Errors at the extremes of angle are due to the regression equations, which were not designed to cover as wide a range of angles as the geometric parameters causing larger errors at the extremes, this is particularly obvious in the vasti. In addition small differences in the positions of the joint centres, where a few millimetres offset can produce a very significant change, would tend to be more sensitive at the extreme angles.

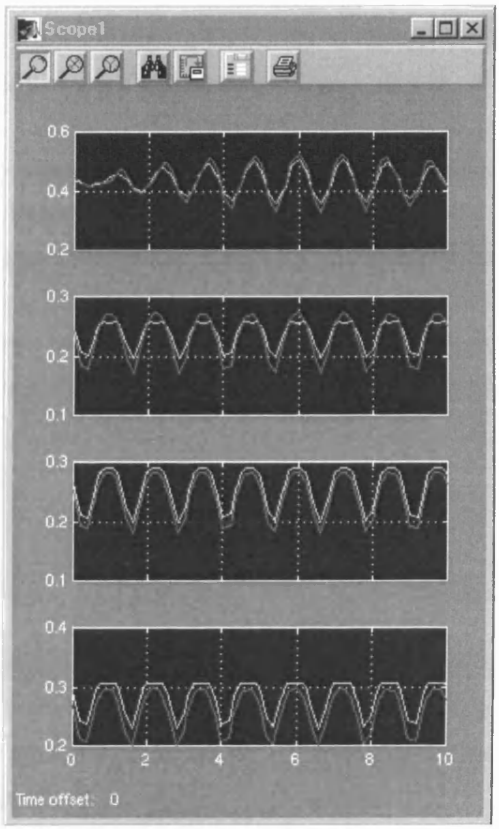

Figure 6.12: Lengths of the quadriceps: rectus femoris and vastus medialis, vastus intermedius and vastus lateralis respectively. Regression equation outputs - yellow, geometrically calculated - magenta

The most significant error occurs in semitendinosus (Figure 6.11), which shows a constant offset of almost 10 cm. An examination of the parameters from Delp [21] shows that semitendinosus should be the longest of the

hamstrings, which suggests an error in the regression equations rather than the geometric method or, more likely, that significantly different parameters were used to calculate the equations.

The regression equations only covered ten muscles so cannot be used for comparison with all of the muscles used on the model, but do confirm the validity of the geometric system tested here. Other muscles were checked to confirm that over the entire range of joint motion their muscle lengths were in the range of optimal fibre length plus or minus 50% (see figure 2.15).

6.6 Ground Reactions

The most common force acting on the body is the ground reaction force and it is the basic measure in the biomechanical analysis of human movement [34].

A two-part viscoelastic foot model developed by Gilchrist and Winter [38] was used to simulate ground reaction forces in the model.

Nine spring/damper elements are used to calculate forces along the sole of the foot, six along the main foot and three on the toes. Each is assumed to maintain the same orientation during all phases of gait.

The following equation models the damping behaviour of each of the elements:

$$c = \begin{cases} 0, & x \leq 0 \\ c_1 \times ([\frac{x}{x_1}]^2 \times 3 - 2[\frac{x}{x_1}]), & 0 \leq x \leq x_1 \\ c_1, & x \geq x_1 \end{cases}$$

Vertical and horizontal damping are modelled using the same equation, but where vertical damping uses spring compression to dictate the conditional components of the equation, horizontal damping uses the vertical force.

The following parameters describe the system:

	Parameters	Values
Vertical:		
Spring Stiffness	k	4000 Nm^{-1}
Spring resting length	l_0	0.0226 m
Critical compression	x_1	0.005 m
Maximum damping	c_1	300 Nsm^{-1}
Anterior/posterior:		

Critical vertical force	x_1	100 N
Maximum damping	c_1	400 Nsm^{-1}

The damping coefficient c can be vertical or horizontal as appropriate and the variable x represents spring compression or vertical force respectively.

This foot model also includes spring/damper parameters for the internal joint moments required to maintain accurate foot motion. These springs and dampers provide control of foot angle throughout the stance phase and include all muscle, ligament and internal friction effects. As such they are inappropriate for this model as control ligament and muscle actions are calculated separately.

6.7 Summary

In summary, a forward-dynamics, sagittal-plane model of the human locomotor apparatus has been developed to simulate motion over the gait cycle supplying both joint angle data and ground reactions in three degrees-of-freedom. A publication describing the model is included in Appendix D [73].

The dynamics of a ten-segment, pin-jointed locomotive apparatus are described by a general set of equations developed from LaGrange's equations. Parameters for segment lengths, masses and moments of inertia allow the model to be adapted to a specific individual.

Ground reactions are applied using a three-point approximation to the sole of the foot. When at least two points are in contact with the floor, ground reactions can be calculated in three degrees-of-freedom. Friction is assumed to be always sufficient to prevent the feet from slipping.

A Hill-type actuator model incorporating a two-element muscle in series with a tendon describes Musculotendon behaviour. Four length-force and velocity-force relationships describe the mechanical characteristics.

Muscle tissue excitation levels as stimulated by neural signals are approximated by an activation dynamics equation. This mimics the chemical changes occurring within the muscle fibres during excitation. The contraction dynamics described by the Hill-type actuator simulate the mechanical changes then produced. The generic model produced is scaled to each of the muscles using muscle-tendon specific parameters.

The effects of the muscles on the segments in terms of forces and moments are found using basic geometry means at the musculotendon attachment sites and other contact points.

Of the model components, the ligaments came from Piazza and Delp ([85]), the Hill-type musculotendon model from Zajac et. al. ([119]), the ground reaction system from Gilchrist and Winter ([38]) and the default parameters from Delp, Lariviere and Gagnon and Piazza and Delp ([21, 68, 85]). The motion dynamics and geometric muscle force application sections were developed specifically for this project as well as the integration of the foreign components into the system.

Chapter 7

Sliding-Mode Control and Muscle Activation Strategies

7.1 Introduction

Forward and inverse dynamics models require extreme accuracy in their mathematical description including detailed knowledge of physical parameters. For biological systems such as the human body, which include wide diversity between individuals as well as variation in performance from moment to moment, this is extremely difficult.

The model described in chapter 6 is a forward-dynamics neuro-musculoskeletal model, which by itself is of little use in gait analysis. The human locomotive apparatus forms too unstable a system to generate useful results under open-loop conditions; the simulated individual tends to fall over after only a very short period of time. Implementation of a controller is needed in order to drive the model's joints and segments to follow a specific set of trajectories.

In the human body, control is applied using visual, tactile and balance sensors, the modelling of which are far beyond the scope of this project. Instead a reference tracking control system was developed to force the simulation to follow motion patterns collected by kinematic gait analysis.

Sliding-mode control has also been shown to be a viable technique in the control of motion via FES both in modelling [49, 50, 51, 61, 71, 97] and in use on human subjects [52].

A large number of sliding-mode controlled models have been developed to deal with knee joint angle control [49, 50, 51, 52, 71, 97], and there are others designed for gait simulation and robot gait control [5, 15, 30, 75]. In

addition, other non-linear control techniques have also been applied to these problems [79, 80, 99] and some recent examples exist of the use of linear controllers for limb movement [51, 98], a technique becoming increasingly rarely represented in the literature of this field.

Schauer and Hunt [99] and Negard et. al. [79] both describe alternative non-linear control techniques for motion control, however it was decided that the sliding-mode method was most appropriate for several reasons: the chief advantages of this technique lies in it's order reduction properties and insensitivity to the problems of system complexity, variation and unmodelled dynamics [29, 103]. In addition, the high frequency switching of the controller (see Section 7.2) could in principle produce antagonism and an increasing amount of information points to the existence of stable positive force feedback control occurring in human movement [94, 93], which sliding-mode techniques can produce.

In 1993 Chang and Hurmuzlu [15] published details of a five segment, sliding-mode controller driven, planar model to simulate bipedal gait. The model described aims to generate human-like gait based on five constraint relations and four parameters rather than through trajectory tracking. In this way the reaching phase can be avoided and the evolution of tracking errors controlled directly. However, a later publication concerning the model [30] shows that, as might be expected, poor agreement is produced between human gait patterns and those generated by the model.

For the model being constructed here, it was decided that the trajectories followed should be as close a match to normal gait patterns as possible to minimise the effort required [2]. Motion tracking was the seen to be the best way to achieve this.

Jezernik and Riener [51] presented a sliding-mode controller for the motion tracking of the knee joint, however the equations presented drive the angular velocity rather than the angular acceleration as is required by the model described in Chapter 6. In addition, being concerned only with the knee joint this controller may not expand well to the rest of the locomotor apparatus. For these reasons this technique was rejected as a basis for the controller.

The system described in this thesis is entirely simulated and there are therefore no problems with unmeasurable states or restricted output information and no limits on the control magnitude or rate. Some of the control

systems mentioned above address these issues and when FES muscle controllers are developed on this model they would require similar consideration. However the basic controller (which will drive the rest of the simulated body while the FES controllers activate particular muscles) requires only that performance be maximised in the sense of precise sliding and fast reachability. Designing for unmeasurable states or restricted output information would be inappropriate in this context.

Likewise chattering, which is extremely undesirable in a mechanical actuation system in robotics is also not a problem during simulation and in fact produces antagonism in the muscles of the model (see Chapters 8 and 9), which is a useful trait.

It was ultimately decided that a suitable controller would be developed from the same control law used by Lim et. al. [71] who produced a hip, knee and ankle joint tracking model. Of the control systems examined, this one was closest to the requirements of the model, deriving from second-order sliding-mode techniques and producing good angle tracking of three joints simultaneously.

The details of the sliding-mode system are described in section 7.3. It has been suggested that 'minimum metabolic energy per unit distance travelled is a valid measure of walking performance' [2]. As there are many more muscles than there are joints, some optimisation is necessary in order to find the muscle activation pattern at every stage of the simulation that uses the least energy. The muscle activation strategies devised to minimise energy use are detailed in section 7.4.

7.2 Principles of Sliding Mode Control

Sliding-mode techniques form part of a class of systems known as variable structure control systems (VSCS), which evolved in Russia in the 1960s, only emerging to the rest of the world in the mid 1970s [29].

The defining characteristic of VSCS is a *control law* that is deliberately changed as the system operates according to a set of predefined rules. In this way a set of individually inappropriate and often mutually contradictory control laws are combined to provide effective closed-loop system performance.

An example system takes the form:

$$\ddot{x} = f(x, \dot{x}) + u \tag{7.1}$$

Where x, $\dot{x}$ and $\ddot{x}$ are the position, velocity and acceleration of the error in the system variable to be controlled respectively and u is the system input. The function f is an arbitrary function relating the position and velocity to the acceleration. A sliding-mode controller has a two-state control law, the condition of which is dictated by a *switching function*. A switching function 's' appropriate for the system (7.1) typically takes the form:

$$s(x, \dot{x}) = \lambda x + \dot{x} \tag{7.2}$$

Where λ is a strictly positive design scalar. The control strategy seeks to force s to zero, as a result of which the dynamics are then forced to lie on the line referred to as the *sliding surface* or *switching surface*, shown in phase space in figure 7.1. The control law is specifically designed to force the system state to this surface.

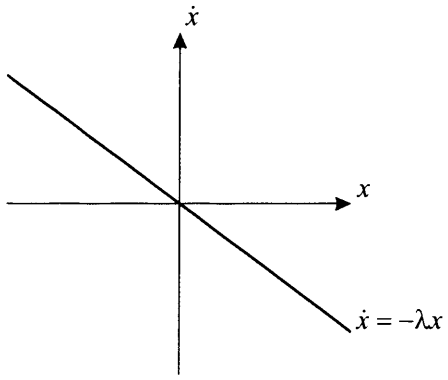

Figure 7.1: Phase portrait of a sliding surface

Differentiating (7.2) and substituting (7.1):

$$\begin{aligned} \dot{s}(x, \dot{x}) &= \lambda \dot{x} + \ddot{x} \\ &= \lambda \dot{x} + f(x, \dot{x}) + u \end{aligned}$$

When $s = 0$ and therefore $\dot{s} = 0$:

$$u_{eq} = -\lambda \dot{x} - f(x, \dot{x})$$

u_{eq} is referred to as the equivalent control action. Note that this is not the control action experienced directly by the plant, but the effective control action experienced by application of the discontinuous controller. For sliding-mode reachability, s and $\dot{s}$ must have opposite signs. This ensures that the system trajectories always tend towards the sliding surface.

Let:

$$u = -\lambda\dot{x} - \rho \times sgn(s)$$

Where ρ is a positive design constant. Thus:

$$\dot{s} = f(x, \dot{x}) - \rho \times sgn(s) \tag{7.3}$$

As long as $\rho > |f|$, s and $\dot{s}$ have opposite signs. Ensuring that the velocity and position errors have opposing signs in this way ensures that the system is constantly pushing towards zero error. However, sliding-mode systems are not asymptotically stable. As ρ is a constant, the control action inevitably overshoots the sliding surface, producing a high frequency oscillation about it. For this reason s and $\dot{s}$ only equal zero on average during sliding-mode conditions, hence the equivalent control action. Under infinite frequency switching, the system would be constrained to remain on the line:

$$\dot{x} = -\lambda x$$

This results in a first order decay as the trajectories 'slide' towards the origin (Figure 7.2). This behaviour is termed *ideal sliding mode* [29, 103]. To ensure sliding-mode conditions are reached the design parameters must be chosen so that the general reachability condition $s\dot{s} < 0$ is satisfied.

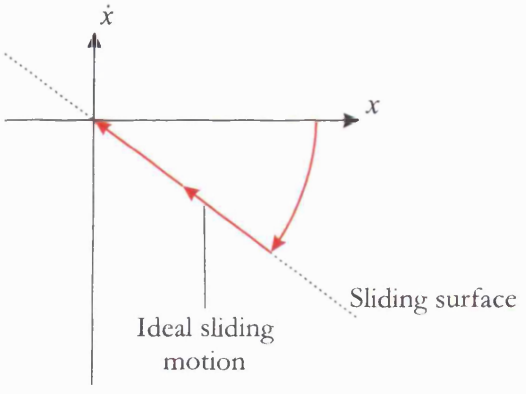

Figure 7.2: Ideal sliding motion

This reduction to a first-order decay occurs regardless of the complexity of the second-order plant being controlled and continues for as long as the control action is powerful enough to maintain the sliding-motion, i.e. to satisfy the reachability condition. The controller also cancels any disturbance

in the closed loop system without requiring any knowledge of the disturbance. This insensitivity to unmodelled dynamics and parameter inaccuracies gives sliding-mode techniques an advantage in the control of simulated human motion. In addition, computation of the equivalent control action can be used for modelling neuromuscular control.

7.3 Design of Sliding Mode Controller

A modified control law from Edwards & Spurgeon [29] (pp. 11-15) is used to control the model presented in chapter 6:

$$u(t) = -\ddot{x}_r - (\lambda + \Phi)\dot{x}(t) - \Phi\lambda x(t) - \rho sgn(s(t))$$

The introduction of a linear feedback component provides *asymptotic reaching* of the sliding surface and a further constraint that maintains the trajectories on the sliding surface once they have reached it. Φ is a positive design scalar designed to accomplish this. It also allows a smaller value of ρ to be used, which decreases the amplitude of the switching required to maintain sliding motion.

For this new control law, a modified reachability condition applies [29]:

$$s\dot{s} \leq -\Phi s^2 - \mu|s|$$

Where the value chosen for μ must be positive and satisfy the inequality:

$$\rho > \ddot{x}_{max} + \mu$$

For simulation purposes there is no upper limit on the tuning parameters, so values were chosen to ease the design task and to maximise performance in the sense of precise sliding and fast reachability:

$$\lambda = 200$$
$$\rho = 200$$
$$\Phi = 100$$

Using these values the simulated trajectories were constrained to the sliding surface for all of the normal and pathological gait patterns modelled (see Chapter 8).

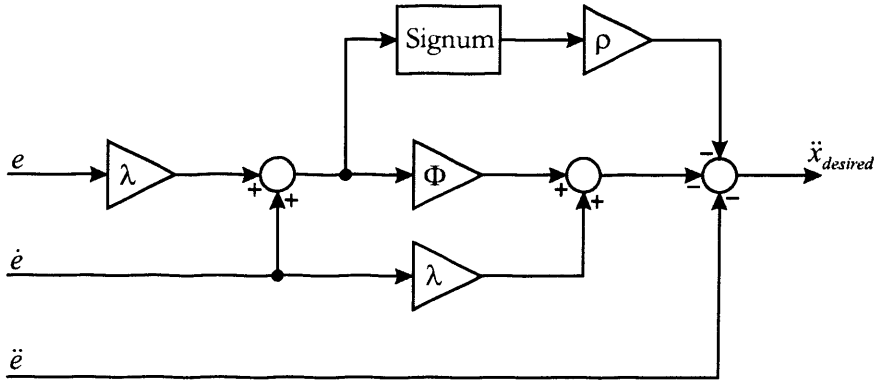

Figure 7.3: Block diagram of controller

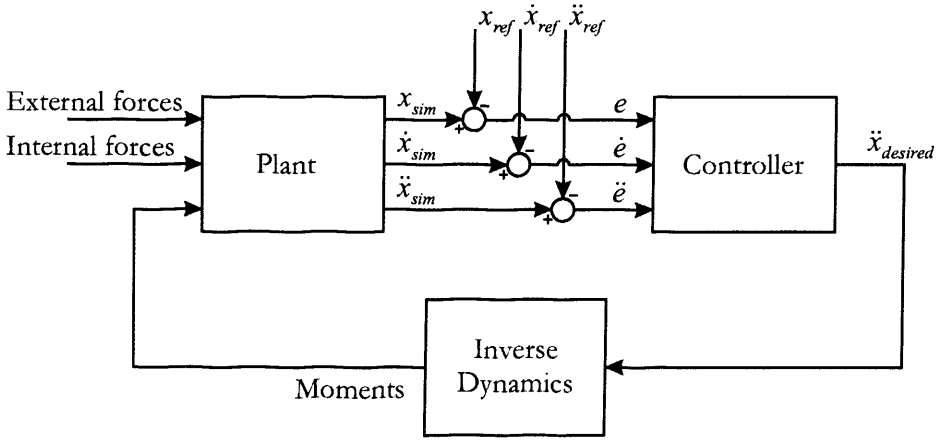

Figure 7.4: Block diagram of controlled system

Values for e and $\dot{e}$ are found by subtracting the reference signals, measured in the gait laboratory and processed as in Chapter 5, from the simulated segment angles and angular velocities respectively. The reference angular velocities, $\ddot{e}$, provide the trajectories should no further control input be necessary.

The output from the controller is then a set of desired accelerations (Figure 7.3), which must be passed through a matrix representing the inverse of the model dynamics to generate the moments required to drive the model (Figure 7.4).

The external forces acting on the plant in figure 7.4 include ground reactions and gravity. The internal forces are ligament and passive muscular forces. The controlling moments represent the active muscle behaviour.

7.3.1 Changes to model

This controller does not operate through the muscles. Moments are generated and applied directly to the body segments and the muscle activation patterns are calculated by optimisation outside the closed loop process (Figure 3.12). Passive muscle action occurs within the plant and the model describing it does not change with the addition of the closed loop controller.

Internal joint moments are calculated without considering the effects of internal joint friction, ligament effects or passive and active muscular behaviour. These parts of the model must be disabled when attempting to analyse joint moments, but enabled when simulating muscle activity.

To generate accurate readings for gait analysis it is useful to replace the ground reactions system detailed in section 6.6 with measured readings matching the trajectories being followed. This removes a source of error and thus allows internal activity to be estimated more accurately.

7.3.2 Testing the Controller

The controller was tested in a similar way to the motion dynamics equations. A series of small tests designed to test the interactions of the various components of the system.

The simulated body would be required to hold position under a variety of forces and accelerations, including gravity and ground reaction. Particular motions would also be generated under force conditions: the raising of a leg,

bending of a knee, etc. Each joint was tested before moving onto combinations of movements. Sample results from five tests are displayed in Table 7.1.

Test	Time (s)	x_t (m)	θ_t (^{c})	θ_1 (^{c})	θ_2 (^{c})	θ_3 (^{c})	θ_4 (^{c})	θ_5 (^{c})	θ_6 (^{c})	θ_7 (^{c})	θ_8 (^{c})	θ_9 (^{c})
C1	1	[0 0]	0	0	0	0	0	0	0	0	0	0
C2	0.5	[0 0]	$5e^{-6}$	$6e^{-6}$	1	$2e^{-6}$	$2e^{-6}$	$2e^{-6}$	$2e^{-6}$	$2e^{-6}$	$3e^{-6}$	$2e^{-6}$
	1	[0 0]	$6e^{-6}$	$6e^{-6}$	1	$2e^{-6}$	$-2e^{-6}$	$2e^{-6}$	$2e^{-6}$	$2e^{-6}$	$3e^{-6}$	$2e^{-6}$
C3	0.5	[0 0]	$-9e^{-6}$	$-1e^{-5}$	0.487	$-4e^{-6}$	-0.487	$3e^{-6}$	$5e^{-8}$	$3e^{-8}$	$2e^{-5}$	$2e^{-6}$
	1	[0 0]	$-1e^{-5}$	$-1e^{-5}$	0.987	$-8e^{-7}$	-0.987	$2e^{-6}$	$1e^{-6}$	$1e^{-6}$	$1e^{-5}$	$2e^{-6}$
C4	0.5	[0 0]	$6e^{-5}$	$-4e^{-6}$	0.5	$-8e^{-6}$	-0.5	$-2e^{-6}$	$4e^{-6}$	$-4e^{-6}$	$-2e^{-5}$	$2e^{-6}$
	1	[0 0]	$1e^{-5}$	$-5e^{-6}$	1	$-5e^{-6}$	-1	$-2e^{-6}$	$-3e^{-6}$	$-3e^{-6}$	$1e^{-5}$	$-2e^{-6}$
C5	0.5	[-0.55 0.025]	-0.722	$8e^{-5}$	0.5	$9e^{-6}$	-0.5	$-3e^{-5}$	$-1e^{-5}$	$9e^{-6}$	$-2e^{-5}$	$-3e^{-6}$
	1	[-2.2 0.955]	-0.701	$8e^{-5}$	1	$2e^{-5}$	-1	$1e^{-5}$	$-7e^{-6}$	$2e^{-5}$	$-4e^{-5}$	$-5e^{-6}$

Table 7.1: Controller test samples: C1, C2, C3, C4 and C5. Data included are the system centre of mass position (x_t), the system angle (ω_t) and the nine joint angles (θ_1 to θ_9) in radians.

Control test 1 (C1): a null test. No force applied and zero initial conditions.

Control test 2 (C2): from zero initial conditions, a desired hip angle of 1 rad is introduced to the controller. This is outside the sliding surface and results in very fast motion to attain the required position followed by the holding the set pose for the remainder of the test.

Control test 3 (C3): from zero initial condition the simulation is required to track to a hip angle of 1 rad and an ankle angle of -1 rads over 1 second despite desired angular velocities of zero. The requirement of zero velocities induces a compromise between tracking and velocity performance and the result accordingly lags behind the desired trajectory by 0.013 radians.

Control test 4 (C4): from zero initial condition the simulation is required to track to a hip angle of 1 rad and an ankle angle of -1 rads over 1 second with appropriate desired angular velocities. Tracking performance here is far better than in C3 as the angular velocity trajectories match the angle trajectories removing the compromise.

Control test 5 (C5): from zero initial condition the simulation is required to track to a hip angle of 1 rad and an ankle angle of -1 rads over 1 second with appropriate desired angular velocities while under a set of randomly selected forces ([250 65]N, [0 488]N, [98 126]N, [-846 0]N, [798

98]N, [-74 25]N, [-789 89]N, [235 -745]N, [46 67]N and [-58 -24]N) acting on the segments. Despite these forces, the system is capable of tracking the required trajectories. Slight increases can be seen in the errors of the zero joint angles, but these are still small enough to be ignored. Small errors are inevitable in unfiltered sliding-mode data as such systems are not asymptotically stable. Switching about the desired value continues constantly.

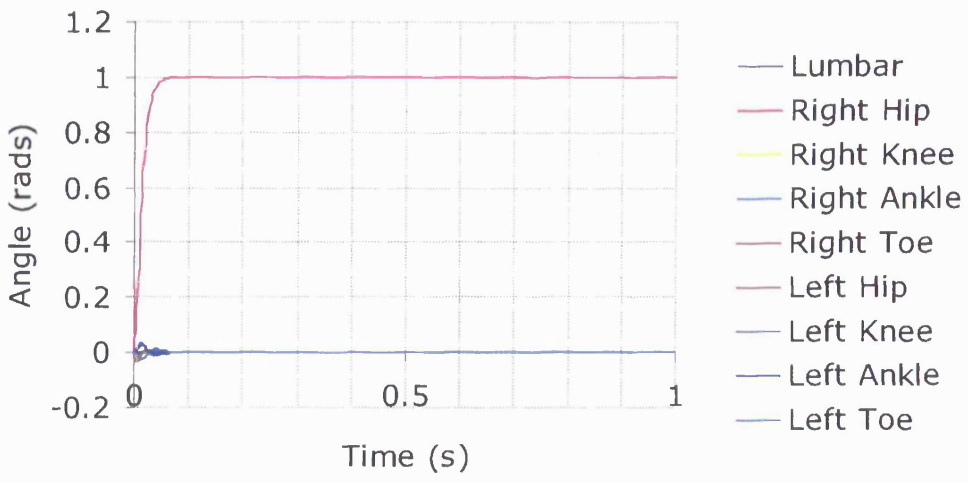

Figure 7.5: Joint angle plot for test C2

Figure 7.5 shows the joint angles generated by test C2 as the system trajectories approach and attain the sliding surface. A full radian is traversed and the system settled well within 0.1 seconds, which is more than fast enough for gait simulation. As the hip joint bends, the segments are shifted with it causing other joints to bend with the segment inertia before the controller reacts to arrest their momentum. This causes the minor deviations seen in the other joints at the beginning of the simulation. This is a rather extreme example where the system is a full radian from the sliding surface and as such, even these minor deviations are much reduced in practice.

7.4 Muscle Activation Strategies

7.4.1 Muscle Groupings

In a purely 2-dimensional model, many of the muscles become redundant. In particular a large number of muscles that cross the hip joint produce chiefly rotation or adduction-abduction moments.

Across the ankle, the peroneus and tibialis posterior muscles are principally evertors and invertors and as such are unnecessary in a sagittal plane

model. There are also a number of small muscles around each joint, particularly in the feet. These are not powerful enough to make a significant impact on gait and were neglected in every model examined.

Many model builders combine muscles crossing a particular joint into a single actuator for the sake of convenience [25, 89, 90]. Figure 7.6 demonstrates the pattern of the lines of action of the muscles around the legs and it can be seen that many muscles follow very similar paths. In this way, the number of actuators can be reduced to 22. The reduction in complexity is appealing but a slightly more accurate way of reducing the effective number of actuators is to apply the same neural input signal to all of the muscles having the same effect across a particular joint or joints. This system requires the same 22 input signals and allows for expansion to individual muscle control should this become desirable.

Figure 7.6: The paths of the major muscles used during gait. Many modellers choose to use actuators representing groups of muscles rather than considering each muscle individually.

For a 2-dimensional model, the muscles can be grouped according to their main action on the body as follows:

- Lumbar flexors: rectus abdominis.
- Lumbar extensors: erector spinae.
- Hip flexors: Iliacas and psoas.
- Hip extensors: gluteus maximus.
- Hip & knee flexors: rectus femoris, sartorius and tensor fasciae latae.

- Hip & knee extensors: biceps femoris long head, semimembranosus and semitendinosus.
- Knee flexors: biceps femoris short head.
- Knee extensors: vastus lateralis, vastus intermedius and vastus medialis.
- Knee & ankle flexors/plantarflexors: gastrocnemius lateral and medial heads, soleus.
- Ankle dorsiflexor: tibialis anterior.
- Ankle plantarflexors & toe flexors: flexor digitorum longus and flexor hallucis longus.
- Ankle dorsiflexors & toe extensors: extensor digitorum longus & extensor hallucis longus.

These muscle groups are applied on both sides of the body except those containing the lumbar muscles.

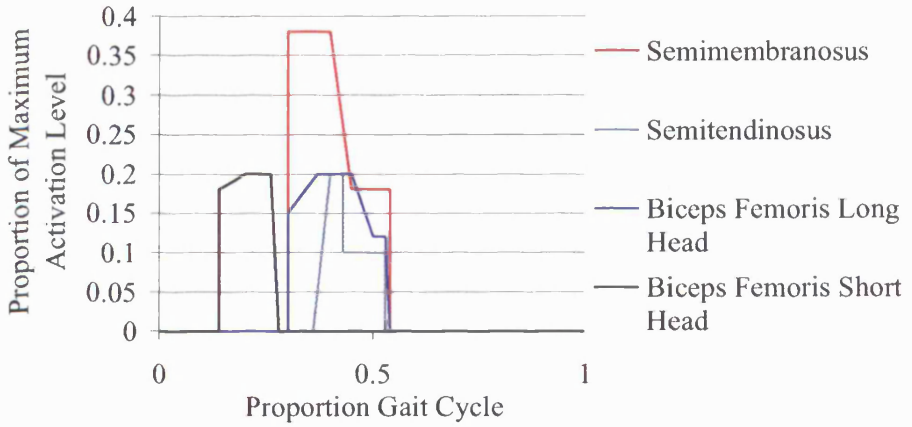

Figure 7.7: Hamstring activation signals during normal gait [84].

In figure 7.7 it can be seen that the biceps femoris short head (black) signal is offset from the biceps femoris long head (cyan), semimembranosus (orange) and semitendinosus (green) signals. This makes combining the muscles into a single group inadvisable. Instead, biceps femoris short head forms one group while the other three form another. It should also be noted that biceps femoris short head crosses only one joint, while the other hamstrings cross two.

There are several groups with only one muscle active within them, which could be merged with similar groups crossing the same joint as well as another. This would reduce the number to be considered. However, gluteus maximus and biceps femoris short head demonstrate sufficiently different activation characteristics during normal gait that this would be unacceptable for them. Combining tibialis anterior with the other dorsiflexing group would

effectively remove independent control of toe extension, making it dependant on ankle movements.

7.4.2 Strategies

Only one pair of antagonistic muscle groups cross each of the toe and lumbar joints. As only single antagonistic pairs are responsible for the motion of the upper body and toe segments, distribution of control moments occurs entirely between these muscles. The activations required are found by dividing the control moment by the maximum muscle moment. This is performed for both muscles in an antagonistic pair and the resulting signals are constrained to be greater than or equal to zero. In this way positive moments are distributed to the group of muscles producing a positive moment about the joint and negative to the group generating a negative moment.

$$activation = \begin{cases} \frac{M_{control}}{M_{muscle\_max}}, & for\ \frac{M_{control}}{M_{muscle\_max}} > 0 \\ 0, & for\ \frac{M_{control}}{M_{muscle\_max}} < 0 \end{cases}$$

A similar approach is used for the tibialis anterior and soleus muscles crossing the ankle joints, but the gastrocnemius activations must be calculated first. The gastrocnemius and soleus muscles both plantarflex the ankle, but the gastrocnemius also flexes the knee joint. The distribution of a plantarflexing ankle moment between them must therefore be based on an optimisation of the ankle and knee moments. Minimising the following within the constraint of activation levels 'A' of 0 to 1 performs this.

$$M_{knee\_minimised} = |M_{knee} - M_{max\_gastroc\_knee} A_{gastroc}|$$

Where:

$$M_{ankle} = A_{soleus} \times M_{max\_soleus\_ankle} + A_{gastroc} \times M_{max\_gastroc\_ankle}$$

An additional constraint ensures that neither muscle can be activated excessively higher than the other to produce a more realistic outcome:

$$|A^2_{gastroc} - A^2_{soleus}| \leq 0.25$$

A total of six muscle groups then remain crossing the hip and/or knee joints of each leg. A similar optimisation approach is used to find activation signals for them.

Individual minimisation calculations are made for each knee and hip joint by the same process as above, i.e. using the muscle groups crossing both joints first. In each case, the moment about the un-minimised joint is then dealt with by the remaining muscle group crossing it. The calculation which results in the smallest activation levels is then selected.

7.5 General Troubleshooting

Data samples used in motion tracking are subject to a series of minor problems which produce anomalies in the results. This section aims to address these problems and provide viable solutions for them.

7.5.1 Initial Conditions

The sliding-mode controller relies on a switching function that produces a high frequency signal on the output (7.2). Filtering is therefore necessary to produce a readable output but the initial condition values needed for these filters are unlikely to be available. A settling time of between ten and thirty percent of the gait cycle (depending on the bandwidth of the filter) is therefore needed. Figure 7.8 shows the long settling time required by a filter with a bandwidth large enough to smooth the switching component of the signal. Improved filters can reduce this delay, but without knowledge of the initial conditions it cannot be eliminated.

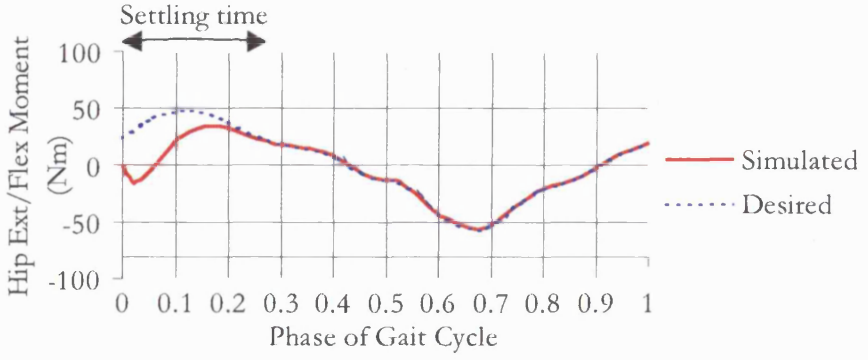

Figure 7.8: Hip moment settling time with a high bandwidth filter

The solution to this problem is to run the simulation for two gait cycles by repeating the motion tracking data inputs. The filter conditions at the end of the first cycle act as a close approximate to the initial conditions needed for the second. As can be seen from figure 7.9 the second gait cycle does not suffer from the settling problems of the first and can therefore be used for analysis.

7.5.2 Tracking Start-End Transients

Human gait is a complex and variable process, and as such the data at the beginning and end of a gait cycle is extremely unlikely to match. When repeating gait cycles these unmatched points from the end of one cycle to the beginning of the next produce transients in the joint moments, which

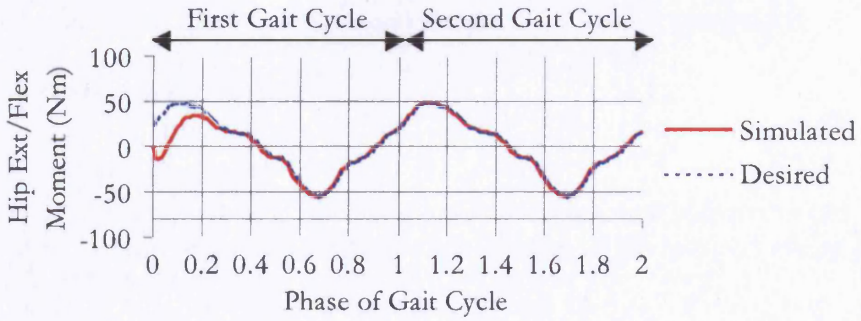

Figure 7.9: Repeating gait cycles. The second (from 1 to 2) needs no settling time.

when unfiltered can be orders of magnitude larger than the signals around them. The 'Raw Data' curves of figure 7.10 show transients after filtering and it can be seen that the disturbances are of a low enough frequency that attempting to remove them altogether is infeasible.

Data is often normalised separately for each leg (i.e. the data for each legs starts at its own heel-strike) and the left leg data must therefore be offset by half a gait cycle for the purposes of simulation. The end-start transients are therefore also offset and as the legs are connected via the pelvis, smaller secondary transients are passed on to the opposite legs half a cycle out of phase with the main transients (Figure 7.10).

When considering only the angles, it would seem quite a simple matter to filter out any mismatch before the motion tracking data is entered into the model, but the controller uses angular velocity and acceleration as well which being differentiated from the angles amplify the problem. Smoothing the tracking data over the required gait cycles therefore has limited effect and even appears to increase the secondary transients (Figure 7.10).

A smooth transition is needed between the end and the start of each gait cycle and the only way to ensure this is to remove the data points to either side of the transition and interpolate a new set. Joint angles follow smooth curves during gait, which makes this a viable option and less than ten percent of the data will require alteration.

For a 51 frame data set the following Matlab commands replace the first and last two frames with new data interpolated from four frames on each side:

The trajectory data is held in a matrix called 'Traj'. The use of cubic spline interpolation provides much better smoothing to the differentiated angular velocities and angular accelerations than linear interpolation.

The moments generated from interpolated data have almost no trace of the transients, as can be seen in figure 7.10, and the results produced have the smooth curves expected of such a closely optimised system as the human

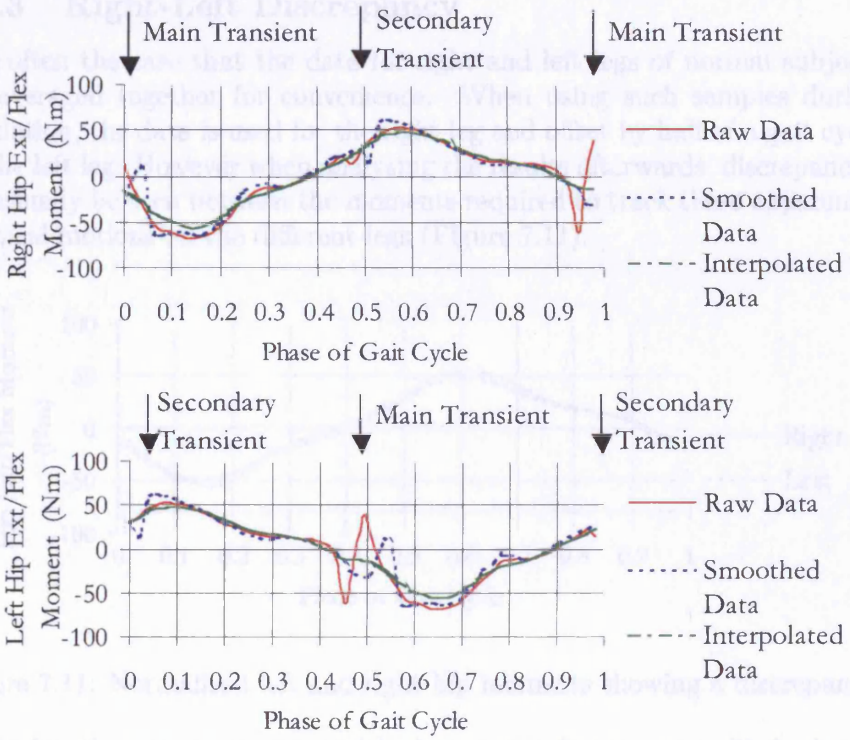

Figure 7.10: Hip moments using different techniques to remove transients

```
% Interpolate beginning and end
yi=interp1([1:4 9:12]',[Trajectories(noofframes-5:noofframes-2,:) ...
            Trajectories(3:6,:)],1:12,'spline');
Trajectories(noofframes-1:noofframes,:)=yi(5:6,:);
Trajectories(1:2,:)=yi(7:8,:);
```

locomotive apparatus [2].

While replacing data is not ideal as some important features could be lost, it is the only viable alternative when samples of several gait cycles are not taken in the first place.

7.5.3 Right-Left Discrepancy

It is often the case that the data for right and left legs of normal subjects are averaged together for convenience. When using such samples during simulation, the data is used for the right leg and offset by half of a gait cycle for the left leg. However when analysing the results afterwards, discrepancies can usually be seen between the moments required to track these apparently identical motions on the different legs (Figure 7.11).

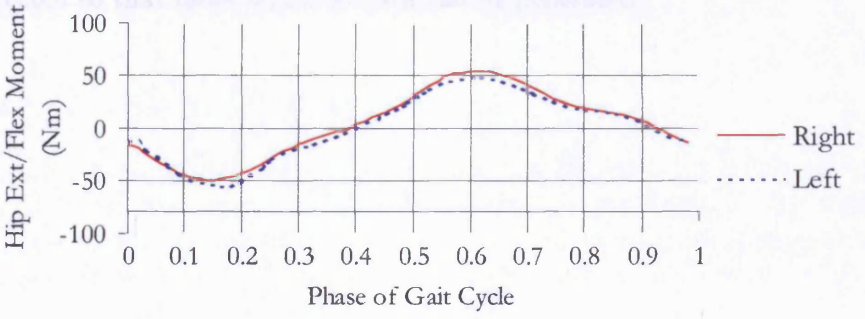

Figure 7.11: Normalised left and right hip moments showing a discrepancy

Rather than errors in the model, these anomalies are more likely due to the movement of the pelvis and upper body, which do not move symmetrically over the legs. It is generally the case that one leg will be dominant and that one leg will be slightly longer than the other. This makes asymmetry unavoidable. For accurate modelling and analysis this method of averaging is unwise as it ignores this fundamental aspect of gait.

The problem can be solved by averaging the pelvis and upper body data samples with the same data offset by half of a gait cycle. This will make the gait pattern entirely symmetrical. Alternatively, the discrepancies are generally small enough to be ignored.

7.6 Summary

A sliding-mode controller has been applied to the model to provide accurate motion tracking of sampled gait data and muscle activation strategies have been developed to predict muscle behaviour during the simulated locomotion.

A modified controller from Edwards & Spurgeon [29] is used to ensure a fast acquisition of the sliding surface. Parameters were selected to be high enough to ensure stability, with no upper limit imposed.

Minor modifications were made to the model to generate better motion tracking and joint moment results; active muscle behaviour is not included in the controller and ground reaction forces are taken from sampled data, rather than calculated by the model.

Muscles activation signals were grouped according to the actions of the muscles in order to reduce the number of signals required and thereby simplify analysis.

Optimisation criteria were then applied in order to minimise the energy usage required to follow the reference gait trajectories by controlling the muscle activity patterns.

Three problems with the controlled data outputs were then identified and corrected so that more accurate data can be generated.

Chapter 8

Simulated Kinematics and Muscle Activity

8.1 Introduction

Ten normal kinematic data samples were used to drive the model in order to assess the motion tracking, moment and muscle activation performances (all of the files from Table 5.1). The results are presented here.

8.2 Motion Tracking

Figure 8.1 below shows the average motion tracking results for the ten data files. The red lines are the simulated joint angles generated by the model, while the blue lines represent the average of the trajectories being tracked. The cyan lines are one standard deviation to either side of these reference trajectories, found by the equation:

$$\sum \frac{(x_i - m)}{\sqrt{n-1}}$$

Where x_i is the sample trajectory, m is the mean trajectory and n is the number of samples.

It can be seen that the simulated trajectories stay well within the one standard deviation range. The largest error can be seen in the pelvis angle, which differs from the reference value by up to 1.71 degrees. The errors in the pelvis angles coincide with the minimum hip angles as the ligaments preventing hyperextension at the hip joints begin to act in these regions. The ligaments take effect from -20 degrees, so only a few of the samples are influenced, but the action of the ligaments is so strong that a marked influence is visible on the average.

During normal gait the hip hyperextension ligaments provide a non-muscular, and therefore energy efficient, braking mechanism during opposite loading response. The gait pattern of an individual is optimised to make

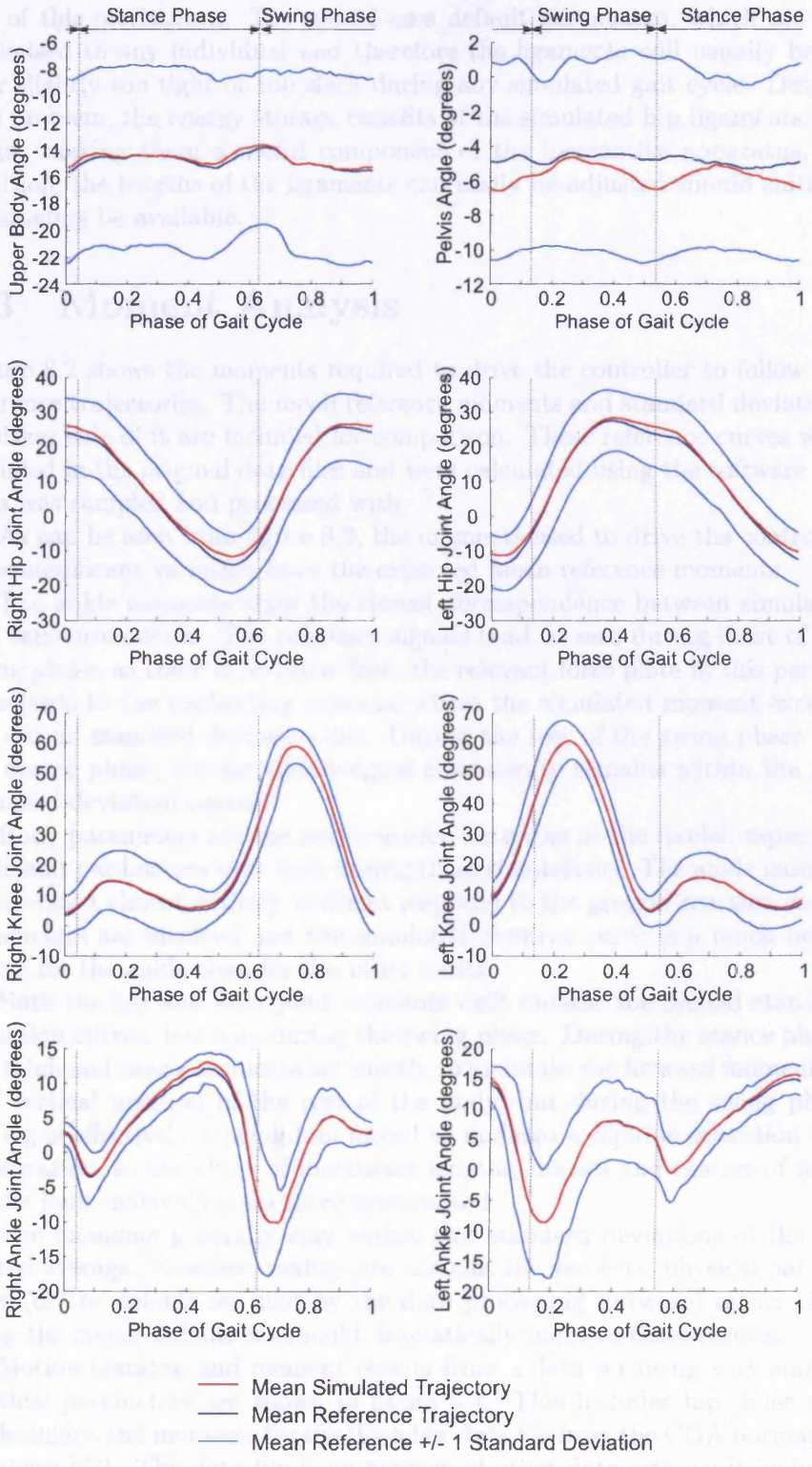

Figure 8.1: Average joint angle motion tracking results

use of this mechanism. The model uses default parameters, which are not optimised to any individual and therefore the ligaments will usually be either slightly too tight or too slack during any simulated gait cycle. Despite this problem, the energy storage benefits of the simulated hip ligaments still occur, making them a useful component of the locomotive apparatus. In addition, the lengths of the ligaments can easily be adjusted should suitable parameters be available.

8.3 Moment Analysis

Figure 8.2 shows the moments required to drive the controller to follow the reference trajectories. The mean reference moments and standard deviations to either side of it are included for comparison. These reference curves were included in the original data files and were calculated using the software the data was sampled and processed with.

As can be seen from figure 8.2, the moments used to drive the controller show significant variation from the expected mean reference moments.

The ankle moments show the closest correspondence between simulated and reference curves. The reference signals tend to zero during most of the swing phase, as there is no input from the relevant force plate in this period. This leads to the misleading outcome where the simulated moment exceeds the second standard deviation line. During the rest of the swing phase and the stance phase, the simulated signal consistently remains within the first standard deviation curves.

Body parameters are the major source for errors in the model, especially as default parameters were used during these simulations. The ankle moment is generated almost entirely in direct response to the ground reaction so few parameters are involved and the simulated moment curve is a much better match for the ankle than for the other joints.

Both the hip and knee joint moments drift outside the second standard deviation curves, but only during the swing phase. During the stance phase, the thigh and shank segments act mostly to maintain the forward momentum and vertical position of the rest of the body, but during the swing phase the leg is effectively a pendulum forced to undergo a rapid acceleration and deceleration, so the effect of inaccurate lengths, masses and centres of mass on the joint moments is far more pronounced.

The moments generally stay within two standard deviations of the expected average. However, taking into account the subjects' physical parameters (or the default set used by the data processing software) rather than using the model default set should dramatically improve these results.

Motion tracking and moment results from a data set using very similar physical parameters are shown in figure 8.3. This includes hip, knee and ankle angles and moments for the 'Dundee' data file from the CGA normative database [63]. The data file is an average of other data sets, so it includes

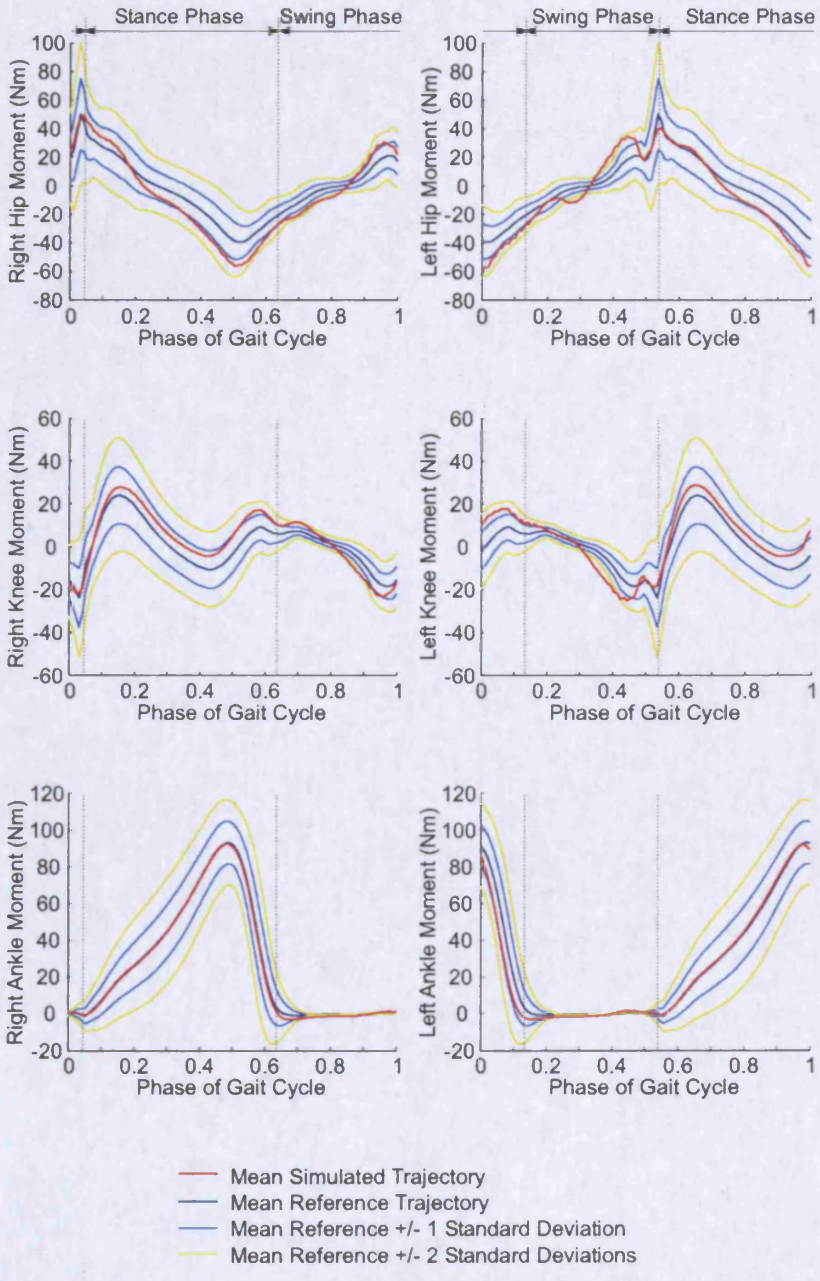

Figure 8.2: Average joint moments during motion tracking

the standard deviation curves shown in figure 8.3.

The motion tracking results are so close a match as to be almost indistinguishable by eye from the reference trajectories, with maximum errors of less than 0.25 degrees. Likewise, the moment curves are a closer fit, remaining almost exclusively within the one standard deviation limits. There is still some significant deviation in the swing phase, which is due to the use of a simple pin joint for the modelled knee.

Closely matching data such as this proves only that the methods of calculation were similar, but does not prove that the results accurately represent the activity within the joints.

Accurate parameters are the most important factor in generating accurate moments. Different methods of calculation should all yield the same results if the same segment parameters are used and the closer these values are to the actual physical parameters of the individual being examined, the greater the validity of the result. Ideally in-vitro readings of forces acting inside the joints would be used to validate models such as this, but this is impractical. Techniques are being developed to instrument total joint replacements to take such readings and when available, data from these experiments will be fundamental to the validation of future models.

Even without accurate parameters, the model trajectories provide motion tracking with an error of less than 2% with acceptable deviation in the moments required. This is due to the insensitivity of sliding-mode control techniques to unmodelled dynamics and plant-model mismatches [29]. When modelling or controlling an unpredictable biological system such as the human locomotor apparatus, this is essential.

8.4 Muscle Activity

In the absence of EMG data for all of the data samples, figure 8.4 shows mean simulated muscle activity as compared to normal activity approximations from Perry [84]. The curves of the graphs cannot be expected to be an exact match under these circumstances, but some idea of the model's performance can be obtained. At the top of each graph bars are shown representing the periods where the EMG and activation curves rise above the average for those muscles. This is a common method of assessing the performance of muscle activity estimators and measuring the correlation between EMG signals and simulated muscle activity [74, 81, 122, 123].

The graphs show some correlation between the simulated and reference data, but some disagreements become immediately obvious. Most notably, the rectus femoris muscles are consistently stimulated far more than the reference activity for all of the data samples. This suggests that differences in the musculoskeletal geometry make the rectus femoris a much more desirable choice for activation and accordingly, it provides much of the moment which would normally be distributed throughout other muscles.

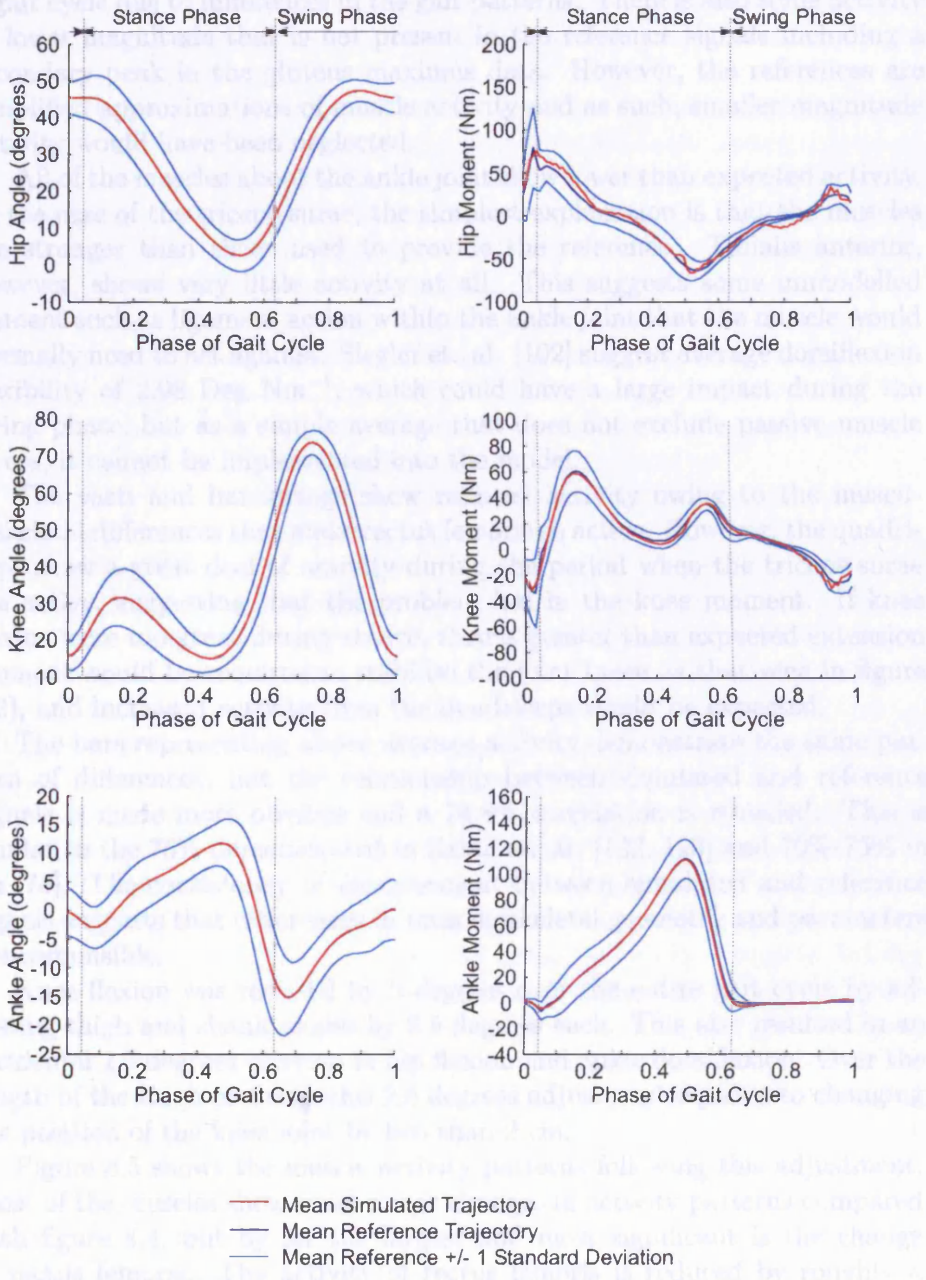

Figure 8.3: Joint angle tracking and resulting moments for the 'Dundee' data file

Gluteus maximus and iliopsoas both show a significant peak of similar proportions to the reference, the iliopsoas in particular offset by around -0.1 of a gait cycle due to differences in the gait patterns. There is also some activity of lower magnitude that is not present in the reference signals including a secondary peak in the gluteus maximus data. However, the references are simplified approximations of muscle activity and as such, smaller magnitude activity would have been neglected.

All of the muscles about the ankle joint show lower than expected activity. In the case of the triceps surae, the simplest explanation is that the muscles are stronger than those used to provide the reference. Tibialis anterior, however, shows very little activity at all. This suggests some unmodelled element such as ligament action within the ankle joint that the muscle would normally need to act against. Siegler et. al. [102] suggest average dorsiflexion flexibility of 2.98 Deg Nm^{-1}, which could have a large impact during the swing phase, but as a simple average that does not exclude passive muscle forces, it cannot be implemented into the model.

The vasti and hamstrings show reduced activity owing to the musculoskeletal differences that make rectus femoris so active. However, the quadriceps show a great deal of activity during the period when the triceps surae are active, suggesting that the problem lies in the knee moment. If knee flexion were too great during stance, then a greater than expected extension moment would be required to stabilise the joint (such as that seen in figure 8.2), and increased activity from the quadriceps would be expected.

The bars representing above average activity demonstrate the same pattern of differences, but the relationship between simulated and reference signals is made more obvious and a 74.8% correlation is revealed. This is similar to the 76% demonstrated in Zajac et. al. [122, 123] and 70%-75% in Lu [74]. The consistency of disagreement between simulated and reference signals suggests that differences in musculoskeletal geometry and parameters are responsible.

Knee flexion was reduced by 5 degrees over the entire gait cycle by adjusting thigh and shank angles by 2.5 degrees each. This also resulted in an incidental 2.5 degrees increase in hip flexion and ankle dorsiflexion. Over the length of the thigh or shank this 2.5 degrees adjustment equates to changing the position of the knee joint by less than 2 cm.

Figure 8.5 shows the muscle activity patterns following this adjustment. Most of the muscles show some minor changes in activity patterns compared with figure 8.4, but by far the largest and most significant is the change in rectus femoris. The activity of rectus femoris is reduced by roughly a third and the activity during the stance phase falls almost entirely below the average activity level, but there is little significant increase in the activity of the other muscles, as the straighter leg requires less support.

While some improvement can be seen in the activation pattern of rectus femoris, the simulated muscle is still far more active than the reference

muscle. The reference signals are a broad simplification of actual muscle activity patterns, which accounts for the low-level activity outside of the main peak, but the magnitude of activity relative to the average is still a little higher than expected due to musculoskeletal differences and variation in the activation strategies used.

Despite the apparent improvements in the rectus femoris activity pattern, the degree of correlation remains unchanged at 74.8% as the activity patterns of other muscles change with the altered load. The vasti in particular show very poor correlation after the adjustment.

It would have been advantageous to further examine techniques to produce a closer match between simulated and reference moments, but time constraints prevented this. Instead, as the reference normal gait samples used were short on EMG data (only one sample providing a useful set) pathological data samples were examined, each including a large quantity of EMG data. This would permit a more accurate muscle activity comparison and test the model's ability to track more extreme gait patterns.

It should be noted that antagonism occurs in opposing muscles crossing the hip and knee joints at several times during the gait cycle including the period when the reference hamstrings and vasti act in opposition. This is not a deliberately programmed-in characteristic of the system, but a benefit of the sliding-mode controller. Previous studies have attempted to predict antagonism [57], but this model generates it according to its fundamental nature. The switching behaviour of the system causes antagonism at periods where the joint angles are most sensitive to changes in moment, the same periods where antagonism would be expected in human gait.

Figure 8.6 shows the muscle activity patterns for the Dundee data file (see Table 5.1), the motion tracking and moment results of which are displayed in figure 8.3. These figures demonstrate that accuracy in skeletal parameters is no guarantee in the accuracy of muscular parameters. The results are similar to those for the average data, with correlation of 74.1%, excessive activity in the rectus femoris muscle, reduced hamstring, vasti and tibialis anterior activity and an extra peak in the gluteus maximus and vasti data. The causes, as before, are oversimplification of the reference signals and differences in the muscle geometry, parameters and gait pattern.

A comparison of simulated muscle activity with real EMG readings is offered in figure 8.7. The data used was extracted from APM, EMG, FPL and KIN files (see the 'man.*' files from Table 5.1 and the processing code description in section 5.4), which demonstrate the poorest correlation between reference and simulated data of the file types used. Figure 8.7 shows muscle activity based on faulty moments due to inaccurate model parameters. As such greater deviation in the results is to be expected and the correlation accordingly falls to 59.5%. However, similar discrepancies occur here as in the other simulations; excessive activity in the rectus femoris, reduced activity in the hamstrings and tibialis anterior and a second peak in the gluteus

maximus curve. In addition, the simulated ankle appears more stable and thus avoids the antagonistic peak in the triceps surae.

Muscle activity within the model shows a pattern that is consistent even with poor quality parameter data. Familiarity with this pattern would permit an estimate to be made of actual muscle activity for gait analysis. Further refinement of the model could improve this, but exact modelling of joint behaviour, muscle geometry and all of the other physical parameters would be required for completely accurate results. Even under these idealised circumstances, the model cannot identify the exact muscle activity within the body because there is no unique solution. The model presents one possible solution based on the parameters designed into it.

8.5 Summary

Human gait is a process optimised for minimum energy use given the individual's muscle strengths and geometries, the ligament actions and the shapes and masses of bones and body segments. Simulation using default parameters equates to forcing an individual to follow the gait pattern of someone else. The ligaments will act against the muscles or fail to act resulting in increased muscle activity, different muscles will act to produce the same motions due to their different geometries and the overall energy use will be increased. Every attempt needs to be made to eliminate these errors when simulating individual gait patterns.

With accurate parameters, the model can provide motion tracking to within 0.25 degrees and with moments that stay almost exclusively well within 1 standard deviation of the expected.

Using default parameters, the motion tracking took place with a maximum error of less than 2 degrees and moments almost exclusively within 2 standard deviations.

In both cases the greatest moment deviation occurred towards the end of the swing cycle where inaccurate body parameters would be most significant.

Muscle activity estimation provided a correlation of 74.8% in measuring activity greater than average, which is consistent with other work in the field [74, 122, 123], but some consistent differences occur suggesting unmodelled joint dynamics and inaccuracies in the muscle parameters. However, taking accurate parametric readings for every muscle and ligament within the body would be more difficult and time consuming than measuring EMG readings directly.

Marker positions from kinematic gait analysis and a weight measurement are enough to estimate segment lengths and masses for motion tracking and moment estimation. The consistent pattern of the muscle activations suggests that variations in this could correlate with variations in actual muscle activity from the norm and therefore default parameters could be used. This will be further explored in the next chapter.

Inevitably, the muscle activations do show some inconsistencies from one to another as gait patterns vary and the errors are augmented or diminished accordingly. As with the consistent error pattern, these should be reduced by greater accuracy in the modelling parameters.

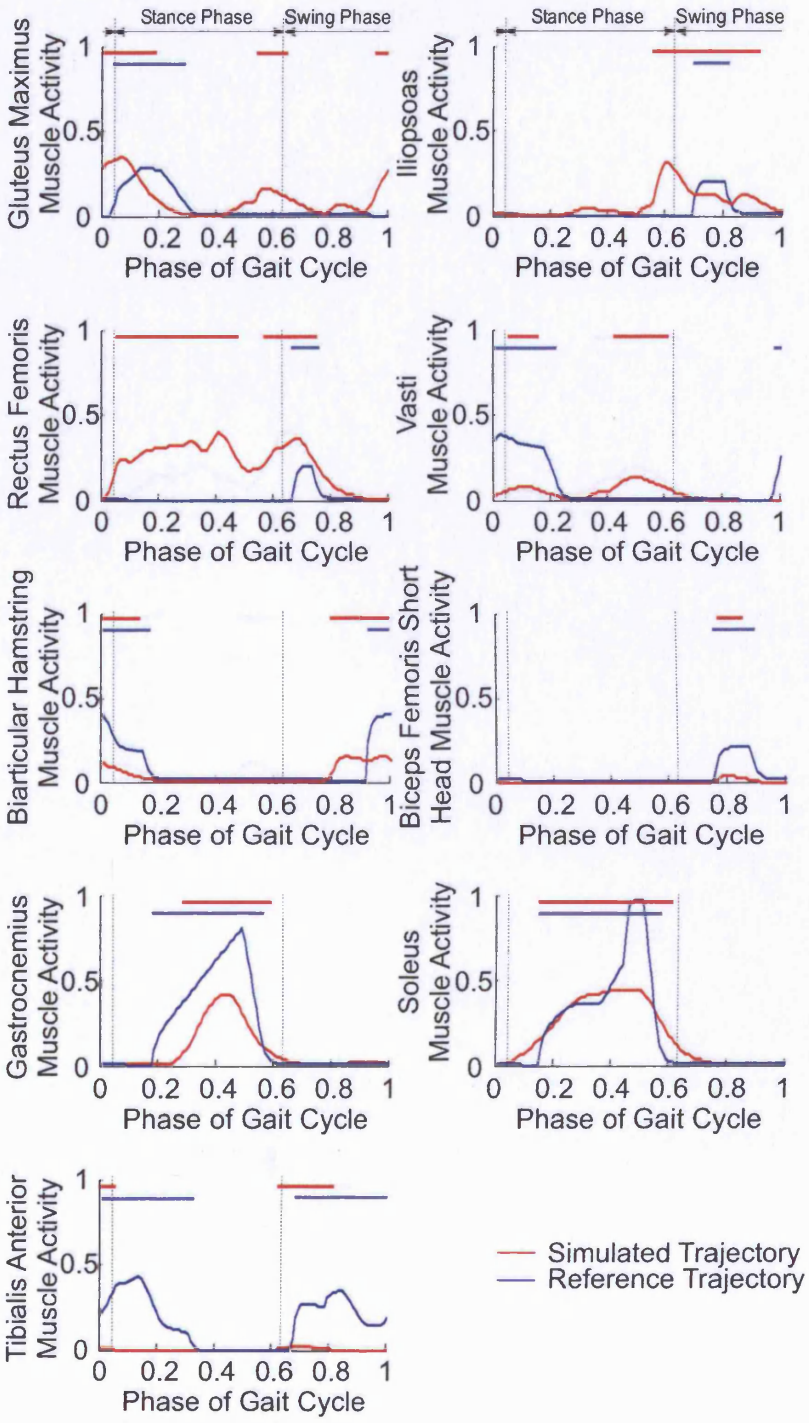

Figure 8.4: Simulated average leg muscle activity compared to approximate data

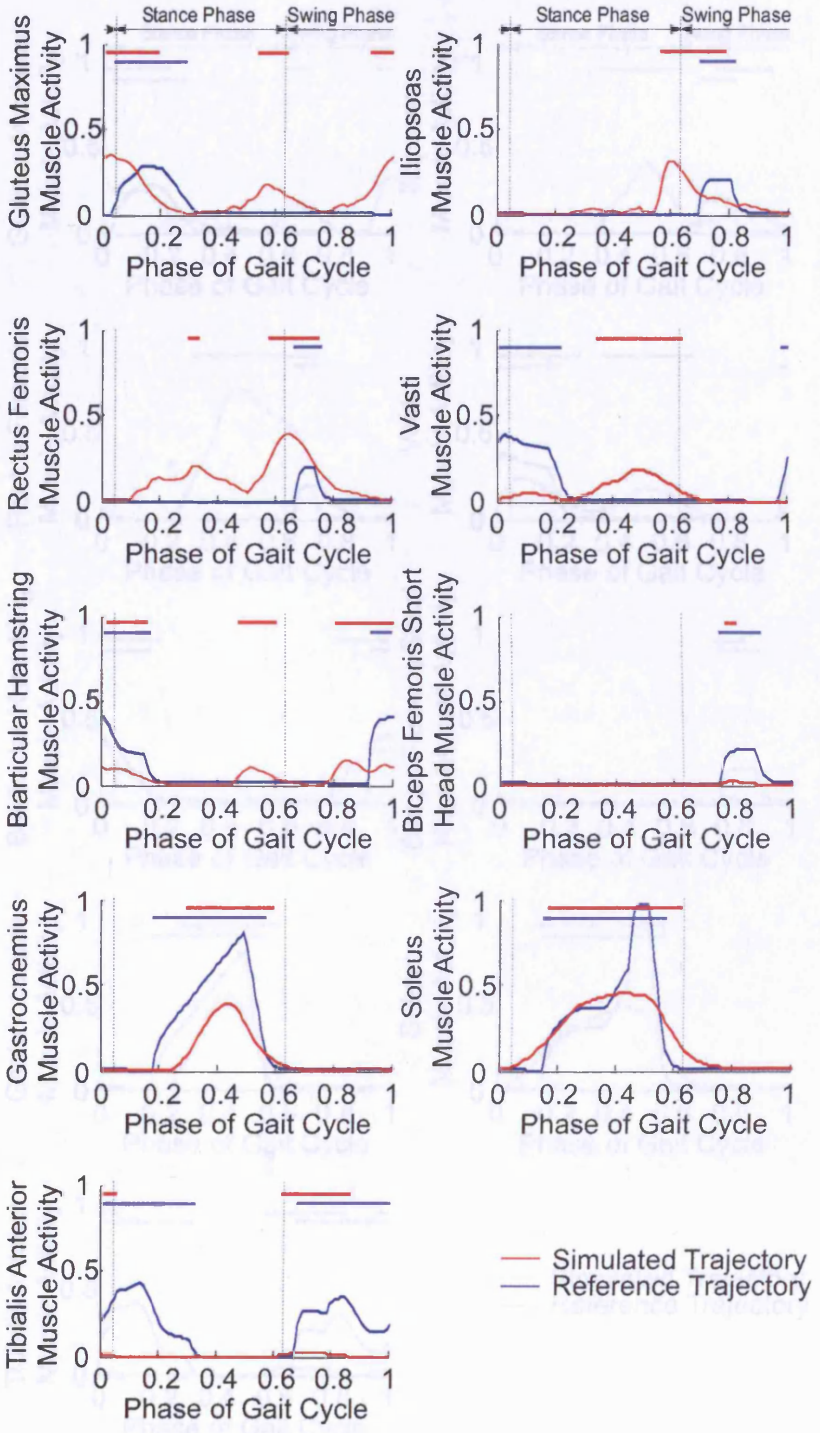

Figure 8.5: Simulated average leg muscle activity with knee joint flexion angle reduced by 5 degrees

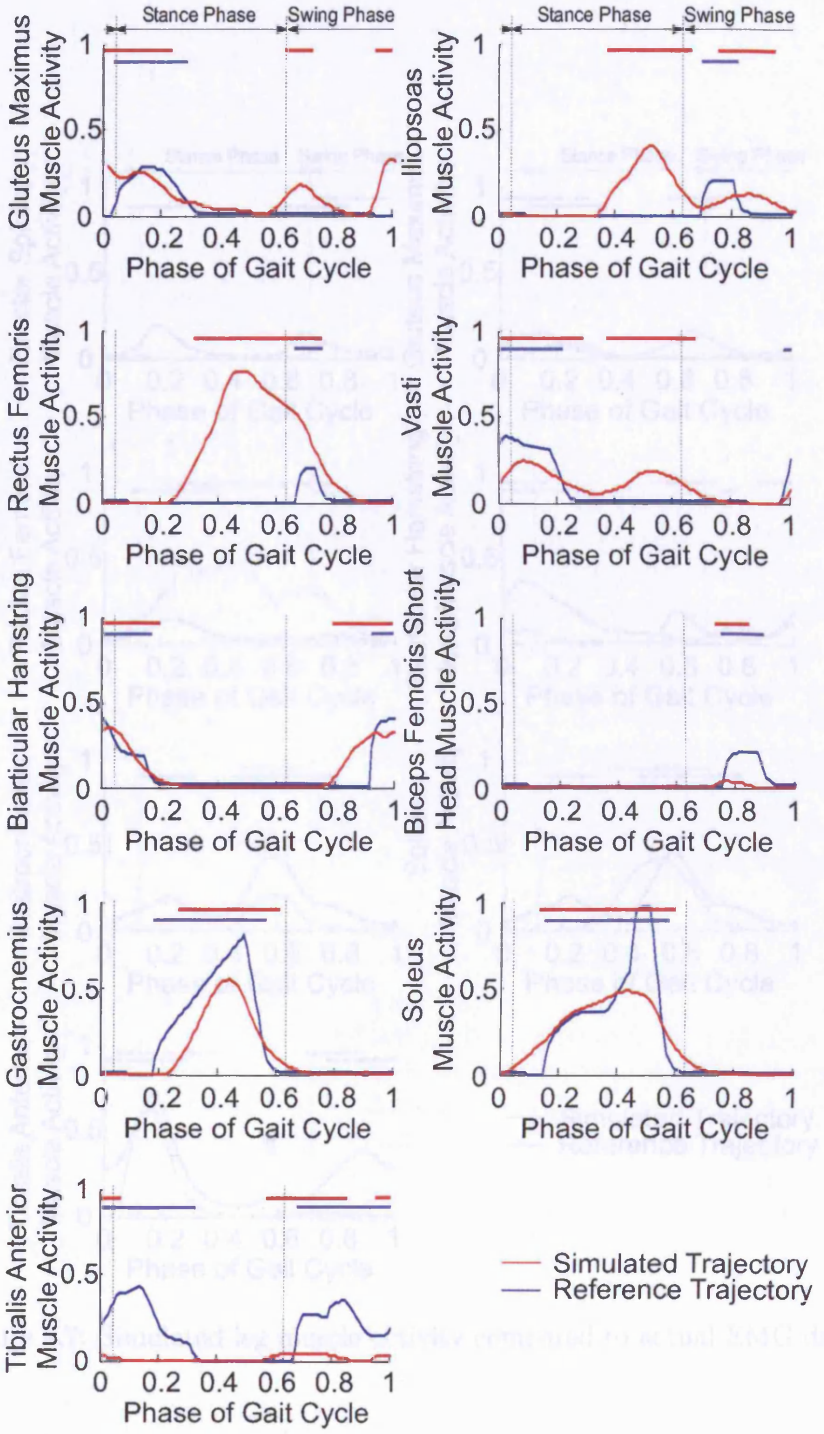

Figure 8.6: Simulated leg muscle activity for the 'Dundee' data file

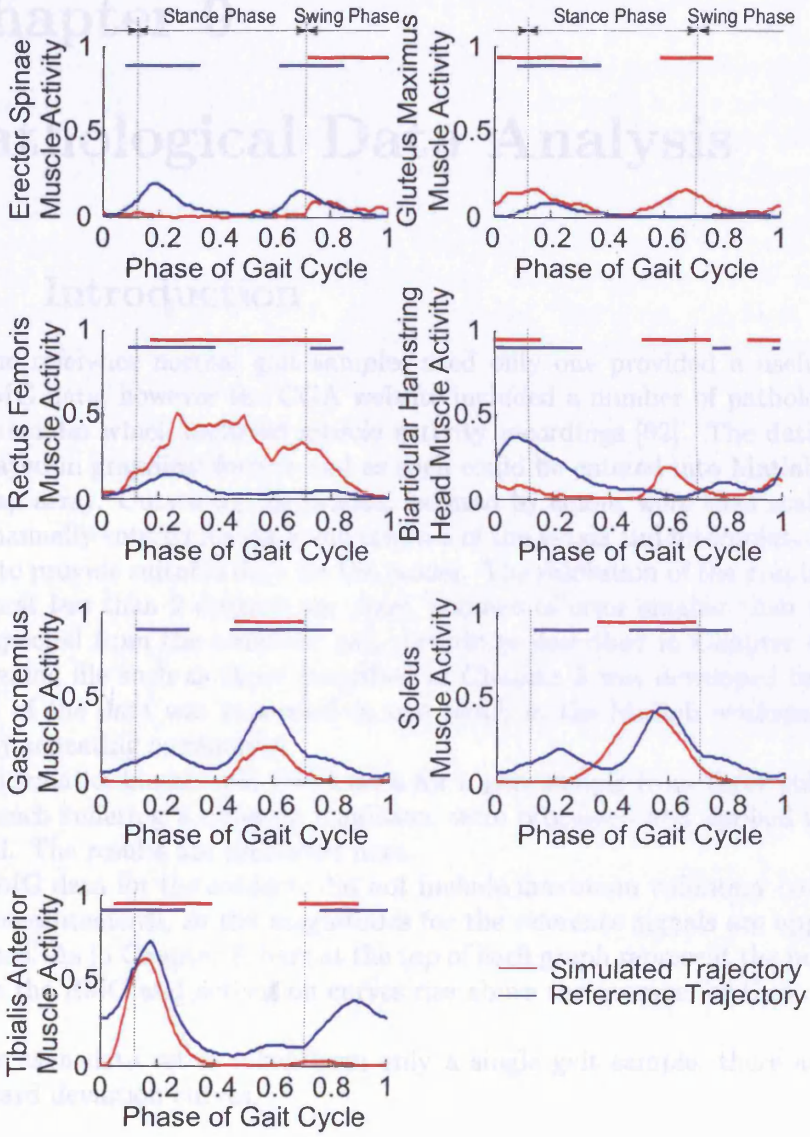

Figure 8.7: Simulated leg muscle activity compared to actual EMG data

Chapter 9

Pathological Data Analysis

9.1 Introduction

Of the reference normal gait samples used only one provided a useful set of EMG data, however the CGA website included a number of pathological gait samples which included muscle activity recordings [62]. The data was displayed in graphical format and as such could be entered into Matlab as a bitmap array. Curves on the graphs, isolated by colour were then scaled to the manually entered maxima and minima of the y-axis and interpolated over time to provide suitable data for the model. The resolution of the graphs was at worst less than 2 degrees per pixel, a range of error smaller than might be expected from the unskilled gait recordings described in Chapter 4. No processing file such as those described in Chapter 5 was developed for this as all of the data was processed in one batch in the Matlab workspace by simply repeating commands.

Kinematic, kinetic and EMG data for a gait sample from three subjects [62], each suffering a different condition, were processed and applied to the model. The results are presented here.

EMG data for the subjects did not include maximum voluntary contraction measurements, so the magnitudes for the reference signals are approximations. As in Chapter 8, bars at the top of each graph represent the periods where the EMG and activation curves rise above the average for those muscles.

As each data set is taken from only a single gait sample, there are no standard deviation curves.

9.2 Femoral Nerve Palsy

This sample was taken from a nine year-old girl with left femoral nerve palsy (obtained from the CGA website [62] 'Femoral nerve palsy'). A femoral nerve transplant took place two years previously, but no gait improvement was observed.

9.2.1 Kinematics and Kinetics

Figure 9.1 shows the kinematic motion tracking results, which as for the normal gait samples are a close match. Likewise the ankle moments in figure 9.2 deviate very little from the reference signals. The simulated hip moments show some correlation to the reference curves, especially the left, but their magnitudes are larger.

The knee moments show a large deviation in flexion moment in the same region as the greatest deviation in knee moment occurred in the normal gait samples. This is caused by differences between the modelled knee and the method used to calculate the reference knee moments. This difference is probably also the major cause of the deviations in the hip moments.

A higher filter cut-off frequency is used for the simulated moments here than for the normal samples. The reference data is from a single sample not an average and is therefore not as smooth. Therefore, the filter must be able to respond more quickly to demonstrate any correlation between the reference and simulated data. The most notable example of this is between 0.55 and 0.8 of the left knee moment curve, where a slower filter would not be able to respond in time.

9.2.2 Muscle Activity

Femoral nerve palsy results in a weakness and reduction in activity of the muscles innervated by the femoral nerve (see table 2.1 in section 2.2.5 for a full list of the muscles). The most significant muscles affected are the quadriceps, so a marked reduction in activity would be expected from them.

The left rectus femoris in figure 9.4 shows no reduction in magnitude in either the simulated or reference signals compared to the normal results, although the first peak does not cover the bulk of the activity period of the triceps surae as would normally be expected from the simulated results (Chapter 8). A second peak occurs where the vasti would normally be active, probably as a compensation, although it is slightly offset from the reference equivalent. The excessive magnitude in the simulated rectus femoris activity is consistent with previous model results.

A reduction can be seen in the activity of the vasti, which is consistent with the pathology of the subject. The simulated results are smaller in magnitude than the reference measurements, but this is consistent with model behaviour. The bars representing above average activity show a correlation of 68.0%, which is slightly above average for the vasti.

The other simulated muscle activity results of figures 9.3 and 9.4 show an average of 70.0% correlation with the measured EMG readings, despite the pattern of deviations typical to the model; excessive activity in the rectus femoris, reduced activity in the hamstrings, vasti and tibialis anterior and a second peak in the gluteus maximus and vasti curves.

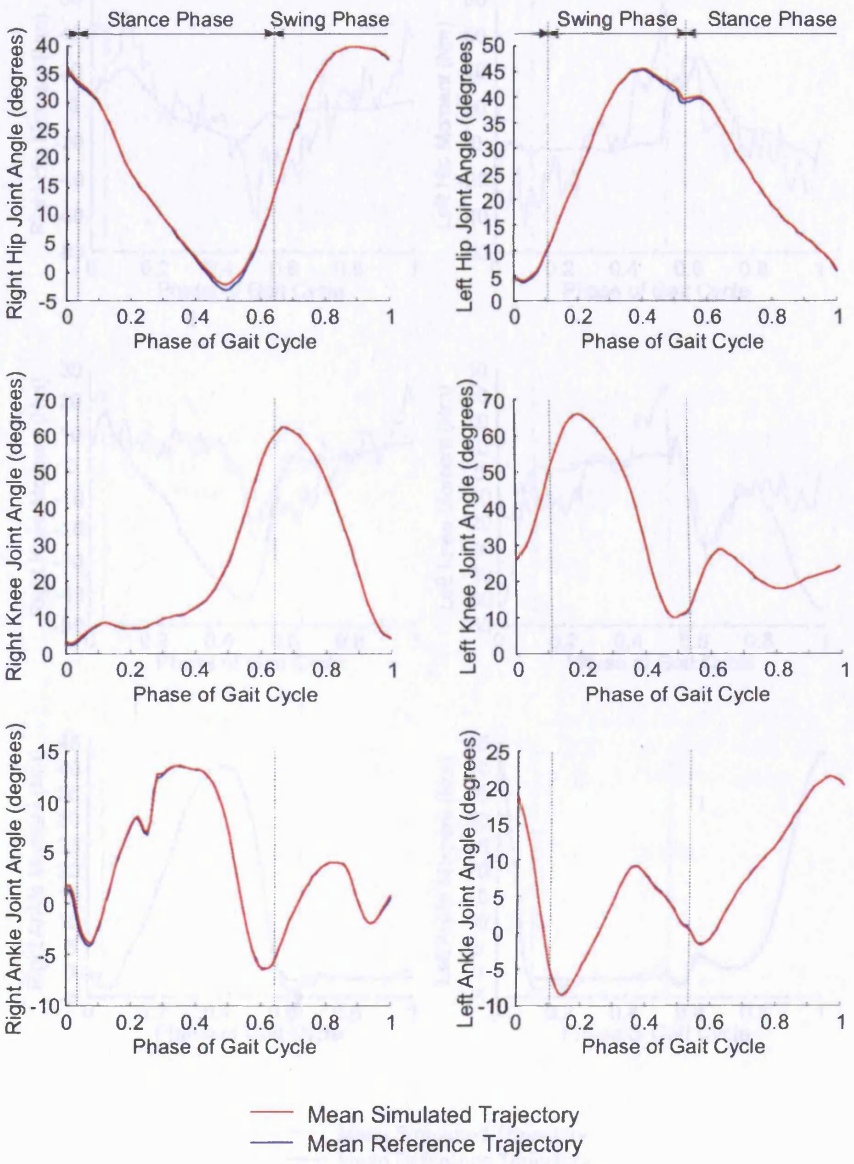

Figure 9.1: Femoral nerve palsy subject joint angle motion tracking results

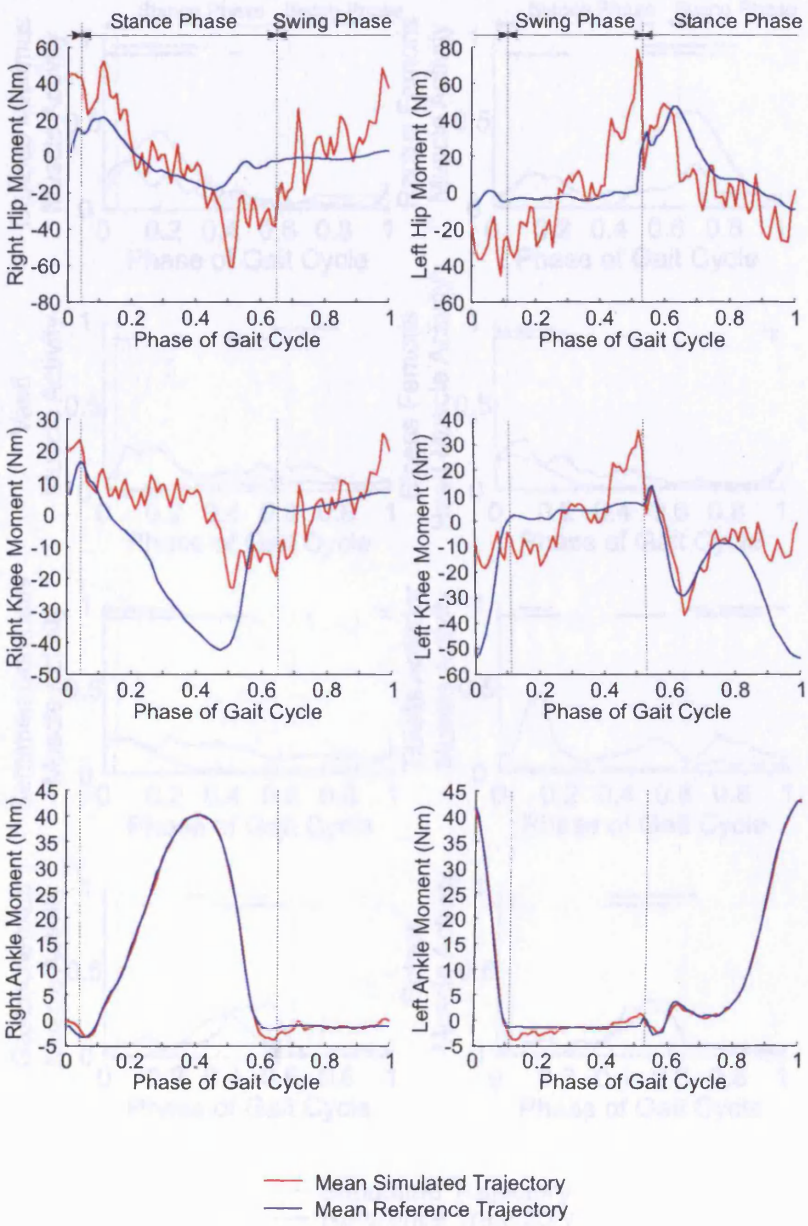

Figure 9.2: Femoral nerve palsy subject joint moments during motion tracking

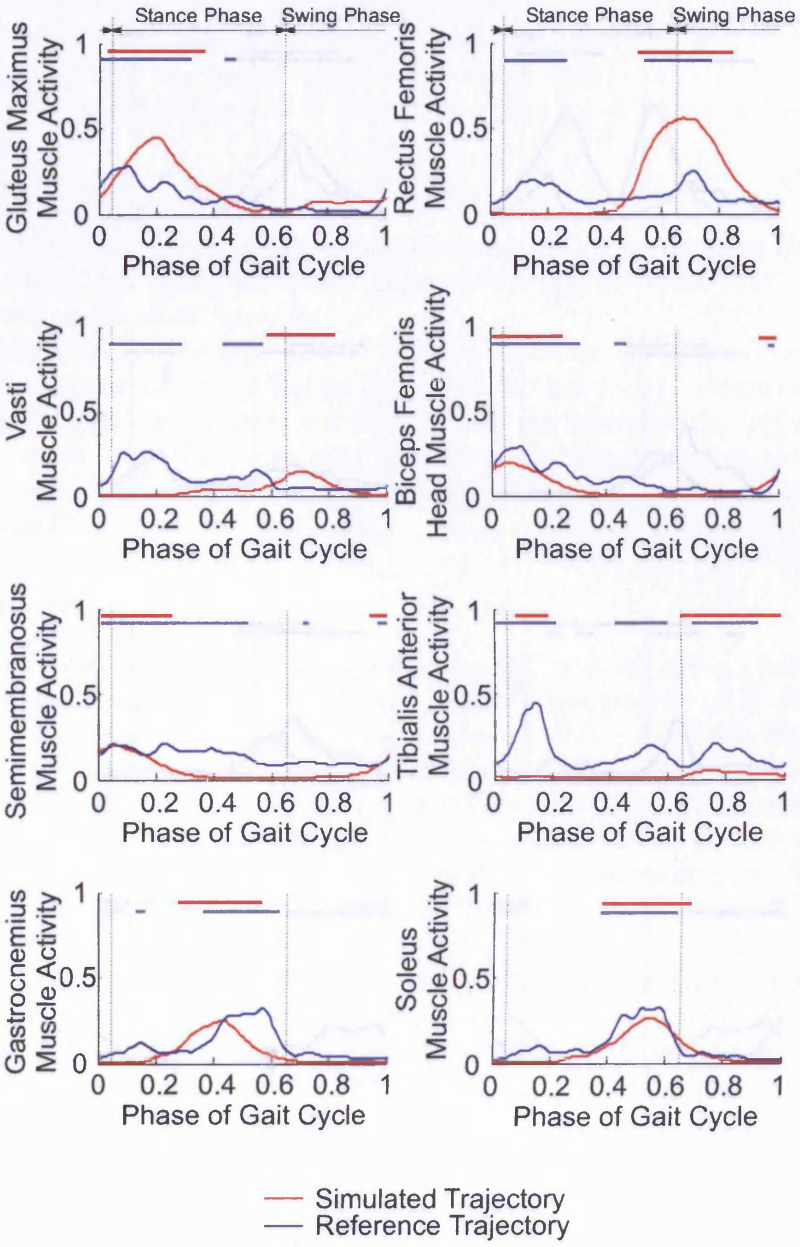

Figure 9.3: Femoral nerve palsy subject right leg simulated muscle activity and EMG measurements

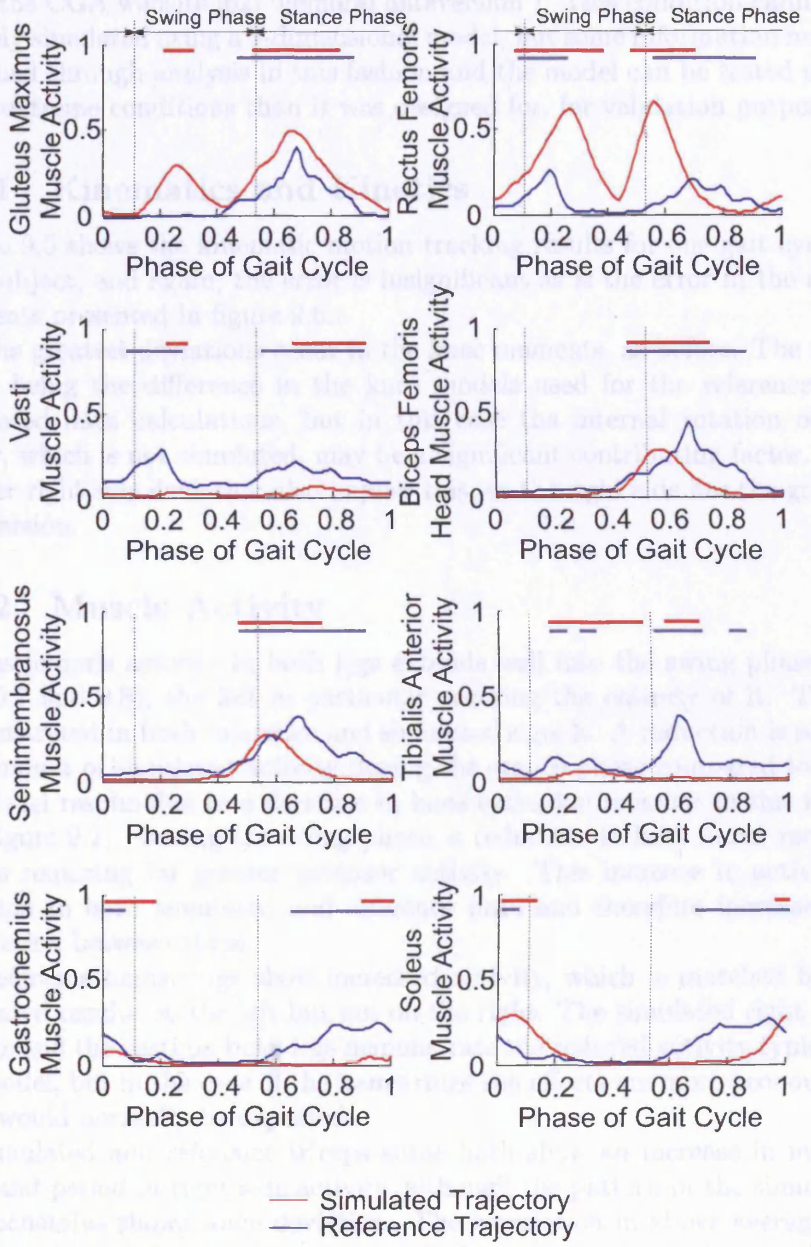

Figure 9.4: Femoral nerve palsy subject left leg simulated muscle activity and EMG measurements

9.3 Femoral Anteversion

This data is from a diplegic nine year-old with femoral anteversion (obtained from the CGA website [62] 'Femoral anteversion'). This condition cannot be entirely simulated using a 2-dimensional model, but some information may be obtained through analysis in this fashion and the model can be tested under more extreme conditions than it was designed for, for validation purposes.

9.3.1 Kinematics and Kinetics

Figure 9.5 shows the kinematic motion tracking results for one gait cycle of this subject, and again, the error is insignificant as is the error in the ankle moments presented in figure 9.6.

The greatest deviations occur in the knee moments, as before. The main cause being the difference in the knee models used for the reference and simulated data calculations, but in this case the internal rotation of the femur, which is not simulated, may be a significant contributing factor. The greater right side deviation also implies this, as the right side has the greater anteversion.

9.3.2 Muscle Activity

Rectus femoris activity in both legs extends well into the swing phase (figures 9.7 and 9.8), the left in particular covering the entirety of it. This is demonstrated in both reference and simulated signals. A reduction is seen in the amount of simulated activity during the stance phase compared to typical model results due to a decrease in knee extension moment in this region (see figure 9.2). During the swing phase, a reduction in knee flexor moment occurs requiring far greater extensor activity. This increase in activity is common to both simulated and reference data and therefore increases the correlation between them.

Reference hamstrings show increased activity, which is matched by the simulated results on the left but not on the right. The simulated right hamstrings and the vasti on both legs demonstrate the reduced activity typical to the model, but in the case of the hamstrings the effects are more pronounced than would normally be expected.

Simulated and reference triceps surae both show an increase in magnitude and period of right side activity, although the pattern of the simulated gastrocnemius shows some deviation. The correlation in above average activation of most of the triceps surae and tibialis anterior muscles is reduced due to the decrease in the ankle moments, which leaves the moment required for unmodelled dynamics and differences in musculoskeletal geometry, thus increasing the error.

As expected the data here does not provide as close a match as the previous sample. The degree of correlation of above average muscle activity

is reduced to 67.4% but this does not preclude the attainment of useful information, particularly with regard to the rectus femoris and left hamstring behaviour, which are two of the most important features of this pathology.

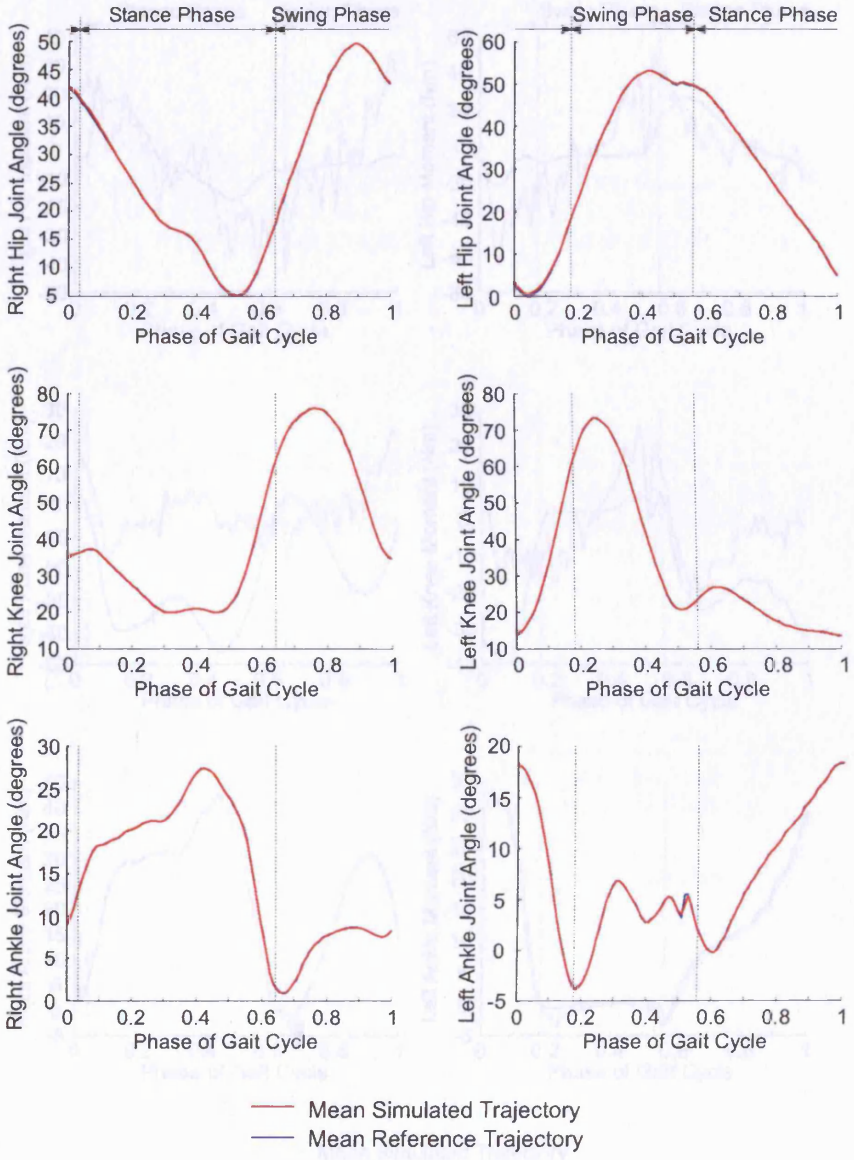

Figure 9.5: Femoral anteversion subject joint angle motion tracking results

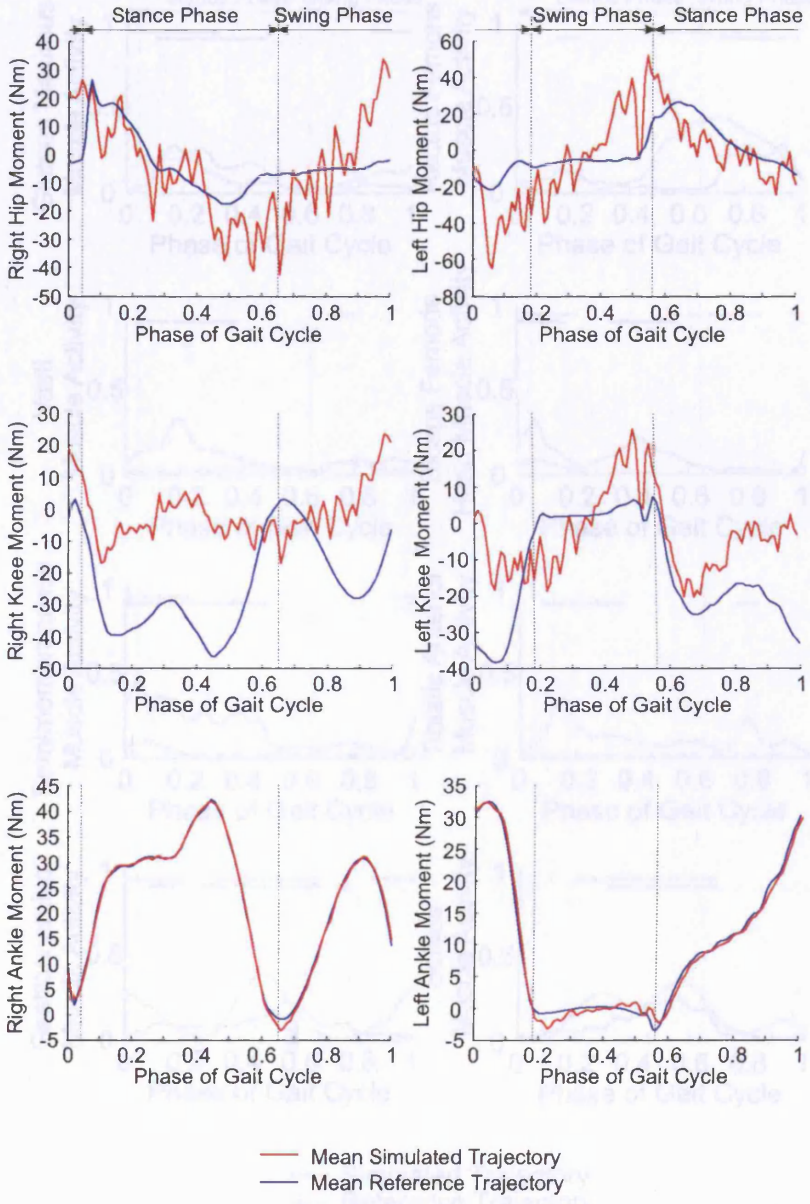

Figure 9.6: Femoral anteversion subject joint moments during motion tracking

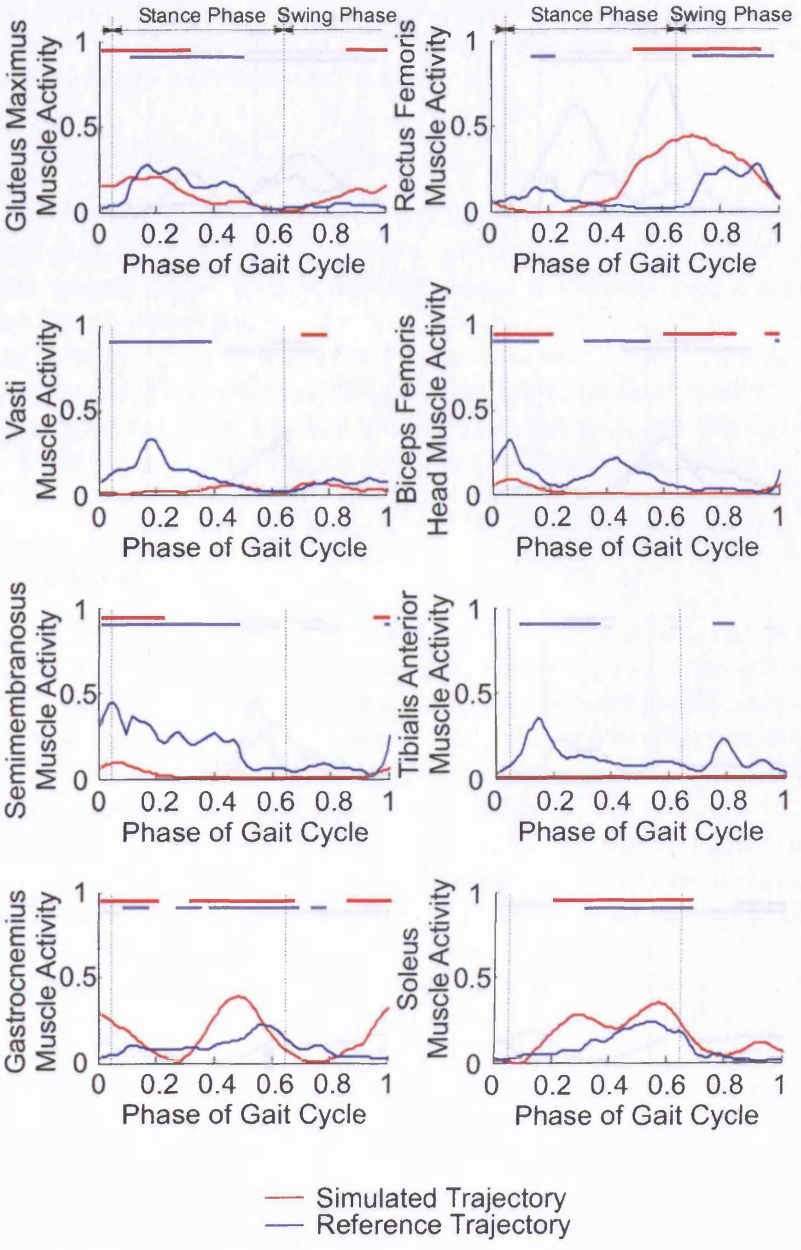

Figure 9.7: Femoral anteversion subject right leg simulated muscle activity and EMG measurements

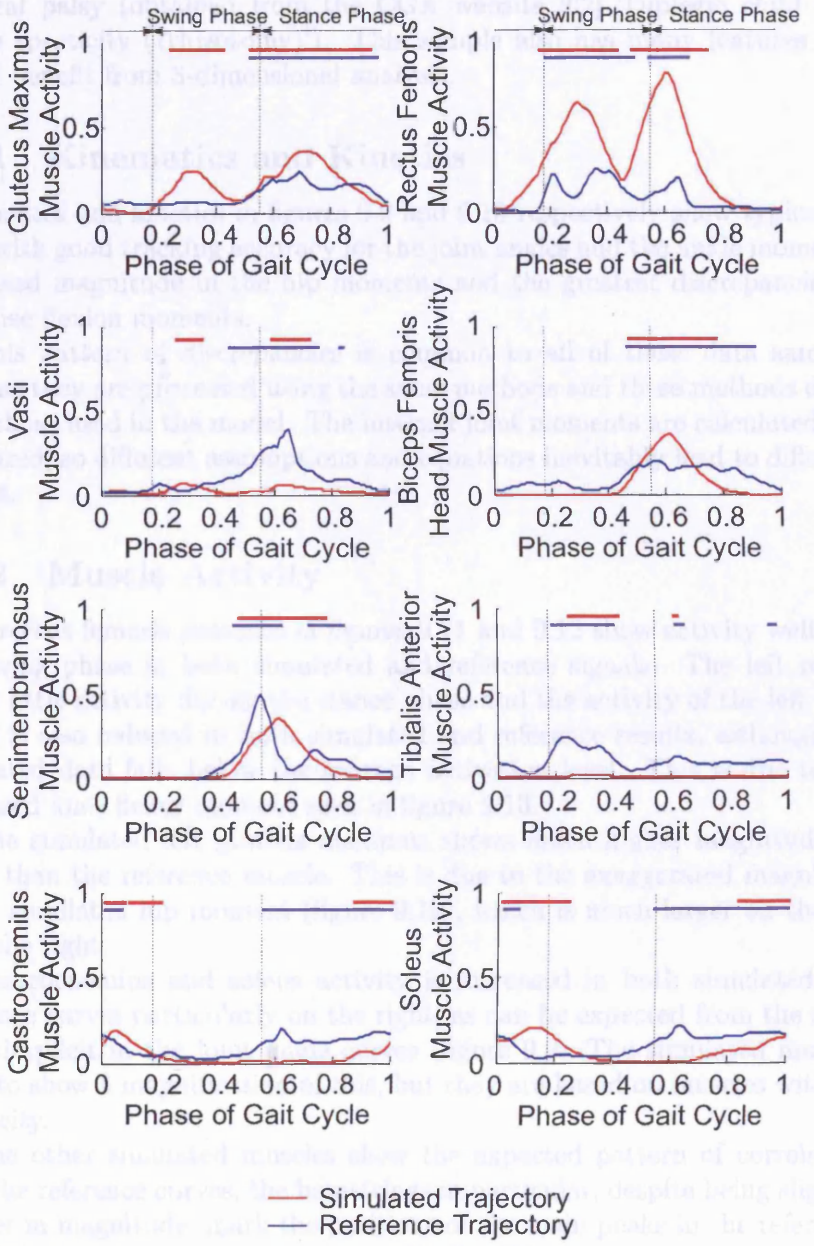

Figure 9.8: Femoral anteversion subject left leg simulated muscle activity and EMG measurements

9.4 Diplegic Idiopathic Cerebral Palsy

This final sample was taken from a ten year-old girl with diplegic idiopathic cerebral palsy (obtained from the CGA website [62] 'Diplegic child with severe spasticity (?rhizotomy)'). This sample also has many features that would benefit from 3-dimensional analysis.

9.4.1 Kinematics and Kinetics

Kinematics and kinetics in figures 9.9 and 9.10 respectively show typical results with good tracking accuracy for the joint angles and the ankle moments, increased magnitude in the hip moments and the greatest discrepancies in the knee flexion moments.

This pattern of discrepancies is common to all of these data samples because they are processed using the same methods and these methods differ from those used in the model. The internal joint moments are calculated not measured, so different assumptions and equations inevitably lead to different results.

9.4.2 Muscle Activity

Both rectus femoris patterns in figures 9.11 and 9.12 show activity well into the swing phase in both simulated and reference signals. The left rectus shows little activity during the stance phase and the activity of the left vasti group is also reduced in both simulated and reference results, although the simulated data falls below the average activation level. This is due to the increased knee flexor moment seen in figure 9.10.

The simulated left gluteus maximus shows much higher magnitude activity than the reference muscle. This is due to the exaggerated magnitude of the simulated hip moment (figure 9.10), which is much larger on the left than the right.

Gastrocnemius and soleus activity is increased in both simulated and reference curves particularly on the right, as can be expected from the spasticity implicit in the joint angle curves (figure 9.9. The simulated muscles seem to show a magnification of this, but they are based on muscles without spasticity.

The other simulated muscles show the expected pattern of correlation with the reference curves, the hamstrings in particular, despite being slightly smaller in magnitude, mark the positions of the main peaks in the reference signals and demonstrate correlations of 81%-89%.

The average correlation for this gait cycle is 69.7%.

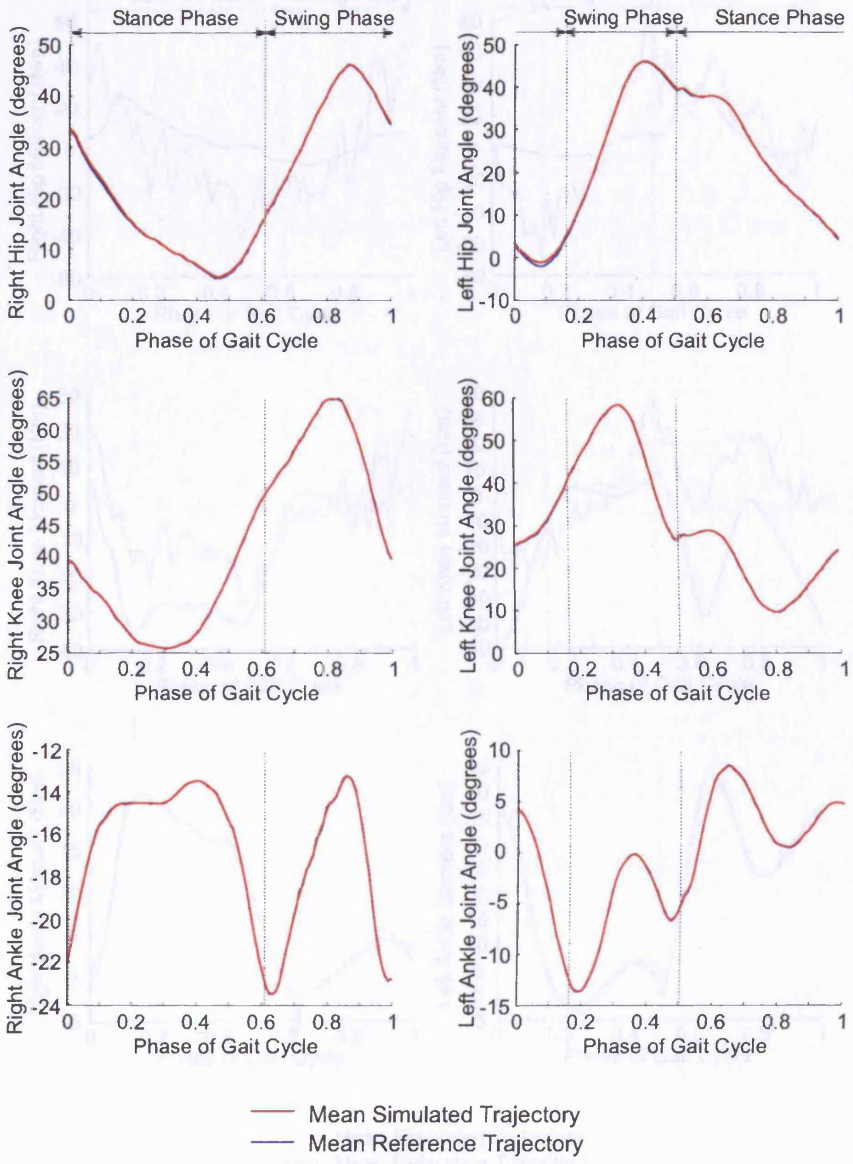

Figure 9.9: Diplegic idiopathic cerebral palsy subject joint angle motion tracking results

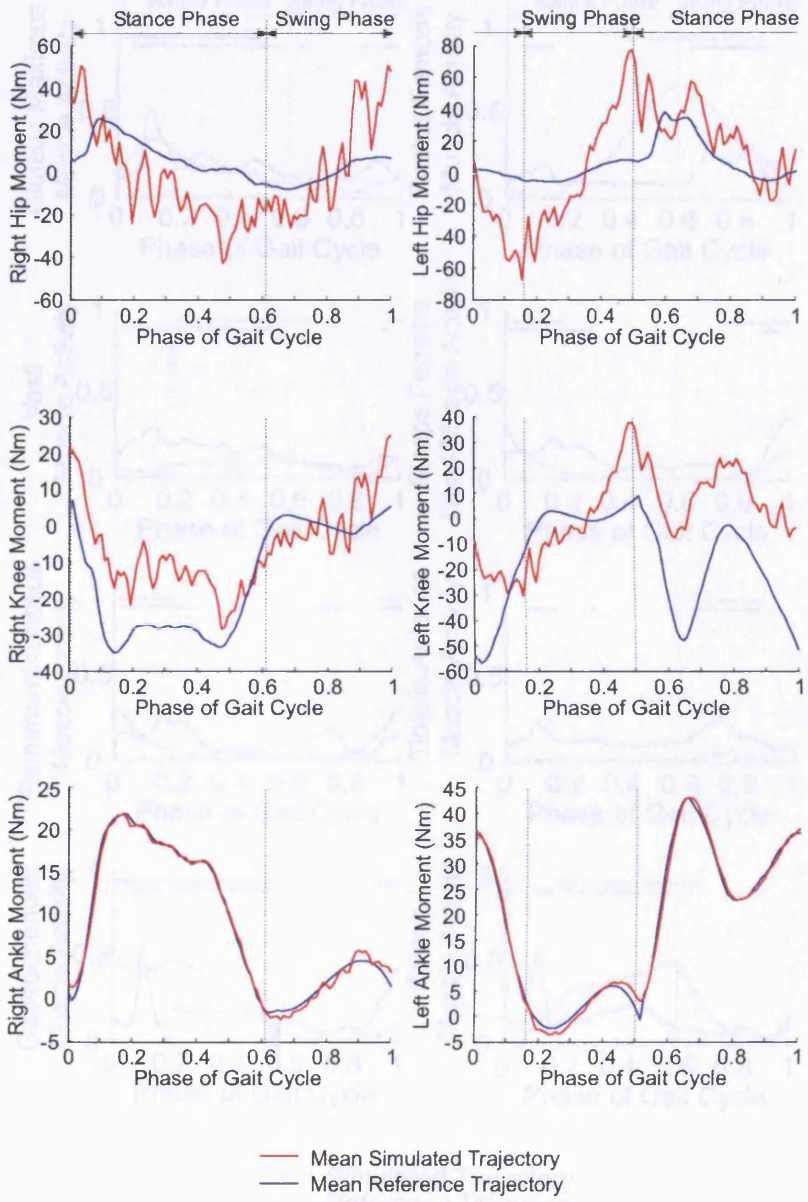

Figure 9.10: Diplegic idiopathic cerebral palsy subject joint moments during motion tracking

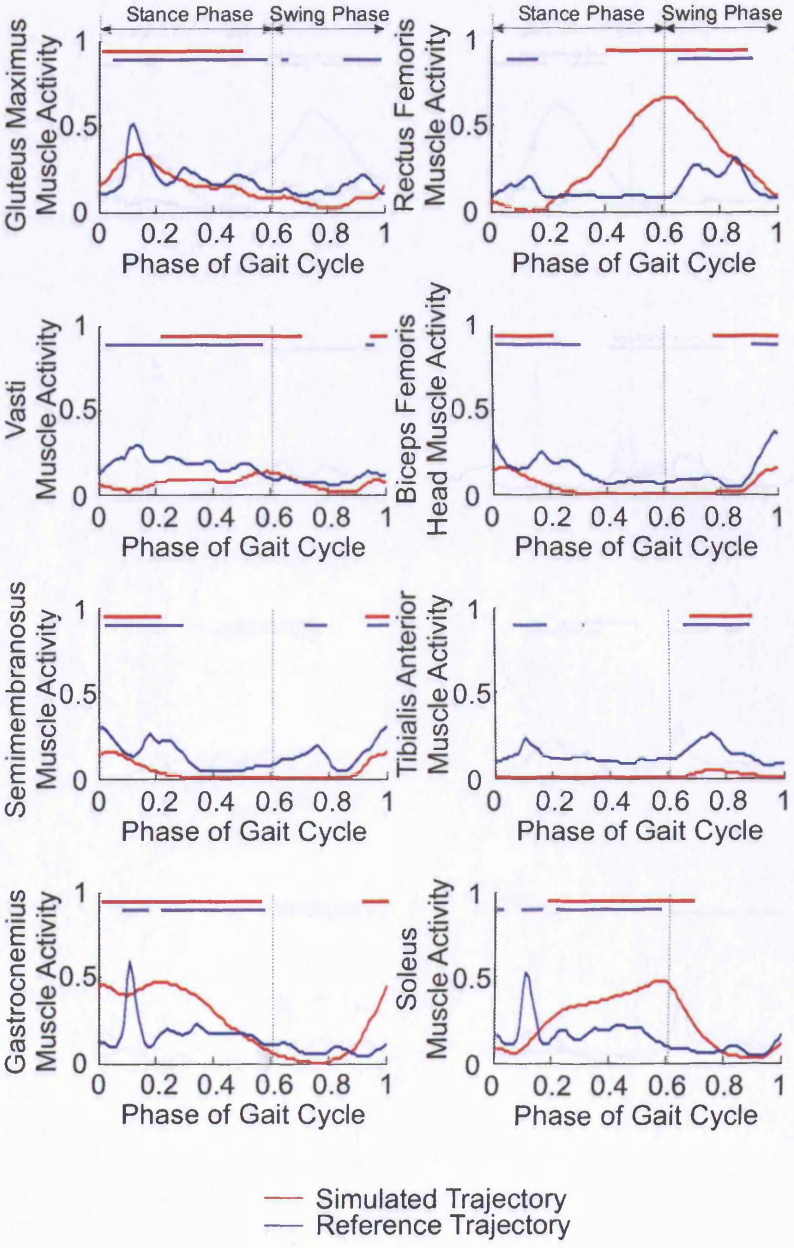

Figure 9.11: Diplegic idiopathic cerebral palsy subject right leg simulated muscle activity and EMG measurements

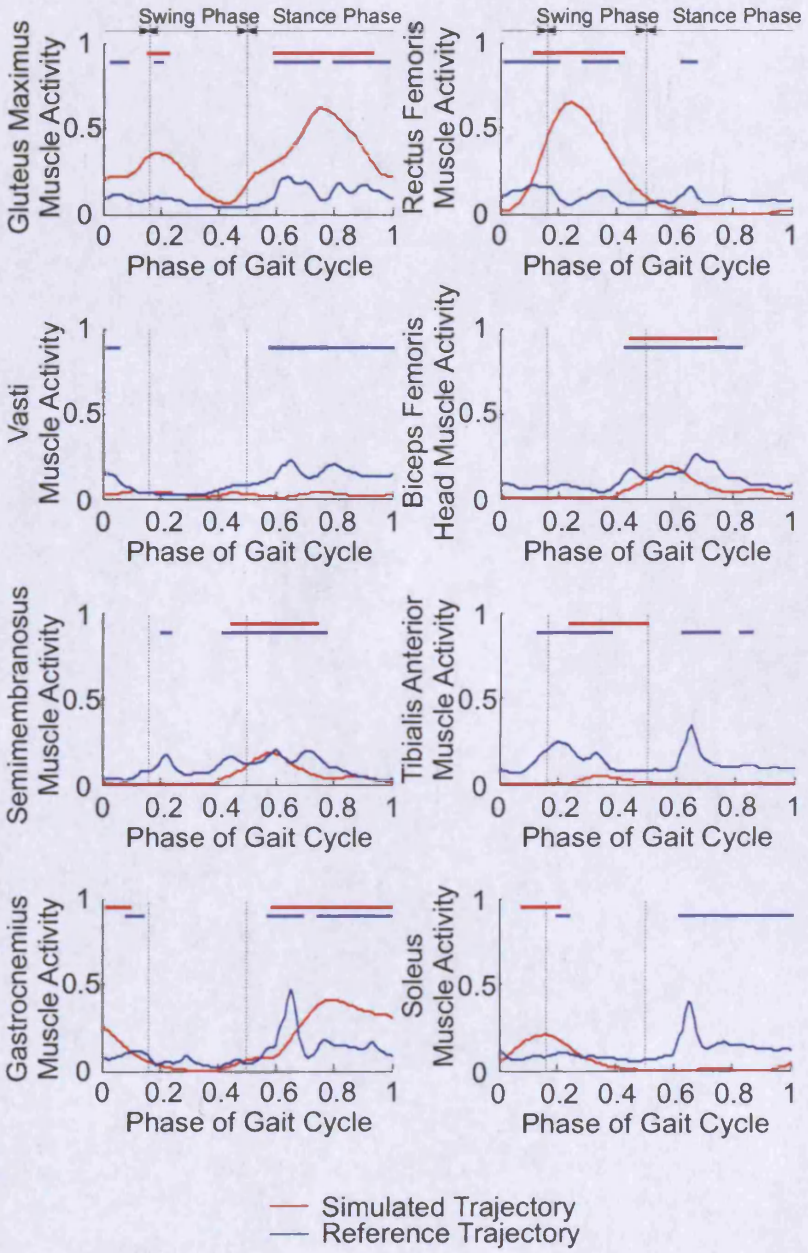

Figure 9.12: Diplegic idiopathic cerebral palsy subject left leg simulated muscle activity and EMG measurements

9.5 Summary

As was expected, the model performs motion tracking of any gait samples entered into it with errors small enough to be neglected. The model would also be capable of tracking other motions and with minor modifications could simulate sit-to-stand and stand-to-sit trajectories.

Some deviation was seen from the reference moments, due to a combination of the use of a pin joint model for the knee and the different calculations used to generate these moments in the simulation. The use of different calculations does not mean that either is wrong, as they may be calculated relative to slightly different points and be based on different assumptions. Without accurate in-vitro measurements from inside the joints the validity of any method cannot be fully verified.

Despite analysing 3-dimensional pathologies with a 2-dimensional model, the muscle activations show correlations of 67.4%-70.0% with the reference EMG signals. Inevitably there are some unaccounted for variations, but for the most part the differences in the standard simulation pattern reveal the same behaviour in the reference signals. This correlation is lower than the 74.8% for the normal gait samples, but this is to be expected with 3-dimensional pathologies.

Provided that the ever-present deviations of excessive activity in the rectus femoris, reduced activity in the hamstrings, vasti and tibialis anterior and a second peak in the gluteus maximus curve are accounted for, the simulation can be used to estimate the activity occurring in the muscles of a subject from kinematic and kinetic data samples. While it would certainly be possible to build in a function to automatically adjust and remove these differences, without a mathematical basis for doing so this would be unwise and could lead to further errors. Tailoring the system parameters to given individuals would help reduce these differences and would be an important step in the process of developing muscle stimulation controllers for them, as is the long term aim of the project. In addition, the controllers will be developed using sliding-mode techniques, and it is exactly these sort of plant-model mismatches to which sliding-mode controllers are insensitive [29].

The model can therefore function as a first stage, non-invasive muscle activity estimator, and as a basis for the development of sliding-mode muscle stimulation controllers.

Chapter 10

Conclusions and Future Work

10.1 Conclusions

As a result of the work detailed in this thesis, conclusions can be drawn in several areas including neuro-musculo-skeletal modelling, motion tracking of human gait using sliding-mode techniques and simulation of optimised muscle activity in such a system. All of these areas relate to the aims of providing a versatile and expandable gait analysis and therapy tool for future research and platform for further development, in particular as a basis for the development of muscle stimulation controllers for subjects of limited gait capability through neural dysfunction.

The research motivation driving this project is the disability of those suffering from conditions such as Parkinsonism, head or spinal injury, stroke, multiple sclerosis and cerebral palsy. Where a failure or reduction in quality of the neural activation signals to muscles involved in gait occurs the locomotive capacity of the subject is diminished, causing loss of speed, stability and confidence. FES techniques combined with adequate sliding-mode controllers could provide a means for subjects with these conditions to walk more normally improving their stability, freedom and thus, quality of life.

To this end a series of objectives was laid out in Chapter 1, the first of which was the construction of a forward-dynamics neuro-musculo-skeletal model capable of simulating human gait. Chapter 6 lays out the details of the construction of a 10 segment, pin-jointed, sagittal plane model developed using LaGrange's equations driven by 52 musculotendon actuators based on a modified Hill-type model. A default set of parameters can be used and modified as necessary to adapt the model to a given individual (Appendix C).

Restriction of the model to the sagittal plane allowed quicker construction and simulation, while scope was left for future expansion to 3-dimensions. The majority of gait motion takes place in the sagittal plane, especially for normal subjects, but for pathological patterns in particular there may be very important features in the frontal and horizontal plane motions, such as

Trendelenberg sign or circumduction which are neglected by the model. A 2-dimensional model would be incapable of simulating these correctly, but the model could be of use with other gait pathologies and with gait patterns corrected through the use of muscle stimulation controllers, e.g. if a foot drop is corrected then circumduction need no longer occur.

Open-loop locomotive gait modelling is impractical at best as the system is fundamentally unstable. The second objective therefore, was the development of a controller to force the model to follow observed gait trajectory data from real subjects.

To this end, Chapter 3 describes common methods and equipment employed to collect gait data and details the wealth of information that can be obtained through gait analysis.

Chapter 4 explains the actual methods used to collect data for the purposes of this project; kinematic data was collected using an infra red video capturing system (Qualysis Inc.), kinetic data was calculated based on readings from a force plate (Bertec Inc.) embedded in the capture surface and muscle activity data was measured using a four-channel EMG system (BIOPAC Inc.). The Internet was used as a source for further data samples.

Chapter 5 lays out the processing performed on the collected data samples to transform them into viable input files for the model. For each sample format a unique processing function was created for this purpose. Each of these functions is examined in Chapter 5 and presented in Appendix B.

Development of the controller that fulfils the second objective is described in Chapter 7. For the first time, the unique properties of variable structure control systems in the form of sliding-mode control techniques have been successfully implemented into a gait tracking system. In finite time, the control law forces the system trajectories to the sliding-surface and maintains them there for the remainder of the simulation. This provides precise tracking of simulated outputs to reference inputs with errors of less than 2 degrees with even the most inaccurate of parameters (Chapter 8).

The difference between reference and simulated moments required to drive the model through the trajectories input depends upon the accuracy of the parameters used in the model and the similarity between the methods used to calculate the reference moments with the motion dynamics of the model. Assumptions are made about the positions of the joints and centres of mass relative to the markers. These assumptions vary from method to method, so inevitably the resulting moments will differ. In addition the use of a pin joint for the modelled knee increases the inaccuracy. Despite this, for the normal samples used, the moments remain almost exclusively within a 2 standard deviation range of the reference (Chapter 8). The error is greater in the case of the pathological samples, due to greater deviations in the calculation methods.

Without exact initial conditions, some settling time of the system is inevitable. For this reason, during each simulation the gait cycle was repeated,

with some interpolation to smooth the end-start transition, and only the second cycle was used for analysis.

Use of the controller output signals to estimate the muscle activity required to produce the gait pattern being followed was the third objective. With many more muscles than controller outputs, some optimisation was needed. The muscles were grouped according to their actions on the joints that they crossed. Each muscle in a group would be assumed to have the same activation signal as the others. A set of optimisation criteria designed to minimise the total energy use by finding the pattern of minimum muscle activity required to perform the motion was then laid out based on the assumption that energy use and muscle activity are directly proportional (Chapter 7).

Muscle activity patterns do show some correlation with the expected results. The normal gait patterns tested averaged 74.8% correlation of signals exceeding the average for the muscle activity being examined, while the pathological patterns simulated averaged 69.0%. Pathological cycles may average lower correlation due to the increased lateral motion of the gait trajectories that the 2-dimensional model cannot simulate. The model cannot generate an exact match to the patterns due to parameter differences and the fact that the system does not allow for a unique solution. However, in general the regions of significant activity in the reference EMG signals correspond to the regions of significant activity in the simulated signals. This occurs despite the discrepancies in the moment curves as the same methods used to calculate the joint moments are used to calculate the maximum muscle moments. The activations are found by dividing joint moments by maximum muscle moments, thus the discrepancies act against each other and better fitting results are produced than might otherwise be expected.

Muscle activity generated by the model shows certain predictable deviations from the EMG reference signals. Variation to this characteristic structure corresponds to variations in the EMG signals as demonstrated in Chapter 9, allowing an experienced user to estimate the actual muscle activity of a subject being motion tracked by the model. When developing an FES system based on the model, however, these variations become unacceptable. The use of sliding-mode techniques greatly reduces this problem. Sliding-mode controllers are insensitive to plant-model mismatches, rejecting uncertainty and unmodelled dynamics while the sliding-surface is maintained [29]. As such the system would only generate as much activity as is necessary for the movement, producing an activation profile appropriate for each unique subject just as the activation pattern generated during simulation is appropriate for the unique characteristics of the model.

The switching behaviour of sliding-mode controllers offers another benefit in the form of antagonism. Muscles crossing opposite sides of the same joint are in some cases activated simultaneously in order to stabilise the joint. High frequency switching by the controller produces the same effect. When forces

and body mass are unstably balanced about a joint it becomes sensitive to small changes in moment. The switching function causes the moments to switch back and forth from positive to negative, activating muscles on either side of the joint, thus producing antagonism in similar periods as it occurs in real subjects.

In addition, an increasing amount of information points to the existence of positive force feedback control occuring in human movement [94, 93]. Linear control systems typically become unstable under positive feedback conditions, but provided the reachability conditions are met, a sliding-mode controller can remain stable [29].

The final objective laid out in the introduction was to provide an environment for the development of FES muscle stimulation controllers. The model has been shown to simulate normal and pathological gait patterns to an acceptable accuracy despite the lack of accurate physical parameters, and when tailored to an individual this precision increases further (Chapters 8 and 9). As such the model is an acceptable substitute for a test subject and can be used for the development of muscle stimulation controllers without fear of injury or discomfort.

The model can simulate how the activity pattern of the subjects other muscles may respond to the influence of an FES system and thus test the validity of the system. While no system can provide an exact prediction of a subject's neuro-muscular behaviour, the model has been shown to generate similar results to experimental EMG readings and thus can be assumed to offer one possible acceptable solution.

Musculotendon parameters used in research are almost exclusively acquired through cadaver measurements [21, 33, 113] and therefore matching kinematic, kinetic and EMG data cannot be collected. Obtaining in-vitro measurements of the sizes and geometries of every muscle used in gait is an enormous task involving complex, expensive and impractical techniques such as ultrasonography and MRI [47, 48, 117]. The insensitivity to plant-model mismatches of sliding-mode techniques makes this problem of little importance, as accurate parameters are not necessary to generate appropriate outcomes with this method [29].

Deformity can easily be programmed into the system by adjusting the existing parameters, and spasticity can be taken into account by adding constant stimulation to the muscle input signal and adding the output to the relevant joint moment(s).

As a forward-dynamics neuro-musculo-skeletal model with an integral sliding-mode controller and optimised muscle activity estimator, the model can function both as a powerful tool for gait analysis and non-invasive EMG estimation and as a platform for the development of FES controllers for subjects with neuro-muscular gait anomalies. This fulfils all of the objectives laid out in the introduction.

10.2 Future Work

The main limitations of the model are its 2-dimensional nature and the modelling of the knee as a simple pin joint. These should be the principal considerations for a future modelling project. Both require a substantial reworking of the motion dynamics of the model, so should be performed together. The muscles are already described in 3-dimensions, so very little work would be required to adapt them, but the optimisation procedure would need reworking as more muscle groups become relevant for 3-dimensional analysis.

The hip is a ball and socket joint with a 'feasible error range' in the centre of rotation of more than 1 cm [23]. It can therefore be effectively modelled by a fixed centre of rotation in the pelvis (minor deviations during rotation being well within this range). The ankle joint complex should be modelled as separate talocrural and subtalar joints with fixed axes of rotation relative to the proximal segment. The ankle joints rotate about a fixed point with translations small enough to be neglected, so they can be modelled as pin joints. The knee joint shows significant translation relative to any chosen centre of rotation, so for accurate simulation this must be built into the model. A mathematical description of knee joint translation with rotation can be found in the parameters supplied by Delp to the ISB website [21].

Development of FES controllers using the model and testing their performance first in simulation and then on real subjects is a natural progression of the work laid out here. Limits can be applied to the output moments generated by the controller based on the predicted muscle activity in order to simulate inadequate neural stimulation of the muscles affected by a given subject's condition. A sliding-mode controller can then be developed to stimulate the required muscle models as necessary to maintain the input trajectory.

Muscles behave slightly differently under FES than neural stimulus, so an electrically stimulated muscle model such as that described in Durfee and Palmer [28] should be used as well as consideration made of previously developed closed-loop FES muscle force controllers [17, 18, 56, 114].

These FES controllers would be much smaller than the model and could therefore be copied into a piece of portable hardware to be carried by a subject in order to drive a muscle stimulation system to correct their gait abnormality. Each controller would be unique to the subject it was developed for and in the early stages, regular checks and adjustments would be required as the subject's gait pattern adapted to the system.

The model is versatile enough to be used for other types of research including sports science, arthritis research and robotics.

Motion tracking of any movement of the lower limbs is possible, so analysis of loading and stress is possible during physical activity including sports. This would be of use not only in a medical context, but also in the design of equipment.

Some research has already been carried out in the University of Leicester

Department of Engineering concerning whether muscle activation patterns can be a cause of, or contributing factor to, arthritis [69, 70, 71, 72]. The previous research focused on the knee joint with a sagittal plane knee model. The model developed for this study could be used to analyse hip, knee and ankle joints bilaterally.

By replacing musculotendon actuators with motors or pneumatics the model could be used in robotics simulation and research.

The model developed here provides a sound basis for future research projects, not only to extend the original motivation for which it was developed, but also branching out into other related fields. Further development of the model will enhance its value as a research tool.

Bibliography

[1] J. J. Abbas and H. J. Chizeck. Neural network control of functional neuromuscular stimulation systems: Computer simulation studies. *IEEE Transactions on Biomedical Engineering*, 42(11):1117–1127, 1995.

[2] F.C. Anderson and M.G. Pandy. Dynamic optimization of human walking. *Journal of Biomechanics*, 34(5):381–390, 2001.

[3] K. Arabi and M.A. Sawan. Electronic design of a multichannel programmable implant for neuromuscular electrical stimulation. *IEEE Transactions on Rehabilitation Engineering*, 7(2):204–214, 1999.

[4] J.V. Basmajian and C.J. De Luca. *Muscles Alive.* Williams & Wilkins, 5th edition, 1985.

[5] A. Benallegue, N.K. M'Sirdi, and N. Manamani. Learning control and sliding mode control for a pneumatic legged robot. In *Proceedings of the IEEE-Syst. Man and Cybernetics, IMACS*, Hammamet, Tunisia, April 1998.

[6] M. Bijak, C. Hofer, H. Lanmuller, W. Mayr, S. Sauermann, E. Unger, and H. Kern. Personal computer supported eight channel surface stimulator for paraplegic walking: first results. *Artificial Organs*, 23:424–427, 1999.

[7] L. Blankevoort and R. Huiskes. Validation of a three-dimensional model of the knee. *Journal of Biomechanics*, 29(7):955–961, 1996.

[8] R.A. Brand, R.D. Crowninshield, and C.E. Wittstock. A model for lower muscular anatomy. *Journal of Biomechanics*, 19:589–596, 1986.

[9] T.I.H. Brown, Ying Huang, D.L. Morgan, U. Proske, and A. Wise. A new strategy for controlling the level of activation in artificially stimulated muscle. *IEEE Transactions on Rehabilitation Engineering*, 7(2):167–173, 1999.

[10] J.H. Burridge, P.N. Taylor, S.A. Hagan, and I.D. Wood, D.E. an Swain. The effect of common peroneal nerve stimulation on quadriceps spasticity in hemiplegia. *Physiotherapy*, 83(2):82–89, 1997.

[11] J.H. Burridge and D. Wood. Invited symposium: The role of fes assisted movements in the rehabilitation of motor impaired persons (8 presentations in this symposium) two channel stimulation for hemiplegic gait. control algorithms, selection of muscle groups and the results of a preliminary clinical trial.

[12] C3D.ORG. C3d data file format information. *Motion Lab Systems, Inc. (www.c3d.org)*, 2003.

[13] D. R. Carter and G. S. Beaupré. *Skeletal Function and Form.* Cambridge University Press, 2001.

[14] J. Case. *Sensory Mechanisms.* The Macmillan Company, 1966.

[15] T.-H. Chang and Y. Hurmuzlu. Sliding control without reching phase and its application to bipedal locomotion. *Journal of Dynamic Systems, Measurement and Control*, 115:447–455, 1993.

[16] Peripheral Systems Lab. Computer Science Department at the École Polytechnique Fédèrale de Lausanne. The visible human server. *http://visiblehuman.epfl.ch/index.php*, 2003.

[17] P. E. Crago, J. T. Mortimer, and P. H. Peckham. Closed-loop control of force during electrical stimulation of muscle. *IEEE Transactions on Biomedical Engineering*, 27(6):306–311, 1980.

[18] P. E. Crago, P. H. Peckham, and G. B. Thrope. Modulation of muscle force by recruitment during intramuscular stimulation. *IEEE Transactions on Biomedical Engineering*, 27(12):679–684, 1980.

[19] R. Davoodi, B.J. Andrews, and G.D. Wheeler. Manual and automaitc control of fes-assisted indoor rowing exercise.

[20] D.T. Davy and M.L. Audu. Dynamic optimisation techniques for predicting muscle forces in the swing phase of gait. *Journal of Biomechanics*, 10:187–201, 1987.

[21] S.L. Delp. Parameters for a model of the lower limb. *International Society of Biomechanics website (http://isb.ri.ccf.org./data/delp/)*, 1990.

[22] S.L. Delp, J.P. Loan, M.G. Hoy, F.E. Zajac, E.L. Topp, and J.M. Rosen. An interactive graphics-based model of the lower extremity to study orthopaedic surgical procedures. *IEEE Transactions on Biomedical Engineering*, 37:757–767, 1990.

[23] S.L. Delp and W. Maloney. Effects of hip centre location on the moment-generating capacity of the muscles. *Journal of Biomechanics*, 26(4/5):485–499, 1993.

[24] S.L. Delp and F.E. Zajac. Force and moment generating capacity of lower extremity muscles before and after tendon lengthening. *Clinical Orthopaedics and Related Research*, 284:247–259, 1992.

[25] S.J. Dorgan and T. Fuhr. Mathematical modelling and control of human skeletal dynamics. *Engineering Science and Engineering Journal*, 8(4):185–192, 1999.

[26] S.J. Dorgan and R.B. Reillr. A model for human skin impedance during surface functional neuromuscular stimulation. *IEEE Transactions on Rehabilitation Engineering*, 7(3):341–348, 1999.

[27] W.K. Durfee. Task-based methods for evaluating electrically stimulated antagonist muscle controllers. *IEEE Transactions on Biomedical Engineering*, 36:309–321, 1988.

[28] W.K. Durfee and K. I. Palmer. Estimation of force-activations, force-length and force velocity properties in isolated electrically stimulated muscle. *IEEE Transactions on Biomedical Engineering*, 41(3):205–216, 1994.

[29] C. Edwards and S.K. Spurgeon. *Sliding Mode Control Theory and Applications.* Taylor and Francis LTD., 1998.

[30] A. Ephanov and Y. Hurmuzlu. Generating pathological gait patterns via the use of robotic locomotion models. 1997.

[31] M. Ferrarin, F. Palazzo, R. Riener, and J. Quintern. Model-based control of fes-induced single joint movements. *IEEE Transactions on Neural Systems and Rehabilitation Engineering*, 9(3):245–258, 2001.

[32] M. Ferrarin and A. Pedotti. The relationship between electrical stimulus and joint torque: a dynamic model. *IEEE Transactions on Rehabilitation Engineering*, 8(3):342–352, 2000.

[33] J.A. Friederich and R.A. Brand. Muscle fibre architecture in the human lower limb. *Journal of Biomechanics*, 23:91–95, 1990.

[34] M. Fritz and K. Peikenkamp. Simulation of the influence of sports surfaces on vertical ground reaction forces during landing. *Medical and Biological Engineering & Computing*, 41:11–17, 2003.

[35] S.S. Galen and M.H. Granat. Study of the effect of functional electrical stimulation (fes) on walking in children undergoing botulinum toxin a therapy. In *FESnet 2002 conference proceedings (fesnet.eng.gla.ac.uk/conference/2002.html)*, 2002.

[36] P. Gallien, R. Brissot, M. Eyssette, L. Tell, M. Barat, L. Wiart, and H. Petit. Restoration of gait by functional electrical stimulation for spinal cord injured patients. *Paraplegia*, 33:660–664, 1995.

[37] M. Gföhler, A.J. van Soest, and L.J.R. Casius. Can fes cycling be improved by releasing the ankle joint? In *IX International Symposium on Computer Simulation in Biomechanics*, Sydney, Australia, July 2003.

[38] L.A. Gilchrist and D.A. Winter. A two-part viscoelastic foot model for use in gait simulations. *Journal of Biomechanics*, 29(6):795–798, 1996.

[39] M. Glanz, S. Klawansky, W. Stason, C. Berkey, and T.C. Chalmers. Functional electrostimulation in poststroke rehabilitation: A meta-analysis of the randomized controlled trials. *Archives of Physical Medicine and Rehabilitation*, 77(6):549–553, 1996.

[40] D. Graupe. Emg pattern analysis for patient-responsive control of fes in paraplegics for walker supported walking. *IEEE Transactions on Biomedical Engineering*, 36:711–719, 1989.

[41] J. Hamill and K.M. Knutzen. *Biomechanical Basis of Human Movement.* Williams & Williams, 1995.

[42] H. Hatze. A complete set of control equations for the human musculoskeletal system. *Journal of Biomechanics*, 10:799–805, 1977.

[43] D. Hawkins and M. L. Hull. A method for determining lower-extremity muscle-tendon lengths during flexion/extension movements. *Journal of Biomechanics*, 23:487–494, 1990.

[44] M.G. Hoy, F.E. Zajac, and M.E. Gordon. A musculoskeletal model of the human lower extremity: The effect of muscle, tendon, and moment arm on the moment-angle relationship of musculotendon actuators at the hip, knee, and ankle. *Journal of Biomechanics*, 23:157–169, 1990.

[45] K.J. Hunt, B. Stone, N. Negård, and T. Schauer. Fes cycling with electric motor assist. In *1st FESnet Conference*, pages 7–9, Glasgow, Scotland, 2002.

[46] M. Ilic, D. Vasiljevic, and D.B. Popovic. A programmable electronic stimulator for fes systems. *IEEE TRansactions on Rehabilitation Engineering*, 2(4):234–239, 1994.

[47] M. Ito, H. Akimo, and T. Fukunaga. In vivo moment arm determination using b-mode ultrasonography. *Journal of Biomechanics*, 33:215–218, 2000.

[48] S. V. S. Jan, D. J. Giurintano, D. E. Thompson, and M. Rooze. Joint kinematics from medical imaging data. *IEEE Transactions on Biomedical Engineering*, 44(12):1175–1184, 1997.

[49] S. Jezernik, Inderbitzin P., T. Keller, and R. Riener. Sliding mode control of functional electrical stimulation for knee joint angle tracking. In *Proceedings of the 7th Vienna International Workshop on Functional Electrical Stimulation*, pages 160–163, 2001.

[50] S. Jezernik, Inderbitzin P., T. Keller, and R. Riener. A novel sliding mode controller for functional electrical stimulation. In *Proc. of the 15th IFAC World Congress on Automatic Control*, pages 199–203, 2002.

[51] S. Jezernik and R. Riener. A computer simulation of tuned pid and continuous sliding mode fes control. In *Proceedings of the International Biomechatronics Workshop*, pages 37–41, 1999.

[52] S. Jezernik, R.G.V. Wassink, and T. Keller. Sliding mode closed loop control of fes: Controlling the shank movement. *IEEE Transactions on Biomedical Engineering*, 51(2):263–272, 2004.

[53] C.A. Johnson, D. Wood, I.D. Swain, A.M. Tromans, P. Strike, and J.H. Burridge. A pilot study to investigate the combined use of botulinum neurotoxin type a and functional electrical stimulation, with physiotherapy, in the treatment of spastic dropped foot in subacute stroke. *Artificial Organs*, 26(3):263–266, 2002.

[54] M.W. Johnson, P.H. Peckham, N. Bhadra, K.L. Kilgore, M.M. Gazdik, and M.W. Kieth. Implantable transducer for two-degree of freedom joint angle sensing. *IEEE Transactions on Rehabilitation Engineering*, 7(3):349–359, 1999.

[55] E.R. Kandel, J.H. Schwartz, and T.M. Jessell. *Principles of Neural Science*. Appleton & Lange, 4th edition, 1991.

[56] Z. Z. Karu, W. K. Durfee, and A. M. Barzilai. Reducing muscle fatigue by stimulating with n-let pulse trains. *IEEE Transactions on Biomedical Engineering*, 42(8):809–817, 1995.

[57] K. R. Kaufman, E. Y. S. Chao, and H. E. Rubash. Predication of antagonistic muscle forces using inverse dynamic optimization during flexion/extension of the knee. *Transactions of the ASME Journal of Biomedical Engineering*, 121:316–322, 1999.

[58] T. Keller, M.R. Popovic, I.P.I. Pappas, and P.Y Müller. Transcutaneous functional electrical stimulator "compex motion". *Artificial Organs*, 26(3):219–223, 2002.

[59] G. Khang and F.E. Zajac. Paraplegic standing controlled by functional neuromuscular stimulation: Part 1 computer model and control-system design. *IEEE Transactions on Biomedical Engineering*, 36(9):873–884, 1989.

[60] G. Khang and F.E. Zajac. Paraplegic standing controlled by functional neuromuscular stimulation: Part 2 computer simulation studies. *IEEE Transactions on Biomedical Engineering*, 36(9):885–894, 1989.

[61] P. Kiriazov. Control design in computer simulation of human movement: Biologically plausible methods. In *VIII International Symposium on Computer Simulation in Biomechanics*, July 2001.

[62] C. Kirtley, Kranzl A., and Kopf A. Pathological gait samples including kinematic, kinetic and emg measurements. *CGA website. (http://guardian.curtin.edu.au/cga/case.html)*, 2003.

[63] C. Kirtley and J. Linskell. Kinematic and kinetic gait samples including some emg measurements. *CGA Normative Gait Database. (http://www.univie.ac.at/cga/data/index.html)*, 2003.

[64] R. Kobetic and E.B. Marsolais. Synthesis of paraplegic gait with multichannel functional neuromuscular stimulation. *IEEE Transactions on Rehabilitaion Engineering*, 2(2):66–79, 1994.

[65] R.D. Komitek, J.B. Stiehl, D.A. Dennis, R.D. Paxson, and R.W. Soutas-Little. Mathematical model of the lower extremity joint reaction forces using kane's method of dynamics. *Journal of Biomechanics*, 31:185–189, 1998.

[66] T. Komura, P. Prokopow, and A. Nagano. Evaluation of the influence of muscle deactivation on other muscles and joints during gait motion. *Journal of Biomechanics*, 37(4):425–436, 2004.

[67] S.H. Koozekanani and J. Duerk. Determination of body segment parameters and their effect in the calculation of the position of the center of pressure during postural sway. *IEEE Transactions on Biomedical Engineering*, 32:67–69, 1985.

[68] C. Larivière and D. Gagnon. The influence of trunk modelling on 3d biomechanical analysis of simple and complex lifting tasks. *Journal of Clinical Biomechanics*, 14:449–461, 1999.

[69] C. L. Lim, N. B. Jones, S. K. Spurgeon, and J. J. A. Scott. Modelling of knee joint movement during walking - understanding the implications of knee osteoarthritis. Unpublished draft, 2000.

[70] C. L. Lim, N. B. Jones, S. K. Spurgeon, and J. J. A. Scott. Modelling of knee joint muscles during the swing phase of gait - a forward dynamics approach using matlab/simulink. *Simulation Modelling Practice and Theory*, 11:91–107, 2003.

[71] C. L. Lim, N. B. Jones, S. K. Spurgeon, and J. J. A. Scott. Reconstruction of human neuromuscular control signals using a sliding mode control technique. *Simulation Modelling Practice and Theory*, 11:223–235, 2003.

[72] C.L. Lim. *Models of human knee movements for internal signal estimation.* PhD thesis, University of Leicester Department of Engineering, 2002.

[73] S. Lister, N. B. Jones, W. Peasgood, and S. K. Spurgeon. A neuro-musculo-skeletal model for the simulation of normal and pathological human gait patterns. In *Proceedings of the IEEE EMBSS UK & RoI PG Conference in Biomedical Engineering and Medical Physics*, page 4, 2002.

[74] T. Lu. Muscle recruitment strategies of the human locomotor system during normal walking: A mechanical perspective. *Biomedical Engineering Applications Basis Communications*, 11:191–202, 1999.

[75] N. Manamani, N. Nadjar-Gauthier, and N.K. M'Sirdi. Sliding-mode control for a pneumatic robot leg. In *Proceedings of the European Control Conference*, pages 699–710, Brussels, Belgium, July 1997.

[76] W.D. Memberg, P.H. Peckham, and M.W. Keith. A suurgically-implanted intramuscular electrode for an implantable neuromuscular stimulation system. *Ieee Transactions on Rehabiliation Engineering*, 2(2):80–91, 1994.

[77] M.M. Mirbagheri, M. Ladouceur, H. Barbeau, and R.E. Kearney. The effects of log term fes assisted walking on intrinsic and reflex dynamic stiffness in spastic spinal-cord-injured subjects. *IEEE Transactions on Neural Systems and Rehabilitation Engineering*, 10(4):280–289, 2002.

[78] J. Mizrahi, M. Levy, H. Ring, E. Isakov, and A. Liberson. Emg as an indicator of fatigue in isometrically fes-activated paralyzed muscles. *IEEE Transactions on Rehabilitation Engineering*, 2(2):57–65, 1994.

[79] N.O. Negârd, T. Schauer, and J. Raisch. Robust nonlinear control of knee-joint angle: A simulation study. In *Proceedings of the 3rd Wismar Symposium on Automatic Control*, 2002.

[80] N.O. Negârd, T. Schauer, and J. Raisch. Robust nonlinear control of single limb movement. In *Proc. of the 5th IFAC Symposium on Modelling and Control in Biomedical Systems (Including Biological Systems)*, 2003.

[81] M. Nordin and V.H. Frankel. *Basic Biomechanics of the Musculoskeletal System.* Lippincott, Williams & Wilkins, 3rd edition, 2001.

[82] National Library of Medicine (US). The visible human project. *http://www.nlm.nih.gov/research/visible/visible_human.html*, 2003.

[83] M. G. Pandy and N. Berme. Synthesis of human walking: A planar model for single support. *Journal of Biomechanics*, 21(12):1053–1060, 1988.

[84] J. Perry. *Gait Analysis.* SLACK, Thorofare, NJ, 1992.

[85] S.J. Piazza and S.L. Delp. The influence of muscles on knee flexion during the swing phase of gait. *Journal of Biomechanics*, 29:723–733, 1996.

[86] D.A. Pierre. *Optimization Theory with Applications.* John Wiley and Sons, Inc., 1969.

[87] D. Poboroniuc, M.S.and Wood, N. Donaldson, T. Fuhr, and R. Riener. Closed-loop control for fes-based restoration of standing in paraplegia. In *2nd World Congress of the International Society of Physical and Rehabilitation Medicine - ISPRM*, pages 201–204, Prague, Czech Republic, May 2003.

[88] M.S. Poboroniuc, T. Fuhr, R. Riener, and N. Donaldson. Closed-loop control for fes-supported standing-up and sitting-down. In *Proceedings of the 7th Annual IFESS Conference*, pages 307–309, Ljubljana, Slovenia, 2003.

[89] D. Popovic and S. Jonic. Control of bipedal locomotion assisted with functional electrical stimulation. In *Proceedings of the American Control Conference*, volume 2, pages 1238–1242, 1999.

[90] D. Popovic, R.B. Stein, M.N. Oguztoreli, M. Lebiedowska, and S. Jonic. Optimal control of walking with functional electrical stimulation: A computer simulation study. *IEEE Transactions on Rehabilitation Engineering*, 7(1):69–79, 1999.

[91] S. D. Prentice, A. E. Patla, and D. A. Stacey. Artificial neural network model for the generation of muscle activation patterns for human locomotion. *Journal of Electromyography and Kinesiology*, 11:19–30, 2001.

[92] D. D. Pringle, A. M. Seger, and J. Ponichtera-Mulcare. Locomotive function in individuals with multiple sclerosis. In *Proceedings of the Southern Conference Biomedical Engineering*, pages 433–436, 1996.

[93] A. Prochazka, Gillard D., and D. J. Bennet. Implications of positive feedback in the control of movement. *Journal of Neurophysiology*, 77:3237–3251, 1997.

[94] A. Prochazka, Gillard D., and D. J. Bennet. Positive force feedback control of muscles. *Journal of Neurophysiology*, 77:3226–3236, 1997.

[95] R. Riener and T. Fuhr. Patient-driven control of fes-supported standing up: a simulation study. *IEEE Transaciton on Rehabilitation Engineering*, 6(2):113–124, 1998.

[96] R. Riener, J. Quintern, and G. Schmidt. Biomechanicsl model of the human knee evaluated by neuromuscular stimulation. *Journal of Biomechanics*, 1996.

[97] T. Schauer, W. Holderbaum, and K.J. Hunt. Sliding-mode control of knee-joint angle: experimental results. In *Proceedings of the International Functional Electrical Stimulation Society 2002 Conference*, pages 316–318, 2003.

[98] T. Schauer and K.J. Hunt. Linear modelling and controller design for the single limb movement of paraplegics using fes. In *Preprints of the 4th IFAC Symposium on Modelling and Control in Biomedical Systems*, Greifswald, Germany, March-April 2000.

[99] T. Schauer and K.J. Hunt. Nonlinear predictive control of knee-joint angle using fes. In *IFESS Conference 2000*, Aalborg, Denmark, June 2000.

[100] Y. Shimada, K. Sato, E. Abe, H. Kagaya, K. Ebata, M. Oba, and M. Sato. Clinical experience of funcational electrical stimulation in complete paraplegia. *Spinal Cord*, 34:615–619, 1996.

[101] G. Shue, P.E. Crago, and H.J. Chizeck. Muscle-joint models incorporating activation dynamics, moment-angle and moment-velocity properties. *IEEE Transactions on Biomedical Engineering*, 42:212–222, 1995.

[102] S. Siegler, S. Lapointe, R. Nobilini, and A.T. Berman. Six-degrees-of-freedom instrumented linkage for measuring the flexibility characteristics of the ankle joint complex. *Journal of Biomechanics*, 39(7):943–947, 1996.

[103] J. J. E. Slotine and W. Li. *Applied Nonlinear Control.* Prentice-Hall, Inc., 1991.

[104] K.D. Strange and J.A. Hoffer. Restoration of use of paralyzed limb muscles using sensory nerve signals for state control of fes-assisted walking. *IEEE Transactions on Rehabilitation Engineering*, 7(3):289–300, 1999.

[105] I.D. Swain, J.H. Burridge, C.A. Johnson, G.E. Mann, P.N. Taylor, and P.A. Wright. The efficacy of functional electrical stimulation in improving walking ability of people with multiple sclerosis. In *Proceedings of the 5th Annual Conference of the IFESS Society*, pages 55–58, 2000.

[106] P.N. Taylor, J.H. Burridge, Dunkerley, D.E. Wood, J.A. Norton, S. Singleton, and I.D. Swain. Clinical use of the odstock dropped foot stimulator. its effect on the speed and effort of walking. *Archives of Physical Medicine and Rehabilitation*, 80:1577–1583, 1999.

[107] P.N. Taylor, J.H. Burridge, A.L. Dunkerley, A. Lamb, D.E. Wood, J.A. Norton, and I.D. Swain. Patients perceptions of the odstock dropped foot stimulator (odfs). *Clinical Rehabilitation*, 13:333–340, 1999.

[108] T.A. Thrasher and M.R. Popovic. Fes-assisted walking for rehabilitation of incomplete spinal cord injury. In *Proceedings of the IFESS Conference*, Brisbane, Australia, July 2003.

[109] M. Trew and T. Everett. *Human Movement AN INTRODUCTORY TEXT.* Harcourt International, 4th edition, 2001.

[110] C. L. Vaughan. Gaitlab format data files (i.e. apm, emg, fpl, & kin). *International Society of Biomechanics Biomechanical Data Resources (http://www.isbweb.org/data.index.html)*, 2003.

[111] T. Watanabe, R. Futami, N. Hoshimiya, and Y. Handa. An approach to a muscle model with a stimulaus frequency-force relationship for fes applications. *IEEE Transactions on Rehabilitation Engineering*, 7(1):12–18, 1999.

[112] M. W. Whittle. *Gait Analysis an Introduction.* Reed Educational and Professional Publishing LTD., 1996.

[113] R.R. Wickiewicz, T.L. Roy and V.R. Edgerton. Muscle architecture of the human lower limb. *Clinical Orthopaedics and Related Research*, 179:275–283, 1983.

[114] G. F. Wilhere, P. E. Crago, and H. J. Chizeck. Design and evaluation of a digital closed-loop controller for the regulation of muscle force by recruitment modulation. *IEEE Transactions on Biomedical Engineering*, 32(9):668–676, 1985.

[115] D. A. Winter. Kinemaitcs and kinetic patterns in human gait: Variability and compensating effects. *Human Movement Science*, 3:51–76, 1984.

[116] D. A. Winter. Biomechanics of normal and pathological gait: Implications for understanding human locomotor control. *Journal of Motor Behaviour*, 21(4):337–355, 1989.

[117] S. Wood, D. J. Pearsall, R. Ross, and J. G. Reid. Trunk muscle parameters determined from mri for lean to obese males. *Clinical Biomechanics*, 11(3):139–144, 1996.

[118] www.emgsrus.com. C3d files for biomechanics. *Motion Lab Systems, Inc. (http://www.emgsrus.com/c3dformat.htm)*, 2003.

[119] E.L. Zajac, F.E. Topp and P.J. Stevenson. A dimensionless musculotendon model. In *Proceedings of the 8th Annual Conference of the Engineering in Medicine and Biology Society*, pages 601–604, 1986.

[120] F.E. Zajac. Muscle and tendon: Properties, models, scaling and application to biomechanics and motor control. *Critical Reviews Biomedical Engineering*, 17:359–411, 1989.

[121] F.E. Zajac. Muscle coordination of movement - a perspective. *Journal of Biomechanics*, 26(Supplement):109–124, 1993.

[122] F.E. Zajac, R. R. Neptune, and S. A. Kautz. Biomechanics and muscle coordination of human walking part i: Introduction to concepts, power transfer, dynamics and simulations. *Gait and Posture*, 16:215–232, 2002.

[123] F.E. Zajac, R. R. Neptune, and S. A. Kautz. Biomechanics and muscle coordination of human walking part ii: Lessons from dynamical simulations and clinical implications. *Gait and Posture*, 17:1–17, 2003.

Appendices

Appendix A

Anatomical Marker Positioning

The following are descriptions of the marker positions used when taking kinematic gait samples for the model.

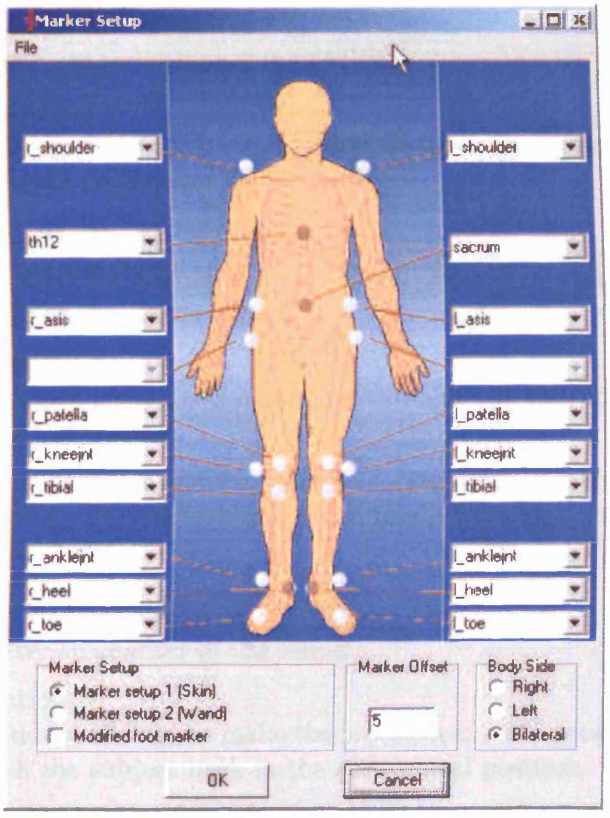

Marker Positioning.

SHOULDER

On the superior surface of the acromion.

Marker application:

Apply the marker approximately 1 cm medially of the lateral edge, centrally fore-aft.

12th Thoracic Vertebra (TH 12)

On the spinous process of the 12th thoracic vertebra

Marker application:

Find the L3-L4 interspace at the same level as the tops of the iliac crests. Then palpate the spinous processes from L3 up to TH12 and apply the marker.

The shoulder markers and 12th thoracic vertebra marker describe a plane used to calculate the angle of the upper body relative to the plane running through the pelvis markers

ASIS

At the anterior superior iliac spine (ASIS).

Marker application:

Follow the iliac crest to the anterior and distal to the spine at the end of the crest and apply the marker there.

SACRUM

On the sacrum on a horizontal line with the two ASIS markers when the subject is in the anatomical position.

Marker application:

Apply the marker on the medial line through the sacrum horizontally level with the ASIS markers

The two ASIS markers and the sacrum marker define the transverse plane through the pelvis. The angle of this plane relative to the system axes is the pelvis angle.

GREATER TROCHANTER

At the greater trochanter of the femur.

Marker application:

Flex and Adduct the hip to make the trochanter more prominent. Apply the marker with the subject back in the anatomical position.

The greater trochanter marker is only used in unilateral measurements

PATELLA

Along the central line of the patella, 1 cm proximally of the superior edge.

Marker application:

Palpate the edges of the patella, and apply the marker centrally, approximately one cm above the top edge. If the patella is dislocated, apply the marker at the central line of the thigh instead of at the central line of the patella.

KNEE JOINT

Laterally on the knee joint line. Centrally on the lateral aspect of the knee when the patella is excluded.

Marker application:

Find the line between the lateral condyles of the femur and tibia and apply the marker centrally on the lateral aspect of the knee ignoring the patella.

TIBIAL TUBEROSITY

On the tibial tuberosity.

Marker application:

Apply the marker on the middle of the tubercle with special care in the lateral-medial direction as the calculations are very sensitive to inaccuracy in this direction.

ANKLE

At the lateral malleolus.

Marker application:

Centrally on the malleolus

TOE

On the foot between the 2nd and 3rd metatarsal bones, 10-15 mm proximally of the metatarsal heads.

Marker application:

Apply the marker between the 2nd and 3rd metatarsal bones, 10-15 mm proximally of the metatarsal heads.

HEEL

On the posterior of calcaneus, in the same horizontal plane as the toe marker.

Marker application:

Apply the marker centrally on the posterior heel, at the same horizontal plane as the toe marker. If the marker is too close to the floor and there is a risk it may be knocked off during gait, the toe marker should be moved proximally and the heel marker raised into the same horizontal plane.

Appendix B

Data Processing Code

Matlab function for processing data from TSV, _A.TSV and QGT files

```
function processtsv(fpl,tsv,qgt,TotalMass,TotalHeight,...
   freq,start,stop)

%TotalMass=input('Mass (kg): ');
%TotalHeight=input('Height (m): ');
%freq=input('Camera Frequency (Hz): ');
%start=input('Start frame: ');
%stop=input('Stop frame: ');

% Establish filenames
name=qgt;
fpl=[fpl,'.tsv'];
mtsv=[tsv,'.tsv'];
atsv=[tsv,'_A.tsv'];
qgt=[qgt,'.qgt'];

% Input data
fplmarkers=dlmread(fpl,'\t',10,0)/1000;
groundreaction=dlmread(atsv,'\t',[12+start,0,12+stop,5]);
%z,x,y

Trajectories=dlmread(qgt,'\t',[289+start,0,289+stop,23]);

thoracicmarker=dlmread(mtsv,'\t',[9+start,0,9+stop,2])/1000;
%x,(z),y

Rightanklemarker=dlmread(mtsv,'\t',...
   [9+start,21,9+stop,23])/1000;
Leftanklemarker=dlmread(mtsv,'\t',...
   [9+start,45,9+stop,47])/1000;

% Define parameters
noofframes=size(thoracicmarker,1);
halfcycle=round(noofframes/2);
```

```
Timestep=1/freq;
StepSize=0.0005;
TotalTime=noofframes*timestep*2 timestep;
GaitPhase=[0:timestep:TotalTime]';
Walkingdirection=sign(thoracicmarker(noofframes,1) ...
     thoracicmarker(1,1));

% Angles

Trajectories=Trajectories(:,[23 20 1 4 7 7 10 13 16...
     16])*pi/180;
% Select required trajectories and convert to radians

Pelvis_Trajectory=Trajectories(:,2);
Body_Trajectory= Trajectories(:,1) Pelvis_Trajectory;
R_Thigh_Trajectory=Trajectories(:,3)+Pelvis_Trajectory;
R_Shank_Trajectory= Trajectories(:,4)+R_Thigh_Trajectory;
R_Foot_Trajectory=Trajectories(:,5)+R_Shank_Trajectory;
R_Toes_Trajectory=R_Foot_Trajectory;
L_Thigh_Trajectory=Trajectories(:,7)+Pelvis_Trajectory;
L_Shank_Trajectory= Trajectories(:,8)+L_Thigh_Trajectory;
L_Foot_Trajectory=Trajectories(:,9)+L_Shank_Trajectory;
L_Toes_Trajectory=L_Foot_Trajectory;

Trajectories=[Body_Trajectory,Pelvis_Trajectory,...
     R_Thigh_Trajectory,R_Shank_Trajectory,...
     R_Foot_Trajectory,R_Toes_Trajectory,...
     L_Thigh_Trajectory,L_Shank_Trajectory,...
     L_Foot_Trajectory,L_Toes_Trajectory];

% Interpolate beginning and end to provide a smooth
% transition when repeating data
yi=interp1([1:4 9:12]',[Trajectories(noofframes ...
     5:noofframes 2,:);Trajectories(3:6,:)],1:12,'spline');
Trajectories(noofframes 1:noofframes,:)=yi(5:6,:);
Trajectories(1:2,:)=yi(7:8,:);

Trajectories=[Trajectories;Trajectories];
% Repeat trajectories

[x,AngularVelocities]=gradient(Trajectories,timestep);
[X,AngularAccelerations]=gradient(AngularVelocities,...
     timestep);

% Offset ankle markers to find ankle joints

Rightanklejoint(:,1)=rightanklemarker(:,1)...
     +0.0315*walkingdirection*cos(R_Shank_Trajectory)
     +0.01*sin(R_Shank_Trajectory);
Rightanklejoint(:,2)=rightanklemarker(:,3)...
      0.0315*walkingdirection*Sin(R_Shank_Trajectory)...
     +0.01*cos(R_Shank_Trajectory);
Leftanklejoint(:,1)=leftanklemarker(:,1)...
     +0.0315*walkingdirection*Cos(R_Shank_Trajectory)...
     +0.01*sin(R_Shank_Trajectory);
Leftanklejoint(:,2)=leftanklemarker(:,3) ...
```

```
    0.0315*walkingdirection*Sin(R_Shank_Trajectory)...
    +0.01*cos(R_Shank_Trajectory);


% Ground reactions

% Average centre of force plate
avfplm=sum(fplmarkers(:,1:12))/size(fplmarkers(:,1:12),1);
fplc(1)=sum(avfplm([1,4,7,10]))/4;
fplc(2)=sum(avfplm([3,6,9,12]))/4;

% Zero offset ground reactions
offset=(groundreaction(1,:)+groundreaction(noofframes,:))/2;
for i=1:6
    groundreaction(:,i)=groundreaction(:,i)-offset(i);
end

sensitivity=[60.92    0.61  -0.94   0.465  0.2375  -0.7125
             -0.68   61.6    0.41  -0.14   0.3375  -0.25
             -1.68   -0.34 191.79   0.15   0.3625   2.1625
              0.015  -3.82  -0.16  35.19   0.075   -0.0125
              3.65   -0.085  0.14   0.2   61.9875  -0.025
              0.045   0      0.04   0.225 -0.4     35.6875];

% Adjust ground reactions according to sensitivity matrix
for i=1:noofframes
    groundreaction(i,:)=(sensitivity*groundreaction(i,:)')';
end
forcex=groundreaction(:,2)*walkingdirection;% Ensure +ve
forcey=groundreaction(:,3);

% Find point where ground reaction first exceeds 100N
j=0; k=0;
while j<1 ; k=k+1; j=groundreaction(k,3)>100; end


% Calculate ground reaction moments, establish ground
% reaction forces and moments and duplicate and offset for
% opposite leg
if (rightanklejoint(k,1)-fplc(1))^2<(leftanklejoint(k,1)-...
    fplc(1))^2
        Momentarm=[rightanklejoint(:,1)-fplc(1),...
    rightanklejoint(:,2)-fplc(2)];
       Momentz=(groundreaction(:,2).*momentarm(:,2)-...
       Groundreaction(:,3).*momentarm(:,1)-...
       groundreaction(:,4))*walkingdirection;
    Force(:,1)=forcex;
    Force(:,2)=forcey;
    Force(:,5)=momentz;
    Force(:,3)=[forcex(halfcycle+1:noofframes,1);...
       forcex(1:halfcycle,1)];
    Force(:,4)=[forcey(halfcycle+1:noofframes,1);...
       forcey(1:halfcycle,1)];
    Force(:,6)=[momentz(halfcycle+1:noofframes,1);...
       Momentz(1:halfcycle,1)];
else
```

```
    Momentarm=[leftanklejoint(:,1)-fplc(1),...
       leftanklejoint(:,2)-fplc(2)];
    Momentz=(groundreaction(:,2).*momentarm(:,2)...
       -groundreaction(:,3).*Momentarm(:,1)...
       -groundreaction(:,4))*walkingdirection;
    Force(:,1)=[forcex(halfcycle+1:nooframes,1);...
       forcex(1:halfcycle,1)];
    Force(:,2)=[forcey(halfcycle+1:nooframes,1);...
       forcey(1:halfcycle,1)];
    Force(:,5)=[momentz(halfcycle+1:nooframes,1);...
       momentz(1:halfcycle,1)];
    Force(:,3)=forcex;
    Force(:,4)=forcey;
    Force(:,6)=momentz;
end

GroundReactions=[Force;Force]; % Repeat ground reactions


% Body centre of mass accelerations

[x,Velocities]=gradient(thoracicmarker(:,[1,3]),timestep);
Velocities(:,1)=Velocities(:,1).*sign(Velocities(:,1)); %
Ensure positive
InitialVelocity=Velocities(1,:);
[x,Accelerations]=gradient(Velocities,timestep);

Acc=[Accelerations;Accelerations]; % Repeat accelerations


% Save all relevant data
Save(name,'TotalMass','TotalHeight','TotalTime',...
    'StepSize','InitialVelocity','GaitPhase','Acc',...
    'GroundReactions','Trajectories','AngularVelocities',...
    'AngularAccelerations','Body_Trajectory',...
    'Pelvis_Trajectory','R_Thigh_Trajectory',...
    'R_Shank_Trajectory','R_Foot_Trajectory',...
    'R_Toes_Trajectory','L_Thigh_Trajectory',...
    'L_Shank_Trajectory','L_Foot_Trajectory',...
    'L_Toes_Trajectory')
```

Matlab function for processing data from GCD files

```
function processgcd(gcdhtm,cadence)

% Establish filename
name=gcdhtm;
gcdhtm=[gcdhtm,'.htm'];

% Input data
TotalTime=dlmread(gcdhtm,' ',[cadence+2,0,cadence+2,0])*2;
InitialVelocity=[dlmread(gcdhtm,' ',[cadence+20,0,...
         cadence+20,0])/1000,0];

GroundReactions=dlmread(gcdhtm,' ',[cadence+1738,0,...
      cadence+1788,2]);%x,-,y
TotalMass=sum(GroundReactions(:,3))*2/(9.81*51);
Momentz=dlmread(gcdhtm,' ',[cadence+958,0,cadence+1008,0])...
   *TotalMass;

GRSD=[dlmread(gcdhtm,' ',[cadence+1738,6,cadence+1788,6]),...
      dlmread(gcdhtm,' ',[cadence+1738,8,cadence+1788,8])];
Moments=[dlmread(gcdhtm,' ',[cadence+646,0,cadence+696,1])...
      *TotalMass,dlmread(gcdhtm,' ',[cadence+802,0,...
      cadence+852,1])*TotalMass,dlmread(gcdhtm,' ',...
      [cadence+958,0,cadence+1008,1])*TotalMass];
Moments=Moments(:,[1 3 5 2 4 6]);

Pelvis_Trajectory=-dlmread(gcdhtm,' ',[cadence+22,0,...
      cadence+72,0])*pi/180;
Hip=dlmread(gcdhtm,' ',[cadence+178,0,cadence+228,0])*pi/180;
Knee=dlmread(gcdhtm,' ',[cadence+334,0,cadence+384,0])...
   *pi/180;
Ankle=dlmread(gcdhtm,' ',[cadence+490,0,cadence+540,0])...
   *pi/180;
PelvisSD=-dlmread(gcdhtm,' ',[cadence+22,1,cadence+72,1])...
   *pi/180;
HipSD=dlmread(gcdhtm,' ',[cadence+178,1,cadence+228,1])...
   *pi/180;
KneeSD=dlmread(gcdhtm,' ',[cadence+334,1,cadence+384,1])...
   *pi/180;
AnkleSD=dlmread(gcdhtm,' ',[cadence+490,1,cadence+540,1])...
   *pi/180;

% Define parameters
TotalHeight=1.75;
noofframes=51;
timestep=TotalTime/(51*2);
TotalTime=TotalTime-timestep;
StepSize=0.0005;
GaitPhase=[0:timestep:TotalTime]';

%Ground reactions
```

```
Force(:,1)=GroundReactions(:,1);
Force(:,2)=GroundReactions(:,3);
Force(:,5)=Momentz(:,1);
Force(:,3)=[GroundReactions(27:51,1);...
      GroundReactions(1:26,1)];
% Offset for other foot
Force(:,4)=[GroundReactions(27:51,3);...
      GroundReactions(1:26,3)];
Force(:,6)=[Momentz(27:51,1);Momentz(1:26,1)];

GroundReactions=[Force;Force]; % Repeat cycle


% Body centre of mass accelerations

Accelerations=0; % No data available
Accelerations(1:51,1:2)=0;

Acc=[Accelerations;Accelerations]; % Repeat cycle


% Angles

Body_Trajectory=Pelvis_Trajectory;
R_Thigh_Trajectory=Hip+Pelvis_Trajectory;
R_Shank_Trajectory=-Knee+R_Thigh_Trajectory;
R_Foot_Trajectory=Ankle+R_Shank_Trajectory;
R_Toes_Trajectory=R_Foot_Trajectory;
L_Thigh_Trajectory=[Hip(27:51,1);Hip(1:26,1)]...
   +Pelvis_Trajectory;
L_Shank_Trajectory=-[Knee(27:51,1);Knee(1:26,1)]...
   +L_Thigh_Trajectory;
L_Foot_Trajectory=[Ankle(27:51,1);Ankle(1:26,1)]...
   +L_Shank_Trajectory;
L_Toes_Trajectory=L_Foot_Trajectory;

Trajectories=[Body_Trajectory,Pelvis_Trajectory,...
      R_Thigh_Trajectory,R_Shank_Trajectory,...
      R_Foot_Trajectory,R_Toes_Trajectory,...
      L_Thigh_Trajectory,L_Shank_Trajectory,...
      L_Foot_Trajectory,L_Toes_Trajectory];
TrajectoriesSD=[PelvisSD,HipSD,KneeSD,AnkleSD];

% Interpolate beginning and end to provide a smooth
% transition when repeating data
yi=interp1([1:4 9:12]',[Trajectories(noofframes-5:...
      noofframes-2,:);Trajectories(3:6,:)],1:12,'spline');
Trajectories(noofframes-1:noofframes,:)=yi(5:6,:);
Trajectories(1:2,:)=yi(7:8,:);

Trajectories=[Trajectories;Trajectories]; % Repeat cycle
[x,AngularVelocities]=gradient(Trajectories,timestep);
[x,AngularAccelerations]=gradient(AngularVelocities,...
   timestep);

% Save all relevant data
```

```
Save(name,'TotalMass','TotalHeight','TotalTime',...
    'StepSize','InitialVelocity','GaitPhase','Acc',...
    'GroundReactions','Trajectories','AngularVelocities',...
    'AngularAccelerations','Body_Trajectory',...
    'Pelvis_Trajectory','R_Thigh_Trajectory',...
    'R_Shank_Trajectory','R_Foot_Trajectory',...
    'R_Toes_Trajectory','L_Thigh_Trajectory',...
    'L_Shank_Trajectory','L_Foot_Trajectory',...
    'L_Toes_Trajectory','TrajectoriesSD','Moments','GRSD')
```

Matlab function for processing data from APM, EMG, FPL, and KIN files

```
function processaefk(filename)

% Establish filenames
apm=[filename,'.apm'];
emg=[filename,'.emg'];
fpl=[filename,'.fpl'];
kin=[filename,'.kin'];

% Input data
parameters=dlmread(apm,' ');
muscleactivity=dlmread(emg,' ');
groundreaction=dlmread(fpl,' ');
kinematics=dlmread(kin,' ');

% Define parameters
TotalMass=parameters(1);
TotalHeight=(1.75/0.85)*sum(parameters([3,4,7,8]))/2;
timestep=0.02;
noofframes=size(kinematics,1)/15;

groundreaction=[groundreaction(1:2:noofframes*2,:),...
      groundreaction(2:2:noofframes*2,:)]; % Sort data

% Find point where first ground reaction first exceeds 100N
j=0; a=0;
while j<1 ; a=a+1; j=groundreaction(a,3)>100; end

% Find point where first ground reaction falls below 100N
b=a;
while j==1 ; b=b+1; j=groundreaction(b,3)>100; end

% Find point where second ground reaction first exceeds 100N
j=0; c=0;
while j<1 ; c=c+1; j=groundreaction(c,9)>100; end

% Find point where second ground reaction falls below 100N
d=c;
while j==1 ; d=d+1; j=groundreaction(d,9)>100; end

if c>a
    start=a;              % 'start' and 'stop' mark the gait
    stop=a+(c+d)-(a+b);   % cycle that contains ground
else                      % reaction data for both feet.
    start=c;
    stop=c+(a+b)-(c+d);
end

% Sort kinematic data into a more convenient form
righttoemarker=kinematics([1:15:noofframes*15],:);
rightheelmarker=kinematics([2:15:noofframes*15],:);
```

```
Rightanklemarker=kinematics([3:15:noofframes*15],:);
rightkneemarker=kinematics([5:15:noofframes*15],:);
righttrochmarker=kinematics([6:15:noofframes*15],:);
rightasismarker=kinematics([7:15:noofframes*15],:);
lefttoemarker=kinematics([8:15:noofframes*15],:);
leftheelmarker=kinematics([9:15:noofframes*15],:);
leftanklemarker=kinematics([10:15:noofframes*15],:);
leftkneemarker=kinematics([12:15:noofframes*15],:);
lefttrochmarker=kinematics([13:15:noofframes*15],:);
leftasismarker=kinematics([14:15:noofframes*15],:);
sacrummarker=kinematics([15:15:noofframes*15],:);


% Angles
Pelvis_Trajectory=-atan(((rightasismarker(:,3)...
   +leftasismarker(:,3))/2-sacrummarker(:,3))...
   ./((rightasismarker(:,1)+leftasismarker(:,1))/2 ...
   -sacrummarker(:,1)));
Body_Trajectory=Pelvis_Trajectory;
R_Thigh_Trajectory=-atan((righttrochmarker(:,1)...
   -rightkneemarker(:,1))./(righttrochmarker(:,3)...
   -rightkneemarker(:,3)));
R_Shank_Trajectory=-atan((rightkneemarker(:,1)...
   -rightanklemarker(:,1))./(rightkneemarker(:,3)...
   -rightanklemarker(:,3)));
R_Foot_Trajectory=atan((righttoemarker(:,3)...
   -rightheelmarker(:,3))./(righttoemarker(:,1)...
   -rightheelmarker(:,1)));
R_Toes_Trajectory=R_Foot_Trajectory;
L_Thigh_Trajectory=-atan((lefttrochmarker(:,1)...
   -leftkneemarker(:,1))./(lefttrochmarker(:,3)...
   -leftkneemarker(:,3)));
L_Shank_Trajectory=-atan((leftkneemarker(:,1)...
   -leftanklemarker(:,1))./(leftkneemarker(:,3)...
   -leftanklemarker(:,3)));
L_Foot_Trajectory=atan((lefttoemarker(:,3)...
   -leftheelmarker(:,3))./(lefttoemarker(:,1)...
   -leftheelmarker(:,1)));
L_Toes_Trajectory=L_Foot_Trajectory;

Trajectories=[Body_Trajectory,Pelvis_Trajectory,...
      R_Thigh_Trajectory,R_Shank_Trajectory,...
      R_Foot_Trajectory,R_Toes_Trajectory,...
      L_Thigh_Trajectory,L_Shank_Trajectory,...
      L_Foot_Trajectory,L_Toes_Trajectory];


% Offset ankle markers to find ankle joints

rightanklejoint(:,1)=rightanklemarker(:,1)+0.0315...
   *cos(R_Shank_Trajectory)+0.01*sin(R_Shank_Trajectory);
rightanklejoint(:,2)=rightanklemarker(:,3)-0.0315...
   *sin(R_Shank_Trajectory)+0.01*cos(R_Shank_Trajectory);
leftanklejoint(:,1)=leftanklemarker(:,1)+0.0315...
   *cos(R_Shank_Trajectory)+0.01*sin(R_Shank_Trajectory);
leftanklejoint(:,2)=leftanklemarker(:,3)-0.0315...
```

```
   *sin(R_Shank_Trajectory)+0.01*cos(R_Shank_Trajectory);


% Calculate ground reaction forces and moments
if (rightanklejoint(a,1)-groundreaction(a,4))^2 ...
   <(leftanklejoint(a,1)-groundreaction(a,4))^2
Force(:,1)=groundreaction(:,1)*sign(sacrummarker...
   (nooffframes,1)-sacrummarker(1,1)); % Ensure positive
    Force(:,2)=groundreaction(:,3);
    Force(:,5)=(groundreaction(:,1).*rightanklejoint(:,2)...
       -groundreaction(:,3).*(rightanklejoint(:,1)...
       -groundreaction(:,4)))*sign(sacrummarker...
       (nooffframes,1)-sacrummarker(1,1));
    Force(:,3)=groundreaction(:,7)*sign(sacrummarker...
       (nooffframes,1)-sacrummarker(1,1)); % Ensure positive
    Force(:,4)=groundreaction(:,9);
    Force(:,6)=(groundreaction(:,7).*leftanklejoint(:,2)...
       -groundreaction(:,9).*(leftanklejoint(:,1)...
       -groundreaction(:,10)))*sign(sacrummarker...
       (nooffframes,1)-sacrummarker(1,1));
else
   Force(:,1)=groundreaction(:,7)*sign(sacrummarker...
      (nooffframes,1)-sacrummarker(1,1)); % Ensure positive
    Force(:,2)=groundreaction(:,9);
    Force(:,5)=(groundreaction(:,7).*rightanklejoint(:,2)...
       -groundreaction(:,9).*(rightanklejoint(:,1)...
       -groundreaction(:,10)))*sign(sacrummarker...
       (nooffframes,1)-sacrummarker(1,1));
    Force(:,3)=groundreaction(:,1)*sign(sacrummarker...
       (nooffframes,1)-sacrummarker(1,1)); % Ensure positive
    Force(:,4)=groundreaction(:,3);
    Force(:,6)=(groundreaction(:,1).*leftanklejoint(:,2)...
    -groundreaction(:,3).*(leftanklejoint(:,1)...
    -groundreaction(:,4)))*sign(sacrummarker...
    (nooffframes,1)-sacrummarker(1,1));
end

if c>a % Left or right leg first? Trim and wrap
   GroundReactions(1:stop-start+1,[1:2,5])=Force(...
      [start:stop-start+1,1:start-1],[1:2,5]);
   GroundReactions(1:stop-start+1,[3:4,6])=Force(...
      [stop+1:stop+start,start+start:stop],[3:4,6]);
else
   GroundReactions([1:2,5],:)=Force([1:2,5],...
      [stop+1:stop+start,start+start:stop]);
   GroundReactions([3:4,6],:)=Force([3:4,6],...
      [start:stop-start+1,1:start-1]);
end
GroundReactions=[GroundReactions;GroundReactions];

nooffframes=stop-start+1; % Trim frames


% Reorder EMG signals into a more convenient form
Muscles=['Erector Spinae    ';'Gluteus Maximus  ';...
      'Gluteus Medius    ';'Hamstrings       ';...
```

```
      'Rectus Femoris    ';'Adductor Longus  ';...
      'Tibialis Anterior';'Triceps Surae     '];

for i=0:8:(noofframes-1)*8
    EMG(i/8+1,:)=muscleactivity(i+1:i+8,1)';
end


% Body centre of mass accelerations
% Sacrum marker data is used in the abscence of thoracic
[x,Velocities]=gradient(sacrummarker(:,[1,3]),timestep);
Velocities(:,1)=Velocities(:,1).*sign(Velocities(:,1));
InitialVelocity=Velocities(1,:);
[x,Accelerations]=gradient(Velocities,timestep);

Accelerations=Accelerations(start:stop,:); % Trim to 1 cycle
Acc=[Accelerations;Accelerations]; % Repeat cycle


% Other parameters
TotalTime=2*noofframes*timestep-timestep;
StepSize=0.0005;
GaitPhase=[0:timestep:TotalTime]';

Trajectories=Trajectories(start:stop,:); % Trim to 1 cycle

% Interpolate beginning and end to provide a smooth
% transition when repeating data
yi=interp1([1:4 9:12]',[Trajectories(noofframes-5:...
   noofframes-2,:);Trajectories(3:6,:)],1:12,'spline');
Trajectories(noofframes-1:noofframes,:)=yi(5:6,:);
Trajectories(1:2,:)=yi(7:8,:);

Trajectories=[Trajectories;Trajectories]; % Repeat cycle
[x,AngularVelocities]=gradient(Trajectories,timestep);
[x,AngularAccelerations]=gradient(AngularVelocities,...
   timestep);


% Save all relevant data
save(filename,'TotalMass','TotalHeight','TotalTime',...
   'StepSize','InitialVelocity','GaitPhase','Acc',...
   'GroundReactions','Trajectories','AngularVelocities',...
   'AngularAccelerations','Body_Trajectory',...
   'Pelvis_Trajectory','R_Thigh_Trajectory',...
   'R_Shank_Trajectory','R_Foot_Trajectory',...
   'R_Toes_Trajectory','L_Thigh_Trajectory',...
   'L_Shank_Trajectory','L_Foot_Trajectory',...
   'L_Toes_Trajectory','Muscles','EMG')
```

Appendix C

Default Model Parameters

The parameters that follow are presented in the Matlab format; the format in which they are used by the model.

```
%--------------------------------*
% General Simulation Parameters *
%--------------------------------*

TotalTime=1.1;
StepSize=0.0005;
TotalHeight=1.75;
TotalMass=77.02;
InitialVelocity=[1.3 0];

%----------*
% Segments *
%----------*

% Segment Masses

R_Toe_mass = 0.01;
R_Foot_mass = 0.99;
R_Shank_mass = 3.86;
R_Thigh_mass = 9.74;
Pelvis_mass = 9.94;
Body_mass = 35.88;
L_Thigh_mass = 9.74;
L_Shank_mass = 3.86;
L_Foot_mass = 0.99;
L_Toe_mass = 0.01;

% Centre of Mass Positions relative to the proximal joint of
% the relevant segment.
% 3-dimensional values are required for accurate muscle
% geometry calculations

Body_CofG = [0 0 0];
Pelvis_CofG = [0 -0.0650 0];
```

```
R_Thigh_CofG = [0 -0.172 0];
R_Shank_CofG = [0 -0.185 0];
R_Foot_CofG = [0.0312 -0.0420 0];
R_Toe_CofG = [0.010 0 0];
L_Thigh_CofG = [0 -0.172 0];
L_Shank_CofG = [0 -0.185 0];
L_Foot_CofG = [0.0312 -0.0420 0];
L_Toe_CofG = [0.010 0 0];

%--------*
% Joints *
%--------*

% Vector distance from the proximal joint to the distal joint
along the axes
% of the relevant segment

% Body Centre of Gravity to Lumbar Joint

Lumbar_CofR = [0 -0.135 0];

% Lumbar Joint to Hip Joints

R_Hip_CofR = [0 -0.131 0.0835];

L_Hip_CofR = [0 -0.131 -0.0835];

% Hip Joints to Knee Joints

R_Knee_CofR = [0 -0.400 0];

L_Knee_CofR = [0 -0.400 0];

% Knee Joints to Ankle (Talocrural) Joints

R_Talocrural_CofR = [0 -0.430 0];

L_Talocrural_CofR = [0 -0.430 0];

% Ankle Joints to Toe Joints (base of second metatarsal taken
from the iris)

R_Toe_CofR = [0.130 -0.044 0.001];

L_Toe_CofR = [0.130 -0.044 -0.001];
```

```
%---------*
% Muscles *
%---------*

% Muscle parameters include geometric attachment sites and
% wrapping points (where the muscle path is diverted by bones,
% ligaments or other tissues) relative to the axes of the
% segment contacted by the muscle.

% Some wrapping points are angle dependant and the angle limits
% are included

% Where more than one contact point occurs on the same segment,
% a static length can be calculated by the dot product of the
% coordinates to save processing later

% A set of four parameters for the modified Hill-type
% musculotendon actuator model are also included for each
% muscle. These are: the maximum voluntary force that can be
% generated by the muscle, optimal muscle fibre lengths
% (at which the greatest force can be generated), tendon slack
% lengths and muscle fibre pennation angles.

% Muscle data is grouped for convenience according to groups
% crossed and angle dependant wrapping points. This gives the
% groups: lumbar, hip, quad, thigh, gastroc, ankle.

% Lumbar
% ------

% Erector Spinae
Lumbar_Body_Origins(1,:) = [-0.0300 0 0.0500];
Lumbar_Pelvis_Insertions(1,:) = [-0.1349 0.0176 0.0320];

Lumbar_forces_max(1,:) = 800.0;
Lumbar_optimal_fibre_lengths(1,:) = 0.0800;
Lumbar_tendon_slack_lengths(1,:) = 0.1064;
Lumbar_pennation_angle(1,:) = 0.0;

Lumbar_Body_Origins(5,:) = [-0.030 0 -0.050];
Lumbar_Pelvis_Insertions(5,:) = [-0.1349 0.0176 -0.0320];

Lumbar_forces_max(5,:) = 800.0;
Lumbar_optimal_fibre_lengths(5,:) = 0.0800;
Lumbar_tendon_slack_lengths(5,:) = 0.1064;
Lumbar_pennation_angles(5,:) = 0.0;

% External Oblique
Lumbar_Body_Origins(2,:) = [0.05 -0.06 0.05];
Lumbar_Pelvis_Insertions(2,:) = [-0.0855 0.04450 0.0766];

Lumbar_forces_max(2,:) = 300.0;
Lumbar_optimal_fibre_lengths(2,:) = 0.0500;
Lumbar_tendon_slack_lengths(2,:) = 0.0883;
Lumbar_pennation_angles(2,:) = 0.0;

Lumbar_Body_Origins(6,:) = [0.05 -0.06 -0.05];
```

```
Lumbar_Pelvis_Insertions(6,:) = [-0.0855 0.04450 -0.0766];

Lumbar_forces_max(6,:) = 300.0;
Lumbar_optimal_fibre_lengths(6,:) = 0.0500;
Lumbar_tendon_slack_lengths(6,:) = 0.0883;
Lumbar_pennation_angles(6,:) = 0.0;

% Internal Oblique
Lumbar_Body_Origins(3,:) = [-0.05 -0.06 0.05];
Lumbar_Pelvis_Insertions(3,:) = [-0.0563 0.04450 0.0766];

Lumbar_forces_max(3,:) = 300.0;
Lumbar_optimal_fibre_lengths(3,:) = 0.050;
Lumbar_tendon_slack_lengths(3,:) = 0.0883;
Lumbar_pennation_angles(3,:) = 0.0;

Lumbar_Body_Origins(7,:) = [-0.05 -0.06 -0.05];
Lumbar_Pelvis_Insertions(7,:) = [-0.0563 0.04450 -0.0766];

Lumbar_forces_max(7,:) = 300.0;
Lumbar_optimal_fibre_lengths(7,:) = 0.050;
Lumbar_tendon_slack_lengths(7,:) = 0.0883;
Lumbar_pennation_angles(7,:) = 0.0;

% Rectus Abdominis
Lumbar_Body_Origins(4,:) = [0.0709 0 0.05];
Lumbar_Pelvis_Insertions(4,:) = [-0.0316 -0.0836 0.0169];

Lumbar_forces_max(4,:) = 800.0;
Lumbar_optimal_fibre_lengths(4,:) = 0.080;
Lumbar_tendon_slack_lengths(4,:) = 0.2072;
Lumbar_pennation_angles(4,:) = 0.0;

Lumbar_Body_Origins(8,:) = [0.0709 0 -0.05];
Lumbar_Pelvis_Insertions(8,:) = [-0.0316 -0.0836 -0.0169];

Lumbar_forces_max(8,:) = 800.0;
Lumbar_optimal_fibre_lengths(8,:) = 0.080;
Lumbar_tendon_slack_lengths(8,:) = 0.2072;
Lumbar_pennation_angles(8,:) = 0.0;

% Gluteus
%--------

% Gluteus Maximus (superior component)
R_GMax1_Origin = [-0.1195  0.0612 0.0700];
R_Hip_Pelvis_Origins(1,:) = [-0.1291  0.0012 0.0886];
R_Hip_Thigh_Insertions(1,:) = [-0.0457 -0.0248 0.0392];
R_GMax1_Insertion = [-0.0277 -0.0566 0.0470];

R_Hip_Static(1,:) = (dot((R_Hip_Pelvis_Origins(1,:)-
R_GMax1_Origin),...
   (R_Hip_Pelvis_Origins(1,:)-R_GMax1_Origin)))^0.5...
   + (dot((R_GMax1_Insertion-R_Hip_Thigh_Insertions(1,:)),...
   (R_GMax1_Insertion-R_Hip_Thigh_Insertions(1,:))))^0.5;

R_Hip_forces_max(1,:) = 382.0;
```

```
R_Hip_optimal_fibre_lengths(1,:) = 0.1420;
R_Hip_tendon_slack_lengths(1,:) = 0.1250;
R_Hip_pennation_angles(1,:) = 5.0;

L_GMax1_Origin = [-0.1195  0.0612 -0.0700];
L_Hip_Pelvis_Origins(1,:) = [-0.1291  0.0012 -0.0886];
L_Hip_Thigh_Insertions(1,:) = [-0.0457 -0.0248 -0.0392];
L_GMax1_Insertion = [-0.0277 -0.0566 -0.0470];

L_Hip_Static(1,:) = (dot((L_Hip_Pelvis_Origins(1,:)-
L_GMax1_Origin),...
   (L_Hip_Pelvis_Origins(1,:)-L_GMax1_Origin)))^0.5...
   + (dot((L_GMax1_Insertion-L_Hip_Thigh_Insertions(1,:)),...
   (L_GMax1_Insertion-L_Hip_Thigh_Insertions(1,:))))^0.5;

L_Hip_forces_max(1,:) = 382.0;
L_Hip_optimal_fibre_lengths(1,:) = 0.1420;
L_Hip_tendon_slack_lengths(1,:) = 0.1250;
L_Hip_pennation_angles(1,:) = 5.0;

% Gluteus Maximus (middle component)
R_GMax2_Origin = [-0.1349  0.0176 0.0563];
R_Hip_Pelvis_Origins(2,:) = [-0.1376 -0.0520 0.0914];
R_Hip_Thigh_Insertions(2,:) = [-0.0426 -0.0530 0.0293];
R_GMax2_Insertion = [-0.0156 -0.1016 0.0419];

R_Hip_Static(2,:) = (dot((R_Hip_Pelvis_Origins(2,:)-
R_GMax2_Origin),...
   (R_Hip_Pelvis_Origins(2,:)-R_GMax2_Origin)))^0.5...
   + (dot((R_GMax2_Insertion-R_Hip_Thigh_Insertions(2,:)),...
   (R_GMax2_Insertion-R_Hip_Thigh_Insertions(2,:))))^0.5;

R_Hip_forces_max(2,:) = 546.0;
R_Hip_optimal_fibre_lengths(2,:) = 0.1470;
R_Hip_tendon_slack_lengths(2,:) = 0.1270;
R_Hip_pennation_angles(2,:) = 0.0;

L_GMax2_Origin = [-0.1349  0.0176 -0.0563];
L_Hip_Pelvis_Origins(2,:) = [-0.1376 -0.0520 -0.0914];
L_Hip_Thigh_Insertions(2,:) = [-0.0426 -0.0530 -0.0293];
L_GMax2_Insertion = [-0.0156 -0.1016 -0.0419];

L_Hip_Static(2,:) = (dot((L_Hip_Pelvis_Origins(2,:)-
L_GMax2_Origin),...
   (L_Hip_Pelvis_Origins(2,:)-L_GMax2_Origin)))^0.5...
   + (dot((L_GMax2_Insertion-L_Hip_Thigh_Insertions(2,:)),...
   (L_GMax2_Insertion-L_Hip_Thigh_Insertions(2,:))))^0.5;

L_Hip_forces_max(2,:) = 546.0;
L_Hip_optimal_fibre_lengths(2,:) = 0.1470;
L_Hip_tendon_slack_lengths(2,:) = 0.1270;
L_Hip_pennation_angles(2,:) = 0.0;

% Gluteus Maximus (inferior component)
R_GMax3_Origin = [-0.1556 -0.0314 0.0058];
R_Hip_Pelvis_Origins(3,:) = [-0.1529 -0.1052 0.0403];
R_Hip_Thigh_Insertions(3,:) = [-0.0299 -0.1041 0.0135];
```

```
R_GMax3_Insertion = [-0.0060 -0.1419 0.0411];

R_Hip_Static(3,:) = (dot((R_Hip_Pelvis_Origins(3,:)-
R_GMax3_Origin),...
   (R_Hip_Pelvis_Origins(3,:)-R_GMax3_Origin)))^0.5...
   + (dot((R_GMax3_Insertion-R_Hip_Thigh_Insertions(3,:)),...
   (R_GMax3_Insertion-R_Hip_Thigh_Insertions(3,:))))^0.5;

R_Hip_forces_max(3,:) = 368.0;
R_Hip_optimal_fibre_lengths(3,:) = 0.1440;
R_Hip_tendon_slack_lengths(3,:) = 0.1450;
R_Hip_pennation_angles(3,:) = 5.0;

L_GMax3_Origin = [-0.1556 -0.0314 -0.0058];
L_Hip_Pelvis_Origins(3,:) = [-0.1529 -0.1052 -0.0403];
L_Hip_Thigh_Insertions(3,:) = [-0.0299 -0.1041 -0.0135];
L_GMax3_Insertion = [-0.0060 -0.1419 -0.0411];

L_Hip_Static(3,:) = (dot((L_Hip_Pelvis_Origins(3,:)-
L_GMax3_Origin),...
   (L_Hip_Pelvis_Origins(3,:)-L_GMax3_Origin)))^0.5...
   + (dot((L_GMax3_Insertion-L_Hip_Thigh_Insertions(3,:)),...
   (L_GMax3_Insertion-L_Hip_Thigh_Insertions(3,:))))^0.5;

L_Hip_forces_max(3,:) = 368.0;
L_Hip_optimal_fibre_lengths(3,:) = 0.1440;
L_Hip_tendon_slack_lengths(3,:) = 0.1450;
L_Hip_pennation_angles(3,:) = 5.0;

% Gluteus Medius (anterior compartment)
R_Hip_Pelvis_Origins(4,:) = [-0.0408  0.0304 0.1209];
R_Hip_Thigh_Insertions(4,:) = [-0.0218 -0.0117 0.0555];

R_Hip_forces_max(4,:) = 546.0;
R_Hip_optimal_fibre_lengths(4,:) = 0.0535;
R_Hip_tendon_slack_lengths(4,:) = 0.0780;
R_Hip_pennation_angles(4,:) = 8.0;

L_Hip_Pelvis_Origins(4,:) = [-0.0408  0.0304 -0.1209];
L_Hip_Thigh_Insertions(4,:) = [-0.0218 -0.0117 -0.0555];

L_Hip_forces_max(4,:) = 546.0;
L_Hip_optimal_fibre_lengths(4,:) = 0.0535;
L_Hip_tendon_slack_lengths(4,:) = 0.0780;
L_Hip_pennation_angles(4,:) = 8.0;

% Gluteus Medius (middle compartment)
R_Hip_Pelvis_Origins(5,:) = [-0.0855  0.04450 0.0766];
R_Hip_Thigh_Insertions(5,:) = [-0.0258 -0.0058  0.0527];

R_Hip_forces_max(5,:) = 382.0;
R_Hip_optimal_fibre_lengths(5,:) = 0.0845;
R_Hip_tendon_slack_lengths(5,:) = 0.0530;
R_Hip_pennation_angles(5,:) = 0.0;

L_Hip_Pelvis_Origins(5,:) = [-0.0855  0.04450 -0.0766];
L_Hip_Thigh_Insertions(5,:) = [-0.0258 -0.0058  -0.0527];
```

```
L_Hip_forces_max(5,:) = 382.0;
L_Hip_optimal_fibre_lengths(5,:) = 0.0845;
L_Hip_tendon_slack_lengths(5,:) = 0.0530;
L_Hip_pennation_angles(5,:) = 0.0;

% Gluteus Medius (posterior compartment)
R_Hip_Pelvis_Origins(6,:) = [-0.1223  0.0105 0.0648];
R_Hip_Thigh_Insertions(6,:) = [-0.0309 -0.0047 0.0518];

R_Hip_forces_max(6,:) = 435.0;
R_Hip_optimal_fibre_lengths(6,:) = 0.0646;
R_Hip_tendon_slack_lengths(6,:) = 0.0530;
R_Hip_pennation_angles(6,:) = 19.0;

L_Hip_Pelvis_Origins(6,:) = [-0.1223  0.0105 -0.0648];
L_Hip_Thigh_Insertions(6,:) = [-0.0309 -0.0047 -0.0518];

L_Hip_forces_max(6,:) = 435.0;
L_Hip_optimal_fibre_lengths(6,:) = 0.0646;
L_Hip_tendon_slack_lengths(6,:) = 0.0530;
L_Hip_pennation_angles(6,:) = 19.0;

% Gluteus Minimus (anterior compartment)
R_Hip_Pelvis_Origins(7,:) = [-0.0467 -0.0080 0.1056];
R_Hip_Thigh_Insertions(7,:) = [-0.0072 -0.0104 0.0560];

R_Hip_forces_max(7,:) = 180.0;
R_Hip_optimal_fibre_lengths(7,:) = 0.0680;
R_Hip_tendon_slack_lengths(7,:) = 0.0160;
R_Hip_pennation_angles(7,:) = 10.0;

L_Hip_Pelvis_Origins(7,:) = [-0.0467 -0.0080 -0.1056];
L_Hip_Thigh_Insertions(7,:) = [-0.0072 -0.0104 -0.0560];

L_Hip_forces_max(7,:) = 180.0;
L_Hip_optimal_fibre_lengths(7,:) = 0.0680;
L_Hip_tendon_slack_lengths(7,:) = 0.0160;
L_Hip_pennation_angles(7,:) = 10.0;

% Gluteus Minimus (middle compartment)
R_Hip_Pelvis_Origins(8,:) = [-0.0633 -0.0065 0.0991];
R_Hip_Thigh_Insertions(8,:) = [-0.0096 -0.0104 0.0560];

R_Hip_forces_max(8,:) = 190.0;
R_Hip_optimal_fibre_lengths(8,:) = 0.0560;
R_Hip_tendon_slack_lengths(8,:) = 0.0260;
R_Hip_pennation_angles(8,:) = 0.0;

L_Hip_Pelvis_Origins(8,:) = [-0.0633 -0.0065 -0.0991];
L_Hip_Thigh_Insertions(8,:) = [-0.0096 -0.0104 -0.0560];

L_Hip_forces_max(8,:) = 190.0;
L_Hip_optimal_fibre_lengths(8,:) = 0.0560;
L_Hip_tendon_slack_lengths(8,:) = 0.0260;
L_Hip_pennation_angles(8,:) = 0.0;

% Gluteus Minimus (posterior compartment)
```

```
R_Hip_Pelvis_Origins(9,:) = [-0.0834 -0.0063 0.0856];
R_Hip_Thigh_Insertions(9,:) = [-0.0135 -0.0083 0.0550];

R_Hip_forces_max(9,:) = 215.0;
R_Hip_optimal_fibre_lengths(9,:) = 0.0380;
R_Hip_tendon_slack_lengths(9,:) = 0.0510;
R_Hip_pennation_angles(9,:) = 1.0;

L_Hip_Pelvis_Origins(9,:) = [-0.0834 -0.0063 -0.0856];
L_Hip_Thigh_Insertions(9,:) = [-0.0135 -0.0083 -0.0550];

L_Hip_forces_max(9,:) = 215.0;
L_Hip_optimal_fibre_lengths(9,:) = 0.0380;
L_Hip_tendon_slack_lengths(9,:) = 0.0510;
L_Hip_pennation_angles(9,:) = 1.0;


% Deep Hip
% --------

% Psoas
R_Psoas_Origin = [-0.0647  0.0887 0.0289];
R_Hip_Pelvis_Origins(10,:) = [-0.0238 -0.0570 0.0759];
R_Hip_Thigh_Insertions(10,:) = [0.0016 -0.0507 0.0038];
R_Psoas_Insertion = [-0.0188 -0.0597 0.0104];

R_Hip_Static(10,:) = (dot((R_Hip_Pelvis_Origins(10,:)-
R_Psoas_Origin),...
   (R_Hip_Pelvis_Origins(10,:)-R_Psoas_Origin)))^0.5...
   + (dot((R_Psoas_Insertion-R_Hip_Thigh_Insertions(10,:)),...
   (R_Psoas_Insertion-R_Hip_Thigh_Insertions(10,:))))^0.5;

R_Hip_forces_max(10,:) = 371.0;
R_Hip_optimal_fibre_lengths(10,:) = 0.1040;
R_Hip_tendon_slack_lengths(10,:) = 0.1300;
R_Hip_pennation_angles(10,:) = 8.0;

L_Psoas_Origin = [-0.0647  0.0887 -0.0289];
L_Hip_Pelvis_Origins(10,:) = [-0.0238 -0.0570 -0.0759];
L_Hip_Thigh_Insertions(10,:) = [0.0016 -0.0507 -0.0038];
L_Psoas_Insertion = [-0.0188 -0.0597 -0.0104];

L_Hip_Static(10,:) = (dot((L_Hip_Pelvis_Origins(10,:)-
L_Psoas_Origin),...
   (L_Hip_Pelvis_Origins(10,:)-L_Psoas_Origin)))^0.5...
   + (dot((L_Psoas_Insertion-L_Hip_Thigh_Insertions(10,:)),...
   (L_Psoas_Insertion-L_Hip_Thigh_Insertions(10,:))))^0.5;

L_Hip_forces_max(10,:) = 371.0;
L_Hip_optimal_fibre_lengths(10,:) = 0.1040;
L_Hip_tendon_slack_lengths(10,:) = 0.1300;
L_Hip_pennation_angles(10,:) = 8.0;

% Iliacus
R_Il_Origin = [-0.0674  0.0365 0.0854];
R_Hip_Pelvis_Origins(11,:) = [-0.0218 -0.0550 0.0851];
R_Hip_Thigh_Insertions(11,:) = [0.0017 -0.0543 0.0057];
```

```
R_Il_Insertion = [-0.0193 -0.0621 0.0129];

R_Hip_Static(11,:) = (dot((R_Hip_Pelvis_Origins(11,:)-
R_Il_Origin),...
   (R_Hip_Pelvis_Origins(11,:)-R_Il_Origin)))^0.5...
   + (dot((R_Il_Insertion-R_Hip_Thigh_Insertions(11,:)),...
   (R_Il_Insertion-R_Hip_Thigh_Insertions(11,:))))^0.5;

R_Hip_forces_max(11,:) = 429.0;
R_Hip_optimal_fibre_lengths(11,:) = 0.1000;
R_Hip_tendon_slack_lengths(11,:) = 0.0900;
R_Hip_pennation_angles(11,:) = 7.0;

L_Il_Origin = [-0.0674  0.0365 -0.0854];
L_Hip_Pelvis_Origins(11,:) = [-0.0218 -0.0550 -0.0851];
L_Hip_Thigh_Insertions(11,:) = [0.0017 -0.0543 -0.0057];
L_Il_Insertion = [-0.0193 -0.0621 -0.0129];

L_Hip_Static(11,:) = (dot((L_Hip_Pelvis_Origins(11,:)-
L_Il_Origin),...
   (L_Hip_Pelvis_Origins(11,:)-L_Il_Origin)))^0.5...
   + (dot((L_Il_Insertion-L_Hip_Thigh_Insertions(11,:)),...
   (L_Il_Insertion-L_Hip_Thigh_Insertions(11,:))))^0.5;

L_Hip_forces_max(11,:) = 429.0;
L_Hip_optimal_fibre_lengths(11,:) = 0.1000;
L_Hip_tendon_slack_lengths(11,:) = 0.0900;
L_Hip_pennation_angles(11,:) = 7.0;

% Pectineus
R_Hip_Pelvis_Origins(12,:) = [-0.0431 -0.0768 0.0451];
R_Hip_Thigh_Insertions(12,:) = [-0.0122 -0.0822 0.0253];

R_Hip_forces_max(12,:) = 177.0;
R_Hip_optimal_fibre_lengths(12,:) = 0.1330;
R_Hip_tendon_slack_lengths(12,:) = 0.0010;
R_Hip_pennation_angles(12,:) = 0.0;

L_Hip_Pelvis_Origins(12,:) = [-0.0431 -0.0768 -0.0451];
L_Hip_Thigh_Insertions(12,:) = [-0.0122 -0.0822 -0.0253];

L_Hip_forces_max(12,:) = 177.0;
L_Hip_optimal_fibre_lengths(12,:) = 0.1330;
L_Hip_tendon_slack_lengths(12,:) = 0.0010;
L_Hip_pennation_angles(12,:) = 0.0;

% Piriformis
R_Pir_Origin = [-0.1396  0.0003 0.0235];
R_Hip_Pelvis_Origins(13,:) = [-0.1193 -0.0276 0.0657];
R_Hip_Thigh_Insertions(13,:) = [-0.0148 -0.0036 0.0437];

R_Hip_Static(13,:) = (dot((R_Hip_Pelvis_Origins(13,:)-
R_Pir_Origin),...
   (R_Hip_Pelvis_Origins(13,:)-R_Pir_Origin)))^0.5;

R_Hip_forces_max(13,:) = 296.0;
R_Hip_optimal_fibre_lengths(13,:) = 0.0260;
```

```
R_Hip_tendon_slack_lengths(13,:) = 0.1150;
R_Hip_pennation_angles(13,:) = 10.0;

L_Pir_Origin = [-0.1396  0.0003 -0.0235];
L_Hip_Pelvis_Origins(13,:) = [-0.1193 -0.0276 -0.0657];
L_Hip_Thigh_Insertions(13,:) = [-0.0148 -0.0036 -0.0437];

L_Hip_Static(13,:) = (dot((L_Hip_Pelvis_Origins(13,:)-
L_Pir_Origin),...
   (L_Hip_Pelvis_Origins(13,:)-L_Pir_Origin)))^0.5;

L_Hip_forces_max(13,:) = 296.0;
L_Hip_optimal_fibre_lengths(13,:) = 0.0260;
L_Hip_tendon_slack_lengths(13,:) = 0.1150;
L_Hip_pennation_angles(13,:) = 10.0;

% Gemelli
R_Hip_Pelvis_Origins(14,:) = [-0.1133 -0.0820 0.0714];
R_Hip_Thigh_Insertions(14,:) = [-0.0142 -0.0033 0.0443];

R_Hip_forces_max(14,:) = 109.0;
R_Hip_optimal_fibre_lengths(14,:) = 0.0240;
R_Hip_tendon_slack_lengths(14,:) = 0.0390;
R_Hip_pennation_angles(14,:) = 0.0;

L_Hip_Pelvis_Origins(14,:) = [-0.1133 -0.0820 -0.0714];
L_Hip_Thigh_Insertions(14,:) = [-0.0142 -0.0033 -0.0443];

L_Hip_forces_max(14,:) = 109.0;
L_Hip_optimal_fibre_lengths(14,:) = 0.0240;
L_Hip_tendon_slack_lengths(14,:) = 0.0390;
L_Hip_pennation_angles(14,:) = 0.0;

% Quadratus Femoris
R_Hip_Pelvis_Origins(15,:) = [-0.1143 -0.1151 0.0520];
R_Hip_Thigh_Insertions(15,:) = [-0.0381 -0.0359 0.0366];

R_Hip_forces_max(15,:) = 254.0;
R_Hip_optimal_fibre_lengths(15,:) = 0.0540;
R_Hip_tendon_slack_lengths(15,:) = 0.0240;
R_Hip_pennation_angles(15,:) = 0.0;

L_Hip_Pelvis_Origins(15,:) = [-0.1143 -0.1151 -0.0520];
L_Hip_Thigh_Insertions(15,:) = [-0.0381 -0.0359 -0.0366];

L_Hip_forces_max(15,:) = 254.0;
L_Hip_optimal_fibre_lengths(15,:) = 0.0540;
L_Hip_tendon_slack_lengths(15,:) = 0.0240;
L_Hip_pennation_angles(15,:) = 0.0;

% Adductors
% ---------

% Adductor Longus
R_Hip_Pelvis_Origins(16,:) = [-0.0316 -0.0836 0.0169];
R_Hip_Thigh_Insertions(16,:) = [0.0050 -0.2111 0.0234];
```

```
R_Hip_forces_max(16,:) = 418.0;
R_Hip_optimal_fibre_lengths(16,:) = 0.1380;
R_Hip_tendon_slack_lengths(16,:) = 0.1100;
R_Hip_pennation_angles(16,:) = 6.0;

L_Hip_Pelvis_Origins(16,:) = [-0.0316 -0.0836 -0.0169];
L_Hip_Thigh_Insertions(16,:) = [0.0050 -0.2111 -0.0234];

L_Hip_forces_max(16,:) = 418.0;
L_Hip_optimal_fibre_lengths(16,:) = 0.1380;
L_Hip_tendon_slack_lengths(16,:) = 0.1100;
L_Hip_pennation_angles(16,:) = 6.0;

% Adductor Brevis
R_Hip_Pelvis_Origins(17,:) = [-0.0587 -0.0915 0.0164];
R_Hip_Thigh_Insertions(17,:) = [0.0009 -0.1196 0.0294];

R_Hip_forces_max(17,:) = 286.0;
R_Hip_optimal_fibre_lengths(17,:) = 0.1330;
R_Hip_tendon_slack_lengths(17,:) = 0.0200;
R_Hip_pennation_angles(17,:) = 0.0;

L_Hip_Pelvis_Origins(17,:) = [-0.0587 -0.0915 -0.0164];
L_Hip_Thigh_Insertions(17,:) = [0.0009 -0.1196 -0.0294];

L_Hip_forces_max(17,:) = 286.0;
L_Hip_optimal_fibre_lengths(17,:) = 0.1330;
L_Hip_tendon_slack_lengths(17,:) = 0.0200;
L_Hip_pennation_angles(17,:) = 0.0;

% Adductor Magnus (superior component)
R_Hip_Pelvis_Origins(18,:) = [-0.0732 -0.1174 0.0255];
R_Hip_Thigh_Insertions(18,:) = [-0.0045 -0.1211 0.0339];

R_Hip_forces_max(18,:) = 346.0;
R_Hip_optimal_fibre_lengths(18,:) = 0.0870;
R_Hip_tendon_slack_lengths(18,:) = 0.0600;
R_Hip_pennation_angles(18,:) = 5.0;

L_Hip_Pelvis_Origins(18,:) = [-0.0732 -0.1174 -0.0255];
L_Hip_Thigh_Insertions(18,:) = [-0.0045 -0.1211 -0.0339];

L_Hip_forces_max(18,:) = 346.0;
L_Hip_optimal_fibre_lengths(18,:) = 0.0870;
L_Hip_tendon_slack_lengths(18,:) = 0.0600;
L_Hip_pennation_angles(18,:) = 5.0;

% Adductor Magnus (middle component)
R_Hip_Pelvis_Origins(19,:) = [-0.0831 -0.1192 0.0308];
R_Hip_Thigh_Insertions(19,:) = [0.0054 -0.2285 0.0227];

R_Hip_forces_max(19,:) = 312.0;
R_Hip_optimal_fibre_lengths(19,:) = 0.1210;
R_Hip_tendon_slack_lengths(19,:) = 0.1300;
R_Hip_pennation_angles(19,:) = 3.0;

L_Hip_Pelvis_Origins(19,:) = [-0.0831 -0.1192 -0.0308];
```

```
L_Hip_Thigh_Insertions(19,:) = [0.0054 -0.2285 -0.0227];

L_Hip_forces_max(19,:) = 312.0;
L_Hip_optimal_fibre_lengths(19,:) = 0.1210;
L_Hip_tendon_slack_lengths(19,:) = 0.1300;
L_Hip_pennation_angles(19,:) = 3.0;

% Adductor Magnus (inferior component)
R_Hip_Pelvis_Origins(20,:) = [-0.0771 -0.1181  0.0276];
R_Hip_Thigh_Insertions(20,:) = [0.0070 -0.3837 -0.0266];

R_Hip_forces_max(20,:) = 444.0;
R_Hip_optimal_fibre_lengths(20,:) = 0.1310;
R_Hip_tendon_slack_lengths(20,:) = 0.2600;
R_Hip_pennation_angles(20,:) = 5.0;

L_Hip_Pelvis_Origins(20,:) = [-0.0771 -0.1181  0.0276];
L_Hip_Thigh_Insertions(20,:) = [0.0070 -0.3837 -0.0266];

L_Hip_forces_max(20,:) = 444.0;
L_Hip_optimal_fibre_lengths(20,:) = 0.1310;
L_Hip_tendon_slack_lengths(20,:) = 0.2600;
L_Hip_pennation_angles(20,:) = 5.0;

% Superficial Thigh
% -----------------

% Sartorius
R_Hip_Pelvis_Origins(21,:) = [-0.0153 -0.0013 0.1242];
R_Hip_Thigh_Insertions(21,:) = [-0.0030 -0.3568 -0.0421];
R_Hip_Thigh_Origins(21,:) = [-0.0030 -0.3568 -0.0421];
R_Hip_Shank_Insertions(21,:) = [-0.0056 -0.0419 -0.0399];
R_Sar_TibiaWrap2 = [ 0.0060 -0.0589 -0.0383];
R_Sar_Insertion = [ 0.0243 -0.0840 -0.0252];

R_Hip_Static(21,:) = (dot((R_Sar_TibiaWrap2-
R_Hip_Shank_Insertions(21,:)),...
   (R_Sar_TibiaWrap2-R_Hip_Shank_Insertions(21,:))))^0.5...
   + (dot((R_Sar_Insertion-R_Sar_TibiaWrap2),...
   (R_Sar_Insertion-R_Sar_TibiaWrap2)))^0.5;

R_Hip_forces_max(21,:) = 104.0;
R_Hip_optimal_fibre_lengths(21,:) = 0.5790;
R_Hip_tendon_slack_lengths(21,:) = 0.0400;
R_Hip_pennation_angles(21,:) = 0.0;

L_Hip_Pelvis_Origins(21,:) = [-0.0153 -0.0013 -0.1242];
L_Hip_Thigh_Insertions(21,:) = [-0.0030 -0.3568 0.0421];
L_Hip_Thigh_Origins(21,:) = [-0.0030 -0.3568 0.0421];
L_Hip_Shank_Insertions(21,:) = [-0.0056 -0.0419 0.0399];
L_Sar_TibiaWrap2 = [ 0.0060 -0.0589 0.0383];
L_Sar_Insertion = [ 0.0243 -0.0840 0.0252];

L_Hip_Static(21,:) = (dot((L_Sar_TibiaWrap2-
L_Hip_Shank_Insertions(21,:))...
   ,(L_Sar_TibiaWrap2-L_Hip_Shank_Insertions(21,:))))^0.5...
   + (dot((L_Sar_Insertion-L_Sar_TibiaWrap2),...
```

```
   (L_Sar_Insertion-L_Sar_TibiaWrap2)))^0.5;

L_Hip_forces_max(21,:) = 104.0;
L_Hip_optimal_fibre_lengths(21,:) = 0.5790;
L_Hip_tendon_slack_lengths(21,:) = 0.0400;
L_Hip_pennation_angles(21,:) = 0.0;

% Tensor Faciae Latae
R_Hip_Pelvis_Origins(22,:) = [-0.0311  0.0214 0.1241];
R_Hip_Thigh_Insertions(22,:) = [0.0294 -0.0995 0.0597];
R_Hip_Thigh_Origins(22,:) = [0.0054 -0.4049 0.0357];
R_Hip_Shank_Insertions(22,:) = [0.0060 -0.0487 0.0297];

R_Hip_Static(22,:) = (dot((R_Hip_Thigh_Origins(22,:)...
   -R_Hip_Thigh_Insertions(22,:)),(R_Hip_Thigh_Origins(22,:)...
   -R_Hip_Thigh_Insertions(22,:))))^0.5;

R_Hip_forces_max(22,:) = 155.0;
R_Hip_optimal_fibre_lengths(22,:) = 0.0950;
R_Hip_tendon_slack_lengths(22,:) = 0.4250;
R_Hip_pennation_angles(22,:) = 3.0;

L_Hip_Pelvis_Origins(22,:) = [-0.0311  0.0214 -0.1241];
L_Hip_Thigh_Insertions(22,:) = [0.0294 -0.0995 -0.0597];
L_Hip_Thigh_Origins(22,:) = [0.0054 -0.4049 -0.0357];
L_Hip_Shank_Insertions(22,:) = [0.0060 -0.0487 -0.0297];

L_Hip_Static(22,:) = (dot((L_Hip_Thigh_Origins(22,:)...
   -L_Hip_Thigh_Insertions(22,:)),(L_Hip_Thigh_Origins(22,:)...
   -L_Hip_Thigh_Insertions(22,:))))^0.5;

L_Hip_forces_max(22,:) = 155.0;
L_Hip_optimal_fibre_lengths(22,:) = 0.0950;
L_Hip_tendon_slack_lengths(22,:) = 0.4250;
L_Hip_pennation_angles(22,:) = 3.0;

% Gracilis
R_Thigh_Pelvis_Origins(1,:) = [-0.0563 -0.1038  0.0079];
R_Thigh_Shank_Insertions(1,:) = [-0.0154 -0.0475 -0.0358];
R_Gra_Insertion = [0.0060 -0.0836 -0.0228];

R_Thigh_Static(1,:) = (dot((R_Thigh_Shank_Insertions(1,:)...
   -R_Gra_Insertion),(R_Thigh_Shank_Insertions(1,:)...
   -R_Gra_Insertion)))^0.5;

R_Thigh_forces_max(1,:) = 108.0;
R_Thigh_optimal_fibre_lengths(1,:) = 0.3520;
R_Thigh_tendon_slack_lengths(1,:) = 0.1400;
R_Thigh_pennation_angles(1,:) = 3.0;

L_Thigh_Pelvis_Origins(1,:) = [-0.0563 -0.1038  -0.0079];
L_Thigh_Shank_Insertions(1,:) = [-0.0154 -0.0475 0.0358];
L_Gra_Insertion = [0.0060 -0.0836 0.0228];

L_Thigh_Static(1,:) = (dot((L_Thigh_Shank_Insertions(1,:)...
   -L_Gra_Insertion),(L_Thigh_Shank_Insertions(1,:)-
L_Gra_Insertion)))^0.5;
```

```
L_Thigh_forces_max(1,:) = 108.0;
L_Thigh_optimal_fibre_lengths(1,:) = 0.3520;
L_Thigh_tendon_slack_lengths(1,:) = 0.1400;
L_Thigh_pennation_angles(1,:) = 3.0;
% Quadriceps Femoris
% ------------------

% Rectus Femoris
R_Quad_Pelvis_Origins(1,:) = [-0.0295 -0.0311  0.0968];
R_Quad_Thigh_Insertions(1,:) = [0.0334 -0.4030  0.0019];
R_Quad_Thigh_Origins(1,:) = [0.0334 -0.4030  0.0019];
R_RF_FemurWrap_Max = -1.46;
R_Quad_Shank_Insertions(1,:) = [0.0121  0.0437 -0.0010];

R_Quad_forces_max(1,:) = 779.0;
R_Quad_optimal_fibre_lengths(1,:) = 0.0840;
R_Quad_tendon_slack_lengths(1,:) = 0.3460;
R_Quad_pennation_angles(1,:) = 5.0;

L_Quad_Pelvis_Origins(1,:) = [-0.0295 -0.0311  -0.0968];
L_Quad_Thigh_Insertions(1,:) = [0.0334 -0.4030  -0.0019];
L_Quad_Thigh_Origins(1,:) = [0.0334 -0.4030  -0.0019];
L_RF_FemurWrap_Max = -1.46;
L_Quad_Shank_Insertions(1,:) = [0.0121  0.0437 0.0010];

L_Quad_forces_max(1,:) = 779.0;
L_Quad_optimal_fibre_lengths(1,:) = 0.0840;
L_Quad_tendon_slack_lengths(1,:) = 0.3460;
L_Quad_pennation_angles(1,:) = 5.0;

% Vastus Medialis
R_VM_Origin = [0.0140 -0.2099 0.0188];
R_Quad_Thigh_Origins(2,:) = [0.0356 -0.2769 0.0009];
R_Quad_Thigh_Origins(3,:) = [0.0370 -0.4048 -0.0125];
R_VM_FemurWrap2_Max = -1.21;
R_Quad_Thigh_Origins(4,:) = [0.0274 -0.4255 -0.0131];
R_VM_FemurWrap3_Max = -1.78;
R_Quad_Shank_Insertions(2,:) = [0.0063  0.0445 -0.0170];

R_Quad_Static(2,:) = (dot((R_Quad_Thigh_Origins(2,:)...
   -R_VM_Origin),(R_Quad_Thigh_Origins(2,:)-R_VM_Origin)))^0.5;

R_Quad_forces_max(2,:) = 1294.0;
R_Quad_optimal_fibre_lengths(2,:) = 0.0890;
R_Quad_tendon_slack_lengths(2,:) = 0.1260;
R_Quad_pennation_angles(2,:) = 5.0;

L_VM_Origin = [0.0140 -0.2099 -0.0188];
L_Quad_Thigh_Origins(2,:) = [0.0356 -0.2769 -0.0009];
L_Quad_Thigh_Origins(3,:) = [0.0370 -0.4048 0.0125];
L_VM_FemurWrap2_Max = -1.21;
L_Quad_Thigh_Origins(4,:) = [0.0274 -0.4255 0.0131];
L_VM_FemurWrap3_Max = -1.78;
L_Quad_Shank_Insertions(2,:) = [0.0063  0.0445 0.0170];

L_Quad_Static(2,:) = (dot((L_Quad_Thigh_Origins(2,:)...
```

```
   -L_VM_Origin),(L_Quad_Thigh_Origins(2,:)-L_VM_Origin)))^0.5;

L_Quad_forces_max(2,:) = 1294.0;
L_Quad_optimal_fibre_lengths(2,:) = 0.0890;
L_Quad_tendon_slack_lengths(2,:) = 0.1260;
L_Quad_pennation_angles(2,:) = 5.0;

% Vastus Intermedius
R_VI_Origin = [0.0290 -0.1924  0.0310];
R_Quad_Thigh_Origins(5,:) = [0.0335 -0.2084  0.0285];
R_Quad_Thigh_Origins(6,:) = [0.0343 -0.4030  0.0055];
R_VI_FemurWrap2_Max = -1.42;
R_Quad_Shank_Insertions(3,:) = [0.0058  0.0480 -0.0006];

R_Quad_Static(3,:) = (dot((R_Quad_Thigh_Origins(5,:)...
   -R_VI_Origin),(R_Quad_Thigh_Origins(5,:)-R_VI_Origin)))^0.5;

R_Quad_forces_max(3,:) = 1365.0;
R_Quad_optimal_fibre_lengths(3,:) = 0.0870;
R_Quad_tendon_slack_lengths(3,:) = 0.1360;
R_Quad_pennation_angles(3,:) = 3.0;

L_VI_Origin = [0.0290 -0.1924  -0.0310];
L_Quad_Thigh_Origins(5,:) = [0.0335 -0.2084  -0.0285];
L_Quad_Thigh_Origins(6,:) = [0.0343 -0.4030  -0.0055];
L_VI_FemurWrap2_Max = -1.42;
L_Quad_Shank_Insertions(3,:) = [0.0058  0.0480 0.0006];

L_Quad_Static(3,:) = (dot((L_Quad_Thigh_Origins(5,:)...
   -L_VI_Origin),(L_Quad_Thigh_Origins(5,:)-L_VI_Origin)))^0.5;

L_Quad_forces_max(3,:) = 1365.0;
L_Quad_optimal_fibre_lengths(3,:) = 0.0870;
L_Quad_tendon_slack_lengths(3,:) = 0.1360;
L_Quad_pennation_angles(3,:) = 3.0;

% Vastus Lateralis
R_VL_Origin = [0.0048 -0.1854 0.0349];
R_Quad_Thigh_Origins(7,:) = [0.0269 -0.2591 0.0409];
R_Quad_Thigh_Origins(8,:) = [0.0361 -0.4030 0.0205];
R_VL_FemurWrap2_Max = -1.21;
R_Quad_Thigh_Origins(9,:) = [0.0253 -0.4243 0.0184];
R_VL_FemurWrap3_Max = -1.92;
R_Quad_Shank_Insertions(4,:) = [0.0103  0.0423 0.0141];

R_Quad_Static(4,:) = (dot((R_Quad_Thigh_Origins(7,:)...
   -R_VL_Origin),(R_Quad_Thigh_Origins(7,:)-R_VL_Origin)))^0.5;

R_Quad_forces_max(4,:) = 1871.0;
R_Quad_optimal_fibre_lengths(4,:) = 0.0840;
R_Quad_tendon_slack_lengths(4,:) = 0.1570;
R_Quad_pennation_angles(4,:) = 5.0;

L_VL_Origin = [0.0048 -0.1854 -0.0349];
L_Quad_Thigh_Origins(7,:) = [0.0269 -0.2591 -0.0409];
L_Quad_Thigh_Origins(8,:) = [0.0361 -0.4030 -0.0205];
L_VL_FemurWrap2_Max = -1.21;
```

```
L_Quad_Thigh_Origins(9,:) = [0.0253 -0.4243 -0.0184];
L_VL_FemurWrap3_Max = -1.92;
L_Quad_Shank_Insertions(4,:) = [0.0103  0.0423 -0.0141];

L_Quad_Static(4,:) = (dot((L_Quad_Thigh_Origins(7,:)...
   -L_VL_Origin),(L_Quad_Thigh_Origins(7,:)-L_VL_Origin)))^0.5;

L_Quad_forces_max(4,:) = 1871.0;
L_Quad_optimal_fibre_lengths(4,:) = 0.0840;
L_Quad_tendon_slack_lengths(4,:) = 0.1570;
L_Quad_pennation_angles(4,:) = 5.0;

% Hamstrings
% ----------

% Biceps Femoris Short Head
R_Hip_Thigh_Origins(23,:) = [0.0050 -0.2111 0.0234];
R_Hip_Shank_Insertions(23,:) = [-0.0101 -0.0725 0.0406];

R_Hip_forces_max(23,:) = 402.0;
R_Hip_optimal_fibre_lengths(23,:) = 0.1730;
R_Hip_tendon_slack_lengths(23,:) = 0.1000;
R_Hip_pennation_angles(23,:) = 23.0;

L_Hip_Thigh_Origins(23,:) = [0.0050 -0.2111 -0.0234];
L_Hip_Shank_Insertions(23,:) = [-0.0101 -0.0725 -0.0406];

L_Hip_forces_max(23,:) = 402.0;
L_Hip_optimal_fibre_lengths(23,:) = 0.1730;
L_Hip_tendon_slack_lengths(23,:) = 0.1000;
L_Hip_pennation_angles(23,:) = 23.0;

% Biceps Femoris Long Head
R_Thigh_Pelvis_Origins(4,:) = [-0.1244 -0.1001 0.0666];
R_Thigh_Shank_Insertions(4,:) = [-0.0081 -0.0729 0.0423];

R_Thigh_forces_max(4,:) = 717.0;
R_Thigh_optimal_fibre_lengths(4,:) = 0.1090;
R_Thigh_tendon_slack_lengths(4,:) = 0.3410;
R_Thigh_pennation_angles(4,:) = 23.0;

L_Thigh_Pelvis_Origins(4,:) = [-0.1244 -0.1001 -0.0666];
L_Thigh_Shank_Insertions(4,:) = [-0.0081 -0.0729 -0.0423];

L_Thigh_forces_max(4,:) = 717.0;
L_Thigh_optimal_fibre_lengths(4,:) = 0.1090;
L_Thigh_tendon_slack_lengths(4,:) = 0.3410;
L_Thigh_pennation_angles(4,:) = 23.0;

% Semimembranosus
R_Thigh_Pelvis_Origins(2,:) = [-0.1192 -0.1015  0.0695];
R_Thigh_Shank_Insertions(2,:) = [-0.0243 -0.0536 -0.0194];

R_Thigh_forces_max(2,:) = 1030.0;
R_Thigh_optimal_fibre_lengths(2,:) = 0.0800;
R_Thigh_tendon_slack_lengths(2,:) = 0.3590;
R_Thigh_pennation_angles(2,:) = 15.0;
```

```
L_Thigh_Pelvis_Origins(2,:) = [-0.1192 -0.1015 -0.0695];
L_Thigh_Shank_Insertions(2,:) = [-0.0243 -0.0536 0.0194];

L_Thigh_forces_max(2,:) = 1030.0;
L_Thigh_optimal_fibre_lengths(2,:) = 0.0800;
L_Thigh_tendon_slack_lengths(2,:) = 0.3590;
L_Thigh_pennation_angles(2,:) = 15.0;

% Semitendinosus
R_Thigh_Pelvis_Origins(3,:) = [-0.1237 -0.1043  0.0603];
R_Thigh_Shank_Insertions(3,:) = [-0.0314 -0.0545 -0.0146];
R_ST_TibiaWrap2 = [-0.0113 -0.0746 -0.0245];
R_ST_Insertion = [0.0027 -0.0956 -0.0193];

R_Thigh_Static(3,:) = (dot((R_ST_TibiaWrap2-
R_Thigh_Shank_Insertions(3,:)...
   ),(R_ST_TibiaWrap2-R_Thigh_Shank_Insertions(3,:))))^0.5...
   + (dot((R_ST_Insertion-R_ST_TibiaWrap2),(R_ST_Insertion...
   -R_ST_TibiaWrap2)))^0.5;

R_Thigh_forces_max(3,:) = 328.0;
R_Thigh_optimal_fibre_lengths(3,:) = 0.2010;
R_Thigh_tendon_slack_lengths(3,:) = 0.2620;
R_Thigh_pennation_angles(3,:) = 5.0;

L_Thigh_Pelvis_Origins(3,:) = [-0.1237 -0.1043 -0.0603];
L_Thigh_Shank_Insertions(3,:) = [-0.0314 -0.0545 0.0146];
L_ST_TibiaWrap2 = [-0.0113 -0.0746 0.0245];
L_ST_Insertion = [0.0027 -0.0956 0.0193];

L_Thigh_Static(3,:) = (dot((L_ST_TibiaWrap2-
L_Thigh_Shank_Insertions(3,:)...
   ),(L_ST_TibiaWrap2-L_Thigh_Shank_Insertions(3,:))))^0.5...
   + (dot((L_ST_Insertion-L_ST_TibiaWrap2)...
   ,(L_ST_Insertion-L_ST_TibiaWrap2)))^0.5;

L_Thigh_forces_max(3,:) = 328.0;
L_Thigh_optimal_fibre_lengths(3,:) = 0.2010;
L_Thigh_tendon_slack_lengths(3,:) = 0.2620;
L_Thigh_pennation_angles(3,:) = 5.0;

% Plantarflexors
% --------------

% Gastrocnemius (medial head)
R_Gastroc_Thigh_Origins(1,:) = [-0.0127 -0.3929 -0.0235];
R_Gastroc_Thigh_Origins(2,:) = [-0.0239 -0.4022 -0.0258];
R_GasMed_FemurWrap_Min = -0.77;
R_Gastroc_Shank_Insertions(1,:) = [-0.0217 -0.0487 -0.0295];
R_Gastroc_Shank_Origins(1,:) = [-0.0217 -0.0487 -0.0295];
R_Gastroc_Calcn_Insertions(1,:) = [0.0044  0.0310 -0.0053];

R_Gastroc_forces_max(1,:) = 1113.0;
R_Gastroc_optimal_fibre_lengths(1,:) = 0.0450;
R_Gastroc_tendon_slack_lengths(1,:) = 0.4080;
R_Gastroc_pennation_angles(1,:) = 17.0;
```

```
L_Gastroc_Thigh_Origins(1,:) = [-0.0127 -0.3929 0.0235];
L_Gastroc_Thigh_Origins(2,:) = [-0.0239 -0.4022 0.0258];
L_GasMed_FemurWrap_Min = -0.77;
L_Gastroc_Shank_Insertions(1,:) = [-0.0217 -0.0487 0.0295];
L_Gastroc_Shank_Origins(1,:) = [-0.0217 -0.0487 0.0295];
L_Gastroc_Calcn_Insertions(1,:) = [0.0044  0.0310 0.0053];

L_Gastroc_forces_max(1,:) = 1113.0;
L_Gastroc_optimal_fibre_lengths(1,:) = 0.0450;
L_Gastroc_tendon_slack_lengths(1,:) = 0.4080;
L_Gastroc_pennation_angles(1,:) = 17.0;

% Gastrocnemius (lateral head)
R_Gastroc_Thigh_Origins(3,:) = [-0.0155 -0.3946  0.0272];
R_Gastroc_Thigh_Origins(4,:) = [-0.0254 -0.4018  0.0274];
R_GasLat_FemurWrap_Min = -0.77;
R_Gastroc_Shank_Insertions(2,:) = [-0.0242 -0.0481  0.0235];
R_Gastroc_Shank_Origins(2,:) = [-0.0242 -0.0481  0.0235];
R_Gastroc_Calcn_Insertions(2,:) = [0.0044  0.0310 -0.0053];

R_Gastroc_forces_max(2,:) = 488.0;
R_Gastroc_optimal_fibre_lengths(2,:) = 0.0640;
R_Gastroc_tendon_slack_lengths(2,:) = 0.3850;
R_Gastroc_pennation_angles(2,:) = 8.0;

L_Gastroc_Thigh_Origins(3,:) = [-0.0155 -0.3946  -0.0272];
L_Gastroc_Thigh_Origins(4,:) = [-0.0254 -0.4018  -0.0274];
L_GasLat_FemurWrap_Min = -0.77;
L_Gastroc_Shank_Insertions(2,:) = [-0.0242 -0.0481  -0.0235];
L_Gastroc_Shank_Origins(2,:) = [-0.0242 -0.0481  -0.0235];
L_Gastroc_Calcn_Insertions(2,:) = [0.0044  0.0310 0.0053];

L_Gastroc_forces_max(2,:) = 488.0;
L_Gastroc_optimal_fibre_lengths(2,:) = 0.0640;
L_Gastroc_tendon_slack_lengths(2,:) = 0.3850;
L_Gastroc_pennation_angles(2,:) = 8.0;

% Soleus
R_Ankle_Shank_Origins(1,:) = [-0.0024 -0.1533 0.0071];
R_Ankle_Calcn_Insertions(1,:) = [0.0044  0.0310 -0.0053];

R_Ankle_forces_max(1,:) = 2839.0;
R_Ankle_optimal_fibre_lengths(1,:) = 0.0300;
R_Ankle_tendon_slack_lengths(1,:) = 0.2680;
R_Ankle_pennation_angles(1,:) = 25.0;

L_Ankle_Shank_Origins(1,:) = [-0.0024 -0.1533 -0.0071];
L_Ankle_Calcn_Insertions(1,:) = [0.0044  0.0310 0.0053];

L_Ankle_forces_max(1,:) = 2839.0;
L_Ankle_optimal_fibre_lengths(1,:) = 0.0300;
L_Ankle_tendon_slack_lengths(1,:) = 0.2680;
L_Ankle_pennation_angles(1,:) = 25.0;

% Invertors
% ---------
```

```
% Tibialis Posterior
R_TP_Origin = [-0.0094 -0.1348 0.0019];
R_Ankle_Shank_Origins(2,:) = [-0.0144 -0.4051 -0.0229];
R_Ankle_Calcn_Insertions(2,:) = [0.0417 0.0334 -0.0286];
R_TP_Insertion = [0.0772 0.0159 -0.0281];

R_Ankle_Static(2,:) = (dot((R_Ankle_Shank_Origins(2,:)-
R_TP_Origin),...
   (R_Ankle_Shank_Origins(2,:)-R_TP_Origin)))^0.5...
   + (dot((R_TP_Insertion-R_Ankle_Calcn_Insertions(2,:)),...
   (R_TP_Insertion-R_Ankle_Calcn_Insertions(2,:))))^0.5;

R_Ankle_forces_max(2,:) = 1270.0;
R_Ankle_optimal_fibre_lengths(2,:) = 0.0310;
R_Ankle_tendon_slack_lengths(2,:) = 0.3100;
R_Ankle_pennation_angles(2,:) = 12.0;

L_TP_Origin = [-0.0094 -0.1348 -0.0019];
L_Ankle_Shank_Origins(2,:) = [-0.0144 -0.4051 0.0229];
L_Ankle_Calcn_Insertions(2,:) = [0.0417 0.0334 0.0286];
L_TP_Insertion = [0.0772 0.0159 0.0281];

L_Ankle_Static(2,:) = (dot((L_Ankle_Shank_Origins(2,:)-
L_TP_Origin),...
   (L_Ankle_Shank_Origins(2,:)-L_TP_Origin)))^0.5...
   + (dot((L_TP_Insertion-L_Ankle_Calcn_Insertions(2,:)),...
   (L_TP_Insertion-L_Ankle_Calcn_Insertions(2,:))))^0.5;

L_Ankle_forces_max(2,:) = 1270.0;
L_Ankle_optimal_fibre_lengths(2,:) = 0.0310;
L_Ankle_tendon_slack_lengths(2,:) = 0.3100;
L_Ankle_pennation_angles(2,:) = 12.0;

% Flexor Hallucis Longus
R_FHL_Origin = [-0.0079 -0.2334  0.0244];
R_Ankle_Shank_Origins(3,:) = [-0.0186 -0.4079 -0.0174];
R_Ankle_Calcn_Insertions(3,:) = [0.0374  0.0276 -0.0241];
R_FHL_CalcnWrap2 = [0.1038  0.0068 -0.0256];
R_Ankle_Calcn_Origins(3,:) = [0.1726 -0.0053 -0.0269];
R_Ankle_Toe_Insertions(3,:) = [0.0155 -0.0064 -0.0265];
R_FHL_Insertion = [0.0562 -0.0102 -0.0181];

R_Ankle_Static(3,:) = (dot((R_Ankle_Shank_Origins(3,:)-
R_FHL_Origin),...
   (R_Ankle_Shank_Origins(3,:)-R_FHL_Origin)))^0.5...
   + (dot((R_FHL_CalcnWrap2-R_Ankle_Calcn_Insertions(3,:)),...
   (R_FHL_CalcnWrap2-R_Ankle_Calcn_Insertions(3,:))))^0.5...
   + (dot((R_Ankle_Calcn_Origins(3,:)-R_FHL_CalcnWrap2),...
   (R_Ankle_Calcn_Origins(3,:)-R_FHL_CalcnWrap2)))^0.5...
   + (dot((R_FHL_Insertion-R_Ankle_Toe_Insertions(3,:)),...
   (R_FHL_Insertion-R_Ankle_Toe_Insertions(3,:))))^0.5;

R_Ankle_forces_max(3,:) = 322.0;
R_Ankle_optimal_fibre_lengths(3,:) = 0.0430;
R_Ankle_tendon_slack_lengths(3,:) = 0.3800;
R_Ankle_pennation_angles(3,:) = 10.0;
```

```
L_FHL_Origin = [-0.0079 -0.2334  -0.0244];
L_Ankle_Shank_Origins(3,:) = [-0.0186 -0.4079 0.0174];
L_Ankle_Calcn_Insertions(3,:) = [0.0374  0.0276 0.0241];
L_FHL_CalcnWrap2 = [0.1038  0.0068 0.0256];
L_Ankle_Calcn_Origins(3,:) = [0.1726 -0.0053 0.0269];
L_Ankle_Toe_Insertions(3,:) = [0.0155 -0.0064 0.0265];
L_FHL_Insertion = [0.0562 -0.0102 0.0181];

L_Ankle_Static(3,:) = (dot((L_Ankle_Shank_Origins(3,:)-
L_FHL_Origin),...
   (L_Ankle_Shank_Origins(3,:)-L_FHL_Origin)))^0.5...
   + (dot((L_FHL_CalcnWrap2-L_Ankle_Calcn_Insertions(3,:)),...
   (L_FHL_CalcnWrap2-L_Ankle_Calcn_Insertions(3,:))))^0.5...
   + (dot((L_Ankle_Calcn_Origins(3,:)-L_FHL_CalcnWrap2),...
   (L_Ankle_Calcn_Origins(3,:)-L_FHL_CalcnWrap2)))^0.5...
   + (dot((L_FHL_Insertion-L_Ankle_Toe_Insertions(3,:)),...
   (L_FHL_Insertion-L_Ankle_Toe_Insertions(3,:))))^0.5;

L_Ankle_forces_max(3,:) = 322.0;
L_Ankle_optimal_fibre_lengths(3,:) = 0.0430;
L_Ankle_tendon_slack_lengths(3,:) = 0.3800;
L_Ankle_pennation_angles(3,:) = 10.0;

%  Flexor digitorum longus
R_FDL_Origin = [-0.0083 -0.2046 -0.0018];
R_Ankle_Shank_Origins(4,:) = [-0.0154 -0.4051 -0.0196];
R_Ankle_Calcn_Insertions(4,:) = [0.0436  0.0315 -0.0280];
R_FDL_CalcnWrap2 = [0.0708  0.0176 -0.0263];
R_Ankle_Calcn_Origins(4,:) = [0.1658 -0.0081 0.0116];
R_Ankle_Toe_Insertions(4,:) = [-0.0019 -0.0078 0.0147];
R_FDL_ToeWrap2 = [0.0285 -0.0071 0.0215];
R_FDL_Insertion = [0.0441 -0.0060 0.0242];

R_Ankle_Static(4,:) = (dot((R_Ankle_Shank_Origins(4,:)-
R_FDL_Origin),...
   (R_Ankle_Shank_Origins(4,:)-R_FDL_Origin)))^0.5...
   + (dot((R_FDL_CalcnWrap2-R_Ankle_Calcn_Insertions(4,:)),...
   (R_FDL_CalcnWrap2-R_Ankle_Calcn_Insertions(4,:))))^0.5...
   + (dot((R_Ankle_Calcn_Origins(4,:)-R_FDL_CalcnWrap2),...
   (R_Ankle_Calcn_Origins(4,:)-R_FDL_CalcnWrap2)))^0.5...
   + (dot((R_FDL_ToeWrap2-R_Ankle_Toe_Insertions(4,:)),...
   (R_FDL_ToeWrap2-R_Ankle_Toe_Insertions(4,:))))^0.5...
   + (dot((R_FDL_Insertion-R_FDL_ToeWrap2),...
   (R_FDL_Insertion-R_FDL_ToeWrap2)))^0.5;

R_Ankle_forces_max(4,:) = 310.0;
R_Ankle_optimal_fibre_lengths(4,:) = 0.0340;
R_Ankle_tendon_slack_lengths(4,:) = 0.4000;
R_Ankle_pennation_angles(4,:) = 7.0;

L_FDL_Origin = [-0.0083 -0.2046 0.0018];
L_Ankle_Shank_Origins(4,:) = [-0.0154 -0.4051 0.0196];
L_Ankle_Calcn_Insertions(4,:) = [0.0436  0.0315 0.0280];
L_FDL_CalcnWrap2 = [0.0708  0.0176 0.0263];
L_Ankle_Calcn_Origins(4,:) = [0.1658 -0.0081 -0.0116];
L_Ankle_Toe_Insertions(4,:) = [-0.0019 -0.0078 -0.0147];
L_FDL_ToeWrap2 = [0.0285 -0.0071 -0.0215];
```

```
L_FDL_Insertion = [0.0441 -0.0060 -0.0242];

L_Ankle_Static(4,:) = (dot((L_Ankle_Shank_Origins(4,:)-
L_FDL_Origin),...
   (L_Ankle_Shank_Origins(4,:)-L_FDL_Origin)))^0.5...
   + (dot((L_FDL_CalcnWrap2-L_Ankle_Calcn_Insertions(4,:)),...
   (L_FDL_CalcnWrap2-L_Ankle_Calcn_Insertions(4,:))))^0.5...
   + (dot((L_Ankle_Calcn_Origins(4,:)-L_FDL_CalcnWrap2),...
   (L_Ankle_Calcn_Origins(4,:)-L_FDL_CalcnWrap2)))^0.5...
   + (dot((L_FDL_ToeWrap2-L_Ankle_Toe_Insertions(4,:)),...
   (L_FDL_ToeWrap2-L_Ankle_Toe_Insertions(4,:))))^0.5...
   + (dot((L_FDL_Insertion-L_FDL_ToeWrap2),...
   (L_FDL_Insertion-L_FDL_ToeWrap2)))^0.5;

L_Ankle_forces_max(4,:) = 310.0;
L_Ankle_optimal_fibre_lengths(4,:) = 0.0340;
L_Ankle_tendon_slack_lengths(4,:) = 0.4000;
L_Ankle_pennation_angles(4,:) = 7.0;

% Evertors
% --------

% Peronius Longus
R_PL_Origin = [0.0005 -0.1568  0.0362];
R_PL_TibiaWrap1 = [-0.0207 -0.4205  0.0286];
R_Ankle_Shank_Origins(5,:) = [-0.0162 -0.4319  0.0289];
R_Ankle_Calcn_Insertions(5,:) = [0.0438  0.0230  0.0221];
R_PL_CalcnWrap2 = [0.0681  0.0106  0.0284];
R_PL_CalcnWrap3 = [0.0852  0.0069  0.0118];
R_PL_Insertion = [0.1203  0.0085 -0.0184];

R_Ankle_Static(5,:) = (dot((R_PL_TibiaWrap1-R_PL_Origin),...
   (R_PL_TibiaWrap1-R_PL_Origin)))^0.5...
   + (dot((R_Ankle_Shank_Origins(5,:)-R_PL_TibiaWrap1),...
   (R_Ankle_Shank_Origins(5,:)-R_PL_TibiaWrap1)))^0.5...
   + (dot((R_PL_CalcnWrap2-R_Ankle_Calcn_Insertions(5,:)),...
   (R_PL_CalcnWrap2-R_Ankle_Calcn_Insertions(5,:))))^0.5...
   + (dot((R_PL_CalcnWrap3-R_PL_CalcnWrap2),...
   (R_PL_CalcnWrap3-R_PL_CalcnWrap2)))^0.5...
   + (dot((R_PL_Insertion-R_PL_CalcnWrap3),...
   (R_PL_Insertion-R_PL_CalcnWrap3)))^0.5;

R_Ankle_forces_max(5,:) = 754.0;
R_Ankle_optimal_fibre_lengths(5,:) = 0.0490;
R_Ankle_tendon_slack_lengths(5,:) = 0.3450;
R_Ankle_pennation_angles(5,:) = 10.0;

L_PL_Origin = [0.0005 -0.1568 -0.0362];
L_PL_TibiaWrap1 = [-0.0207 -0.4205 -0.0286];
L_Ankle_Shank_Origins(5,:) = [-0.0162 -0.4319 -0.0289];
L_Ankle_Calcn_Insertions(5,:) = [0.0438  0.0230 -0.0221];
L_PL_CalcnWrap2 = [0.0681  0.0106 -0.0284];
L_PL_CalcnWrap3 = [0.0852  0.0069 -0.0118];
L_PL_Insertion = [0.1203  0.0085 0.0184];

L_Ankle_Static(5,:) = (dot((L_PL_TibiaWrap1-L_PL_Origin),...
   (L_PL_TibiaWrap1-L_PL_Origin)))^0.5...
```

```
   + (dot((L_Ankle_Shank_Origins(5,:)-L_PL_TibiaWrap1),...
   (L_Ankle_Shank_Origins(5,:)-L_PL_TibiaWrap1)))^0.5...
   + (dot((L_PL_CalcnWrap2-L_Ankle_Calcn_Insertions(5,:)),...
   (L_PL_CalcnWrap2-L_Ankle_Calcn_Insertions(5,:))))^0.5...
   + (dot((L_PL_CalcnWrap3-L_PL_CalcnWrap2),...
   (L_PL_CalcnWrap3-L_PL_CalcnWrap2)))^0.5...
   + (dot((L_PL_Insertion-L_PL_CalcnWrap3),...
   (L_PL_Insertion-L_PL_CalcnWrap3)))^0.5;

L_Ankle_forces_max(5,:) = 754.0;
L_Ankle_optimal_fibre_lengths(5,:) = 0.0490;
L_Ankle_tendon_slack_lengths(5,:) = 0.3450;
L_Ankle_pennation_angles(5,:) = 10.0;

% Peronius Brevis
R_PB_Origin = [-0.0070 -0.2646 0.0325];
R_PB_TibiaWrap1 = [-0.0198 -0.4184 0.0283];
R_Ankle_Shank_Origins(6,:) = [-0.0144 -0.4295 0.0289];
R_Ankle_Calcn_Insertions(6,:) = [0.0471  0.0270 0.0233];
R_PB_Insertion = [0.0677  0.0219 0.0343];

R_Ankle_Static(6,:) = (dot((R_PB_TibiaWrap1-R_PB_Origin),...
   (R_PB_TibiaWrap1-R_PB_Origin)))^0.5...
   + (dot((R_Ankle_Shank_Origins(6,:)-R_PB_TibiaWrap1),...
   (R_Ankle_Shank_Origins(6,:)-R_PB_TibiaWrap1)))^0.5...
   + (dot((R_PB_Insertion-R_Ankle_Calcn_Insertions(6,:)),...
   (R_PB_Insertion-R_Ankle_Calcn_Insertions(6,:))))^0.5;

R_Ankle_forces_max(6,:) = 348.0;
R_Ankle_optimal_fibre_lengths(6,:) = 0.0500;
R_Ankle_tendon_slack_lengths(6,:) = 0.1610;
R_Ankle_pennation_angles(6,:) = 5.0;

L_PB_Origin = [-0.0070 -0.2646 -0.0325];
L_PB_TibiaWrap1 = [-0.0198 -0.4184 -0.0283];
L_Ankle_Shank_Origins(6,:) = [-0.0144 -0.4295 -0.0289];
L_Ankle_Calcn_Insertions(6,:) = [0.0471  0.0270 -0.0233];
L_PB_Insertion = [0.0677  0.0219 -0.0343];

L_Ankle_Static(6,:) = (dot((L_PB_TibiaWrap1-L_PB_Origin),...
   (L_PB_TibiaWrap1-L_PB_Origin)))^0.5...
   + (dot((L_Ankle_Shank_Origins(6,:)-L_PB_TibiaWrap1),...
   (L_Ankle_Shank_Origins(6,:)-L_PB_TibiaWrap1)))^0.5...
   + (dot((L_PB_Insertion-L_Ankle_Calcn_Insertions(6,:)),...
   (L_PB_Insertion-L_Ankle_Calcn_Insertions(6,:))))^0.5;

L_Ankle_forces_max(6,:) = 348.0;
L_Ankle_optimal_fibre_lengths(6,:) = 0.0500;
L_Ankle_tendon_slack_lengths(6,:) = 0.1610;
L_Ankle_pennation_angles(6,:) = 5.0;

% Peronius Tertius
R_PT_Origin = [0.0010 -0.2804 0.0231];
R_Ankle_Shank_Origins(7,:) = [0.0229 -0.4069 0.0159];
R_Ankle_Calcn_Insertions(7,:) = [0.0857  0.0228 0.0299];

R_Ankle_Static(7,:) = (dot((R_Ankle_Shank_Origins(7,:)-...
```

```
   R_PT_Origin),(R_Ankle_Shank_Origins(7,:)-R_PT_Origin)))^0.5;

R_Ankle_forces_max(7,:) = 90.0;
R_Ankle_optimal_fibre_lengths(7,:) = 0.0790;
R_Ankle_tendon_slack_lengths(7,:) = 0.1000;
R_Ankle_pennation_angles(7,:) = 13.0;

L_PT_Origin = [0.0010 -0.2804 -0.0231];
L_Ankle_Shank_Origins(7,:) = [0.0229 -0.4069 -0.0159];
L_Ankle_Calcn_Insertions(7,:) = [0.0857  0.0228 -0.0299];

L_Ankle_Static(7,:) = (dot((L_Ankle_Shank_Origins(7,:)-...
   L_PT_Origin),(L_Ankle_Shank_Origins(7,:)-L_PT_Origin)))^0.5;

L_Ankle_forces_max(7,:) = 90.0;
L_Ankle_optimal_fibre_lengths(7,:) = 0.0790;
L_Ankle_tendon_slack_lengths(7,:) = 0.1000;
L_Ankle_pennation_angles(7,:) = 13.0;

% Dorsiflexors
% ------------

% Tibialis Anterior
R_TA_Origin = [0.0179 -0.1624  0.0115];
R_Ankle_Shank_Origins(8,:) = [0.0329 -0.3951 -0.0177];
R_Ankle_Calcn_Insertions(8,:) = [0.1166  0.0178 -0.0305];

R_Ankle_Static(8,:) = (dot((R_Ankle_Shank_Origins(8,:)-
R_TA_Origin),...
   (R_Ankle_Shank_Origins(8,:)-R_TA_Origin)))^0.5;

R_Ankle_forces_max(8,:) = 603.0;
R_Ankle_optimal_fibre_lengths(8,:) = 0.0980;
R_Ankle_tendon_slack_lengths(8,:) = 0.2230;
R_Ankle_pennation_angles(8,:) = 5.0;

L_TA_Origin = [0.0179 -0.1624  -0.0115];
L_Ankle_Shank_Origins(8,:) = [0.0329 -0.3951 0.0177];
L_Ankle_Calcn_Insertions(8,:) = [0.1166  0.0178 0.0305];

L_Ankle_Static(8,:) = (dot((L_Ankle_Shank_Origins(8,:)-
L_TA_Origin),...
   (L_Ankle_Shank_Origins(8,:)-L_TA_Origin)))^0.5;

L_Ankle_forces_max(8,:) = 603.0;
L_Ankle_optimal_fibre_lengths(8,:) = 0.0980;
L_Ankle_tendon_slack_lengths(8,:) = 0.2230;
L_Ankle_pennation_angles(8,:) = 5.0;

% Extensor Hallucis Longus
R_EHL_Origin = [0.0012 -0.1767  0.0228];
R_Ankle_Shank_Origins(9,:) = [0.0326 -0.3985 -0.0085];
R_Ankle_Calcn_Insertions(9,:) = [0.0970  0.0389 -0.0211];
R_EHL_CalcnWrap2 = [0.1293  0.0309 -0.0257];
R_Ankle_Calcn_Origins(9,:) = [0.1734  0.0139 -0.0280];
R_Ankle_Toe_Insertions(9,:) = [0.0298  0.0041 -0.0245];
R_EHL_Insertion = [0.0563  0.0034 -0.0186];
```

```
R_Ankle_Static(9,:) = (dot((R_Ankle_Shank_Origins(9,:)-
R_EHL_Origin),...
   (R_Ankle_Shank_Origins(9,:)-R_EHL_Origin)))^0.5...
   + (dot((R_EHL_CalcnWrap2-R_Ankle_Calcn_Insertions(9,:)),...
   (R_EHL_CalcnWrap2-R_Ankle_Calcn_Insertions(9,:))))^0.5...
   + (dot((R_Ankle_Calcn_Origins(9,:)-R_EHL_CalcnWrap2),...
   (R_Ankle_Calcn_Origins(9,:)-R_EHL_CalcnWrap2)))^0.5...
   + (dot((R_EHL_Insertion-R_Ankle_Toe_Insertions(9,:)),...
   (R_EHL_Insertion-R_Ankle_Toe_Insertions(9,:))))^0.5;

R_Ankle_forces_max(9,:) = 108.0;
R_Ankle_optimal_fibre_lengths(9,:) = 0.1110;
R_Ankle_tendon_slack_lengths(9,:) = 0.3050;
R_Ankle_pennation_angles(9,:) = 6.0;

L_EHL_Origin = [0.0012 -0.1767 -0.0228];
L_Ankle_Shank_Origins(9,:) = [0.0326 -0.3985 0.0085];
L_Ankle_Calcn_Insertions(9,:) = [0.0970  0.0389 0.0211];
L_EHL_CalcnWrap2 = [0.1293  0.0309 0.0257];
L_Ankle_Calcn_Origins(9,:) = [0.1734  0.0139 0.0280];
L_Ankle_Toe_Insertions(9,:) = [0.0298  0.0041 0.0245];
L_EHL_Insertion = [0.0563  0.0034 0.0186];

L_Ankle_Static(9,:) = (dot((L_Ankle_Shank_Origins(9,:)-
L_EHL_Origin),...
   (L_Ankle_Shank_Origins(9,:)-L_EHL_Origin)))^0.5...
   + (dot((L_EHL_CalcnWrap2-L_Ankle_Calcn_Insertions(9,:)),...
   (L_EHL_CalcnWrap2-L_Ankle_Calcn_Insertions(9,:))))^0.5...
   + (dot((L_Ankle_Calcn_Origins(9,:)-L_EHL_CalcnWrap2),...
   (L_Ankle_Calcn_Origins(9,:)-L_EHL_CalcnWrap2)))^0.5...
   + (dot((L_EHL_Insertion-L_Ankle_Toe_Insertions(9,:)),...
   (L_EHL_Insertion-L_Ankle_Toe_Insertions(9,:))))^0.5;

L_Ankle_forces_max(9,:) = 108.0;
L_Ankle_optimal_fibre_lengths(9,:) = 0.1110;
L_Ankle_tendon_slack_lengths(9,:) = 0.3050;
L_Ankle_pennation_angles(9,:) = 6.0;

% Extensor Digitorum Longus
R_EDL_Origin = [0.0032 -0.1381  0.0276];
R_Ankle_Shank_Origins(10,:) = [0.0289 -0.4007  0.0072];
R_Ankle_Calcn_Insertions(10,:) = [0.0922  0.0388 -0.0001];
R_Ankle_Calcn_Origins(10,:) = [0.1616  0.0055  0.0130];
R_Ankle_Toe_Insertions(10,:) = [0.0003  0.0047  0.0153];
R_EDL_Insertion = [0.0443 -0.0004  0.0250];

R_Ankle_Static(10,:) = (dot((R_Ankle_Shank_Origins(10,:)-
R_EDL_Origin),...
   (R_Ankle_Shank_Origins(10,:)-R_EDL_Origin)))^0.5...
   + (dot((R_Ankle_Calcn_Origins(10,:)-
R_Ankle_Calcn_Insertions(10,:)),...
   (R_Ankle_Calcn_Origins(10,:)-
R_Ankle_Calcn_Insertions(10,:))))^0.5...
   + (dot((R_EDL_Insertion-R_Ankle_Toe_Insertions(10,:)),...
   (R_EDL_Insertion-R_Ankle_Toe_Insertions(10,:))))^0.5;

R_Ankle_forces_max(10,:) = 341.0;
```

```
R_Ankle_optimal_fibre_lengths(10,:) = 0.1020;
R_Ankle_tendon_slack_lengths(10,:) = 0.3450;
R_Ankle_pennation_angles(10,:) = 8.0;

L_EDL_Origin = [0.0032 -0.1381 -0.0276];
L_Ankle_Shank_Origins(10,:) = [0.0289 -0.4007 -0.0072];
L_Ankle_Calcn_Insertions(10,:) = [0.0922  0.0388 0.0001];
L_Ankle_Calcn_Origins(10,:) = [0.1616  0.0055 -0.0130];
L_Ankle_Toe_Insertions(10,:) = [0.0003  0.0047 -0.0153];
L_EDL_Insertion = [0.0443 -0.0004 -0.0250];

L_Ankle_Static(10,:) = (dot((L_Ankle_Shank_Origins(10,:)-
L_EDL_Origin),...
   (L_Ankle_Shank_Origins(10,:)-L_EDL_Origin)))^0.5...
   + (dot((L_Ankle_Calcn_Origins(10,:)-
L_Ankle_Calcn_Insertions(10,:)),...
   (L_Ankle_Calcn_Origins(10,:)-
L_Ankle_Calcn_Insertions(10,:))))^0.5...
   + (dot((L_EDL_Insertion-L_Ankle_Toe_Insertions(10,:)),...
   (L_EDL_Insertion-L_Ankle_Toe_Insertions(10,:))))^0.5;

L_Ankle_forces_max(10,:) = 341.0;
L_Ankle_optimal_fibre_lengths(10,:) = 0.1020;
L_Ankle_tendon_slack_lengths(10,:) = 0.3450;
L_Ankle_pennation_angles(10,:) = 8.0;
```

Appendix D

A Neuro-Musculo-Skeletal Model for the Simulation of Normal and Pathological Gait Patterns

A NEURO-MUSCULO-SKELETAL MODEL FOR THE SIMULATION OF NORMAL AND PATHOLOGICAL HUMAN GAIT PATTERNS

S. Lister[1], N. B. Jones[1], W. Peasgood[1], S. K. Spurgeon[1]
[1]Department of Engineering, University of Leicester, Leicester, UK
sjl25@leicester.ac.uk, nbj1@leicester.ac.uk, wp3@leicester.ac.uk, eon@leicester.ac.uk

Abstract – A scheme to simulate complete human gait cycles using muscle activation signals similar to those found through EMG analysis is described. A 2-dimensional ten-segment model with a two-part foot was developed using LaGrange's equations. A set of parameters allows the model to be individualised to a given subject's physical characteristics. Twenty-four activation signals provide inputs to forty-six muscles grouped according to their actions. Simple tests show that the model behaves in a realistic manner but under open-loop conditions, simulating gait patterns is infeasible. A controller is required to perform trajectory tracking.

I. INTRODUCTION

It is important to understand the motions of human gait and the associated muscle activations. Such knowledge can help in diagnosing gait disorders and in designing appropriate therapies.

Surface electromyograms (EMGs) can read only a short distance into the skin, most of the signal coming from within 25 mm of the surface [1]. The alternative is to use needle electrodes, which can be painful.

A computer model is used to generate a simulation of EMG activity within muscle groups for a given motion. This could be used as a guide to which muscle groups are under-performing and which are attempting to compensate in a given individuals condition.

II. METHODS

A. Dynamics

A set of general equations for modelling pin joint locomotion models was developed from LaGrange's equations. These were used to produce a 10-segment model following example human parameters.

The model incorporates separate torso and pelvis segments to allow pelvic tilt to be modelled while minimising torso motion.

Use of a 2-segment foot with a joint at the metatarsal heads allows more accurate ground reactions to be generated as the heel can lift while the toes remain flat on the ground.

B. Internal Joint Forces

Dampers and springs were applied to the joints to mimic the effects of cartilage and the ligaments that prevent non-physiological motion [2], [3].

C. Ground Reactions

Ground reaction equations were developed based on preventing three points on the sole of each foot (heel, metatarsal head and toe) from passing through the floor.

The point with the greatest vertical force acting on it would also be prevented from sliding horizontally while in contact with the ground. The assumption is made that the coefficient of friction is always sufficient to maintain this.

D. Musculotendon Actuators

Musculotendon behaviour was simulated using a generalised model and parameters then adapt the model to make it appropriate to each muscle [4], [5].

III. TESTING

Simple tests were made at every stage of development. Muscle behaviour was examined at various joint angles and contraction speeds. Ground reactions were tested by dropping the model from small and large distances. The dynamics were tested by applying external forces, accelerations and velocities. The steady-state response of the model was also checked.

When satisfied with all of the components, open-loop testing of the model began using muscle input-signals from the literature and kinematic data collected specifically for this [6]. However, the system is too unstable and non-linear to produce accurate results in open-loop conditions without painstaking, arbitrary manual adjustments.

IV. CONCLUSION

The model does appear to behave in a realistic manner; applying individual forces will change the models posture, gravity makes the model fall over in a way that appears similar to a falling human. However, without generating a gait pattern within acceptable bounds it is not possible to assess the performance of the model as a gait simulator.

A controller is required to force the model to follow a defined trajectory; comparison of the control input with actual EMG signals would then provide a measure of the simulations effectiveness.

REFERENCES

[1] M. W. Whittle, *Gait Analysis an introduction*, Reed Educational and Professional Publishing Ltd, 2nd Ed., 1996.

[2] S. Siegler, S. Lapointe, R. Nobilini, A. T. Berman, "Six-degrees-of-freedom instrumented linkage for measuring the flexibility characteristics of the ankle joint complex", Journal of Biomechanics, vol. 29(7), 1996, pp. 943-947.

[3] S. J. Piazza, S. L. Delp, "The influence of muscles on knee flexion during the swing phase of gait" Journal of Biomechanics vol. 29, 1996, pp. 723-733.

[4] F. E. Zajac, E. L. Topp, P. J. Stevenson, "A Dimensionless Musculotendon Model", Proceedings of the 8th Annual Conference of the Engineering in Medicine and Biology Society, 1986, pp. 601-604